BIO-FUNCTIONALIZATION OF NANOSTRUCTURED ELECTRODES FOR BIOSENSING APPLICATIONS

By

YAN ZHOU

(Under the Direction of Ramaraja P. Ramasamy)

ABSTRACT

Bio-functionalization refers to the modification of surfaces using biomolecules such as peptides, enzymes, DNA, aptamers, antibodies, and viruses etc. Bio-functionalization of electrode surfaces could impart new properties that enable their use in a specific application such as biosensing. This dissertation mainly focused on two types of bio-functionalization of nanostructured electrodes for electrochemical sensing applications. The first was based on enzymes for oxygen sensing applications and the second was based on viruses for bacterial cell isolation and detection applications. In the first application of oxygen sensing, laccase enzyme derived from two different sources, namely *Trametes versicolor* (fungi) and *Bacillus FNT* (thermophilic bacterium) were used for electrode bio-functionalization. Metal oxides were first functionalized with laccase from *Trametes versicolor* (TVL). However, the resulting electrodes exhibited less than ideal stability for electrochemical sensing applications. The limitation was overcome by using a thermophilic bacterium laccase *Bacillus sp. FNT* (FNTL). Multiwall carbon

nanotubes (MWCNT) modified electrode was functionalized with *Bacillus* FNT laccase. The resulting electrodes exhibited excellent electrochemical stability and high enzyme activity compared to TVL functionalized electrodes for oxygen reduction bio-electrocatalysis. A detailed electro-kinetic study was also conducted using FNTL functionalized electrodes for oxygen reduction reaction.

In the second application, new methods were developed for functionalizing electrode surfaces with viruses for whole bacterial cell biosensor applications. Carbon nanotube modified electrode surfaces were functionalized with bacteriophages using a charge-directed, electric-field induced immobilization method developed specifically for myoviruses. The T2 phages functionalized electrodes were established for the capture and electrochemical detection of *Escherichia coli* B.

In order to achieve simultaneous detection of foodborne pathogens from real food matrix, a bacteria separation method was developed by bio-functionalization of magnetic particles using bacteriophages. P100 phages were used to functionalize magnetic particles for selective isolation and enrichment of *Listeria monocytogenes* from complex media. The work was complemented by a demonstration of simultaneous *L. monocytogenes* enrichment and detection using an electrochemical biosensor. To enable preferred orientation of P100 on the magnetic particles, the bacteriophage was genetically engineered to express biotin on the capsid of the phage, which could be crosslinked to the streptavidin present on the magnetic particle surface.

INDEX WORDS: Laccase enzyme, oxygen reduction, bacteriophage, P100, *E. coli, Listeria monocytogenes*, impedance spectroscopy, magnetic separation, bacterial detection, electrochemical sensor, biosensor.

BIO-FUNCTIONALIZATION OF NANOSTRUCTURED ELECTRODES FOR BIOSENSING APPLICATIONS

by

YAN ZHOU

B.S., Hunan University, China, 2012

A Dissertation Submitted to the Graduate Faculty of The University of Georgia in Partial Fulfillment of the Requirements for the Degree

DOCTOR OF PHILOSOPHY

ATHENS, GEORGIA

BIO-FUNCTIONALIZATION OF NANOSTRUCTURED ELECTRODES FOR BIOSENSING APPLICATIONS

by

YAN ZHOU

Major Professor:	Ramaraja Ramasamy
Committee:	John Stickney Michael Johnson Robert Woods

Electronic Version Approved:

Suzanne Barbour
Dean of the Graduate School
The University of Georgia
May 2018

DEDICATION

To my mom, my dad and my family.

ACKNOWLEDGEMENTS

First and foremost, I would like to thank my advisor, Prof. Ramaraja Ramasamy for his guidance, encouragement, and support throughout my Ph.D. study. As his first student from Chemistry department, he has been giving me opportunity to learn the cutting-edge science, professional experimental strategies and the collaborative spirit. Most importantly, he gave me absolute freedom to try out my hypothesis and ideas, which have influenced me in my Ph.D. study and will keep inspiring me in the future. Next, I would like to thank my Ph.D. dissertation committee members: Dr. John Stickney, Dr. Michael Johnson, and Dr. Robert Woods for their advice, suggestions and comments in my candidacy exams and in the dissertation review process.

Being a graduate student majoring in chemistry, lab work is a major part of my daily life. I'll never forget all memories with my best friends in our lab, Narendran Sekar and Yi Fang, with whom I spent most of my time with. I also want to thank my friend and our previous post-doc Dr. Yogeswaran Umasankar, who helped me during my first two years in the lab. I also want to appreciate the help offered by all my friends and collaborators Abhijit, Jackie, Dr. Yajun Yan and Dr. Peter Kner, without whom my PhD work would not been completed in its entirety. I would like to thank all my teachers who instructed me at HNU and UGA. I would also like to thank all my friends at Riverbend and UGA, Dr. Xiao Wang, Dr. Zixuan Li, Dr. Chenyang Li, Dr. Jing Gao, Dr. Qi Gao, Dr. Feng Long, Dr. Shan Gao, Alyssa, Baviththira, Xiaoshi Zeng, Ke Li, who directly and/or indirectly helped and motivated me through the course of my PhD work. It has been a great pleasure to be friends with you all.

It gives me immense pleasure to thank my dad and my mom, my grandparents and all my family members who have been motivating and advising me, right from taking the decision to join PhD at UGA until now. Last, but not the least, I would like to thank my husband, who has always support me and encouraged me from 2009 since we first met.

TABLE OF CONTENTS

Page

CHAPTER 1

INTRODUCTION

1.1 What is a biosensor?

Biosensor is a device that incorporates recognition elements (bioreceptors) with high specificity towards the target analytes. Analytical tools based on biosensors have been widely applied in various applications ranging from environmental monitoring, agriculture, food safety to clinical diagnosis and military applications.[1-3] In the medical field, researchers have developed biosensors for accurate and rapid detection of infectious diseases, tumors, blood glucose and other toxins. In the food industry, biosensors have been developed to detect pathogens in contaminated food samples, or for gases released from spoiled food. In the field of environmental protection, biosensors have been applied for monitoring toxic substances, detecting heavy metals, and bio-corrosion. Since the 1970s, various types of biosensors have been developed and demonstrated for various applications of which a personal diabetes meter (glucose biosensor) is an example of commercially successful biosensor technologies.[3] As shown in Figure 1.1, a typical biosensor consists of three components, an analyte, a bioreceptor and a transducer element. The analyte is the target molecule of interest, which includes but not limited to cells, antibodies, proteins, complex molecules, simple elements or ions contained in a simple or complex media. The bioreceptor is a recognition element that specifically binds to the target analyte(s) and causes

physical or chemical changes, resulting in the generation of a signal for detection (sensing). For example, enzymes, proteins, nucleic acids, bacteriophages or antibodies have been adopted as recognition elements for detection of various analytes. The transducer is a signal translator that translates the interaction between analyte and bioreceptor into electrochemical, electric, magnetic, optical, colorimetric or gravimetric signals to enable qualitative or quantitative detection.

There are several parameters that are used to determine the performance of a biosensor: sensitivity, selectivity, reliable detection range, limit of detection and limit of quantification. The sensitivity of a biosensor is the magnitude of signal change per unit of quantity (mass, volume or concentration) of the analyte.

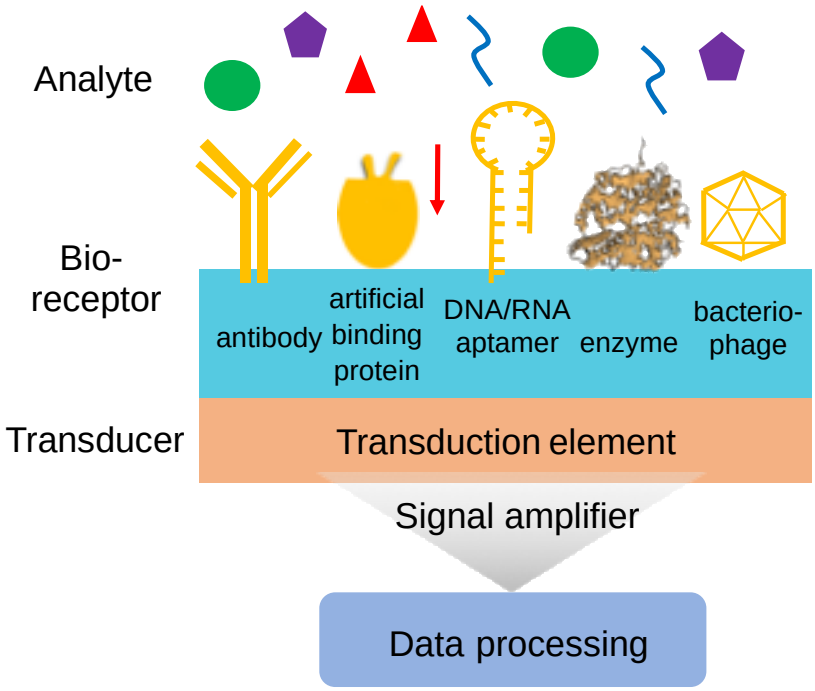

Figure 1.1: Schematic structure and operating principle of a biosensor.

The selectivity of a biosensor is the ability of a bioreceptor to detect a particular analyte while remaining irresponsive towards any other potential contaminants or interfering species

(pseudo-analytes). In the construction of a biosensor, selectivity is the most important parameter of consideration, when choosing the bioreceptors. The reliable range of detection is usually determined by a linear correlation between analyte concentration and sensing signal that can be represented as $y = mc$, where c is the concentration of the analyte, y is the sensing signal, and m is the slope of the linear correlation between y and c, which is also defined as the sensitivity of a biosensor. Biosensors with high sensitivity are advantageous because of their ability to generate significant signal differences even for low variations in the analyte concentrations. Limit of detection (LOD) is the minimum concentration of analyte that can be determined to be statistically different from a blank (noise). The LOD is recommended to be a measurement level of 3σ units above the value of blank, where σ is the standard deviation of the blank.[4] The LOD can be calculated from the slope of linear correlation according to the following equation: $LOD = k\sigma/m$, where $k = 3$, σ = standard deviation of blank, and m = the slope of calibration curve. Limit of quantification (LOQ) is the lowest concentration of an analyte that could be quantitatively measured with acceptable precision and accuracy under the stated condition of test. LOQ is a more conservative estimation of detection limit: $LOQ = k\sigma/m$, where $k = 5\sim10$.[4]

There are additional criteria that determine if a particular biosensing technology is advantageous over other competitive tools: shelf life, thermal and pH stability, cost, test duration, high throughput capability and good reliability. An ideal biosensor must offer high sensitivity towards specific analyte, easy to use, portable, require minimal sample preparation and sample volume, and enable rapid detection at a low cost. Table 1.1 shows the advantages and limitation of biosensors in the field of clinical diagnosis, food safety, and environmental monitoring.[5-7]

Table 1.1: Advantages and limitations of biosensors in clinical diagnosis, food safety, and environmental monitoring.

	Advantages	Limitations
Food safety	• Cost-effective; • Minimal cross-contamination; • High sensitivity and selectivity.	• Need to pre-treat samples; • Variation in sensitivity depending on different transduction elements;
Clinical diagnosis	• Short assay time, point-of-care diagnosis; • Simple sample preparation; • High portability, high-throughput and multiplexing ability.	• Variation in sensitivity based on different transduction elements; • Sensitive to sample matrix heterogeneity.
Environmental monitoring	• High sensitivity and selectivity; • Rapid response.	• Inhibitor interference; • Variable stability due to loss of enzyme activity.

1.1.1 Classification of Biosensors based on recognition element

Biosensors could be classified based on the type of bioreceptors namely enzyme, protein, antibody, virus and deoxyribonucleic acid (DNA) based biosensors. For example, a blood glucose biosensor is considered as an enzymatic biosensor as the biorecognition element is glucose oxidase enzyme.[3] Enzymes could selectively detect target substrates based on their catalytic activity and carry out a biochemical reaction that results in a signal for detection. Enzyme-based biosensors are popular for electrochemical transduction as several approaches have been reported to enhance the communication between the enzymes and the electrode surface in order to generate a signal.[8-10] Nanomaterials, such as carbon nanotubes, or gold nanoparticles (AuNPs), have been utilized to modify the electrode surface, achieving direct electron transfer between enzyme active site and electrode surface. DNA-based biosensor, also named as genosensor, could be used for detection of DNA based on the specific DNA hybridization. It is now explored as an alternative to the classical genetic assays. Recently, DNA sensors have been used to detect genetically modified organisms (GMO).[11] Antibodies and bacteriophages (viruses) can also be used as recognition

molecules which enable biosensing based on affinity interaction. They bind to specific targets based on their intrinsic affinity towards the analyte, which could be utilized for selective detection of the target species. Antibodies as biorecognition element, could interact with the corresponding antigen and the resulting antibody-antigen affinity interaction makes it highly specific and reliable detection to the target analyte. Antibodies are the most popular choice for affinity biosensors, which are also commonly referred to as immunosensors. Bacteriophages, offers high selectivity towards their host bacteria strains and have been explored lately for the detection of pathogenic bacteria.[12,13]

1.1.2 Classification of biosensors based on transduction mode

Biosensors could also be classified based on the mode of transduction. The commonly used transduction modes are optical, electrochemical, colorimetric and piezoelectric transductions. In an optical biosensor, a change in the refractive index or thickness could be observed when the target analyte binds to the biorecognition element. The detection signal could be a change in surface plasma resonance, fluorescence or Raman spectroscopy.[14] Piezoelectric biosensors use oscillating crystals which undergo a frequency shift when a potential is applied. When the target analyte binds to the biorecognition element, a change in the resonance frequency will be produced, which can be used as a signal. Colorimetric biosensors are easy and simple to use due to the ease of detection with naked eyes, as the signal is based on a color change in the system after a recognition molecule interacts with the analyte. Both enzymes and bacteriophages have been used as recognition molecules in colorimetric biosensors.[15] Among the various transduction modes, electrochemical transduction is of particular interest due to their simplicity, fast response and high sensitivity. It is possible to achieve rapid, real-time measurements using electrochemical biosensors. Electrochemical transduction could be potentiometric (voltage signal), amperometric

(current signal) or impedimetric (impedance or resistance signal). The sensitivity of a given biosensor is dependent on both transduction mode and instrument capability. In the following paragraphs, electrochemical transduction is elaborately discussed for specific end applications.

1.1.3 Electrochemical transduction

Electrochemical biosensors have several advantages when compared to other analytical readouts, such as their high sensitivity, low detection limit, easy miniaturization, and real-time possibilities. They do not depend strongly on the reaction volume, and hence very small analyte volumes are sufficient for measurement in most cases. Among the various electrochemical transduction modes, potentiometry is based on the potential difference between a reference electrode and an indicator, or two reference electrodes separated by a selective membrane, where no significant current is observed between them. Amperometry is based on the measurement of the current observed from the electrochemical reduction/oxidation of an electroactive species. Clark oxygen electrodes represent the basis for the simplest forms of amperometric biosensors, where the current is produced due to oxygen reduction and is proportional to the oxygen concentration. Typically, the current is measured at a constant potential and this is referred as amperometry. Impedance is a measurement of resistance and capacitance changes in an electrochemical system, more specifically at the electrode/electrolyte interface. Impedance spectroscopy could help explore the intrinsic property or specific processes that influence the conductivity or resistivity of the electrode interface, in order to monitor changes in electrical properties arising from biorecognition events at the electrode surfaces. Therefore, it is a useful tool in the development and analysis of biosensors. Researchers have used electrochemical impedance spectroscopy (EIS) to characterize the study of polymer degradation, antigen-antibody interaction, binding state of DNA, etc. [16-18] Electrochemical biosensors have been widely used for detection of

various analytes ranging from small molecules to tissues and cells, such as oxygen, glucose, complex carbohydrates, DNAs, tissues, and bacteria. The components of the sensing platforms and the detection approaches play an important role in the performance of the electrochemical biosensors, such as choice of electrode materials and recognition elements, methods used for bio-functionalization of electrodes, and the mode of electrochemical transduction. Detailed discussion on each of the components are discussed in Section 1.2.

1.2 Bio-functionalization of nanostructured electrodes

Bio-functionalization is the process of immobilizing biomolecules onto surfaces to provide biospecificity and/or catalysis activity for reactions in biosensors. Strategies for immobilizing various biomolecules such as proteins, enzymes, antibodies and nucleic acids, onto nanomaterial supports have been extensively studied and widely used in numerous biosensor applications.[17,19-23] Nanostructured electrodes as electrochemical transducers are advantageous for high sensitivity because of the large interfacial area they provide for electrochemical interactions. The nanomaterials can be functionalized with bio-recognition elements using various immobilization strategies (physical adsorption, electrostatic interaction, covalent binding, etc.).[24-27] The following paragraphs in this chapter focus on the development of appropriate bio-functionalization strategies for modified nanostructured electrode surfaces with biorecognition molecules for electrochemical biosensor applications.

1.2.1 Nanomaterials for biosensor platform

In order to increase the sensitivity and obtain a better detection limit in a biosensor, nanomaterials are used as both transduction elements and as immobilization support for biological molecules. The nanomaterials for electrochemical transduction are required to possess electrical conductivity and therefore the preferred choices are metal and metal oxide nanoparticles, carbon

nanotubes, quantum dots, etc.[28-30] Among these various nanomaterials, carbon nanotubes (CNTs) have been widely studied due to their unique electronic structure and tunable electrical conductivity.[31,32] CNTs are also known for their fast electron transfer capability and high chemical stability.[33] CNT could be changed permanently or reversibly through various surface functionalization.[34] CNTs also offer large electro-active area that could create highly porous surface for binding different biomolecules, leading to higher biosensor sensitivity. [35]CNTs are well suited for transduction of electric signals generated upon recognition of a target. Due to the unique properties, CNTs have attracted much attention on their potential in biosensing applications.

Metallic particles, such as gold nanoparticles and silver nanoparticles have been studied for the design of versatile biosensors. Metallic nanoparticles provide unique optical and electrochemical properties, which differ significantly from their bulk counterparts and have been functionalized with biomolecules for various end applications. Gold nanoparticles(AuNPs), for example, can be modified with thiols, disulfides, amines and carboxyl functional groups, which could further be linked to biomolecules such as DNA, proteins or antibodies. AuNPs are mostly used for optical biosensor applications due to their plasmonic properties. For example, gold nanoparticles have been commonly used as transduction element in biosensor that use surface plason resonance (SPR) signals, due to the change in the dielectric constant of gold films during analtye-binding events.[30 36,37]

Metal oxides (MOx) nanomaterials also possess several favorable properties for bio-electrochemical applications. They have been used in various applications due to their biocompatibility, photochemical and semiconducting properties.[38] Intrinsic n-type semiconducting materials, such as TiO_2, SnO_2, and ZnO, can be used for electronic signal transduction in bio-electrochemical devices with no significant ohmic drop due to the low currents involved in the

bio-electrochemical systems. The presence of surface hydroxyl groups on MO nanomaterials offers the possibility for surface functionalization that can reliably link to the biomolecules such as enzymes, and therefore, offer huge prospects as transducers for enzyme-based biosensors.

1.2.2 Commonly used biomolecule functionalization approaches

Multiple strategies for the immobilization of biomolecules to nanostructured electrodes have been extensively explored to improve the sensitivity of the biosensors. The high surface-to-volume ratio allows a maximum number of biomolecules to be immobilized by covalent and non-covalent functionalization for different transducers. Herein, we classify immobilization strategies of biomolecules onto nanostructured electrode surface into two categories: covalent immobilization and non-covalent immobilization.

Non-covalent immobilization methods include: (1) Physical adsorption, based on hydrophobic interaction, electrostatic interaction and π-π stacking and (2) Affinity interaction, based on the specific interactions such as antibody to antigen, streptavidin to biotin, etc. Direct physical adsorption is simple and easy to perform, for example, by soaking the support materials into a solution containing biomolecules like enzymes, in order for the biomolecules to get adsorbed on the nanomaterials.[39] However, physical bonding is generally too weak to keep the biomolecule immobilized on the supporting surface for extended duration and this method is prone to biomolecule leaching out from the nanostructured support matrix.

Table 1.2: Approaches for bio-functionalization of nanomaterials.

Functional groups of nanomaterials	Coupling agent	Active site on biomolecules
-OH	Silane and NHS ester	NH_2
-COOH	EDC, and NHS ester	NH_2
$-NH_2$	EDC	-COOH

Covalent immobilization methods are based on the chemical covalent linkage between the biomolecules and nanomaterials. The linkage could be achieved through various functional groups, such as hydroxyl group (-OH), amine group ($-NH_2$), carboxyl group (-COOH), sulfhydryl group (-SH) etc. Depending on the functional group at the nanomaterial surface, an activation step may be needed for biomolecule immobilization. In Table 1.2, some examples of the functional groups and coupling agent are presented for biomolecule immobilization.

1.3 State-of-the-art in enzyme catalyzed O_2 reduction reaction

Oxygen reduction reaction (ORR) is one of the most important and highly explored electrochemical reactions because of its applicability in devices such as O_2 sensors and fuel cells. For electrochemical oxygen reduction reaction, the desired mechanism is a four-electron reduction of oxygen to water. The sluggish kinetics of ORR can be typically attributed to the strength of the O=O bond (498 kJ/mol) that must be broken during the reaction. The ORR kinetics could be increased by lowering the activation energy of the reaction, with the help of a catalyst that adsorbs oxygen molecules. Biocatalysts are good alternatives to transition metal catalysts for ORR due to their high catalytic activity at low to medium temperature and its reproducibility.[29,40,41] Examples of biological catalysts are known to catalyze ORR include enzymes, such as laccase and tyrosinase, which are multi-copper oxidases. Multi-copper oxidases constitute enzymes that couple one electron oxidation of substrate (e.g. an electrode) with the complete four-electron reduction of oxygen to water. Each multi-copper enzyme contains multiple types of Cu atoms (e.g. T1, T2, T3) in their active site that exhibit specificity to many organic substrates including aromatic phenols and amines, with co-substrate of oxygen.[42] Laccase is one of the simplest multi-copper oxidases that could catalyze the reaction of four-electron oxygen reduction to water without the formation of peroxide intermediates, while simultaneously oxidizing phenolic compounds to quinones.

Based on the redox potential at the T1 copper site, laccases could be classified as low or high redox potential enzymatic catalysts. Bacterial and plant laccases are low redox enzymes with E_{T1} smaller than 460 mV vs NHE (versus standard hydrogen electrode), whereas fungi laccases include enzymes with E_{T1} ranging from 460 mV to 790 mV vs NHE.[43]

1.3.1 Type of laccase used in this study

Laccase from *Trametes versicolor*

Laccase from *Trametes versicolor (TVL)* is a multi-copper enzyme that catalyzes the oxidation of many phenolic compounds, diamines, and aromatic amines with simultaneous reduction of oxygen to water molecules.[19] TVL possess high thermodynamic redox potential and catalytic activity, which could be utilized for biofuel cell and biosensor applications. The XRD and spectroscopic studies have revealed that the enzyme consists four copper sites, Type 1, Type 2, and two Type 3 copper sites. In TVL structure, T1 copper is located 6.5Å below the surface of the protein. T2 and T3 copper sites are located close to each and form a trinuclear copper center. T1 copper is connected to T2/T3 trinuclear site via a histidine-cysteine-histidine tripeptide.[44] During the catalytic reaction, the copper ions within the enzyme structure play an important role by shifting their oxidation states between Cu^{2+} and Cu^{+}. In the electrocatalytic reduction of O_2, electrons will first transfer from to T1 copper site and then to T2/T3 trinuclear copper sites. The fully reduced tri-nuclear copper center will then react with oxygen to generate hydrogen peroxide intermediate and finally reduced to water. TVL is the most widely studied laccase enzyme for electrocatalysis of oxygen, because of its high redox potential (700 mV), which is close to the thermodynamic redox potential of ORR at pH 7. The optimal activity of TVL is at a pH of 4 to 5.[45]

Laccase from *Bacillus FNT*

Although laccase is widely distributed in plants and fungi, it has also been reported in few bacteria and archaea. Compared to fungal laccase, bacterial laccases are highly active and possess higher stability at high pH, at high temperatures, and at high concentration of chlorides and copper ions. Laccase from a thermotolerant bacterium *Bacillus FNT* laccase (FNTL) was purified and found to possess high tolerance to abnormal temperatures and pH. This aerobic organism that belongs to *Bacillus* genus, could be grown in a wide range of temperature, from 16 to 70 °C, and pH between 4 and 10.

1.3.2 Catalytic activity of laccase-nanostructured electrodes

In most cases, enzyme biocatalyst attached on the electrode surface may not achieve significant electrical (electron transfer) communication between its active center and the electrode or support material, which is due to the surrounding protein matrix in the enzyme structure that insulates the redox site. Many researchers have explored different approaches to establish electrical communication in enzyme bioelectrodes for a specific electrochemical reaction such as the ORR. In general, electron transfer could be classified into two types: mediated electron transfer and direct electron transfer as shown in Figure 1.2 for the case of laccase. In direct electron transfer (DET), the electrons transfer directly from the electrodes to laccase enzyme via the active copper sites. In this case, no additional redox reactions or species are involved in carrying out the desired reaction. DET requires a specific orientation of enzymes with their active sites close to the electrode surface to facilitate the electron transfer via the tunneling distances.

In mediated electron transfer (MET), a redox active molecule, which serves as a mediator (M), is used to shuttle electrons between enzyme active sites and the electrode surfaces for continuous, electro-enzymatic reduction of oxygen. The orientation dependency of enzymes is

eliminated, and in such cases, enzyme could catalyze the reduction or oxidation of the mediator. The regeneration of the mediator occurs on the electrode surface. In a mediated electron transfer of oxygen reduction reaction, electrons first transfer from electrode to the mediator, the mediator gets reduced and transfer electrons to laccase enzymes. Oxygen is then reduced to water. The reduced mediator interacts with laccase enzyme via a biological oxidation to regenerate itself on the electrode surface. In Chapter 2, mediators such as 2,2'-azino-bis(3-ethylbenzothiazoline-6-sulfonic acid) (ABTS), promazine, and syringaldazine that possess redox potential close to that of the ORR were used to reduce oxygen to water using TVL as the catalyst.

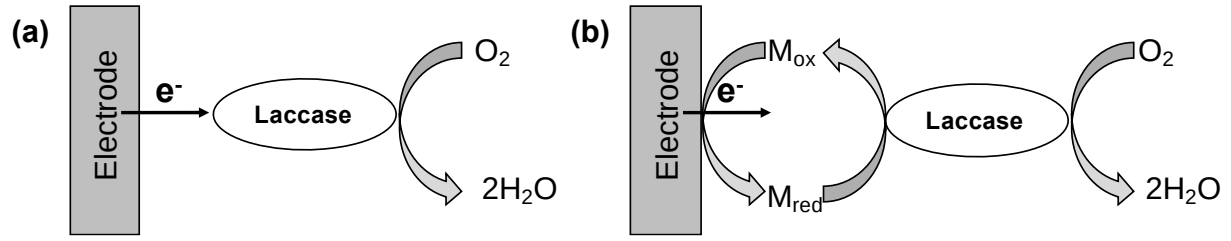

Figure 1.2: The Electron transfer pathway of laccase-catalyzed enzymatic reduction of oxygen to water using laccase: (a) Direct electron transfer; (b) Mediated electron transfer.

Laccase-carbon nanotube nanocomposites

Various strategies have been extensively explored to immobilize enzymes onto CNT supports for biosensor and biofuel cell applications.[46] Based on their different surface functionalities, such as carboxyl, amine or sulfhydryl of proteins, enzymes could be immobilized onto CNT surface through carboxyl groups, amine group, sulfhydryl groups, enzymes could be immobilized onto CNT surface via specific crosslinkers or tethering agents. Single-wall carbon nanotubes (SWCNT) were used first by Mao's team as support for electrocatalyst and for facilitating the electron transfer of laccase.[47] Figure 1.3 describs a laccase immobilization strategy developed earlier in our laboratory using noncovalent functionalization method of CNT via a

heterobifunctional crosslinker pyrenebutanoic acid succinimidyl ester (PBSE) to achieve direct electron transfer between electrode and laccase active sites.[48,49] The rapid electron transfer between laccase and the electrode surface offers considerable promise for maximizing the power density of biofuel cells. In this dissertation research, the electrocatalytic activity of both TVL-CNT and FNTL-CNT bioconjugates have been studied.

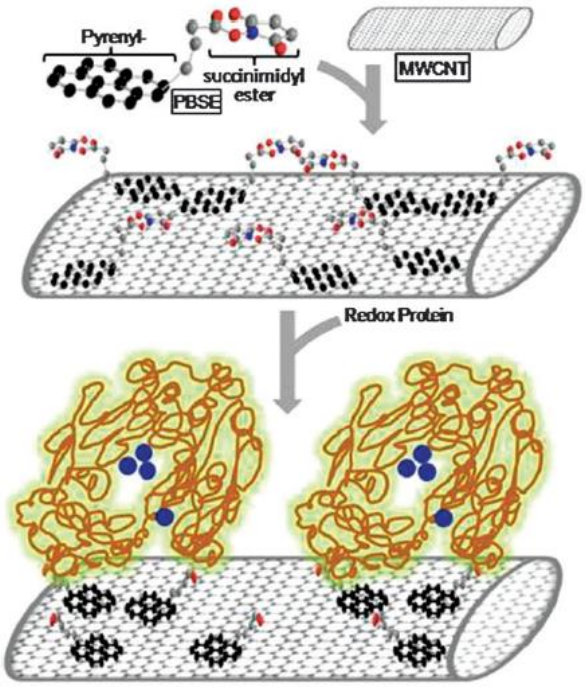

Figure 1.3: Illustration of laccase enzyme immobilization onto PBSE-modified carbon nanotubes. (Reprinted with permission from publisher)[48]

Laccase-metal oxide nanocomposites

Nanostructured metal oxides particles, such as zinc oxide, iron oxide, tin oxide, titanium oxide have been found to exhibit functional biocompatible and exhibit photocatalytic properties. These materials also exhibit higher surface to volume ratio than their bulk counterparts and offer prospects for various types of bio-functionalization. Enzymes could be immobilized onto metal oxide surfaces with improved conformation, orientation and biological activity.[50] In this

dissertation research, metal oxides such as TiO_2, ZnO_2, SnO_2 were functionalized with laccase, and studied as catalysts for oxygen reduction reaction the results of which are discussed in Chapter 2.[29,51]

1.4 State-of-the-art methods for food pathogen detection

Food-borne illnesses are a global problem, causing 48 million illnesses and 3000 deaths each year in the United States and cost around $15 billion annually to the healthcare industry.[52,53] Pathogens, such as *Escherichia coli, Listeria monocytogenes* and *Salmonella spp.* may contaminate food products and cause severe health risks. Quick identification of the existence and source of pathogenic microbes in food could help contain their spread and prevent epidemics.[54-57] The need for the development of detection methods that are rapid, simple, cost effective and offer high sensitivity, specificity is therefore necessary.

Escherichia coli

E. coli consists of diverse group of bacteria. Pathogenic *E. coli* can be categorized into six types, *Shiga toxin-producing E. coli (STEC), Enterotoxigenic E. coli (ETEC), Enteroaggregative E. coli (ESEC), Enteropathogenic E. coli (EPEC), Enteroinvasive E. coli (EIEC), and Diffusely adherent E. coli (DAEC). E. coli* are Gram-negative, facultative anaerobic rods, that belong to the family of *Enterobacteriaceae.* The optimal temperature for *E. coli* to grow is 37 °C. Some *E. coli* strains could cause diarrhea, while others may cause respiratory illness, pneumonia, and breathing problems. *E. coli* is frequently found in contaminated beef, sprouts, lettuce, salami, milk, and water. It can be transmitted through contaminated food or beverages in a short period of one to four days depending on the pathotype.[58]

Listeria monocytogenes

Listeria monocytogenes is a food-borne pathogen frequently found in frozen vegetables, meat, raw

milk, packed salad and raw milk cheese that causes severe foodborne illnesses. It is a Gram-positive, rod-shape and facultative anaerobic bacterium. *L. monocytogenes* could grow over a wide temperature range from -0.4 to 45 °C, under both aerobic and anaerobic conditions, in the presence of salt up to 10% (by weight), and over a wide pH range. It has one of the highest fatality rates among common food-borne pathogens.[59,60] *L. monocytogenes* can cause listeriosis, that primarily affects pregnant woman, newborns and adults with weak immune systems. The symptoms of Listeriosis include high fever, muscle aches, diarrhea and other gastrointestinal symptoms. The symptoms can have duration of days to weeks which vary with different infected individuals. The Food and Drug Administration (FDA) allowable limits for *Listeria monocytogenes* contamination in ready-to-eat (RTE) food products are <1 CFU/25 g of food that supports the growth of *L. monocytogenes* and 100 CFU/g of food that do not support its growth.[61,62]

1.4.1 Conventional methods

Conventional methods for identification and detection of pathogens include microbiological culture techniques, immuno assays, polymerase chain reaction (PCR) based method, DNA based method, immunomagnetic separation (IMS) and microfluidic separation etc.[63] Microbiological culture methods are the "gold standard" for isolation and detection of microorganisms. They are highly reliable and sensitive, which provide both qualitative and quantitative results. In the process of food sample preparation, a pre-enrichment step is needed due to the low levels of heterogeneous distributed pathogens in food matrix. In order to enhance the identification and detection of specific pathogens, several steps have been implemented with pre-enrichment, such as selective enrichment and plating, biochemical screening and serological confirmations. In the first enrichment step, food samples are incubated in non-selective medium to revive the bacterial cells to normal growing condition. This step usually takes 18-24 hours,

followed by further specific enrichment using selective medium to increase the bacterial concentration. Finally, a selective plating is needed to identify the target bacteria cells. Although the microbiological culture based methods are highly reliable and established, they are time-consuming, laborious, and require skilled experts, rendering them unsuitable for rapid identification of pathogens in contaminated food samples.[59]

1.4.2 Emerging technologies

Researchers have refined the improved culture-based detection method by replacing the selective enrichment and plating step with more rapid immunological or PCR based assays. Emerging technologies for pathogen detection include DNA hybridization, enzyme-linked immunosorbent assay (ELISA), PCR methods, biosensors, immunomagnetic separations, and microfluidic devices. These rapid assays exhibit high degree of sensitivity and selectivity towards the target analyte and are easy to use for field applications.[64,65]

Immunoassays are based on the interaction between antigen and antibody. The specific antibody-antigen reaction is capable of detecting analyte in low concentrations. Immuno assays based on polyclonal or monoclonal antibodies includes enzyme immuno assays (e.g. ELISA), immunofluorescent assays, and chemiluminescence immuno assays, etc. ELISA is the most widely used immunoassays for bacterial detection. In ELISA, antibodies that are specific towards target bacteria are immobilized on a solid substrate and bacterial samples are then incubated with the immobilized antibody. Followed by the addition of a secondary antibody labeled with an enzyme, a sandwich complex is formed with the layered structure: first antibody, target bacteria and secondary antibody. The signal generated from the labeled enzyme activity in the secondary antibody is detected, which is directly related to the number of bacteria cells. The enzyme and its substrate or product should not be present in the samples for assay.

Nucleic acid-based assays for pathogen detection are based on the selection of a specific target gene sequence. This unique sequence could be derived from DNA or RNA and detected by DNA hybridization. To increase the sensitivity of the detection, the sequence could be amplified by thermocycling using PCR, which is capable of producing more than a billion copies of the target sequence from one copy in a single reaction. However, both viable (live) and nonviable (dead) bacterial cells are detected by nucleic acid-based method, and therefore could not distinguish between a contaminated sample that contains a live pathogen versus one that contains dead cells. During preparation process for PCR, a selective pre-enrichment step is still needed in order to avoid the interference from other components present in the food matrix.

1.4.3 Need for pre-enrichment or enrichment of samples for testing

As mentioned previously, rapid detection could provide sensitive, specific and real-time detection compared to conventional microbiological methods. However, it is still necessary to use additional procedures for enriching the sample in order to generate sufficient sample for positive detection and to increase the signal-to-noise ratio in the measurements. Several bacterial cell separation and isolation techniques have been studied, including filtration, centrifugation, immunomagnetic separation (IMS) and microfluidic separation. In immunomagnetic separation, magnetic particles surfaces are functionalized with antibodies that target specific bacterial cells. The antibody coated magnetic particles are then exposed to solutions containing contaminated food. With an external magnetic field, the target bacterial cells can be captured by the antibody functionalized magnetic particles and that simplifies separation and concentration of bacterial cells. As an alternate to immunomagnetic separation, magnetic particles could also be modified with bacteriophages for isolation and identification of target bacteria.[66] This method of viro-

magnetic separation could be coupled with immunoassays, biosensors, or other detection tools for simultaneous isolation and detection of target bacterial cells.

1.4.4 Biosensors for bacterial detection

Biosensor are capable of reliable detection of bacterial cells and are considered as good alternatives for traditional microbiological or biochemical methods discussed above. Biosensors for bacterial detection could be classified into two broad categories: direct detection and secondary detection biosensors. In direct detection method, the biosensors are designed to directly detect bacterial cells using a variety of recognition elements discussed earlier, whereas in secondary detection method, a pre-processing step is needed to disrupt bacteria cell structure, resulting in liberation of cell components. These components including ions, small proteins, nucleic acids, and secreted exotoxins can be targeted as an analyte using a suitable recognition molecule for an indirect detection of the corresponding bacteria.[67]

Nucleic acid as recognition element

Nucleic acid-based biosensor is a secondary detection method, as it needs to identify the host bacteria gene which requires cell wall breaking.[68] In nuclei acid-based biosensors, DNA or RNA are the recognition elements for pathogen detection. The fundamental principle is based on the sequence complementarity of the recognition sequence and target bacteria sequence. For example, in a DNA based biosensor, PCR is used to amplify the host bacteria DNA sequence which is further used in the event of hybridization on the biosensor detection platform. RNA could be similarly amplified by reverse transcription PCR using RNA polymerase. The development of DNA microarrays provides opportunities for detection of multiple pathogens from food matrix using the same sensing platform.[69] DNA-based biosensors are highly stable in various solvent and buffers, making them suitable to be used in a wide range of food samples. There is an increasing

number of commercially available nucleic acid-based detection kits for rapid detection of pathogenic bacteria in food samples. Although using nucleic acid as recognition element are popular for pathogen detection, they also have several drawbacks that limit their application, such as the substantial requirement on the purity of nucleic acid, the loss of activity/degradation of nucleic acid, the incapability to differentiate viable cells.

Antibody as recognition element

As mentioned previously in section 1.1.1, antibodies have been extensively explored as recognition element for biosensor applications. In the case of pathogen detection, antibodies can also be used as detection probe upon immobilization on biosensor surfaces. Both polyclonal and monoclonal antibodies have been employed for detection of pathogens. Antibodies have been integrated into different biosensor platforms, such as optical, electrochemical, magnetic and piezoelectric biosensors.[23] Although highly specific to the target host bacteria, they are very susceptible to harsh environmental conditions. Antibodies are prone to activity loss with suboptimal temperature and pH conditions.[16] The short life time of antibodies makes them less suitable for field testing such as pathogen detection in a food processing plant.

Bacteriophage as recognition element

Phages are bacteria-specific viruses consisting of nucleic acid, protein capsid, sheath and tail fibers such as the T4 myoviridea phages. The protein tail fibers serve as recognition element, which can recognize its host bacterium through the bacterial surface receptor to which the phage binds and injects its genetic material (DNA/RNA). Most phage sizes are approximately 100-200 nm. Bacteriophages could distinguish viable bacteria cells from inactive bacteria cells, and therefore possess greater advantages over antibodies as recognition molecules. They could only replicate themselves in viable host bacterial cells and make multiple copies of themselves during

an infection. Moreover, bacteriophages are inexpensive and robust compared to antibodies. They are also stable in harsh environmental conditions, such as acidic and high temperature conditions. The use of bacteriophage as recognition element for pathogen detection will be discussed in detail in section 1.4.5. Table 1.3 provides a list of commercially available detection kits for detection of pathogens use the various detection methods described above, along with their limit of detection.

Table 1.3: A list of commercially available detection kits for foodborne pathogen detection.

Pathogen	Product	Detection method	LOD
E. coli O157:H7	Onar® Bacteria	PCR	N/A
	RubyGlow™	Luminescence	1 CFU
	VIDAS	Immunoassay	N/A
	ANSR®	DNA Hybridization	1 CFU
	MicroSEQ™	DNA Hybridization	1-3 CFU
Listeria	BAX® System X5	DNA Hybridization	
	ANSR®	DNA Hybridization	4 CFU
	VIDAS	Immunoassay	N/A
	MICRO-ID *Listeria*	Enzymatic assay	N/A
	Sample 6	Bacteriophage based biosensor	1 CFU

1.4.5 Bacteriophage-based biosensors for bacteria detection

Phages may be virulent or temperate which determines their interaction with the host bacteria cells. Virulent bacteriophages are capable of lysing the bacterial cells, whereas temperate bacteriophages can either induce the lytic cycle or integrate their genome with the host bacteria cell genome. Virulent phages have been recognized as biorecognition elements or antimicrobial agents in many studies. Many studies have been conducted on the detection or regulation of pathogens using the specific bacteriophages as recognition molecules.[70-72]

Lysis-dependent bacterial cell detection

Bacteriophages can only self-replicate within target host bacteria cells. Upon binding and attachment to bacteria cell, the phage particles will then take over the bacteria cell machinery system to replicate its genetic material, synthesize necessary assembly proteins and break cell wall.

The host cells will be lysed, and the progeny phages will be released together with many intracellular components. The released phages will then propagate by infecting other viable host bacterial cells and initiate a new lytic cycle. The number of phages could be quantified by plaque assay as illustrated in Figure 1.4. The released intracellular components such as enzymes, proteins or DNA could also be used as an indicators (markers) for the detection of pathogens. Researchers have developed lysis-based detection methods using intracellular components, such as β-galactosidase, adenosine triphosphate (ATP), or adenylate kinase as indicator. The resulting enzyme activity could be quantified by ELISA, colorimetric and electrochemical strategies.[15,73,74]

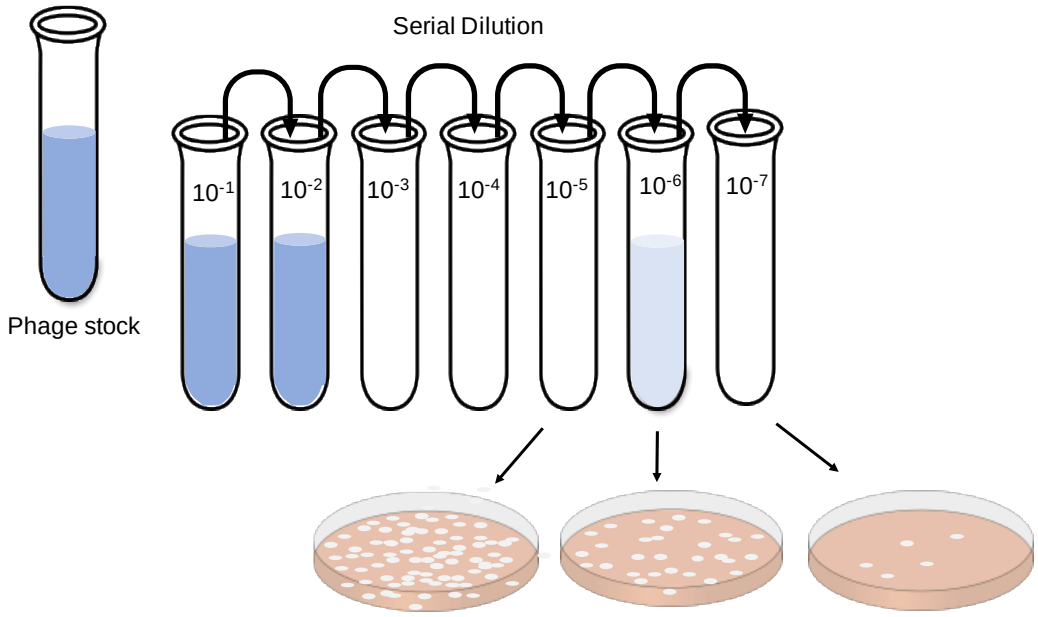

Figure 1.4: Quantification of phage numbers using plaque assay and subsequent plaque counting on petri dishes.

To increase the sensitivity and selectivity of the biosensor, researchers have genetically engineered bacteriophages to possess a desired functionality. The engineered phages are able to transfer the genes to the host bacteria cells, initiating the expression or amplification of the gene product. Lu et al. have genetically engineered a phage DNA with fluorescence tag, which would

be transferred to all progeny phages after host cell lysis.[75] The fluorescence labeled phages act as a detection probes after cell lysis. This reporter phage-based technique has been successfully studied for the detection of several food pathogens, such as *E. coli, Salmonella, Staphylococcus aureus* and *Listeria monocytogenes*.[76,77] These techniques could be used to eliminate the secondary enrichment step and shorten the detection time to about 6-24 h compared to three to four days detection by conventional methods.[72]

Whole cell Detection

The development of whole cell bacteria detection is challenging since it requires detection of analytes that are larger than typical analytes such as protein, and bacteria surface display several epitopes that may lead to nonspecific interaction with the recognition element functionalized sensor surface. Bacteria cells are 0.5 to 5 μm in size with spherical, rod shape, spirochete or spiral shape morphologies. The cell wall of bacteria contains mainly peptidoglycan, a negatively charged polymer matrix. In whole cell bacteria detection, the antigens present on the cell membrane, such as proteins, peptidoglycan, and lipopolysaccharides can be treated as the target for biorecognition. Bacteriophage, in this case, recognizes the bacteria cell by binding onto the specific bacteria receptor protein on cell membrane.[67] In order to detect the target bacteria, bacteriophages are required to be immobilized onto the surface of the transducer. High titer of phages is required to achieve high surface loading of phages, which in turn influences the sensitivity of the sensing system. Salmonella P22 was immobilized on gold substrate to capture *Salmonella. Typhimurium* by surface plasmon resonance.[78]

1.4.6 Immobilization of bacteriophages on biosensor platforms

The key challenge in employing bacteriophages as recognition molecule on a transduction platform is achieving the desired oriented immobilization of phage particles on the transducer

surfaces. The purity of phages is also a key factor for effective immobilization of phages on surfaces. The binding of bacteriophages onto a biosensor surface could be achieved through physical adsorption, chemical immobilization, or affinity interaction.

Immobilization via physical adsorption

Physical immobilization of bacteriophages on surfaces is based on van der walls force, or electrostatic interaction, which could be achieved by simple incubation of sensor platform in a phage containing solution. Physical immobilization of phages has been used for detection of *E. coli and Salmonella.*[79,80] Immobilization has also been carried out through electrostatic interaction between phage capsid and the surface of interest.[81] Most phages carry a net negative charge in their structure with negatively charged capsid (head) and positively charged tail fibers.[82] The charge difference could be used to immobilize phages on a positively charged surface through electrostatic interaction. Cademaritiri et al. have reported bacteriophage immobilization on positively charged silica particles.[70] The disadvantage of physical adsorption of phages is the weak interaction between surface and phages that may cause leakage during long-term storage, which leads to inconsistent and unstable phage density.

Immobilization via chemical linkage

The transducer surface of a biosensor could be functionalized by chemical immobilization of bacteriophages.[14,83] In both physical and chemical immobilization methods, there are two factors that may affect the successful immobilization the phages. Firstly, the purity of bacteriophages is critical to achieve a high density of phages on the biosensor platform. In the process of phage propagation, phages are amplified by infecting the host bacteria strains to obtain the progeny phages. The lysate contains bacteria proteins, intracellular ions and lipid which could affect the immobilization efficiency of phages on sensor surfaces. Therefore, to remove the

interfering components, a phage purification step is usually needed, which include filtration, ultra-high-speed centrifugation, poly ethylene glycol precipitation, and size exclusion chromatograph.[72] Secondly, either simple chemical and physical immobilization alone cannot achieve the desired orientation of phage on sensor surfaces. Typically, the desired orientation is a tail-up and head-down fashion on the electrode, so the tail is exposed to capture bacteria. One approach to achieve the desired orientation of phage on biosensor surface is to genetically engineer bacteriophages with affinity tags that can orient the head towards the surface and exposing the tail towards the electrolyte.

Immobilization via affinity interaction

Bacteriophages can be used to display proteins or peptides on their surfaces using a method commonly referred to phage display. Phage display was developed to investigate the affinity interaction between proteins or peptides to a variety of substrates, such as small molecules, proteins or even entire cells. Lamda phage, T4, T2, T7, M13 phages have been widely studied for phage display techniques. Edgar et al. have demonstrated the oriented immobilization of phages on quantum dots through biotin-streptavidin affinity interaction. Quantum dots were functionalized with streptavidin on which T4 bacteriophages expressing biotin on the capsid were immobilized on the surface. This type of oriented immobilization of phages could help in highly selective recognition of the target bacteria.[76]

1.5 Specific Objectives and Organization of Chapters

Chapter 2: *Trametes versicolor* Laccase Modified Metal Oxide (MOx) Nanoconjugates for Oxygen Reduction Reaction

a) Characterization of laccase-MOx nanoconjugates catalyzed oxygen reduction reaction through electrochemical techniques such as cyclic voltammetry and open circuit potential.

b) Studying the direct/mediated electron transfer behavior of laccase-MOx nanoconjugates.

c) Potential dynamic study of laccase-MOx nanoconjugates.

d) Evaluating the stability of laccase-MOx nanoconjugates.

Chapter 3: Kinetic study of Oxygen Reduction Reaction Catalyzed by Thermophilic Laccase.

a) Characterization of *Bacillus* FNT laccase modified carbon nanotube for oxygen reduction reaction.

b) Studying the kinetics of oxygen reduction reaction using rotating disk electrode.

c) Elucidating the electrochemical rate constant and electron transfer rate of oxygen reduction reaction.

Chapter 4: Charge-Directed Immobilization of Bacteriophage on Nanostructured Electrode for Whole-Cell Electrochemical Biosensors.

a) Electric field-induced immobilization of bacteriophage on carbon nanotube modified electrode surface.

b) Characterization of immobilized bacteriophage on carbon nanotubes through fluorescence microscopy.

c) Quantitative analysis of phage-modified biosensor using variable concentration of bacteria cells.

d) Elucidating the selectivity and sensitivity of the biosensor.

Chapter 5: Isolation and Separation of *Listeria Monocytogenes* Using Bacteriophage P100-Modified Magnetic Particles

a) Studying the importance of magnetic particles sizes, bacteriophage numbers, and bacteriophage immobilization strategy on bacteriophage coupling ratio.

b) Studying the capture of *L. monocytogenes* from food samples using bacteriophage P100-functionalized magnetic particles (PMMP).

c) Characterization of the magnetic captured *L. monocytogenes* using fluorescence microscopy and scanning electron microscopy.

Chapter 6: Impedimetric Detection of *Listeria Monocytogenes* using Phage-modified Magnetic particles.

a) Quantitative analysis of the impedimetric biosensor using variable concentration of bacteria cells separated by PMMP.

b) Manipulation of the sensing platform using magnetic field.

Chapter 7: Construction of Enhanced Green Fluorescence Protein Labeled Biotinylated Bacteriophage P100 for Detection of *Listeria monocytogenes*

a) Cloning of biotin carboxyl carrier protein gene and enhanced green fluorescence protein gene in PZE12-luc plasmid.

b) Construction of PDL276-Y5 shuttle vector.

c) Restriction endonuclease digestion and determination of sequence of the constructed PDL276-Y5 shuttle vector.

Chapter 8. Conclusion and future directions

CHAPTER 2

LACCASE-TiO_2 NANOCONJUGATES AS CATALYSTS FOR OXYGEN REDUCTION IN BIOCATHODES

This chapter is a consolidation of the following journal publications:

- Yan Zhou, Yogeswaran Umasankar, and Ramaraja P. Ramasamy. 2015, *Journal of The Electrochemical Society*, 162 (14) H911-H917
  Reprinted here with permission of publisher.

- Yan Zhou, Yogeswaran Umasankar, and Ramaraja P. Ramasamy. 2014, *ECS Transactions* 61 (25), 9-15
  Reprinted here with permission of publisher.

Abstract:

A new type of conjugate bio-electrocatalyst has been developed using an enzyme (laccase from *Trametes versicolor*) and metal oxide (TiO_2) nanoparticles for the enzymatic reduction of oxygen. A screen-printed carbon electrode (SPE) modified with silylated TiO_2 nanoparticles ($sTiO_2$) was used as a support for immobilizing the enzyme through two crosslinking agents. The surface activity of crosslinked laccase was determined to be 1.24 U/cm^2. Cyclic voltammetry characterization of the laccase-$sTiO_2$ nanoconjugates as bio-electrocatalysts for O_2 reduction revealed that the nanoconjugates displayed competitive activity via direct electron transport, relative to literature, and excellent activity via mediated electron transfer. In mediated electron transfer, 2, 2'-azino-bis (3-ethylbenzothiazoline-6-sulphonic acid) (ABTS) was used as mediator and yielded the highest current for oxygen reduction. The length of the crosslinker used for enzyme immobilization was found to have a significant influence over the electron transfer between the nanoparticles and the enzyme. The results demonstrate that metal oxides, despite their low conductivity, can be used as enzyme supports for bio-electrocatalytic applications with selected molecular tethering agents.

Keywords: Laccase, metal oxide, crosslinkers, enzyme immobilization, direct electron transfer, mediated electron transfer.

2.1 Introduction

The electrochemical reduction of oxygen to water is one of the most studied reactions in electro-catalysis, particularly in bio-fuel cell cathodes.[84,85] Laccase is a metallo-enzyme that catalyzes this reduction.[44,86-88] It has been studied as an electro-catalyst for oxygen biosensors and enzymatic biofuel cell cathodes due to its high thermodynamic potential and excellent biocatalytic properties.[89-91] In laccase, the electrons are received from the substrate or electrode by the T1 copper center of the redox site, which is located close to the substrate-binding pocket. The electrons are then transferred to the tri-nuclear cluster (T2 and two T3 copper centers), where they reduce molecular O_2 to form water.[86,92,93] One of the critical issues in enzyme bio-electrocatalysis is the establishment of sufficient electrical communication between the enzyme redox site and the electrode.[94] This can be achieved by either, (a) a direct electron transfer (DET) between the enzyme active site and electrode, or (b) using redox shuttle for a mediated electron transfer (MET). In most cases, DET requires a short distance between the enzyme active center and the electrode surface to facilitate electron tunneling and is relatively arduous to accomplish;[95] however, in the case of MET, the enzyme orientation becomes less relevant, thus multiple immobilization strategies may be employed.

When a redox enzyme like laccase is adsorbed on to the surface of an electrode, its electro-activity is highly dependent on its orientation. This is due to the influence of the surrounding protein matrix that electrically insulates the enzyme redox center from the external surface.[96] It is theorized that only ~1% of the enzyme molecules are immobilized with the preferred orientation for electrochemical activity when they are physically adsorbed on to the electrode surface.[42,89,97] This issue can be overcome by electrically wiring the enzyme to the electrode using established immobilization methods.[92,42,98] Another issue is the low active site loading on the electrode due to

the large size of enzymes compared to metallic catalysts. This can be overcome by providing a large surface area for enzyme immobilization by using nanomaterials as an enzyme support.

A myriad of literature has been published on immobilizing enzymes on carbon structures, polymer matrices, or gold for bio-electrochemical applications,[19,37,41,87,88,99-102] some strategies of which are based on complex procedures for enzyme immobilization.[9,103-106] Among groups that have explored using metal oxides as immobilization supports for enzymes,[107-110] few have used metal oxide nanostructures in the place of carbon or gold as immobilization supports for enzymatic electrochemical catalysis reactions.[21,111,112] Metal oxide (MO) nanomaterials possess several favorable properties for bio-electrocatalytic applications. First, metal oxide nanoparticles are less expensive alternatives to metallic nanomaterials, such as Au, Pt, and carbon nanotubes. Second, intrinsic n-type semiconducting materials, such as TiO_2, SnO_2, and ZnO, can be used for electronic signal transduction in bio-electrochemical devices with no significant ohmic drop due to the low currents involved in the bio-electrochemical systems. The presence of surface hydroxyl groups on TiO_2 nanomaterials offer the possibility for surface functionalization that can reliably link to the enzyme redox center, and, therefore, offer huge benefits for enzyme based bio-electrocatalysis.[110,113]

In this work, we immobilized laccase on silylated TiO_2 (*s*TiO_2) nanoparticles to prepare laccase-*s*TiO_2 nanoconjugates. By using this new immobilization support, laccase was covalently bound through different molecular tethering agents that allow transfer of electrons and oxygen. Two molecular crosslinkers were used, dithiobis-(succinimidyl propionate) (DSP) and 1,5-difluoro-2,4-dinitrobenzene (DFDNB), which are homo-bifunctional compounds that contain an amine-reactive group on either sides, but differ in chain length. The terminal succinimidyl group in DSP is capable of reacting and covalently binding with the NH_2 group present in biomolecules.

DFDNB, a short length aryl halide crosslinker with two fluorine atoms, can react to primary amines and yield stable arylamine bonds. To the best of our knowledge, this is the first reported work on evaluation of laccase-*s*TiO_2 nanoconjugates electro-catalytic activity in both direct and mediated oxygen reduction reaction.

2.2 Experimental

2.2.1 Materials:

TiO_2 nanoparticles (~20 nm diameter), ZnO nanoparticles (~50nm diameter), SnO_2 nanoparticles(~100nm diameter) and the silane-coupling agent, (3-aminopropyl)-triethoxysilane (APTES) were purchased from Sigma-Aldrich (St. Louis, MO). Stabilized 40 nm gold nanoparticles were purchased from Cytodiagnostics (Canada). Dimethyl sulfoxide (DMSO) was used as the solvent for both the preparation of molecular crosslinkers namely dithiobis-(succinimidyl propionate) (DSP), and 1,5-difluoro-2,4-dinitrobenzene (DFDNB). Syringaldazine, 2,2'-azino-bis (3-ethylbenzothiazoline-6-sulphonic acid) (ABTS) and promazine, all obtained from Sigma-Aldrich, were used as received for mediator studies. Laccase from *Trametes versicolor* (Sigma-Aldrich) was purchased and dialyzed as previously reported.[114] The enzymatic activity was assayed by measuring the oxidation of syringaldazine at 530 nm for 10 minutes.[115] One unit of laccase will produce an absorbance of 0.001 per minute at 530 nm, pH 6.5 and 30℃in a 3 mL reaction volume using syringaldazine as substrate.[116] All spectrophotometric measurements were carried out on a Thermo Scientific Multiskan GO 1510 Spectrophotometer coupled with temperature control. All buffers were prepared using nano-pure distilled water (18 MΩ conductivity). All glassware was dried overnight at 75°C to remove adsorbed water. Industrial grade O_2 and N_2 (Airgas) were used for all electrochemical experiments.

2.2.2 Silylation of TiO_2 nanoparticles

For silylation of the metal oxide nanoparticles, the TiO_2 nanoparticles were first suspended in water (de-ionized) for 30 min. The TiO_2 suspension was then centrifuged and dried to remove the non-adsorbed water. The dried TiO_2 nanoparticles contain OH groups on the surface, which are suitable for silylation reaction. The silylation reaction was carried out in solution of 15 % APTES (in toluene solvent) for a period of 5 h at a temperature around the boiling point of toluene (110 – 115°C). The suspension of silylated TiO_2 nanoparticles was then centrifuged, washed with toluene to remove unreacted APTES and finally washed twice with ethanol. Subsequently, the silylated TiO_2 nanoparticles ($s$$TiO_2$) were dried overnight at 110°C and then resuspended in water. A known quantity of the resulting $s$$TiO_2$ nanoparticle suspension was deposited onto a screen-printed carbon electrode (3 mm diameter) and dried. The electrode thus modified with $s$$TiO_2$ nanoparticles was used for enzyme immobilization.

2.2.3 Enzyme immobilization

The $s$$TiO_2$ nanoparticles on the electrode serve as the immobilization support for laccase. The enzyme immobilization was carried out in two steps as described in Figure 2.1. The first step is the attachment of the molecular crosslinker to $s$$TiO_2$ nanostructures. The molecular crosslinker was either dithiobis-(succinimidyl propionate) (DSP), or 1,5-difluoro-2,4-dinitrobenzene (DFDNB). The optimum concentrations of molecular crosslinkers were optimized by measuring the catalytic current using different crosslinker concentrations, DSP (0.2, 2mM, 10mM, 50mM), DFDNB (0.1mM, 1mM, 10mM, 20mM). The optimal concentrations were determined to be 10 mM and 1 mM for DSP and DFDNB as crosslinkers, respectively. For preparing the nanoconjugates, about 4 µL of 10 mM DSP or 1 mM DFDNB solution was dropped onto the $s$$TiO_2$ modified electrode and allowed to react for 15 min at room temperature. The amine-reactive

groups of the crosslinkers react with terminal NH_2 groups of APTES on the *s*TiO_2 to form molecular tethers around *s*TiO_2 nanoparticles as shown in Figure 2.1. After 15 min, the excess unreacted DSP or DFDNB was removed by washing the electrode with DMSO first and then with 0.01 M pH 7 phosphate buffer, to prepare the electrode for enzyme immobilization. 6 µL of laccase solution (5 mg/mL) was dropped onto the modified electrode and kept on ice for 30 min. The amine reactive groups on the other terminus of the crosslinkers covalently bind to the surface amines of laccase. For control experiments, electrodes were prepared by drop-casting laccase directly onto *s*TiO_2 without any molecular crosslinker. After 30 minutes, the modified electrode was washed to remove unreacted enzymes with acetate buffer and then transferred into the voltammetry cell for testing. The pH of the electrochemical experiment was optimized by measuring the catalytic current generated in buffer of varied pH (4, 4.5, 5, 5.8, and 7.5), the cyclic voltammograms are shown in Figure 2.S1. Based on preliminary experiments, the optimized pH for electrochemical experiments was determined to be 4.5.

For comparative studies using established nanomaterials, gold nanoparticles (AuNP) were also studied as enzyme supports. Stabilized AuNP were centrifuged for 30 min at 4500 G prior to use to remove contaminants. Then, the particles were re-suspended in distilled water. Laccase was immobilized on to the AuNPs-coated SPE using DSP as the crosslinker. The DSP has a disulfide group that is required for the self-assembly onto the gold surface.[117,118] A Bradford assay was used to determine the amount of enzymes washed away during the rinsing procedure. The enzyme loading on the electrode was then determined through the mass difference between the total enzymes deposited on the electrodes (30 µg) and the enzymes that washed away during the rinsing procedure.

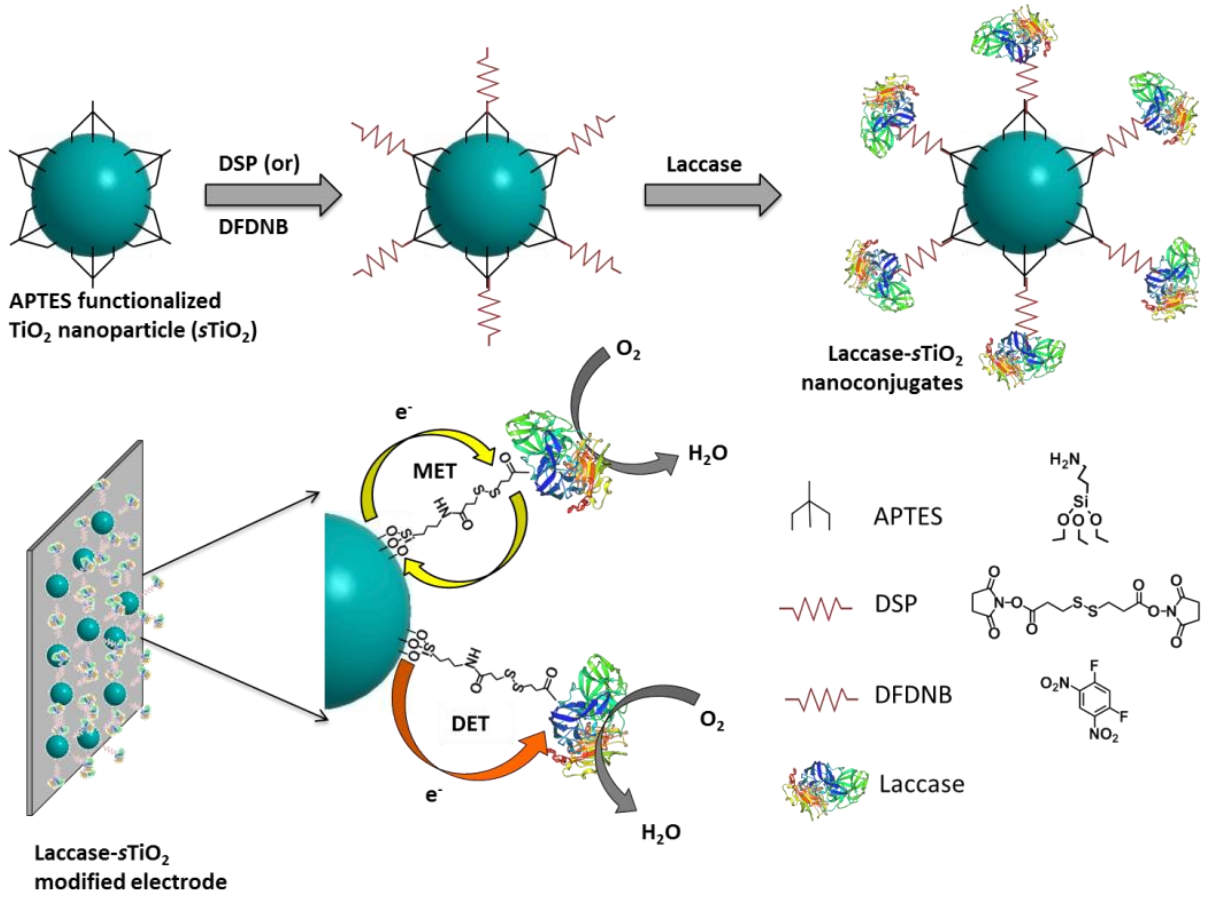

Figure 2.1: Schematic of the stepwise method for laccase-sTiO_2 nanoconjugates preparation (top). An exploded view of the modified electrode showing the laccase attachment on to sTiO_2 via DSP crosslinker (bottom). The chemical structures of APTES and the crosslinkers are also shown.

2.2.4 Characterization studies

Scanning electron microscopy (SEM) images of the modified electrodes were obtained using FEI Inspect FEG electron microscope. For SEM imaging, the sample was prepared by drop-casting the solution of sTiO_2 on HNO_3 treated silica wafer and allowed to dry at room temperature. For enzyme containing samples, the laccase-TiO_2 conjugates were prepared on silica wafer rather than on the electrode. Fourier transform infrared spectroscopy (FTIR) measurements were performed on the TiO_2 and sTiO_2 nanoparticles in a Nicolet 6700 FTIR instrument using the KBr pellet method. Cyclic voltammetry (CV) tests were performed using CHI-920c potentiostat (CH

Instruments) in a 5mL voltammetry cell containing 0.2 M sodium acetate buffer pH 4.5 as the electrolyte, unless otherwise stated. The working electrode was a screen-printed carbon strip modified with the *s*TiO_2 nanoparticles either with or without laccase enzyme. The screen-printed carbon electrodes (TE100) were purchased from CH Instruments with surface area of 0.071cm^2. A Pt wire counter electrode and 3M Ag/AgCl reference electrodes, both also from CH Instruments, completed the setup. All potentials reported are with respect to the reference electrode. The measurements were carried out at ambient temperature (~25°C). For CV tests, the working electrode was scanned from 0.6 to 0 V at a scan rate of 0.02 Vs^{-1}. For oxygen reduction reaction studies, the electrolyte was purged with O_2 for 15 min. For control experiments, the electrolyte was purged with N_2 for 30 min.

2.3 Results and Discussion

2.3.1 Characterization of the nanoparticles

The stepwise procedure to functionalize the TiO_2 nanoparticles with laccase is shown in Figure 2.1. First, the TiO_2 nanoparticles were silylated using (3-aminopropyl)-triethoxysilane (APTES). APTES attaches to the TiO_2 surface by replacing the surface OH groups to form the Si-O bond. Then, either dithiobis-(succinimidyl propionate) (DSP), or 1, 5-difluoro-2,4-dinitrobenzene (DFDNB) was used as a molecular crosslinker to create amine-reactive groups on sTiO_2, which was then used for enzyme attachment. The silylation of the TiO_2 nanoparticles was confirmed using FTIR measurements before and after silylation. Figure 2.2 shows the FTIR spectra of TiO_2 nanoparticles before and after APTES functionalization. The broad peak at 660 cm^{-1} corresponds to TiO_2 itself. The difference in the intensity of the TiO_2 peaks between the two spectra at 660 cm^{-1} could be due to a difference in the surface OH between these samples, which determine the surface coverage of TiO_2 by APTES. The peaks characteristic to the APTES are the

C-N peak at 1078 cm^{-1} and Si-O-R peak at 1024cm^{-1}.[119,120] The peak around 3650~3300 cm^{-1} could be attributed to N-H stretching and the peak at 1631 cm^{-1} could be attributed to N-H bending vibrations of the amine groups present in APTES. Furthermore, the peak at 2921 cm^{-1} corresponds to the alkanes in APTES. The identification of these peaks confirms successful silylation of TiO_2.

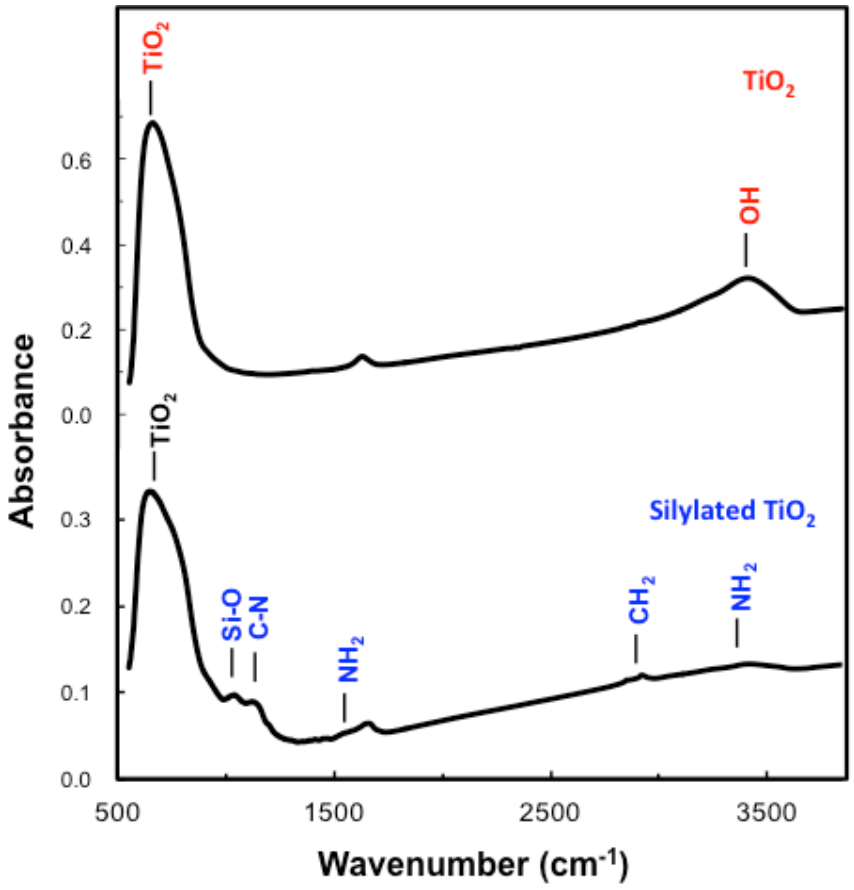

Figure 2.2: FTIR spectra of TiO_2 (above) and *s*TiO_2 (below). The peaks corresponding to the functional groups representative of APTES functionalization can be seen for *s*TiO_2.

The morphology of bare *s*TiO_2 and laccase immobilized *s*TiO_2 modified electrodes were studied using scanning electronic microscopy. The SEM images given in Figure 2.3a shows that the *s*TiO_2 nanoparticles on the electrode surface have an average diameter of ~50 nm, which suggest a small extent of particle aggregation during silylation. In Figure 2.3b, the SEM image of the laccase-immobilized *s*TiO_2 nanoparticles, the morphology indicates the immobilization

methods did not significantly vary the particle size or the morphology of the surface but it did cause particle agglomeration to a small extant.

2.3.2 Bio-electrocatalytic activity of laccase-TiO_2 nanoconjugates

The bio-electrochemical reduction of oxygen by laccase-*s*TiO_2 nanoconjugates can happen via direct electron transfer (DET) or mediated electron transfer (MET). As depicted in Figure 2.1, in DET, the electrons are directly exchanged between *s*TiO_2 and the redox site of laccase that results in direct electrochemical reduction of oxygen to water.[92] In MET however, the catalyst uses redox shuttles to transfer electrons between *s*TiO_2 and the enzyme (see Figure 2.1). We used cyclic voltammetry (CV) to evaluate the bio-electrocatalytic activity of laccase-*s*TiO_2 nanoconjugates in both direct and mediated modes of electron transfer.

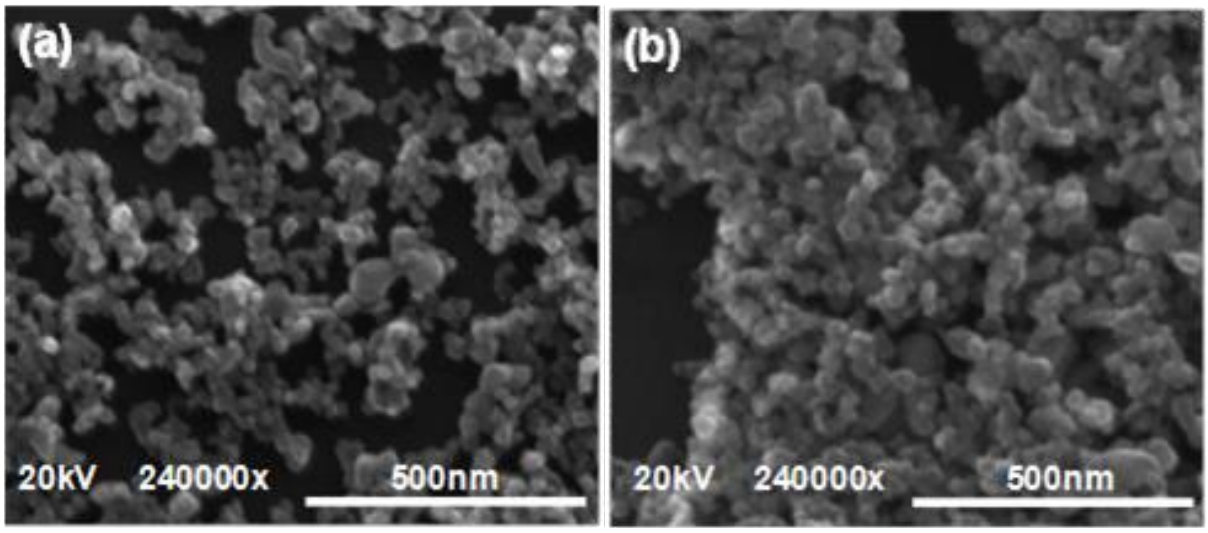

Figure 2.3: SEM images of: (a) *s*TiO_2 nanoparticles and (b) laccase-*s*TiO_2 nanoconjugates.

Direct oxygen reduction

The direct electron transfer (DET) based bio-electrocatalytic activity of the laccase-*s*TiO_2 nanoconjugates were studied using cyclic voltammetry. In direct electrochemical reduction, the electrons from the electrode are directly captured by the T1 copper site of laccase which then

transfer the electrons to the trinuclear copper cluster, where the electrons combine with protons and oxygen to form water.[94] Cyclic voltammograms (CVs) of the modified electrodes in O_2 and N_2 saturated electrolytes are shown in Figure 2.4a for the nanoconjugates prepared using DSP and DFDNB crosslinkers. Control experiments were also performed on *s*TiO_2 nanoparticles without laccase, the voltammogram of which is shown in Figure 2.4a. In order to understand the effectiveness of the molecular crosslinkers for enzyme immobilization, a second control experiment was performed using *s*TiO_2 modified electrode, where laccase was physisorbed onto the *s*TiO_2 with no crosslinkers, the data of which is also included in Figure 2.4a for comparison. The CVs clearly suggest that the molecular crosslinkers are essential for enhancing the surface area of the modified electrodes, resulting in a significant increase in capacitive current. This could be observed in the CVs of DSP and DFDNB modified electrodes that showed higher capacitance than that of the physisorbed sample whereby no crosslinkers were used. The reason is due to the increased number of surface active sites that resulted from the attachment of crosslinkers on *s*TiO_2 surface. When laccase was physisorbed onto *s*TiO_2 nanoparticles sans crosslinkers, the enzyme could have been non-specifically adsorbed on the nanoparticles, completely covering the *s*TiO_2 surface with an insulating protein matrix, making the surface hydrophobic thereby reducing the electrochemical interfacial area. The hydrophobicity between the enzyme and electrode surface could isolate the interface from the enzyme resulting in lower current density.[26] The voltammograms in Figure 2.4a also revealed that the laccase-*s*TiO_2 nanoconjugates prepared using both types of crosslinkers exhibited notable electrocatalytic activity for oxygen reduction. This can be seen in the cathodic wave of the CVs obtained in O_2 saturated electrolyte, which clearly deviates from the CVs obtained in the O_2 deprived electrolyte right from the initial scanning potential at 0.6 V. The onset potential for oxygen reduction was around 0.6 V and the open circuit potentials

were 0.6 and 0.61 V for DSP and DFDNB crosslinked electrodes, respectively. The controls with no laccase did not exhibit any measurable electrocatalytic activity for oxygen reduction. An expanded view of the control CVs from Figure 2.4a are shown as in the supplementary Figure 2.S3 for clarity. Figure 2.4b compares the open circuit and half peak potentials of laccase-*s*TiO_2 nanoconjugates prepared with and without the crosslinkers (physisorbed). The half peak potentials ($Ep_{1/2}$) were calculated upon considering the current at 0.2 V as the peak current.

It can be noticed from the bar charts in Figure 2.4b, that both the OCP and $Ep_{1/2}$ values for the laccase-*s*TiO_2 nanoconjugates prepared using the crosslinkers were significantly higher than that of physisorbed sample. The results indicate that the molecular crosslinker is critical in determining the electrocatalytic activity of the laccase-*s*TiO_2 nanoconjugates. Though the results demonstrate a significant DET-based reduction of oxygen by the laccase-*s*TiO_2 nanoconjugates, the rate at which the cathodic current increases on the CVs suggest that the reactivity of these nanoconjugates is not as high as that of laccase-carbon nanotubes conjugates demonstrated in our previous work.[92,94] This is not surprising as the molecular crosslinkers used in this study do not possess multi-aromatic ring structure as the pyrene-based molecular tethers used for enzyme immobilization on CNTs that facilitate direct electron transfer.[92,94] In order to ensure that the enzymes retained most of its activity even after immobilization on to the *s*TiO_2 nanoparticle, we performed activity evaluation of the immobilized enzymes by measuring the rate of absorbance increase at 530 nm upon oxidation of syringaldazine by immobilized laccase. The surface activity of laccase was determined to be 1.24 U/cm^2 which is close to the value of 1.84 U/cm^2 reported in the literature for laccase immobilized on bulky paper composed of compressed multi-walled carbon nanotubes (CNTs).[121]

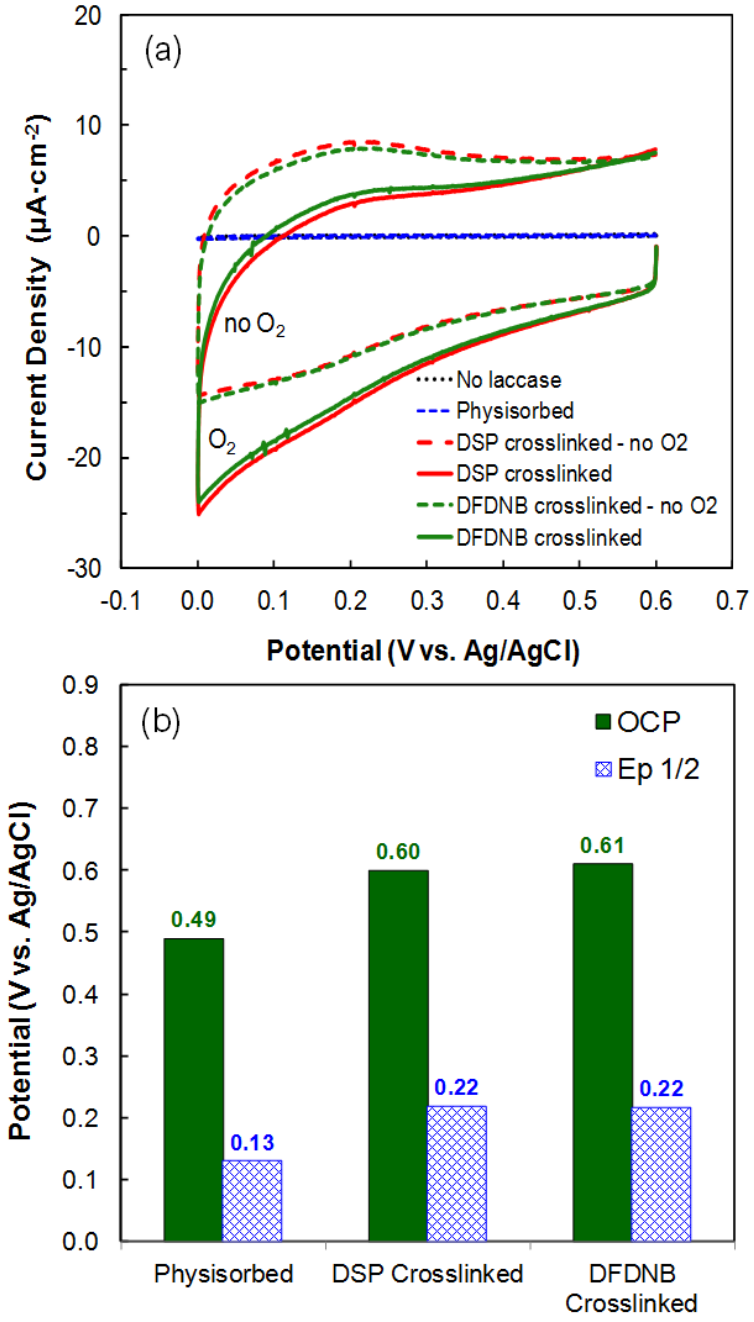

Figure 2.4: (a) Comparison of cyclic voltammograms of laccase-*s*TiO_2 nanoconjugates prepared using DSP or DFDNB crosslinkers in the presence and absence of O_2 in the electrolyte. Controls show the CVs of laccase-*s*TiO_2 prepared without any crosslinker (physisorbed) and the bare *s*TiO_2. The data were obtained in pH 4.5 electrolyte, between 0.6 V and 0 V at a scan rate 0.02 Vs^{-1}. (b) Open circuit potentials (OCP) and half peak potentials ($Ep_{1/2}$) of the nanoconjugates prepared as labeled in the graph.

Besides depositing equivalent amounts of enzyme in all cases, the actual loading on the electrodes differed significantly and was 21.5 ± 2 µg for the DSP crosslinked electrodes, 24.9 ± 2 µg for DFDNB crosslinked electrodes and 13.1 ± 3 µg for physisorbed electrodes; however, the difference in enzyme loading was not the only reason the crosslinked electrodes exhibited better performance than the physisorbed. This is due to the fact that the 'enzyme-loading normalized current' data as shown in supplementary Figure 2.S4, also showed high currents for the cross-linked electrode over physisorbed electrodes.

Furthermore, comparative studies were done between the laccase immobilized on *s*TiO_2 and on gold nanoparticles (AuNP). The experiments were performed under same conditions as those used for laccase-*s*TiO_2 conjugates to achieve the same desired enzyme loading on the nanoparticle surface. The results as shown in supplementary Figure 2.S4, indicates that *s*TiO_2 conjugates exhibited slightly higher electro-catalytic activity for oxygen reduction at high potentials than laccase-AuNP using direct electron transfer. The OCP value for AuNP conjugates is 0.43V *vs.* Ag/AgCl, which is 0.18V lower than that of laccase-*s*TiO_2 conjugates. Therefore, it is reasonable to conclude that the laccase-*s*TiO_2 conjugates suffered no significant conductivity issues during electrocatalysis in the range of current and potentials studied in this work. To further evaluate if the generally low conductivity of metal oxide nanoparticles is particularly disadvantageous for enzyme-based electrocatalysis, O_2 reduction studies were carried out using carefully selected redox mediators as discussed below.

In order to study the effectiveness of the silane functionalization for enzyme immobilization, two different molar ratio of APTES to TiO_2 (APTES/TiO_2) were used for preparation of *s*TiO_2 which are 2.5/1, 4/1. The *s*MO discussed above are all based on 2.5/1 ratio APTES/TiO_2 during silylation process. Compare the two laccase-*s*TiO_2 conjugates with

APTES/TiO_2 molar ratio of 2.5/1 and 4/1, the higher ratio of 4/1 shows enhanced O_2 reduction peak than 2.5/1 ratio. The higher ratio of APTES for surface modification achieved higher surface coverage of amine group that could crosslink with enzyme as well as exhibited higher electrocatalytic activity for O_2 reduction. This can be seen in Figure 2.S5, the CVs of 4/1 ratio *s*TiO_2 nanoconjugates clearly deviates from the CVs obtained from 2.5/1 ratio in O_2 saturated electrolyte.

Mediated oxygen reduction

The mediated electro-catalytic activity of the laccase-*s*TiO_2 nanoconjugates for oxygen reduction was evaluated using redox shuttles (mediators) such as syringaldazine, ABTS, and promazine. The empirically determined mid-point redox potentials for each of the mediators using *s*TiO_2-coated SPE are shown in the supplementary Figure 2.S6a. For syringaldazine, two redox reactions were observed with mid-point redox potentials (E_0) at 0.4 V and 0.62 V. The E_0 for ABTS and promazine redox reactions were 0.48 V and 0.67 V, respectively. The redox potential of the T1 copper site in laccase is 0.58 V vs. Ag/AgCl,[44] which makes the syringaldazine and ABTS viable mediators for oxygen reduction reaction. Although promazine (E_0=0.67 V) falls above the redox potential of T1 site in laccase for the given pH, it was still evaluated as mediator because it can be utilized at higher pH conditions. The redox potential for each of the mediators were also separately examined using bare screen-printed-electrodes, the data for which is shown in Figure 2.S6b for comparison. Similar to the direct electron transfer, the capacitive charging current for *s*TiO_2 supports is about an order of magnitude higher than that of the bare screen-printed-electrode. As depicted in Figure 2.1, in a mediated electron transfer (MET) based reduction of oxygen, the mediators shuttle the electrons between the electrode and the enzyme active site. During this process, the redox shuttles get reduced and oxidized, thereby facilitating the bio-

electrochemical reduction of O_2 to water. While the reduction of the mediator by the electrode is an electrochemical reaction, the oxidation of the mediator by the enzyme is a biochemical reaction. Mediated O_2 reduction was carried out using 0.1 mM of the mediator compound in O_2 saturated, 0.2 M pH 4.5 acetate buffer electrolyte in the voltammetry cell using the laccase-*s*TiO_2 nanoconjugates modified electrodes and the results are shown in Figure 2.5 a-f. To avoid the variability in electrode preparation, the same electrodes used for DET studies were also used for MET. While the CV response is a direct measure of the electrochemical reduction of mediators, it also an indirect measure of the biochemical oxygen reduction by the laccase- *s*TiO_2 nanoconjugates on the electrode. The CVs of the *s*TiO_2 electrodes without enzyme immobilization (control), obtained using each mediators are grouped separately and shown in Figure 2.5 a,c,e for syringaldazine, ABTS and promazine, respectively. An expanded electrochemical window (0.8V~0V) for promazine mediated ORR was also shown in Figure 2.S8. For syringaldazine, an expanded view of Figure 2.5a along with the no mediator controls are shown in the supplementary Figure 2.S7, where the differences are apparent. In the absence of laccase, the CVs show the redox responses of the mediators with clearly defined oxidation and reduction peaks. The immobilization of laccase on *s*TiO_2 nanoparticles brought a significant variation in CV response of the electrodes as shown in Figure 2.5a, c, e for both crosslinked and physisorbed laccase-*s*TiO_2 nanoconjugates. The mediated O_2 reduction was clearly expressed in the CVs for all mediators near the redox potentials of the mediators. The mass-transfer limiting currents (at potentials below 0.3 V) for the electrochemical reduction reaction were much higher than of the corresponding no-enzyme control electrodes. Similar to the DET results, the CV responses of physisorbed laccase-*s*TiO_2 without crosslinkers showed lower electro-activity than their crosslinked peers for all three mediators.

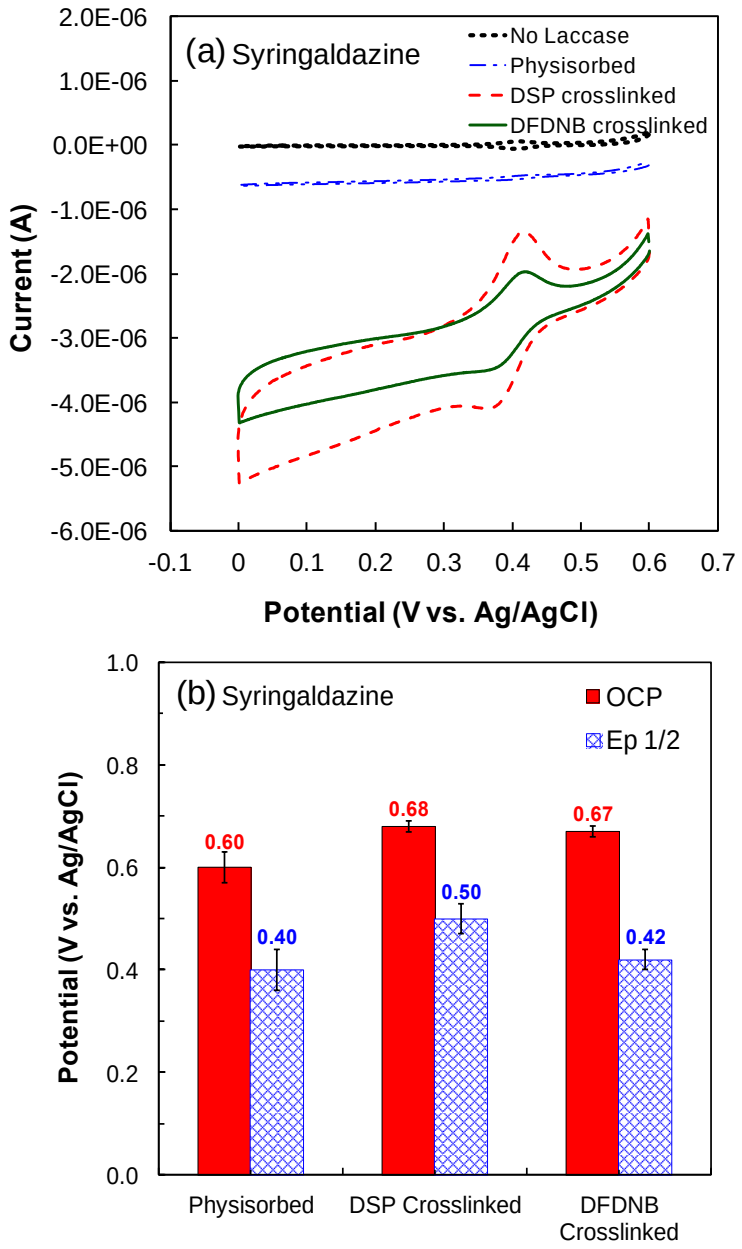

Figure 2.5: (a) CV of the laccase-*s*TiO_2 nanoconjugates obtained in O_2 saturated electrolyte, using Syringaldazine; (b) Open circuit potentials (OCP) and half peak potentials ($Ep_{1/2}$) of the laccase-*s*TiO_2 nanoconjugates prepared with or without the crosslinkers using Syringaldazine.

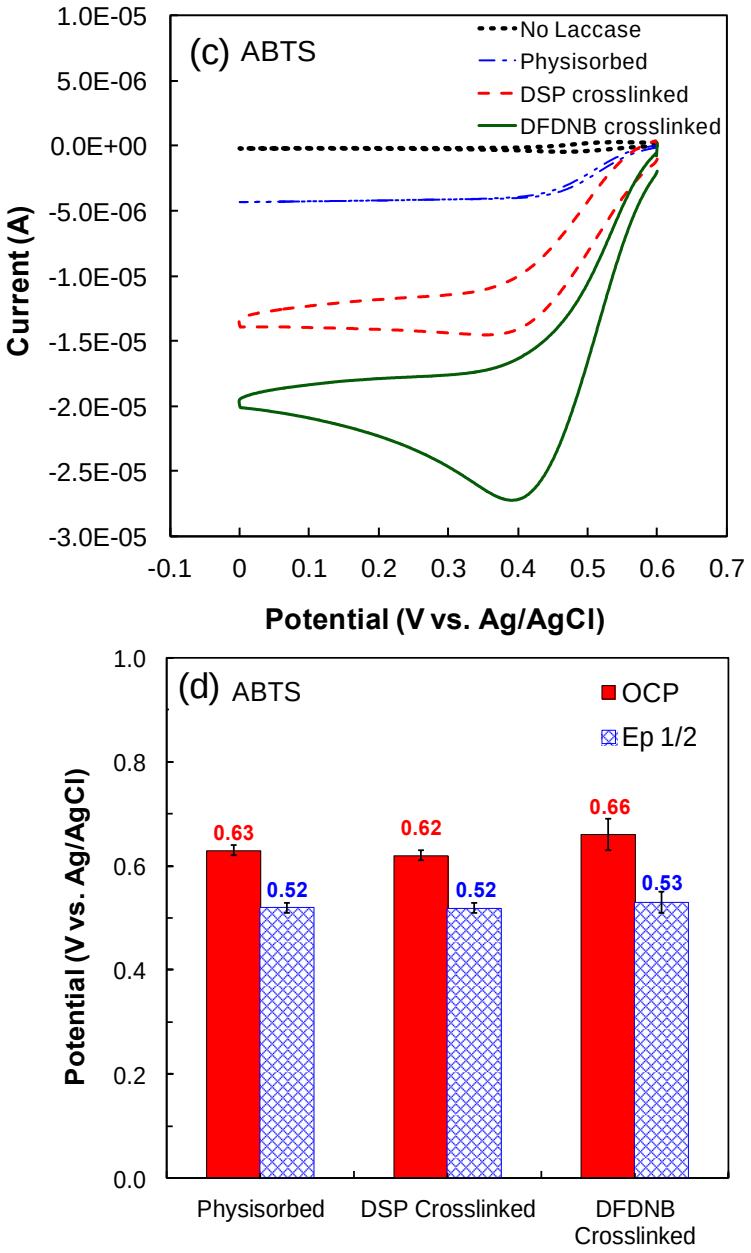

Figure 2.5: (c) CV of the laccase-*s*TiO_2 nanoconjugates obtained in O_2 saturated electrolyte, using ABTS; (d) Open circuit potentials (OCP) and half peak potentials ($Ep_{1/2}$) of the laccase-*s*TiO_2 nanoconjugates prepared with or without the crosslinkers using ABTS.

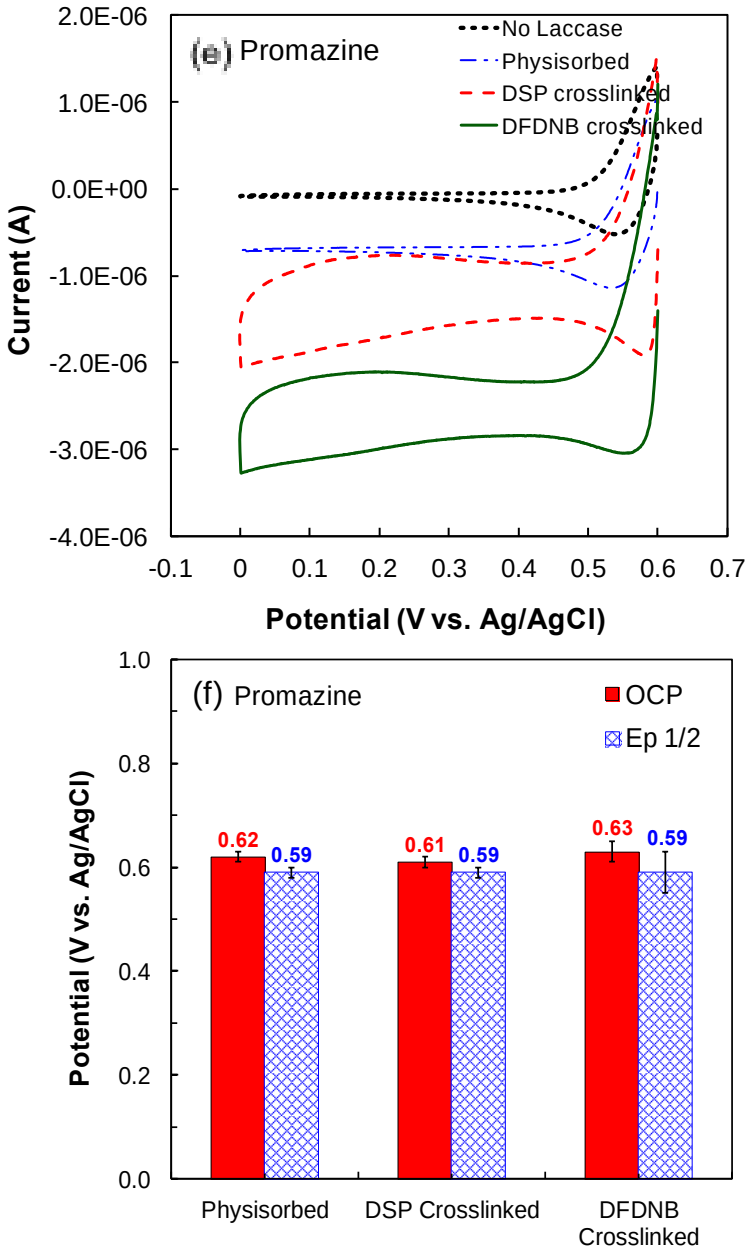

Figure 2.5: (e) CV of the laccase-$sTiO_2$ nanoconjugates obtained in O_2 saturated electrolyte, using Promazine; (f) Open circuit potentials (OCP) and half peak potentials ($Ep_{1/2}$) of the laccase-$sTiO_2$ nanoconjugates prepared with or without the crosslinkers using Promazine.

A distinct dependency in E_0 for the mediators was observed which concurs with the observation of Chakrabory *et al.* for other types of mediators.[122]A cross comparison among the mediators shown in Figure 2.6 revealed that ABTS yielded the highest reduction currents among the three, followed by syringaldazine and promazine. However, it must be noted that when the pH and conditions change, the influence of mediators would also change. Since all the mediators participate in a single electron transfer redox reactions, the difference in the mass-transfer limiting currents could be attributed to the difference in their diffusivities in the electrolyte solution in the terms of low solubility or stability in acid solution.[40,123,124] Moreover, the limiting currents were categorically higher for the DFDNB crosslinked nanoconjugates than for the DSP crosslinked nanoconjugates. Figure 2.5b, d, f showed the OCP and $E_{p1/2}$ values for laccase-*s*TiO_2 nanoconjugates using syringaldazine, ABTS and promazine respectively. Both the open circuit potentials and half peak potentials of the nano-conjugates were significantly higher than those observed in corresponding DET cases.

Among the three mediators, ABTS generated the highest reduction current as observed in Figure 2.5c, it did not translate into high half peak potentials. Similarly, while DFDNB crosslinker appeared to enhance the reduction currents, it did not translate into higher OCP or $E_{p1/2}$ values as shown in Figure 2.5(d-f). This suggested that understanding the effect of the mediators on the activity of nanoconjugates demands a more detailed characterization. The MET results discussed in Figure 2.6 suggest that the conductivity of *s*TiO_2 nanoparticles was not a major limiting factor in determining the electrocatalytic activity of laccase-*s*TiO_2 nano-conjugates. It is also worth noting that, unlike the case in DET, a normalization based on enzyme loading could result in a comparable initial CV performance in mediated electron transfer for both physisorbed and

crosslinked enzymes; however, the physisorbed electrodes quickly lose activity over time due to enzyme dissolution (data not included).

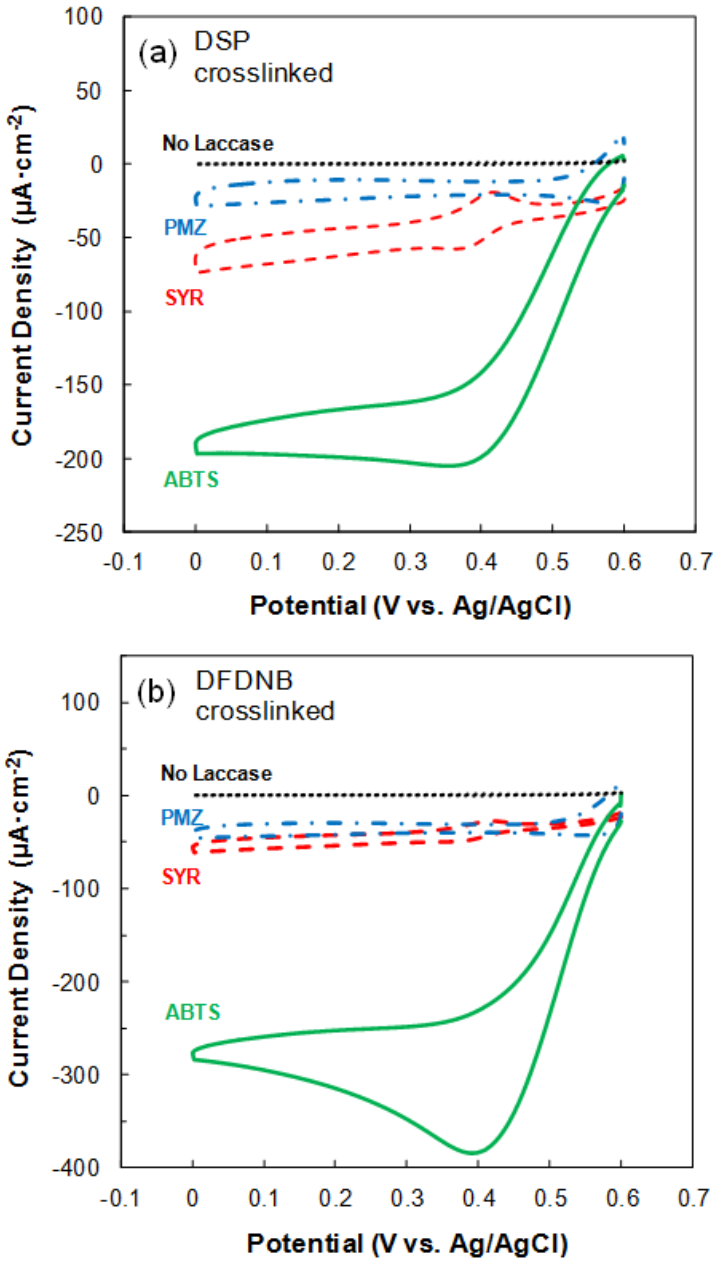

Figure 2.6: Cross comparison of cyclic voltammograms of laccase-sTiO_2 nanoconjugates obtained with (a) DSP as crosslinker, (b) DFDNB as crosslinker using three mediators SYR(syringaldazine), 2,2'-azino-bis(3-ethylbenzothiazoline-6-sulphonic acid) (ABTS) and promazine (PMZ). The data were obtained in pH 4.5 electrolyte, between 0.6 V and 0 V at a scan rate 0.02 Vs^{-1}.

2.3.3 Potentiodynamic polarization

Steady state potentiodynamic polarization tests were performed to eliminate the non-faradaic effects and reveal the true faradaic response of laccase-*s*TiO_2 nanoconjugate modified electrodes. Polarization tests were performed at different applied voltages in O_2 saturated acetate buffer, the current data points were recorded after 15 min at each step. The results shown in Figure 2.7, clearly established the high electro-catalytic activity for the crosslinked nano-conjugates compared to physisorbed nanoconjugates in both DET (Figure 2.7a) and MET (Figure 2.7b) based O_2 reduction. For mediated oxygen reduction (Figure 2.7b), the polarization results were consistent with the CV results where ABTS showed the highest current density for oxygen reduction, followed by syringaldazine and promazine. Also a cross comparison of DET and MET graphs show that the MET based oxygen reduction yielded significantly higher reduction current density. It is also important to note that the MET currents are strongly dependent on the concentrations of mediators. DFDNB, is referred to as a "zero-length" aromatic compound, which is much shorter than long-legged non-aromatic compounds such as DSP. The difference in the chain lengths between DSP and DFDNB could have significant influence on the electron transfer properties of the conjugates, especially when mediators are used. Herein, we compared our work with previously published reports on laccase catalyzed oxygen reduction. Almost every published study in this area were done using on gold/carbon-based nanomaterial supports and the work published for other nanomaterial support differ vastly. For example, both Salaj-Kosla *et al.* and Qiu et al. immobilized laccase using nanoporous gold. Salaj-Kosla *et al.* achieved DET with a current density of 28μA/cm^2 (pH 4.0, 5mV/s), while Qiu *et al.* achieved ~250μA/cm^2 (pH 4.4, 100 mV/s) current density.[37,125]

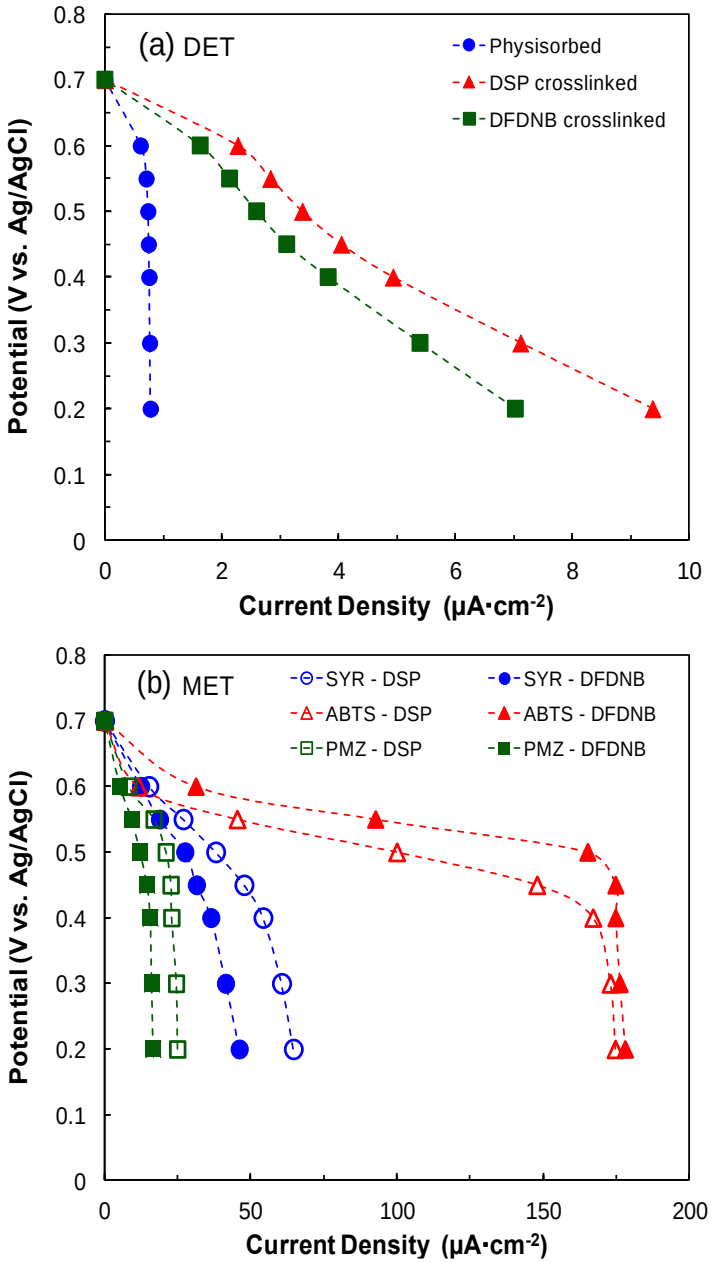

Figure 2.7: (a) Steady state current-voltage behavior of the different laccase-sTiO_2 nanoconjugates modified electrodes for oxygen reduction via direct electron transfer. (b) Steady state current-voltage of the laccase-sTiO_2 nanoconjugates modified electrodes prepared with the crosslinkers the for oxygen reduction via mediated electron transfer, using syringaldazine (SYR), 2,2'-azino-bis(3-ethylbenzothiazoline-6-sulphonic acid) (ABTS) and promazine (PMZ) mediators.

In a different work, Shervedani *et al.* developed methods to immobilize laccase on gold surface and obtained ~25μA/cm^2 current density (pH 7.0, 100 mV/s) in DET which is about two times higher than our results.[126] However, the enzyme loading in their method was three times higher than ours and the scan rate is also much higher than ours (20mV/s). Dagys *et al.* demonstrated laccase-gold nanoparticle assisted ORR with current density of 5-30μA/cm^2 (pH 4.0, 10mV/s) which was comparable with our results.[111] However, our enzyme loading (~20 μg) was much lower than theirs (100 μg). Our work introduces a new class of support material for enzyme electro-catalysis. Continued studies and future publications could provide an indication if this material would be a game changer or not.

2.3.4 Bio-electrocatalytic activity of other laccase-MOx nanoconjugates

Same electrochemical measurements were also applied using ZnO and SnO_2 to achieve laccase nanoconjugates. The CVs obtained from both ZnO and SnO_2 nanoconjugates (Figure 2.8) in the presence of O_2, which deviates from the CVs obtained in the O_2-free electrolyte from the initial scanning potential. OCP and Ep1/2 were shown in Figure 2.9 of 0.62 V and 0.13 V of *s*ZnO, and 0.63 V and 0.22 V of *s*SnO_2.

2.4 Conclusions

We have demonstrated the use of enzyme-metal oxide nanoparticles as bio-nanoconjugate catalysts for an important electrochemical reaction in bio-fuel cells. A reliable method for using molecular wiring of laccase into *s*TiO_2 nanoparticles has been developed and demonstrated in this work. The immobilization seems to retain the enzymatic activity of laccase quite well as observed from the detailed electrochemical experiments. The properties of the molecular crosslinkers particularly possess an important role in determining the spatial position, and hence the electrochemical-activity, of the immobilized enzyme. Despite the generally low conductivity of

the metal oxides-based materials, the *s*TiO_2 nanoparticles showed high electro-activity for the mediated electrochemical oxygen reduction reaction. The reduction of oxygen current density is strongly influenced by the mediator redox potentials. This study also offers an alternative material support of enzyme bio-electrocatalysts and has significant implications for electrochemical biosensors and enzymatic fuel cells where laccase-based catalysts are used for oxygen reduction reactions. Future work in this area would include detailed investigation of the physical properties of metal oxide nanoparticles and crosslinkers and their influence on the electro-catalytic activity of the enzyme. Future studies would also focus on extending this novel immobilization method to other types of enzymes and metal oxides for applications in enzymatic fuel cells and amperometric biosensors.

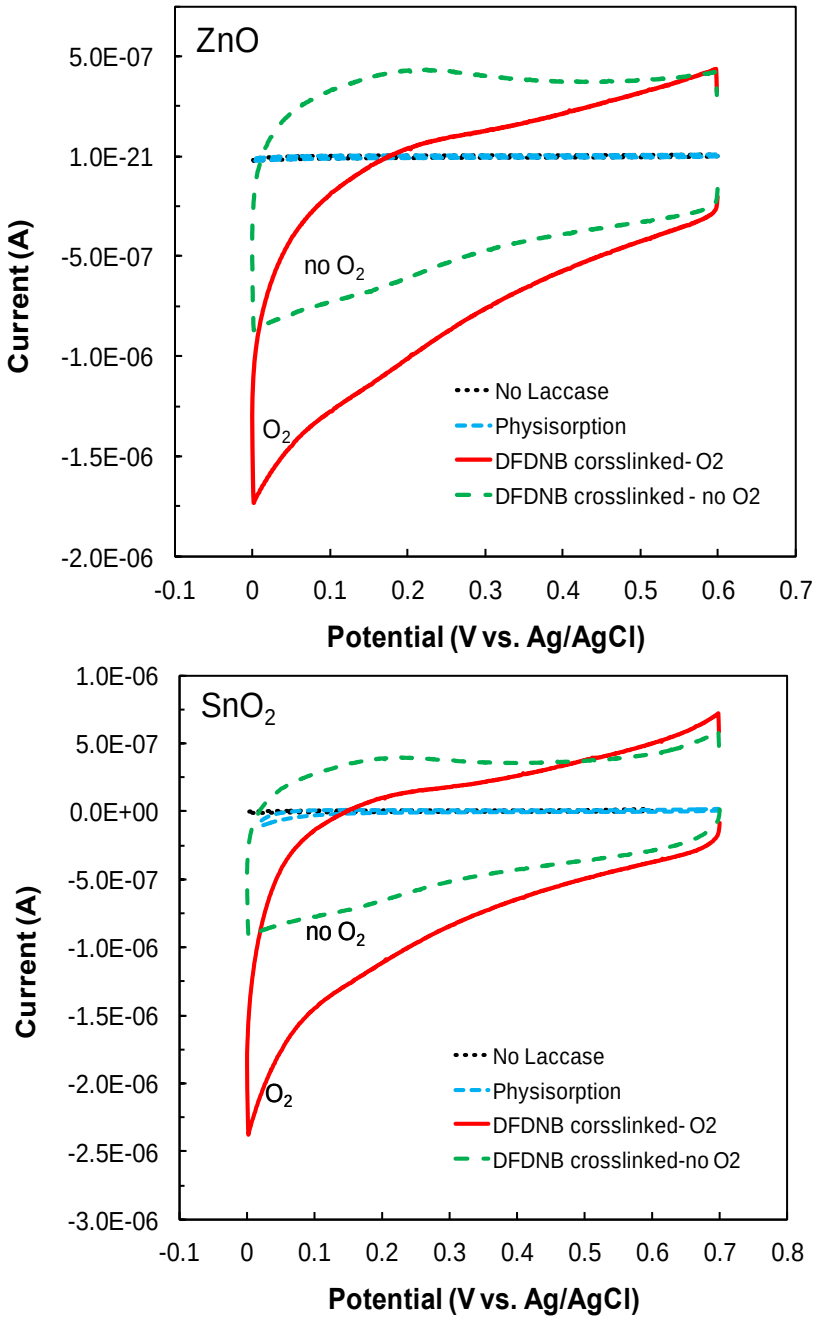

Figure 2.8: Cyclic voltammograms of (a) laccase-*s*ZnO nanoconjugates and (b) laccase-*s*SnO_2 nanoconjugates (c) laccase-*s*TiO_2 nanoconjugates using DFDNB crosslinkers in the presence and absence of O_2 in the electrolyte.

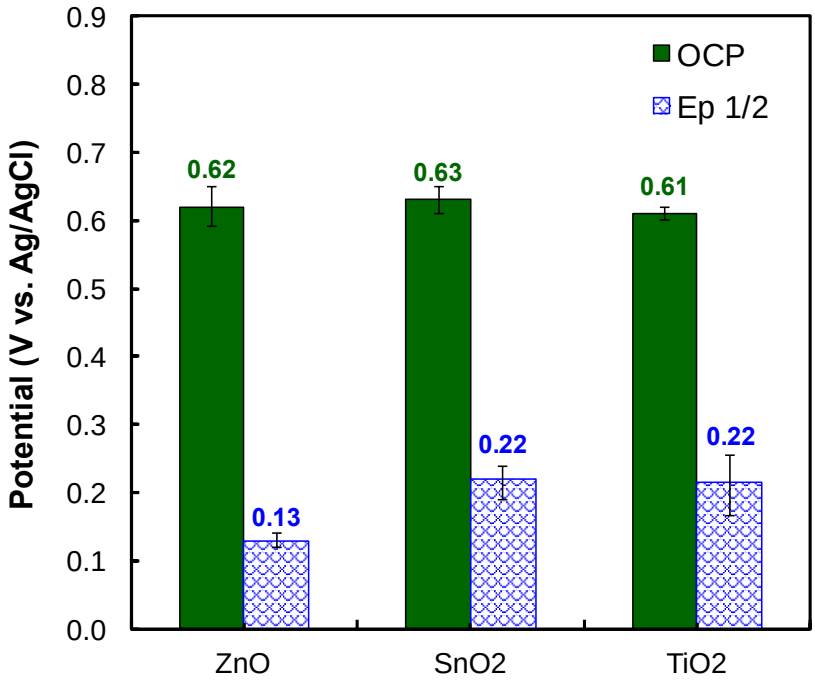

Figure 2.9: OCP and $Ep_{1/2}$ of laccase-sMO nanoconjugates. The data were obtained in pH 4.5 electrolyte.

2.5 Supplementary Data

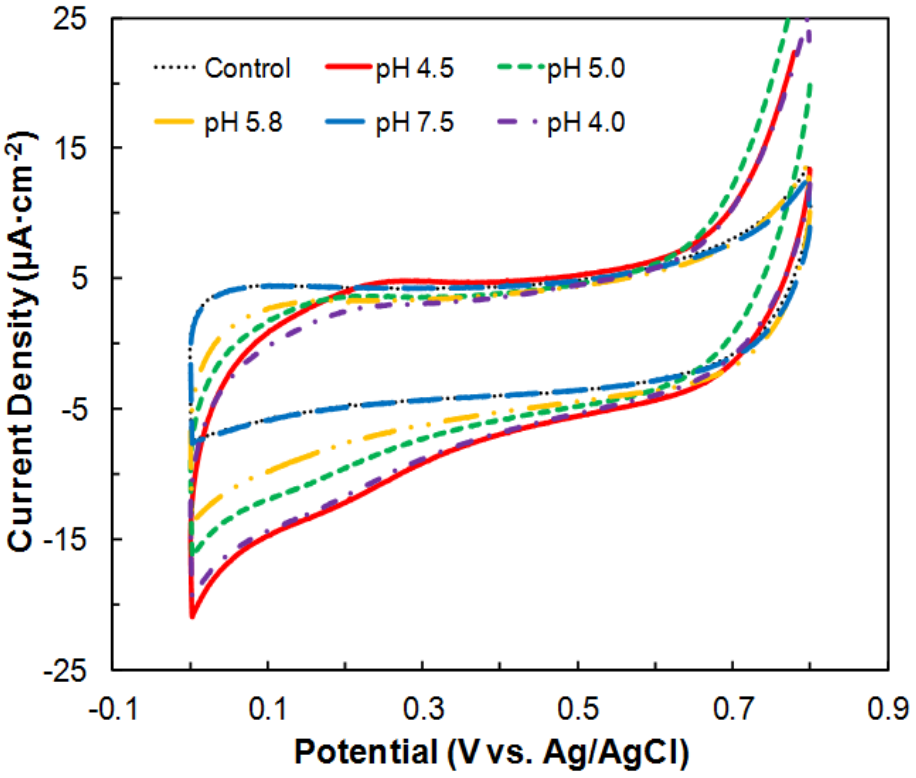

Figure 2.S1: Cyclic voltammograms of $sTiO_2$- laccase nanoconjugates in various pH system for oxygen reduction reaction. pH 4.5 was used as the optimal pH for all electrochemical experiments.

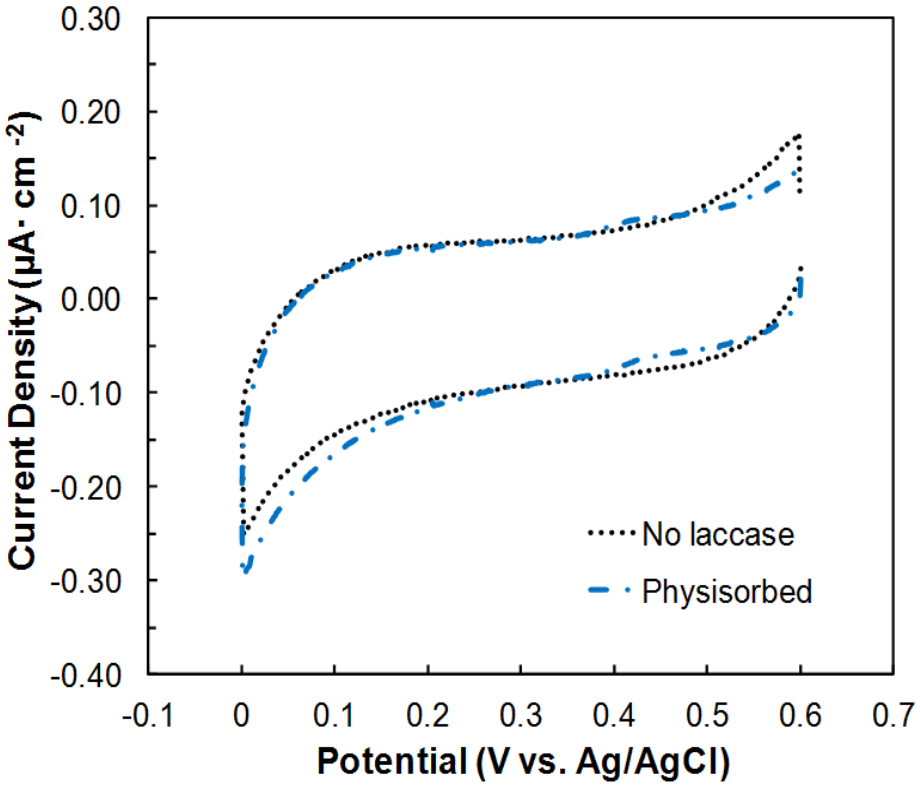

Figure 2.S2: Comparison of the CVs of *s*TiO_2 nanoparticles without laccase and with laccase, where laccase was physisorbed on *s*TiO_2 without any molecular crosslinkers. This figure is an expanded view of the control CVs shown in Figure 2.4a.

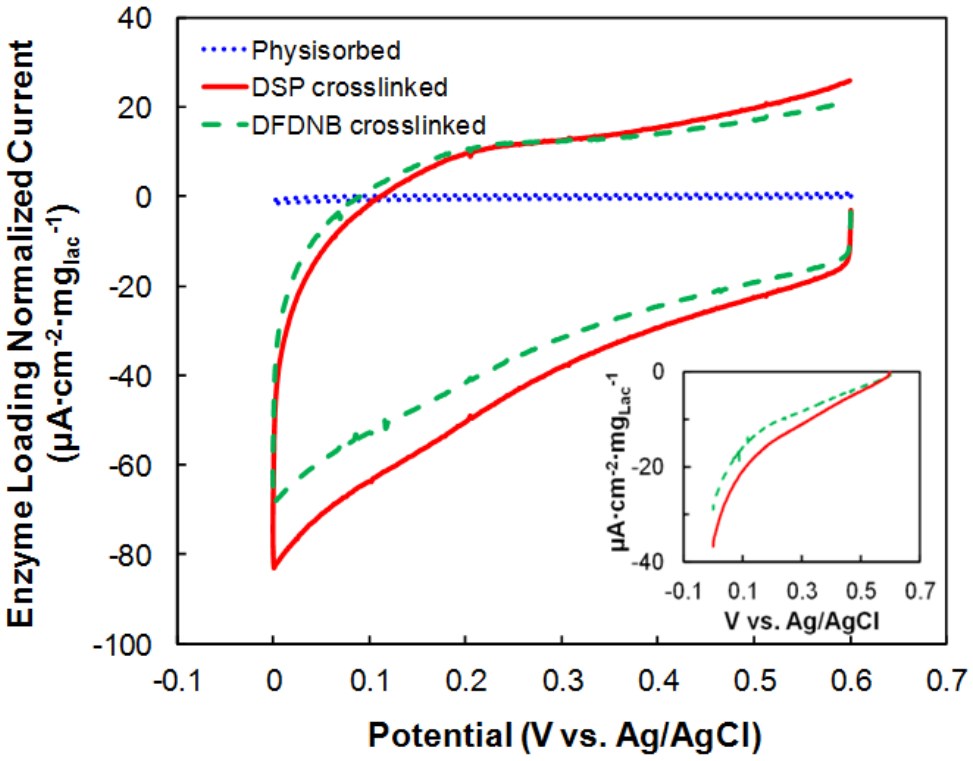

Figure 2.S3: Comparison of CVs for DET based oxygen reduction by physisorbed and crosslinked electrodes. The inset graph represents the capacitive background subtracted currents. The comparison is based on an enzyme loading normalized currents.

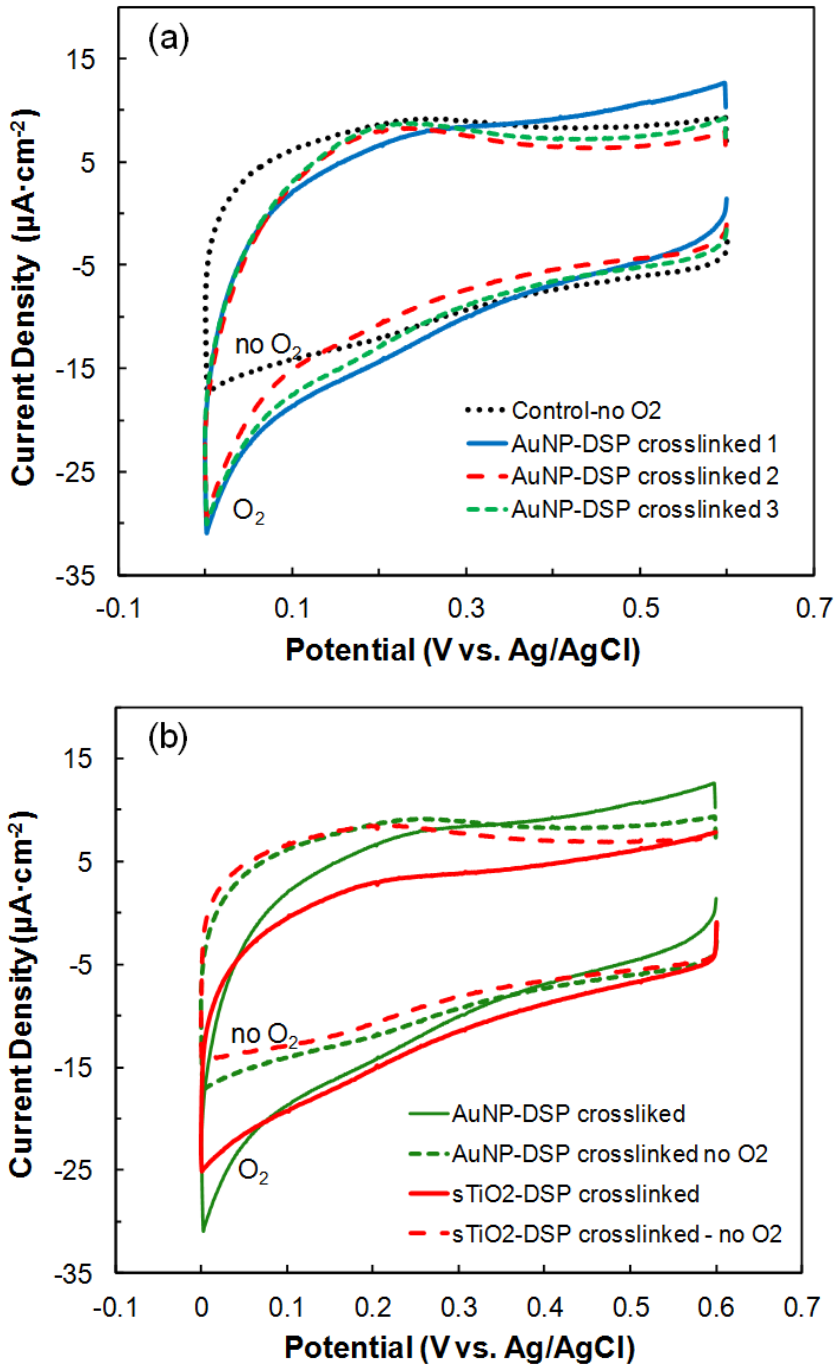

Figure 2.S4. Cyclic voltammograms of (a) triplicate experiments using laccase-AuNP conjugates; (b) Comparison of the cyclic voltammograms of laccase-*s*TiO_2 nanoconjugates and laccase-AuNP nanoconjugates in the presence and absence of O_2 in the electrolyte.

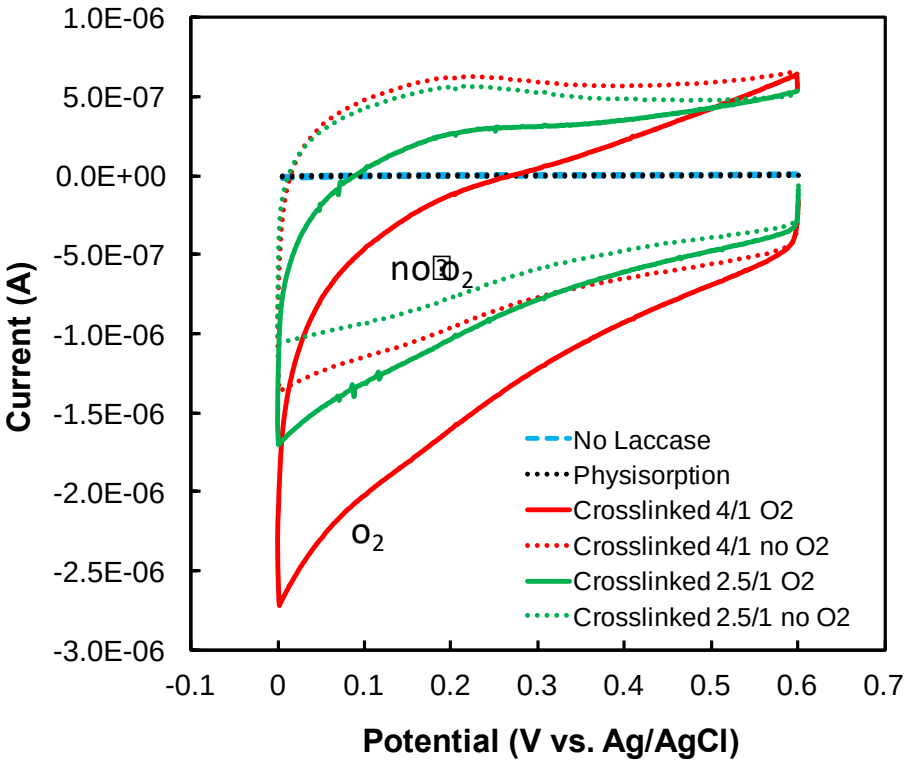

Figure 2.S5. Comparison of cyclic voltammograms of laccase-sTiO_2 nanoconjugates (APTES/ TiO_2 =4/1 or 2.5/1) prepared using DFDNB crosslinkers in the presence and absence of O_2 in the electrolyte. Solid line: O_2 saturated; Dash line: N_2 saturated. The data were obtained in pH 4.5 electrolyte, between 0.6 V and 0 V at a scan rate 0.02 Vs^{-1}.

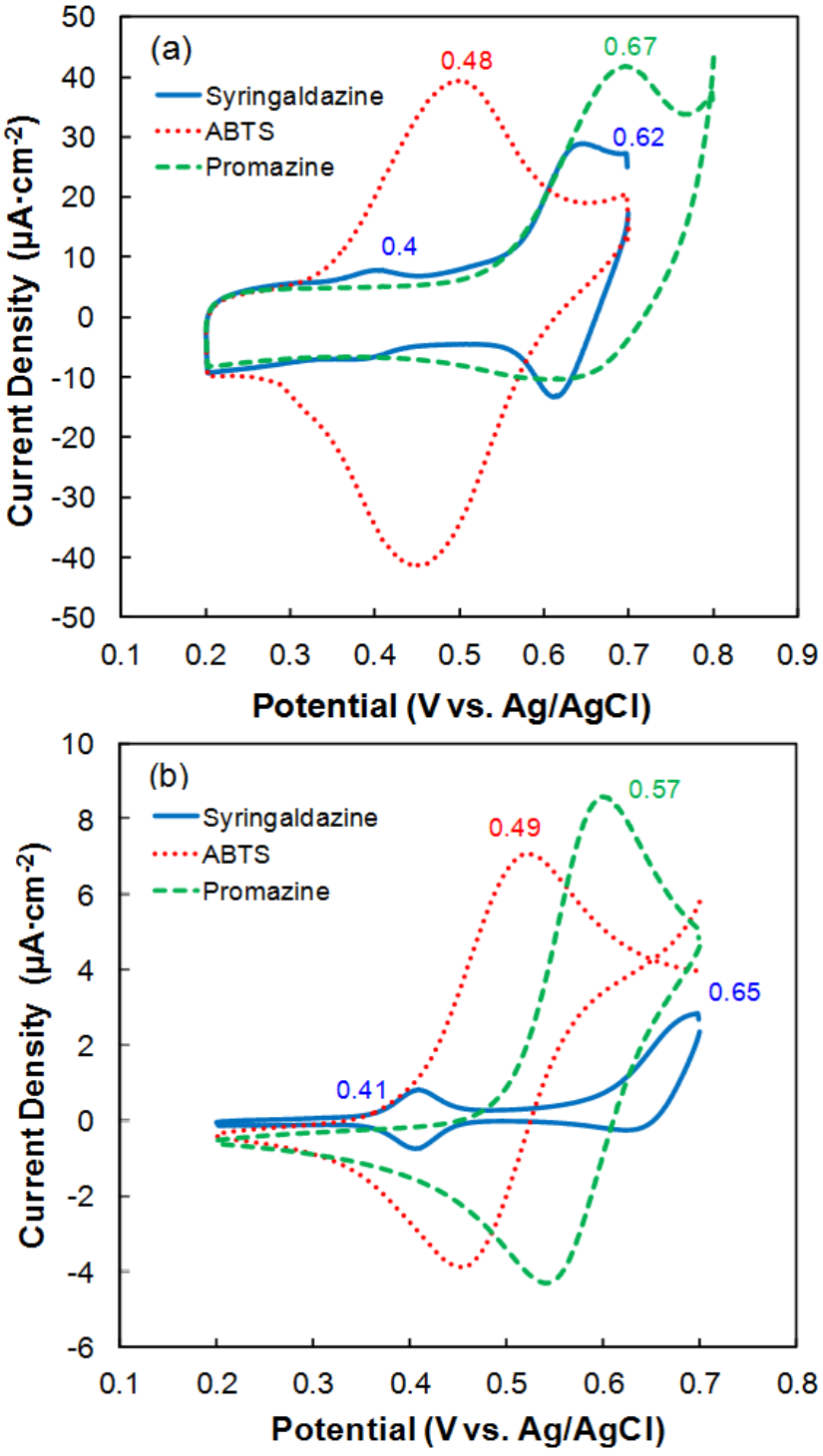

Figure 2.S6. Redox responses of 0.1 mM syringaldazine, ABTS and promazine on (a) $sTiO_2$ modified electrodes, (b) Bare SPE, without laccase.

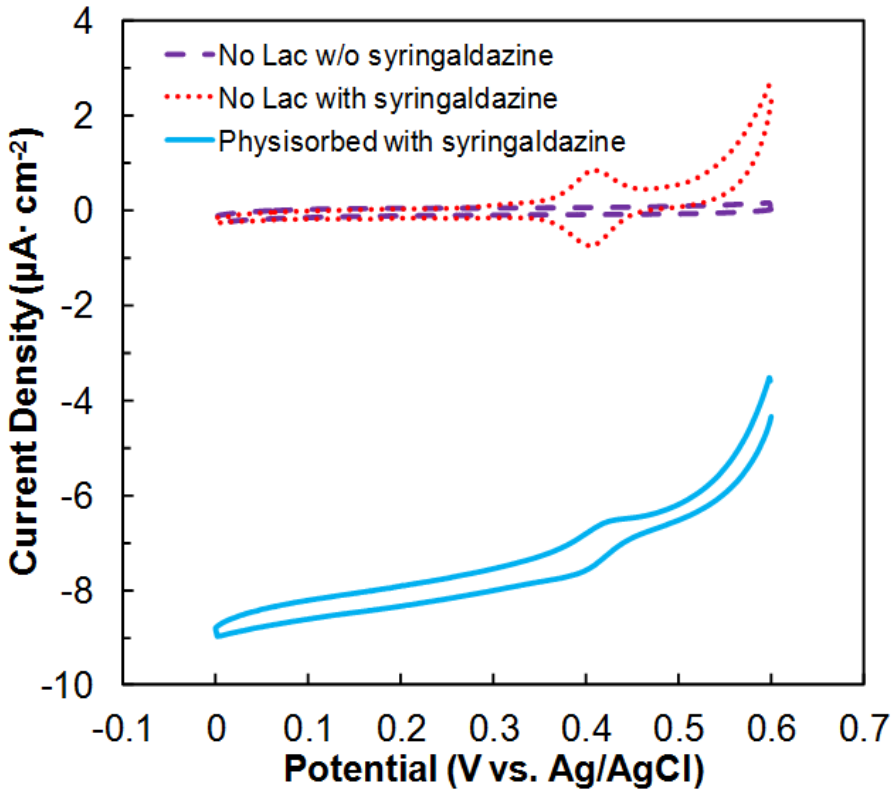

Figure 2.S7. Comparison of the voltammograms of *s*TiO_2 modified electrode in the presence and absence of syringaldazine with the physisorbed laccase (Lac) -*s*TiO_2 modified electrode in the presence of syringaldazine.

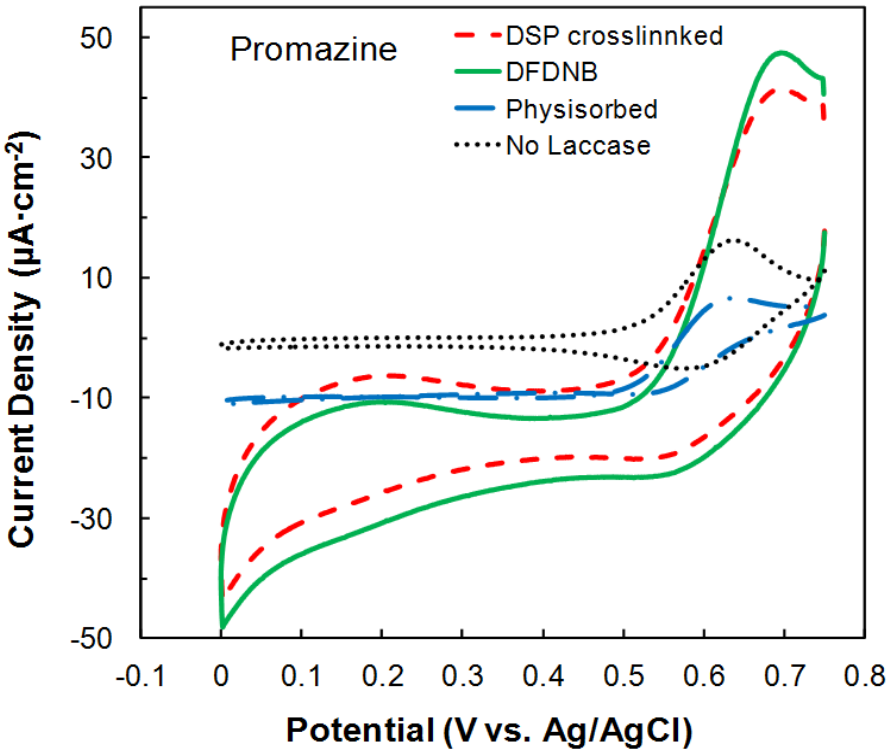

Figure 2.S8. Cyclic voltammograms of the laccase-sTiO_2 nanoconjugates obtained in O_2 saturated pH 4.5 electrolyte, between 0.75 V and 0 V at a scan rate 0.02 Vs^{-1} with promazine as mediator.

CHAPTER 3

KINETIC STUDY OF OXYGEN REDUCTION REACTION CATALYZED BY A THERMOPHILIC LACCASE

Yan Zhou, Nicholas A. Szaro, Joaquín Atalah, Giannina Espina, Jenny M. Blamey and Ramaraja P. Ramasamy. Submitted to Journal of The Electrochemical Society.

Abstract

This article reports the electro-kinetic study of oxygen reduction reaction catalyzed by a new type of enzyme, namely laccase from a thermophilic bacterium, which exhibits superior stability and activity retention compared to fungal laccases. Experiments were performed using a classic tool of electrochemistry, the rotating ring disk electrode (RRDE). *Bacillus sp.* FNT laccase was immobilized onto a multiwall carbon nanotube modified glassy carbon disk electrode using a molecular tethering agent 1-pyrenebutanoic acid succinimidyl ester (PBSE). The conditions for laccase immobilization were optimized to prepare a highly active bioconjugate for the electrochemical reduction of oxygen. The kinetic parameters such as Tafel slopes, number of electrons transferred, electrochemical rate constant and electron transfer rate were calculated from RRDE experiments. The slope value obtained from Tafel plot was close to that of value for the ideal four-electron transfer oxygen reduction, which suggests very high electroactivity of the immobilized *Bacillus sp.* FNT laccase.

Keywords: Multiwall carbon nanotube (MWCNT), thermophilic laccase, oxygen reduction reaction, rotating disk electrode.

3.1 Introduction

The oxygen reduction reaction is one of the most studied reactions in electrocatalysis, particularly in bio-fuel cell cathodes.[127,128] Laccase is one kind of blue multi-copper oxidase that catalyzes the reduction of oxygen. Several studies have discussed using laccase as an electro-catalyst for oxygen biosensors and enzymatic biofuel cell cathodes.[89,90] On a typical laccase modified electrode surface, electrons are received from the electrode by the T1 copper site, followed by transferring to the tri-nuclear cluster (T2 and T3 copper centers), where O_2 will get reduced to water.[86,93] Most of the laccases studied for the oxygen reduction reaction are of fungal origin, such as *Trametes versicolor* (TVL), *Agpergillus niger*, *Pleurotus ostreatus.*[129] As a high potential laccase, TVL is characterized by a high T1 copper redox potential and high catalytic activity between pH 4 and 5.[29,51] TVL has been well studied as an enzyme catalyst on a variety immobilization supports for the electrochemical reduction of oxygen.[87,88,94,101,130] One of the challenges in enzyme electro-catalysis is the insufficient electrical communication between enzyme redox sites and the electrode surface. Several different approaches have been tried to maximize the electrocatalytic activity of the laccase modified electrodes.[94,98] Among various nanomaterials, multiwall carbon nanotubes (MWCNT), have been extensively studied as enzyme immobilization support that provide enlarged surface area and high conductivity, which help to increase the number of enzyme active sites on the electrode.[19,103] In previous work from our laboratory, it has been demonstrated that *Trametes versicolor* laccase (TVL) high electro-catalytic activity for bio-electrochemical reduction of oxygen via direct electron transfer.[94] In that work, TVL laccase was immobilized onto MWCNT-modified electrode surface through molecular tethering agent 1-pyrenebutanoic acid succinimidyl ester (PBSE). This immobilization strategy

has dramatically improved the overall electrocatalytic activity of the laccase-modified electrodes.[92,94]

Though TVL-based enzyme catalysts possess high electrocatalytic activity and could be used in biofuel cell applications, their practical utilization is currently limited by short lifetimes due to enzyme degradation and loss of activity.[89] Thermophilic bacteria laccase, on the other hand, have shown very interesting behavior and functionality in high temperature environment.[131] Thermophilic laccase is generally more resistant to denaturing and loss of activity than their mesophilic counterparts.[132] Few studies have reported the key kinetic parameters of oxygen reduction reaction catalyzed by laccase.[49,133] *Bacillus sp. FNT* is a thermophilic bacterium with optimal growth conditions at pH 8 and 50°C. It was isolated from a hot spring and first characterized at Fundación Biociencia, Chile. The native enzyme was found to have a spore coat with laccase activity and was found to possess a maximum activity at 70 °C and between pH 7 to 8 in our unpublished studies. The *Bacillus FNT* laccase gene was cloned and introduced to *E. coli* BL21 for overexpression and purified to homogeneity. The recombinant *Bacillus FNT laccase* (FNTL) was studied in our previous work.[134] The stability of TVL and FNTL was compared in Figure 3.S1. FNTL exhibited superior stability over 2 weeks compared to TVL. We have demonstrated the high electrocatalytic activity of FNTL-MWCNT tethered composites for oxygen reduction through direct electron transfer with an enhance stability.[134] In that work, FNTL was tethered onto MWCNT surface through a molecular tethering agent PBSE. As depicted in Figure 3.1, PBSE could non-covalently bind onto MWCNT through π-π stacking and covalently bind onto laccase enzyme. In the current work, a comprehensive kinetic analysis of *Bacillus* FNT laccase using hydrodynamic voltammetry measurements obtained with a rotating ring-disk electrode (RRDE) is presented. The key electro-kinetic and mechanistic parameters for the *Bacillus sp. FNT*

derived laccase catalyzed oxygen reduction were determined for the first time. These studies provide a quantitative method of analysis to evaluate the electro-catalytic activity of the catalysis reaction by using laccase functionalized nanocomposites.

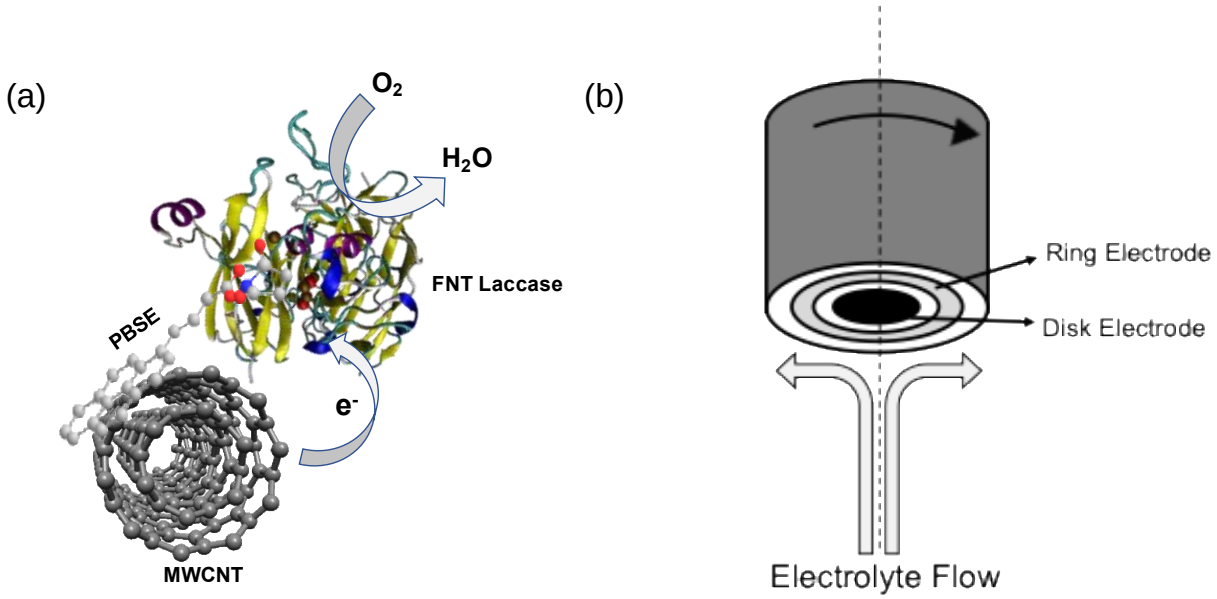

Figure 3.1: (a) Schematic of the FNTL-MWCNT bioconjugates, where FNTL is tethered onto MWNT using pyrenebutanoic acid succinimidyl ester (PBSE). The tethered laccase reduces oxygen to water via direct electron transfer. (b) Rotating ring disk electrode set up for oxygen reduction reaction.

3.2 Experimental

3.2.1 Materials and Instruments

The following chemicals were purchased and used without further purification: multi-walled carbon nanotube (Dropsens, Spain), potassium dihydrogen phosphate (BDH), potassium dibase phosphate. 1-pyrenebutanoic acid succinimidyl ester (PBSE) (Sigma-Aldrich), N,N-dimethyl formamide (DMF). Thermophilic laccase FNT was obtained by cloning and overexpressing in *E. coli* BL21 (New England Biolabs). 100mM of pH 7.0 potassium phosphate

buffer was used as electrolyte. All buffers were prepared using nano-pure distilled water (18 M ohm conductivity). All glassware was dried overnight at 75 °C to remove adsorbed water. Industrial grade O_2 and N_2 (Airgas) were used for all electrochemical experiments. Electrochemical characterization was conducted using a potentiostat CHI-920c (CH Instruments Inc.). A RRDE setup (PINE Instruments Inc., Grove City, PA) was used to carry out the hydrodynamic voltammetry measurements. A glassy carbon disk and platinum ring electrodes were mounted on a rotating shaft controlled by an RPM controller. The glassy carbon disk electrode was polished using an electrode polishing kit consisting 0.3μm aluminum powder. A Ag/AgCl reference electrode and platinum wire auxiliary electrode (both from CH Instrument Inc.) were used for electrochemical measurements. All the electrochemical measurements were carried out at 25 ± 2 °C in a 125 mL voltammetry cell unless otherwise stated. All potentials reported are with respect to the Ag/AgCl reference.

3.2.2 FNTL-MWCNT Composite Preparation

Multiwall carbon nanotube (MWCNT) was used as the immobilization support for laccase. The glassy carbon disk was coated with MWCNT suspension and dried at 70 °C. 10mM PBSE in DMF was dropcasted on the surface of electrode and incubated for 15 min. Followed by washing the electrode with DMF and phosphate buffer (pH =7), laccase enzyme solution was added on the surface of the electrode by dropcasting and incubating for 30 min on ice. The crosslinker PBSE could react with amine group on laccase structure and non-covalently binds to MWCNT surface through π-π stacking. For control experiments, the electrodes were prepared by dropcasting laccase directly onto the MWCNT modified electrode surface without any tethering agent. After 30 min, the modified electrode was washed to removed excess enzymes with phosphate buffer. The prepared electrodes were then ready for electrochemical measurements.

3.2.3 Electrochemical characterization

The electrochemical measurements were conducted in an 125mL electrochemical cell using 100 mM phosphate buffer as electrolyte (pH 7). A bi-potentiostat was used to perform linear sweep voltammetry (LSV) on the disk electrode and at a fixed applied potential on the ring electrode at different disc rotational speeds. For LSV, the disk potential was swept from +0.5 V to -0.9 V at a scan rate of 20 mV/s, while the ring potential was kept constant at +1.0 V. The Tafel plot measurements were obtained on the disk electrode in the potential range of 0.5 V to +0.1 V versus the onset potential for oxygen reduction. The kinetic parameters such as Tafel slope, number of electrons, and rate constants were calculated using the data obtained in voltammogram and Tafel plot measurement.

3.3 Results and discussion

3.3.1 Importance of molecular tethering agent

Figure 3.2 compares the cyclic voltammograms (CVs) of the complete FNTL-MWCNT nanoconjugate catalysts (FNTL, PBSE, MWCNT) with that of the control (catalyst without PBSE or MWCNT). The CVs showed that the molecular tethering agent is essential for enhancing the electron transfer capability, resulting in significant better electrocatalytic activity for oxygen reduction compared to the catalyst that lacked PBSE crosslinker. This can be seen in the cathodic wave of the CV obtained in O_2 saturated electrolyte, which clearly deviates from the CV obtained in the O_2 deprived electrolyte (N_2 saturated electrolyte) at and below 0.37 V. The onset potential for oxygen reduction is 0.37 V and the open circuit potential was 0.46 V. In the absence of MWCNT, the electrode possesses a low surface area that results in low capacitance and low non-faradic currents as shown in the CVs.

3.3.2 Hydrodynamic study

The electro-kinetics of oxygen reduction using FNTL-MWCNT modified electrodes were studied using the RRDE. The RRDE hydrodynamic scheme is shown in Figure 3.1, where a RRDE electrode is immersed in electrolyte containing O_2. On the surface of disk, O_2 is reduced and the products are transferred to ring electrode immediately due to rotation of the electrode. At the ring a potential of +1.0 V *vs* Ag/AgCl was applied to oxidize the reaction product H_2O_2 to O_2. The magnitude of the ring current allows for a direct measurement of the amount of H_2O_2 generated at the disk. High ring currents generally indicate a low electrocatalytic activity of FNTL-MWCNT conjugates for a direct 4-electron reduction of O_2 to water.

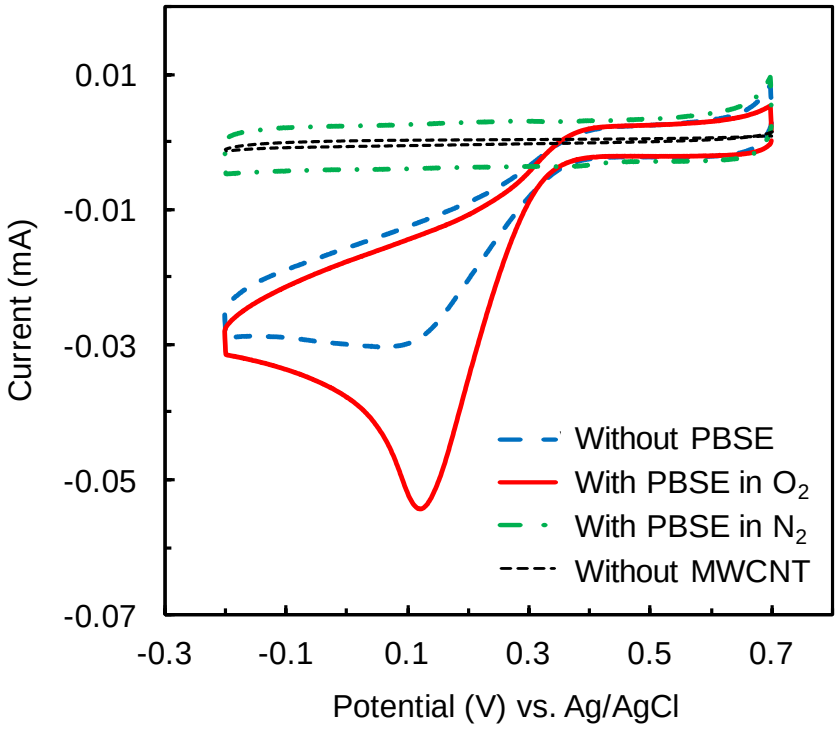

Figure 3.2: Comparison of CVs of the complete and incomplete bio-conjugates using glassy carbon electrode obtained in the presence and absence of O_2.

Due to the high potential applied on the ring electrode, hydrogen peroxide that formed at the disk electrode as a result of incomplete oxygen reduction was able to be reduced to water at the ring

electrode resulting in an oxidation current at the ring. Linear sweep voltammetry (LSV) was conducted using RRDE electrode modified with FNTL-MWCNT nanoconjugates. Disk current (I_D) and ring current (I_R) was monitored at different rotation speed (0 – 1500 rpm) as given in Figure 3.3. The onset potential of oxygen reduction is 0.35 V regardless of the rotation rate. The LSV obtained at 0 rpm clearly showed a significant cathodic wave in O_2 saturated electrolyte at and below 0.35 V with a steep slope. Below 0.15 V, the cathodic disk current started to decrease indicating the mass transfer limitations of O_2 in the solution. With increasing disk rotation speeds, the mass transfer limitation was significantly lowered resulting in high limiting currents (below -0.8V). It is noteworthy that the slopes of oxygen reduction remain the same (1.16 mAV^{-1}) with increasing rotation speeds, indicating a stable electro-catalytic activity of FNTL-MWCNT bioconjugates at all rotation speeds.

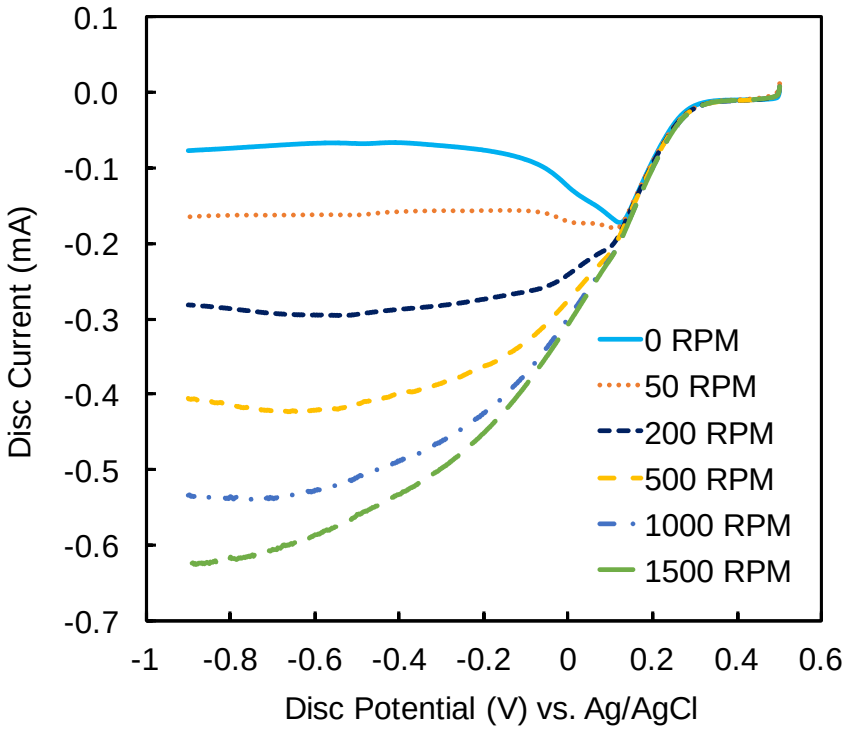

Figure 3.3: Rotating ring disk electrode measurements using linear sweep voltammetry at various disk rotation speeds from 0.6 to -1.0 V at the scan rate of 20 mV s^{-1}. Plot of disk current (I_D) vs disk potential.

3.3.3 Effect of rotation speed

The voltammograms shown in Figure 3.3 were used to understand the relation between I_L and the concentration of O_2. The relation can be described by Levich equation

$$I_L = 0.62nFAD^{2/3}v^{-1/6}\omega^{1/2}c \qquad (1)$$

Where I_L is the limiting current, n is the number of electrons transferred per oxygen molecule, F is the Faraday's constant, A is the electrode surface area (0.196 cm^2), D is the diffusion coefficient (2.6×10^{-5} cm^2s^{-1})[135], ω is the angular rotation rate, v is the kinetic viscosity (cm^2/s) and C is the saturated concentration of oxygen in the bulk (1.22mM)[136]. The I_L values were obtained from the LSV of the disk electrode at -0.9 V at which the rate of O_2 reduction equals the rate of O_2 diffusion. The Levich plot of limiting versus the angular rotation rate of RRDE was plotted in Figure 3.4.

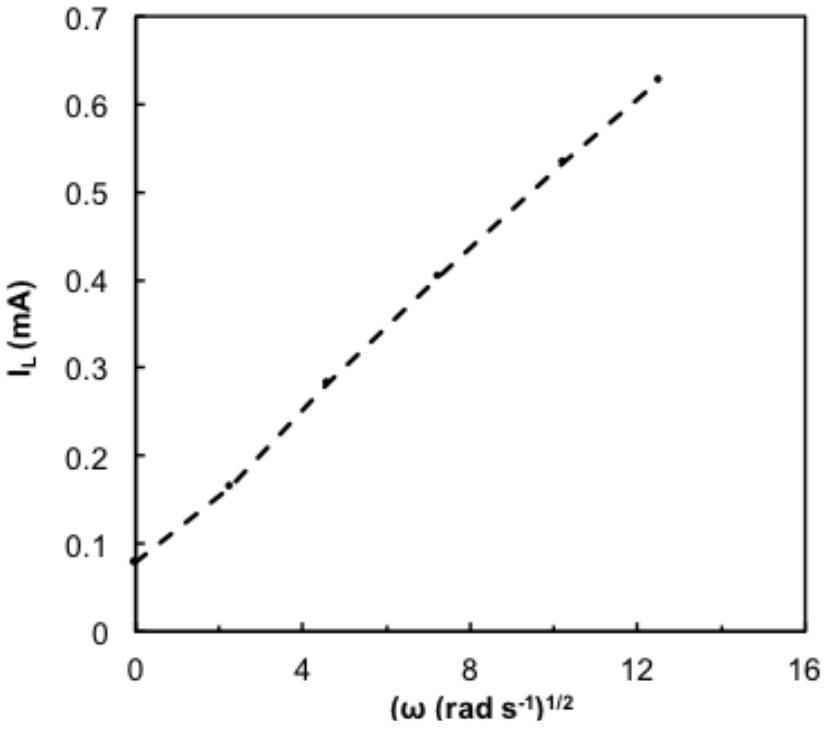

Figure 3.4: Plot showing the Levich regions for ORR by bio-nanocomposite modified disk electrode. Rotation speeds ranged from 0 to 1500 RPM.

In the linear region of the Levich plot, it could be assumed that O_2 can freely diffused to the disk electrode, which indicates the reaction kinetics is faster than the delivery rate of the O_2 to the electrode. The increasing RRDE rotation rate lead to a fast supply of oxygen to electrode surface and greater turbulence near electrode surface.

3.3.4 Koutecky – Levich analysis

The Koutecky- Levich plot of the inverse current versus the inverse angular rotation rate is plotted in Figure 3.5. The slopes shown in the graph were obtained for rotation rates in the range from 200 rpm to 1500 rpm. The slope yielded were 10.9, 11.7 and 11.42 $mA/s^{1/2}$, respectively. Based on the Levich equation, the slope of these plots can be related to the number of electrons transferred in the oxygen reduction:

$$\frac{1}{I} = \frac{1}{I_k} + \frac{1}{I_D} = \frac{1}{I_k} + \frac{1}{0.62nFAc\omega^{1/2}D^{2/3}\upsilon^{-1/6}} = \frac{1}{I_k} + \frac{1}{B\omega^{1/2}} \qquad (2)$$

where I is the measured current, I_k is the kinetic current of the disk electrode given by $I_{kin} = (I_L I)/(I_L-I)$, I_D is the diffusion-limited current, n is the number of electrons transferred, F is the Faraday's constant, A is the surface area of the electrode, c is the bulk concentration of oxygen in the electrolyte, D is the diffusion coefficient of O_2, and υ is the kinetic viscosity of the electrolyte ($9.13 \times 10^{-3} cm^2 s^{-1}$).[137,138] In order to investigate the number of electrons (n) involved in the laccase-MWCNT catalyzed oxygen reduction reaction, the B value in equation (2) was substituted by the slope value obtained in Figure 3.5, and n value was calculated from the slope. The resulting number of electrons transferred per oxygen molecule was between 3.2 and 3.35. These calculated n values were then validated using ring current data in the following analysis.

3.3.5 Ring current analysis

As shown in Figure 3.6, the ring current indicated a difference in H_2O_2 reduction at the ring electrode at various rotational speed and disk potentials.

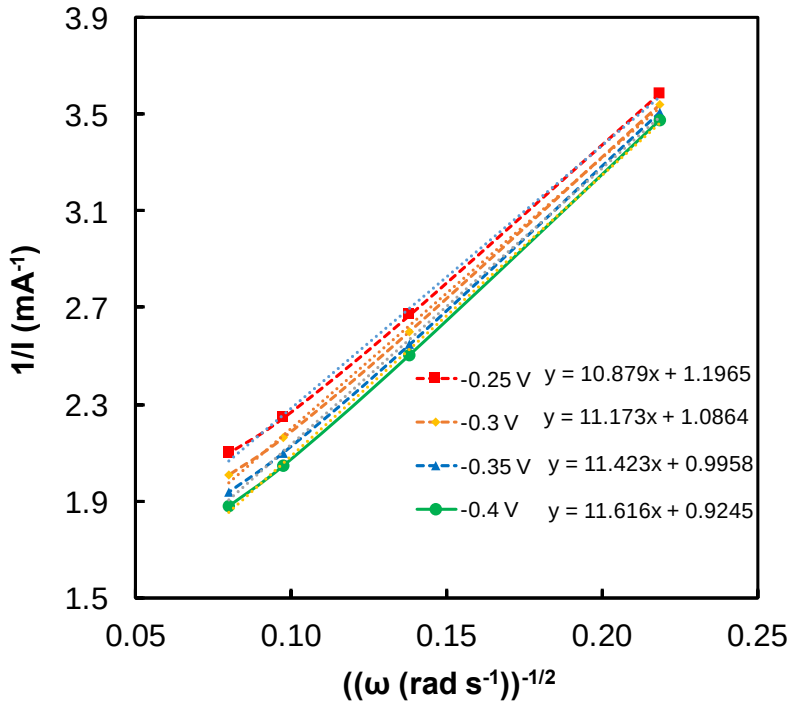

Figure 3.5: Koutecky-Levich plots at various disk potentials (-0.25—-0.4V) outside the kinetics limited region.

The I_R obtained at low rotation rate was lower in the diffusion limiting region compared to the region above the onset potential, this is understandable as the ring current measures the oxidation of H_2O_2 which does not happen at low potentials. I_R also increased with increasing rotation rates and became constant at very high rotation rate. A detailed analysis was conducted to understand the amount of H_2O_2 formation at the disk. The average number of electrons transferred per oxygen molecules could be an indication of the ability of catalyst to catalyze a preferred 4-electron reduction of O_2 over a 2-electron reduction. The number of electrons was calculated by the equation:

$$n = \frac{4}{1+\frac{I_R}{NI}} \qquad (3)$$

where I_R is the ring current and I is the measured disk current, and N is the collection efficiency, which refers to the percentage of H_2O_2 that was collected at the ring electrode. It is a geometric parameter that was experimentally determined to be 0.256 by the manufacture for the RRDE set.[139]

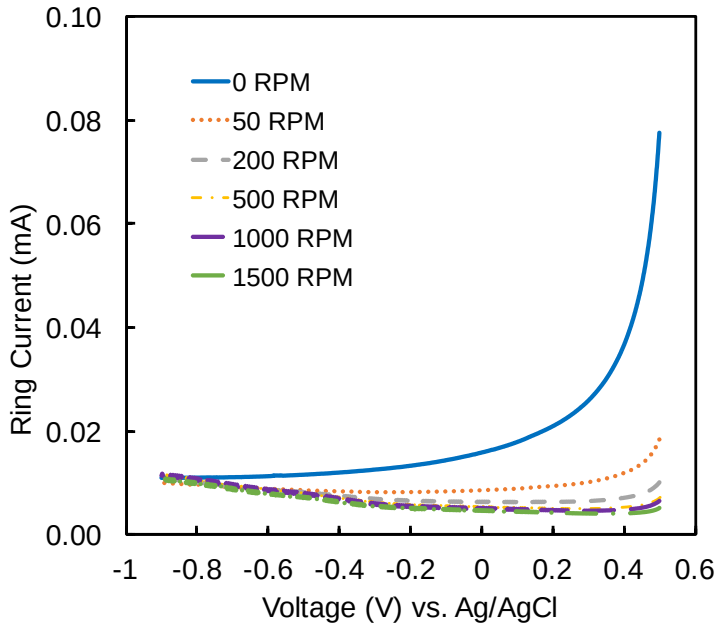

Figure 3.6: Rotating ring disk electrode measurements using linear sweep voltammetry at various disk rotation speeds from 0.6 to -1.0 V at the scan rate of 20 mV s^{-1}. Plot of ring current (I_R) vs disk potential.

A potential range of 0.145 V to -0.9 V was used for the calculation of the number of electrons involved in oxygen reduction reaction using the above equations. The calculated values of n at different rotation rates was plotted against disk potential in Figure 3.7. Figure 3.7 showed high number of electrons involved in the reduction reaction at high rotation rates varying from 3.5 to 3.7, indicating that the catalyst predominantly catalyzes 4-electron reduction of O_2 to water with minimal H_2O_2 formation as intermediate. The results also suggest that FNTL-MWCNT bioconjugates possess high electro–catalytic activity for oxygen reduction reaction.

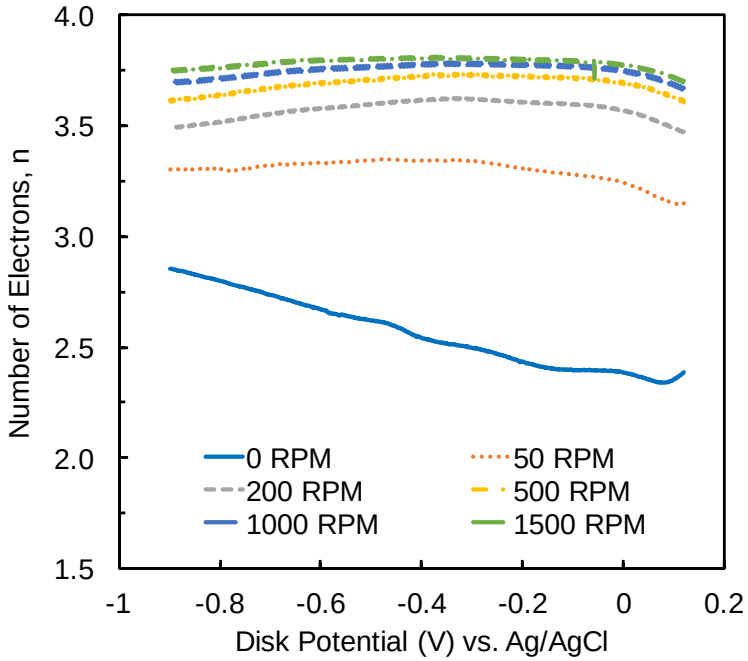

Figure 3.7: Number of electrons as a function of disk potential.

3.3.6 Electrocatalytic activity

The electro-catalytic activity of FNTL-MWCNT bioconjugates for oxygen reduction was also evaluated using Tafel slopes, a key paramaters used for kinetic valuations. The Tafel slopes were obtained from the voltammograms in the kinetic region of oxygen reduction (0.15-0.35V) The Tafel slope in this study is the slope of the linear region in a potential *vs* I_k plot in Figure 3.8, between 1×10^{-3} and 1×10^{-2} mA. The obtained Tafel slope from the above region was 45 mV per decade change of kinetic current and was constant at high rotation rates within Levich region. The theoretical value of Tafel slope for a four-electron reduction of oxygen is 15 mV per decade change in I_k. The closer the experimental value to the theoretical value, the better the electrocatalytic behavior of the catalyst.[136]

3.3.7 Electrochemical rate constant

We have proposed a reaction model of oxygen reduction previously in the bioconjugates-modified electrode, as shown in Figure 3.9a, which is similar to the one reported by Damjanovic.

[92,140] In this model, O_2 in bulk solution first diffuses to disk electrode functionalized with FNTL-MWCNT bionconjugates and get reduced on the electrode surface in two ways: a four-electron O_2 reduction, or a two-electron O_2 reduction. k_1, k_2 and k_3 are the reaction rate constants for each of the reactions on the RRDE surface as depicted in Figure 3.9a. k_1 represents the rate constant of the complete reduction (four-electron reduction) of oxygen to water. k_2 represent the rate constant of the incomplete reduction of oxygen to hydrogen peroxide (two-electron reduction).

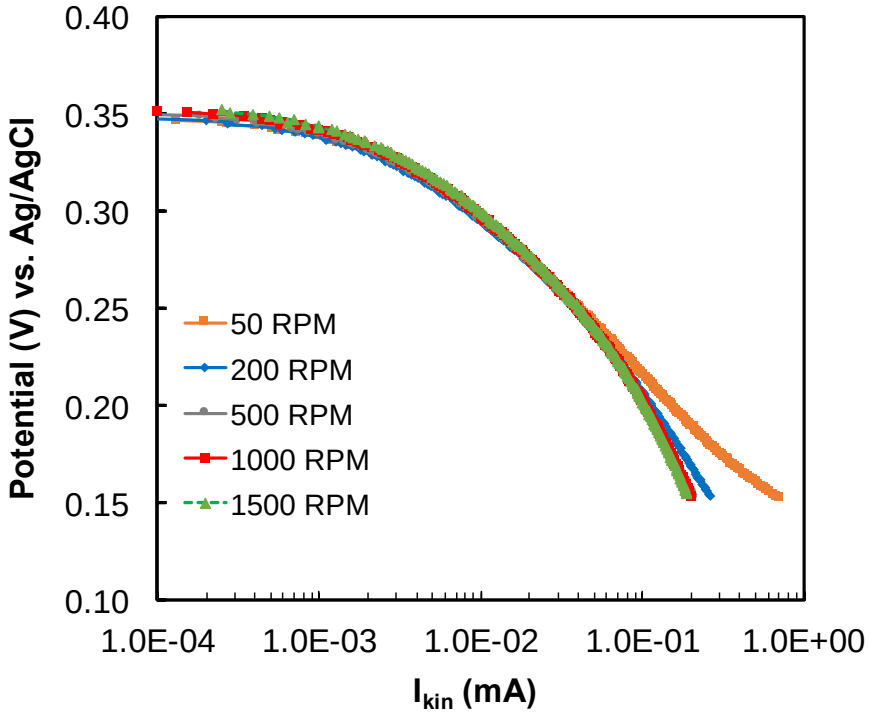

Figure 3.8: Tafel plot obtained from the calculated kinetic current values at different RPM in the kinetic region.

The intermediate hydrogen peroxide that formed on disk electrode partially diffuses to ring electrode, and the remaining hydrogen peroxide diffuses to bulk solution. k_3 represents the rate constant of the reduction of hydrogen peroxide to water on ring electrode. All the rate constants were calculated by the following equations.

$$k_1 = S_2 Z_1 \frac{I_1 N - 1}{I_1 N + 1} \qquad (4)$$

$$k_2 = \frac{2Z_1S_2}{I_1N+1} \quad (5)$$

$$k_3 = \frac{Z_2NS_1}{I_1N+1} \quad (6)$$

$$Z_1 = 0.62D_1^{2/3}\upsilon^{-1/6} \quad (7)$$

$$Z_2 = 0.62D_2^{2/3}\upsilon^{-1/6} \quad (8)$$

where S_1 and I_1 are the slope and intersect of the plot of I_D/I_R *vs* $\omega^{-1/2}$, S_2 is the slope of $I_L/(I_L-I_D)$ *vs* $\omega^{-1/2}$. These plots are shown as Figure 3.S2-S3 in the supporting information. The I_D/I_R *vs* $\omega^{-1/2}$ was plotted at -0.2 V to avoid the kinetic limited condition and the resulting slope S_1 is 329.7 and the intercept is -111.4. Similarly, the slope of $I_L/(I_L-I_D)$ vs $\omega^{-1/2}$ is 251.4. Applying the values in the above equations gives the value of k_1, k_2, and k_3 as 3.21×10^{-1} cm s^{-1}, 2.17×10^{-2} cm s^{-1} and 2.76×10^{-3} cm s^{-1}, respectively. When comparing k_1 and k_2 values, k_1 is one magnitude higher than k_2, indicating that the rate constant for H_2O formation is higher than that of H_2O_2. The rate constant of oxygen reduction reaction using FNTL-MWCNT bioconjugates were two orders of magnitude higher than that of the oxygen reduction on metallic surfaces.[141]

3.3.8 Electron transfer rate

The electron transfer rate of oxygen reduction reaction could be influenced by several factors, such as the conductivity of the electrode, the distance between the catalyst and the electrode, and the intrinsic electro-catalytic activity of the catalyst. The electron transfer rate constant of FNTL-MWCNT bioconjugates catalyzed oxygen reduction reaction could be calculated using the following equation:

$$I_0 = n\mathrm{FAk_{et}c} \quad (9)$$

Where I_0 is the exchange current obtained from Tafel plot, n is the number of electrons, F is the Faraday's constant, A is the electrode surface area, k_{et} is the electron transfer rate constant, c is the

concentration of the analyte in the bulk solution. The exchange current density can be calculated using a current vs overpotential plot also known as Tafel plots. Figure 3.9 shows the log I vs overpotential of the electrochemical oxygen reduction reaction, which can be expressed using the equation

$$I = a + b\,exp(\eta) \qquad (10)$$

Where a and b are empirical fitting constants and η is the overpotential. For this, the disk electrode was swept between 0.1 to 0.5 V (-0.2 to +0.2 V vs onset potential) at 0 RPM. Ideally this plot should be linear. However, it appears nonlinear because of the large voltage window used for sweeping the voltage. From the plot in Figure 3.9, I_0 was calculated by intersecting the tangents at nonlinear regions of the Tafel curve. The obtained values of equilibrium exchange current density (I_0) and the electron transfer rate (k_{et}) were 7.54 $\times 10^{-6}$ A cm^{-2}, and 1.60 $\times 10^{-8}$ cm s^{-1} respectively.

3.4 Conclusion

This work presented a comprehensive detailed electrochemical kinetic study of oxygen reduction reaction by a thermophilic laccase-based bioconjugates. The electro-kinetic parameters for FNTL catalyzed oxygen reduction reaction was reported for the first time. The electro-kinetic parameters such as order of reaction, number of electrons transferred per O_2, Tafel slopes, kinetic rate constant of reactions at the disk electrode, and the electron transfer rate constant are being reported for the first time. These electro-kinetic results demonstrated that laccase present in the bio-nanocomposite has high electro-catalytic activity toward ORR, indicating excellent electro-catalytic activity of the enzyme composite catalysts. The kinetic properties reported in this work can be used as a benchmark for developing new laccase-based catalysts for electrochemical oxygen reduction reactions.

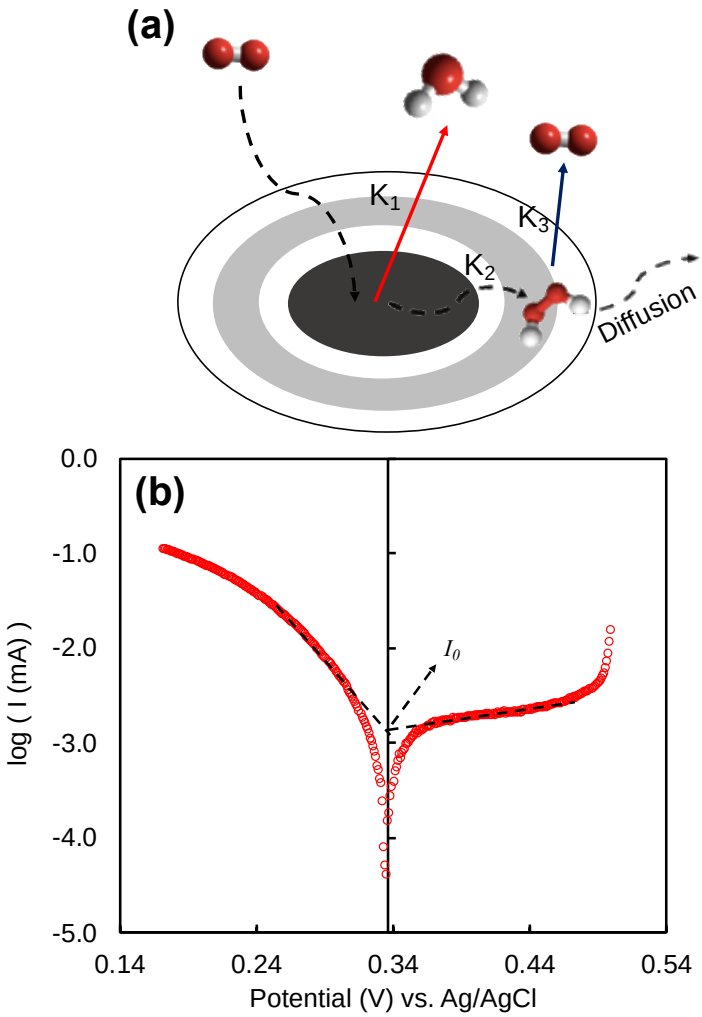

Figure 3.9: (a) Schematic representation of the oxygen reduction reaction mechanism by two different pathways; (b) Linear sweep voltammograms showing Tafel regions at no rotation for the FNTL-MWNT in phosphate buffer (pH 7).

3.5 Supplementary data

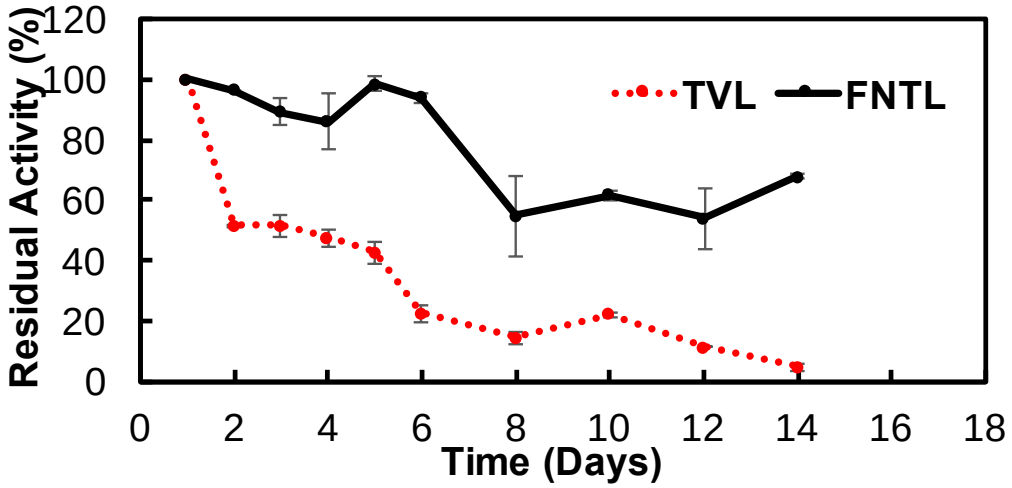

Figure 3.S1: Stability study of laccase residual activity of TVL and FNTL. The residual activity was calculated based on first day's biocatalytic activity measured using standard protocols.

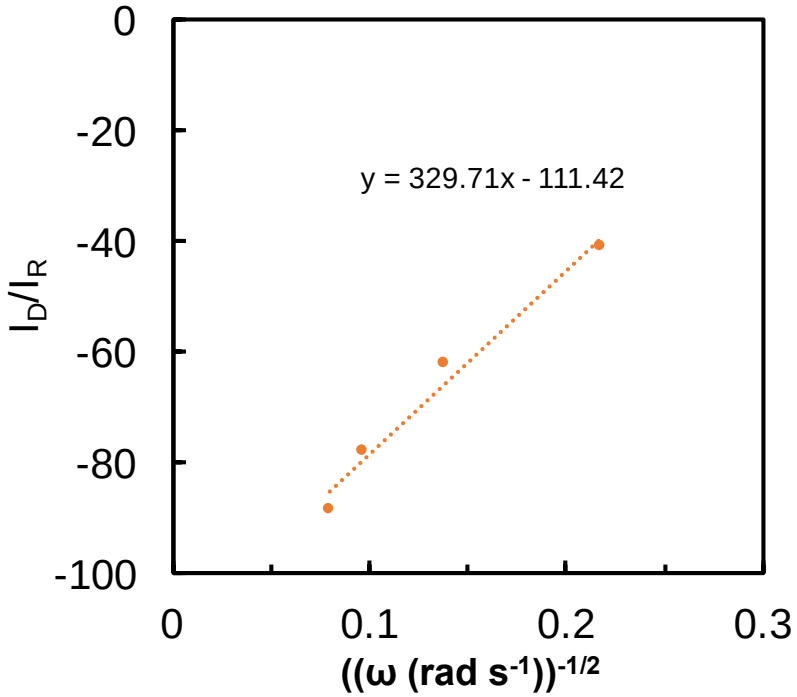

Figure 3.S2: Plot of I_D/I_R versus $\omega^{-1/2}$ to determine the parameters S_1 and I_1.

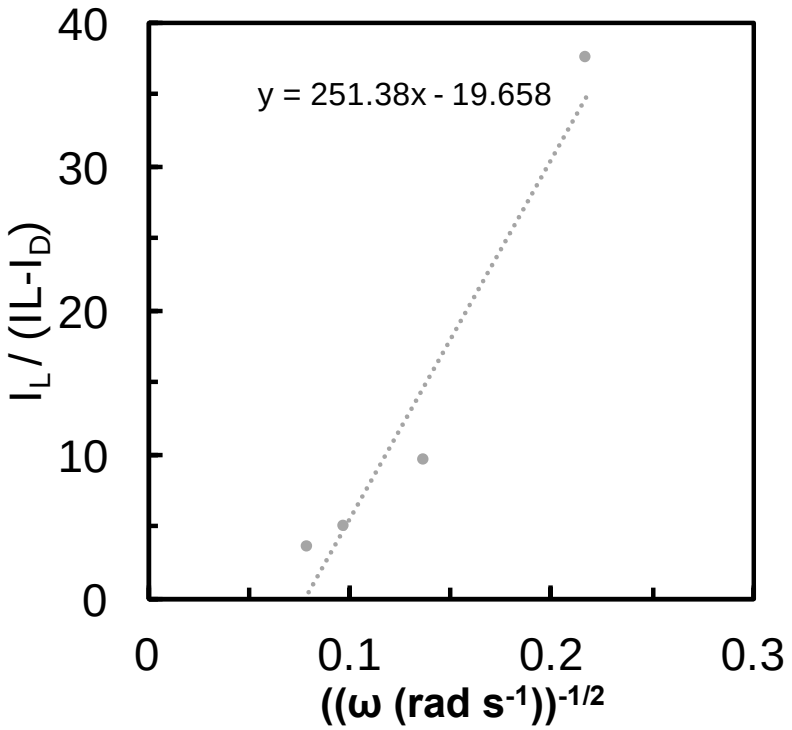

Figure 3.S3: Plot of $I_L/(I_L - I_D)$ versus $\omega^{-1/2}$ to determine the parameter S_2.

CHAPTER 4

CHARGE-DIRECTED IMMOBILIZATION OF BACTERIOPHAGE ON NANOSTRUCTURED ELECTRODE FOR WHOLE CELL ELECTROCHEMICAL BIOSENSORS

This chapter is a consolidation of the following journal publications:

- Yan Zhou, Abhijit Marar, Peter Kner, and Ramaraja P. Ramasamy. 2017, *Analytical Chemistry*, 89 (11), 5734-5741.
  Reprinted here with permission of the publisher.

- Yan Zhou and Ramaraja P. Ramasamy. 2015, *ECS Transaction*, 69, 38, 1-8.
  Reprinted here with permission of the publisher.

Abstract

A new type of carbon nanotube (CNT)-based impedimetric biosensing method has been developed for rapid and selective detection of live bacterial cells. Proof of concept study was conducted using T2 bacteriophage-based biosensors for electrochemical detection of *Escherichia coli* B. The T2 bacteriophage (virus) served as the bio-recognition element, which was immobilized on polyethylenimine (PEI)-functionalized carbon nanotube transducer on glassy carbon electrode. Charge-directed, orientated immobilization of bacteriophage particles on carbon nanotubes was achieved through covalent linkage of phage capsid onto the carbon nanotubes. The presence of the immobilized phage on carbon nanotube modified electrode was confirmed by fluorescence microscopy. Electrochemical impedance spectroscopy (EIS) was used to monitor the changes in the interfacial impedance due to the binding of *E. coli B* to T2 phage on the CNT-modified electrode. The detection was highly selective towards the B strain of *E. coli* as no signal was observed for the non-host K strain of *E. coli.* The presently achievable detection limit of the biosensor is 10^3 CFU/mL.

Keywords: Electrochemical biosensor, bacteria detection, charge-directed immobilization, electric field-induced immobilization, electrochemical impedance spectroscopy.

4.1 Introduction

Bacterial pathogens are universally present in the environment and are important targets for detection and identification in various applications, such as food safety,[142,143] environmental pollution and public health.[142,144] It is important to develop accurate and robust technologies for identification and detection of bacteria in complex matrices. Conventional methods for bacterial identification includes standard microbiology or biochemical procedures, such as culture and cell counting of bacteria, enzyme linked immunosorbent assay (ELISA) and polymerase chain reaction (PCR), etc. While being highly reliable, these methods are also laborious, time-consuming, typically expensive, and require laboratory set up, rendering them unsuitable for rapid screening purposes by an unskilled user outside the laboratory set up.[67] Biosensors are advantageous in this respect, as they are simple, easy to use, and provide rapid response for real time monitoring purposes. Biosensors are devices that incorporate a biological recognition element with high specificity towards target analyte(s). A typical biosensor consists of three components, bioreceptor (enzyme, protein, antibody, DNA and even viruses), transducer element and data processing unit.[67,145] Typically, biosensors can be categorized by the type of bioreceptors, or by the mode of transduction. The transduction mode could be optical, piezo-electric or electrochemical. Electrochemical biosensors are of particular interest because of their simplicity, fast response and high sensitivity.[146-148] The specificity and cost of an electrochemical biosensor is highly dependent on the type of the bio-recognition element being used, such as enzymes, antibodies, DNA/RNA, aptamers or bacteriophages.[149] While aptamers, antibody and enzymes possess high selectivity, they are highly susceptible to damage or loss of activity in harsh environmental conditions for bacterial cell detection. DNA-based detection methods could not distinguish viable cells from dead cells and require rigorous sample processing.[16] On the other hand, bacteriophage (or simply phage)

viruses are inexpensive, ubiquitous in nature, possess robust stability under sub-optimal environmental conditions. As a bio-recognition element, bacteriophages offer high selectivity towards their host bacteria and could discriminate between viable and nonviable cells. A phage could recognize its host bacterium through the bacterial surface receptor, followed by binding onto the bacterial cell. Upon attachment, the phage penetrates the bacterial cell membrane and injects its genetic material (DNA/RNA), which initiate protein synthesis, phage assembly and replication inside the bacterium. This leads to the bacterial cell lysis (break open) and the release of new virus particles. The mechanism reflects a recognition system in which phage particles specifically recognize and bind only to their host bacterial cells and not towards other cells. Thus, bacteriophages represent ideal choice as bio-recognition element for biosensors for bacterial cell detection.[14,76]

An electrochemical biosensing method utilizing phage as a bio-recognition element for whole cell bacteria detection could be developed by immobilizing phage particles on electrode surfaces. The use of nanostructured electrodes for phage immobilization further enhances the sensitivity of electrochemical detection. Towards this end, various approaches have been proposed to immobilize phage on electrochemical biosensor platforms, from a simple physisorption to covalent crosslinking.[79,80,150-152] Much of the efforts in the published literature have been focused on increasing the number of surface phage particles per unit area for signal enhancement purposes, in which the phage was randomly oriented on the surface for either amperometric-based electrochemical biosensor, or surface plasmon resonance-based optical biosensor construction.[14,83,152,153] Since 95% of bacteriophages isolated to date are tailed and possess asymmetric shape, it is important to achieve the desired orientation of phages on the transducer surface to function effectively as a bio-recognition element.[77,82] For *Myoviridae* phages, that

contain a distinct head (capsid)-tail structure such as the T4 phage, it is important to orient the phage in a manner that all the capture proteins (tail fiber) are exposed to target the host bacterial cells. However, a vast majority of the published literature on phage-based biosensors, do not address this problem satisfactorily. Asymmetrical phage particles immobilized on biosensor surface without a preferred orientation generally exhibit low bacteria capture efficiency as shown by Hosseinidoust *et al.* for T4 towards the capture of *E. coli* cells.[154] This underscores the importance of oriented immobilization of phage on electrode surface for biosensing purposes.

Most attempts reported in the literature for attaching phage to a surface were based on a recombinant engineering of phage capsid proteins, such as biotinylation of phage head proteins which immobilize phage in capsid down – tails up fashion.[76,77] There have also been reports about oriented phage immobilization on surfaces without recombinant engineering.[155-157] Most phages have net negative charge, with a negatively charged capsid (head) and positively charged tail fibers. This charge difference between the head and tail fibers of the phage could be utilized for immobilizing phage on electrode surface using electrostatic interaction and electrophoretic deposition. For example, H. Anany *et al.* proposed a method for the oriented immobilization of bacteriophage on positively charged cellulose membrane that attracts large number of phage particles to its surface due to their net negative charge.[155] Han *et al.* proposed the capture of T7 bacteriophage on an indium tin oxide surface through electrophoresis for virus detection. The electrophoretic trapping of phage particles offers a simple method to achieve a controllable array of phages in the correct orientation.[156] Richter *et al.* studied the behavior of phage upon aligned along the electric field and applied the phage-modified substrate for flow cytometry.[157]

In this work, we report our work on the development of an electrochemical biosensing method for bacterial cell detection using phage as a bio recognition element. Here we attempted

an electric field-induced (EFI), charge-directed orientation strategy for immobilizing bacteriophage on carbon nanotube modified electrode surface for electrochemical detection of bacterial cells. Using this immobilization method, a novel T2 bacteriophage-assisted carbon nanotube-based impedimetric biosensor was developed for *E. coli* detection, in which the T2 was immobilized on cationic polymer functionalized multiwall carbon nanotube (CNT) electrodes. T2 phage contains negatively charge on the capsids (heads) and positively charged on the tail fibers. Using electric field-induced immobilization, T2 phages could be oriented on positively charged functionalized CNT matrices to enable the chemical anchoring of phage onto the nanostructured electrode. The resulting T2 phage-modified CNT electrodes were used as biosensors for the detection of *E. coli B* using electrochemical impedance spectroscopy as the detection technique.

4.2 Experimental section

4.2.1 Materials and instruments

The following chemicals were purchased and used without further purification: sodium chloride and sodium phosphate dibasic (both from EMD chemicals), potassium dihydrogen phosphate (BDH), magnesium sulfate heptahydrate (J.T. Baker), 1-pyrenebutanoic acid succinimidyl ester (PBSE) (Sigma Aldrich), polyethylenimine (PEI) (Sigma Aldrich), yeast extract and agar powder (all from Alfa Aesar), tryptone (Amresco). Multi-walled carbon nanotubes (CNT) (diameter 8-15 nm) was obtained from Cheap Tubes Inc. SM buffer was prepared by mixing 5.8 g of NaCl, 2 g of $MgSO_4 \cdot 7H_2O$, 50 mL of 1M Tris-HCl pH 7.5, and 1 mL of 10% (w/v) gelatin in deionized water. Luria-Bertani (LB) medium was prepared by mixing 10 g of tryptone, 5 g of yeast extract and 10 g of NaCl in deionized water and adjusted to pH 7.0. LB-agar medium was prepared by adding 6 g of agar to 400 mL of LB media. 2 g of agar was added to 400 mL of LB media to obtain soft agar medium. 10X phosphate buffered saline (PBS) was prepared by mixing 16 g NaCl,

0.40 g KCl, 2.8 g Na_2HPO_4, and 0.49 g KH_2PO_4 in 200 mL deionized water yielding a buffer solution of pH 7.4. The prepared PBS was further diluted to 1X before use. All media, buffer and glassware were sterilized before use. *E. coli* B and T2 phage were purchased from ATCC (11303 and 11303-B2, respectively). *E. coli* K strain was kindly provided by Dr. Yajun Yan (University of Georgia, Athens). Glassy carbon electrode (GCE) obtained from CH Instruments was used for all electrochemical experiments (3 mm diameter).

Scanning electron microscopy (SEM) images of the modified electrode were obtained using FEI Inspect FEG electron microscope. Attenuated Total Reflectance-Fourier transform infrared spectroscopy (ATR-FTIR) measurements were performed on carbon nanotube coated silica wafer in Nicolet 6700 instrument. Fluorescence images were obtained using EVOS fluorescence microscopy (Invitrogen). Surface charge of carbon nanotubes, bacteria and phage particles were analyzed by ZetaSizer (Malvern). Contact angle measurements to determine hydrophobicity of the CNT electrodes before and after PEI functionalization were performed by a KrüSs DSA 100 using a 1 μL drop of 18 MΩ water (pH 7).

4.2.2 Bacteria preparation and phage propagation

E. coli B (ATCC 11303) were grown in 4 mL of LB medium overnight at 37 °C. 1 mL aliquot of the overnight culture was inoculated into 100 mL of fresh LB, followed by incubation for 3 h at 37 °C in an incubator shaker. 1 mL of the culture was then centrifuged at 4000 g for 10 min to remove medium and washed with 1X PBS buffer for twice before each experiment. Enumeration of bacteria was performed by plate count techniques and expressed in CFU/mL. T2 bacteriophage (wild type) was amplified using soft agar overlay techniques (see detailed method in the Supporting Information). Plaque assay was applied to measure the phage titer and was expressed in PFU/mL prior to use.

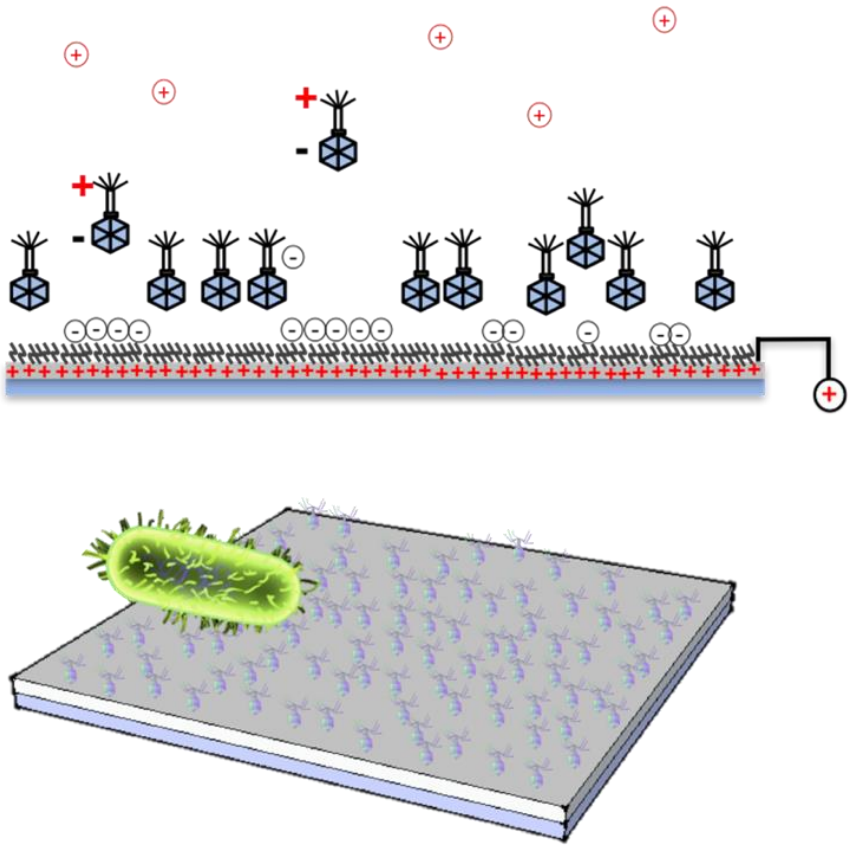

Figure 4.1: Schematic description of the charge-directed orientation and immobilization of bacteriophage onto PEI-functionalized CNT on electrode surface.

4.2.3 Phage immobilization and electrode preparation

Multiwall carbon nanotubes (CNT) was functionalized with polyethylenimine (PEI) to obtain positive surface charge as previously reported (See detailed method in the Supporting Information).[158] To facilitate phage immobilization onto CNT modified electrode surface, a positive potential was applied on working electrode for phage deposition, followed by covalent linkage of phage through PBSE onto PEI-*f*-CNT (see Figure 4.1). Glassy carbon electrode was used as working the electrode and was modified using the following procedure: 2 mg of PEI functionalized multiwall carbon nanotube (PEI-*f*-CNT) was dispersed in 1 mL deionized water. The suspension was ultra-sonicated for 10 min prior to use. 12 µL PEI-*f*-CNT was dropcast on

glassy carbon electrode (GCE) surface and dried. Prior to phage attachment, the PEI-*f*-CNT modified GCE was activated with succinimidyl ester (PBSE) as molecular tethering agent. For this, 4 μL of 10 mM PBSE solution (in DMF) was dropcast on the PEI-*f*-CNT modified GCE electrode and allowed to react for 15 min on ice. The excess unreacted PBSE was removed by rinsing the electrode with DMF, followed by PBS buffer.[48,49,159-161] For electric field-induced immobilization, a positive potential of +0.5 V *vs* Ag/AgCl was applied to the working electrode for 1h in a 1X phosphate buffer solution (PBS) containing bacteriophage (~10^9 PFU/mL) in order to facilitate the charge-directed immobilization process. Finally, the phage immobilized electrode was rinsed using SM buffer and covered with 50 μL *E. coli* B suspension for 30 min. After *E. coli* incubation, the electrode was rinsed with buffer and was used to perform electrochemical impedance measurements. For control experiments, the biosensor was tested in the buffer without bacteria (negative control) and in the buffer with non-host *E. coli* K strain (positive control). Seven-fold serial dilutions (10^2-10^8 CFU/mL) of *E. coli* B were prepared for bacterial cell detection experiments.

4.2.4 Fluorescence imaging of bacteria and phage

To characterize the surface immobilized phage, 100 μL of phage solution (10^{10} PFU/mL) was stained with SYBR gold, a fluorescent nucleic acid dye with EX/EM of 495 nm/537 nm, at a final concentration of 5X for 20 min at room temperature. Free dye was removed by centrifugation (see detailed method in the Supporting Information).[162] Phage was then added to electrochemical cell for electric field-induced immobilization using CNT coated ITO glass slide as working electrode. The reason for using the ITO glass slide as electrode instead of GCE is due to the practical difficulties in accommodating the rod shaped GCE inside the fluorescence microscope. Same experimental procedure as mentioned earlier for GCE was used to immobilize phage onto

ITO surface in dark. The resulting ITO was used for fluorescence characterization (APPENDIX I).[163]

4.2.5 Infectivity of immobilized phage

Phage immobilized CNT coated ITO glass slide was prepared using the same method to study the infectivity of the immobilized phage. The infectivity of the immobilized phage was verified using the disk diffusion technique as reported elsewhere.[164] The agar plates were topped with cut-out electrode discs immobilized with phage particles. The agar plates were inspected on the subsequent day for lysis rings around the electrode disks. ITO glass slides with no phage were used as a negative control.

4.2.6 Electrochemical characterization

Electrochemical characterization was conducted using CHI-920c model potentiostat (CH Instruments Inc, Austin, TX). A conventional three-electrode cell (a working electrode, an Ag/AgCl reference electrode and a Pt wire auxiliary electrode) was used for electrochemical measurements. All the electrochemical measurements were carried out at 25 ºC ± 2 ºC in a 5 mL voltammetry cell containing 5 mM $Fe(CN)_6^{3-/4-}$ (1:1) mixture in 1X PBS buffer, unless otherwise stated. Impedance was measured at the open circuit potential, with a superimposed AC voltage of amplitude 5 mV between frequencies 100 kHz and 10 Hz.

4.3 Results and Discussion

4.3.1 Characterization of PEI-functionalized CNT

Successful functionalization of PEI on CNT was verified using ATR-FTIR measurements of the modified electrode to study the characteristic peaks of the functional groups on the CNT surface. The resulting ATR-FTIR spectra are shown in Figure 4.2. The presence of amide bond due to PEI functionalization of CNT was confirmed by C=O adsorption at 1690 cm^{-1}. The O-H

group resulting from the acid treatment of CNT was observed at 3440 cm^{-1}. In addition, two absorption peaks at 2931 and 2854 cm^{-1} in the spectra could be assigned to CH_2 stretching in the alkyl chain of PEI. Meanwhile, adsorption due to CN stretching was identified at 1370 cm^{-1}. The identification of these peaks confirmed the successful functionalization of CNT with PEI based on the literature.[165]

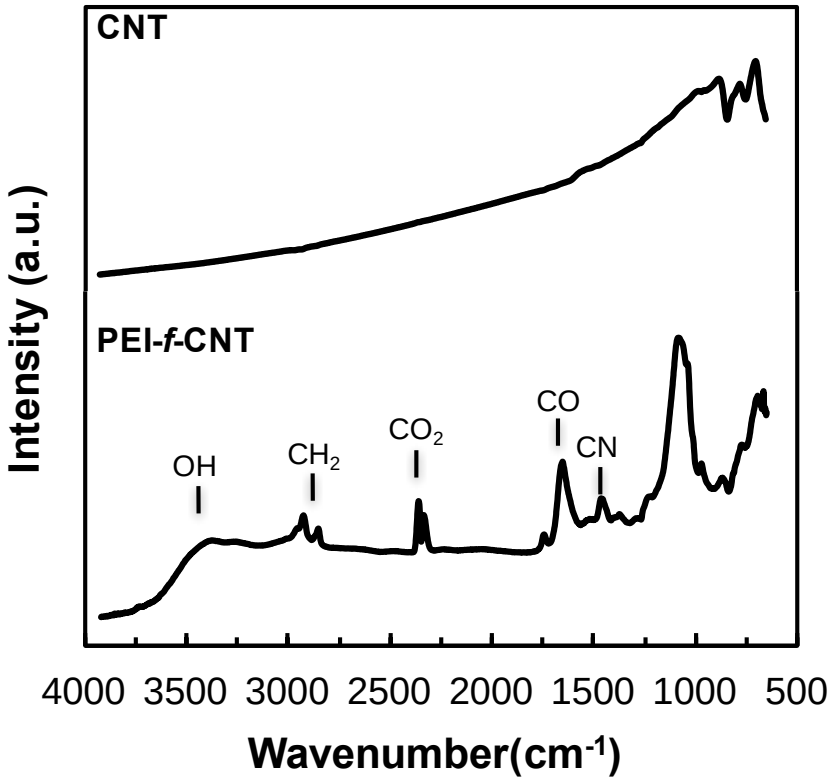

Figure 4.2: ATR-FTIR spectra of unmodified and PEI-*f*-CNT.

Figure 4.3 shows the SEM images of CNT before and after PEI modification differentiating the morphology of the nanostructured electrode before and after cationic polymer functionalization. Some aggregation of CNT occurred after PEI functionalization of CNT with formation of many mesopores as shown in the Figure 4.3. The surface amine functional groups increased the surface energy on CNT and made the surface more hydrophilic resulting in the low contact angle of 29° (see inset in Figure 4.3) for contact between water droplet and the CNT coated surface. On the

other hand, the surface functional groups also altered the surface charge and the zeta potential of CNT. The zeta potentials of CNT, PEI-*f*-CNT in pH 7.4 PBS were -20.2 ± 0.7 mV and +12.4 ± 0.8 mV, respectively. Positively charged PEI-*f*-CNT hence prepared was used as for the immobilization of negatively phage particles in further studies.

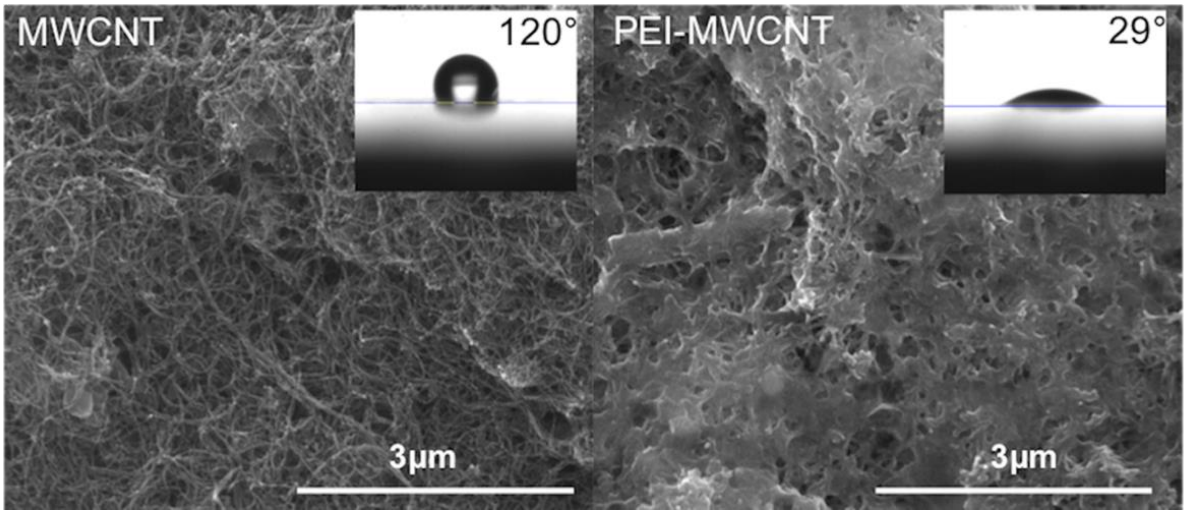

Figure 4.3: SEM images of CNT before and after PEI modification. Inset: Images of water droplet on the substrates and their contact angles.

4.3.2 Characterization of immobilized bacteriophage

Zeta potential measurements elucidate the surface charge and colloidal stability of biological particles. The zeta potential of T2 phage in PBS buffer was measured as -10.0 ± 0.8 mV, resulting in a net negative charge.[155] However the charge distribution varies along the length of the phage with the capsid being more negatively charged and the tail being more positively charged.[155] *E. coli* (ATCC 11303) has zeta potential of -9.7 ± 1.1 mV. In order to achieve the highest capture efficiency of bacteria with immobilized phage particles, T2 phage particles should be immobilized with its positively charged tail-spike proteins exposed to negatively charged bacterial cells. The heads down-tail up fashion of phage on the electrode would help orient the phage towards bacterial cell capture by the exposed tail fibers and this orientation is facilitated

through PEI functionalization of CNT and subsequent electric field-induced immobilization of phage onto PEI-CNT. As previously discussed, the electric field-induced immobilization described in the Figure 4.1 uses the hetero-bifunctional molecular tethering agent PBSE for establishing covalent linkage between the phage and the PEI-*f*-CNT. The aromatic pyrene moiety of the PBSE interacts with CNT side walls through π-π stacking as demonstrated in our previous work,[29,48,49,87,161] while NHS ester moiety binds with primary amine groups in the surface proteins (of T2) to form amide bonds. The PBSE based molecular tethering method has been demonstrated before for enzymes and bacterial cells, but never has been explored before for tethering viruses on CNT.[48] For phage immobilization, the electric field was induced by applying a potential of +0.5 V *vs* Ag/AgCl to the PEI-*f*-CNT electrode for 1 h using 10^9 PFU/mL phage solution. During electric field-induced immobilization, an electrical double layer could form in the proximity of electrode surface on which the phage is deposited (Figure 4.1). The formation of this negative ion layer may decrease the intensity of the electric field inside the electrolyte, resulting in disorientation of phage particles. The orientation of the phage particle are related with Debye length (κ^{-1}) on the CNT surfaces.[157] The phage particles will align along the lines of the electric field within the small volume when κ^{-1} is larger than the size of the phage. When κ^{-1} is smaller than the size of phages, the orientation of the phage particles occurs due to electrostatic interaction.[166,167] In our case, T2 phage is much larger than typical κ^{-1} (few nanometers). Thus, it can be concluded that the immobilized phages were preferentially attached on to the CNT modified electrode in head down-tail up orientation as described in Figure 4.1. To further visualize bacteriophage on electrode surface, T2 bacteriophage were labeled using a DNA intercalating SYBR Gold dye. An electric field was applied as mentioned previously to the PEI-*f*-CNT electrode. The covalent linkage between phage and the CNT is formed by the PBSE as described above.

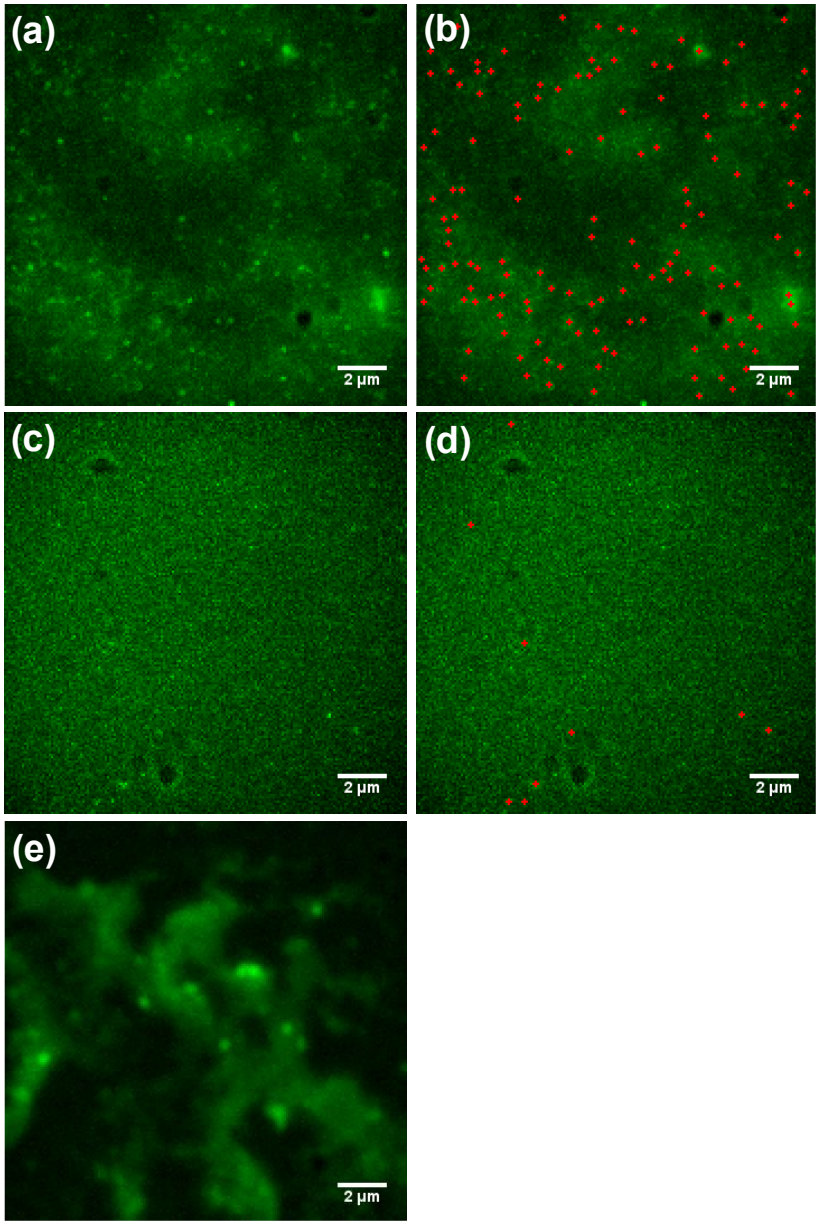

Figure 4.4: Fluorescence images of: (a-b) Surface immobilized phage particles by electric field-induced covalent immobilization; (c-d) Surface immobilized phage particles by covalent immobilization without applying electric field; (e) CNT surface in the absence of phage particles. (b) and (d) are the same images as that of (a) and (c) with the phages highlighted in red color. 140 phage particles were detected in (a), and 9 were detected in (b) using the method described above. The laser power was 114 W/cm^2 for images (a-d) and 343 W/cm^2 for images (e).

The resulting fluorescence images of the immobilized phages are shown in Figure 4.4. The images in Figure 4.4a-b confirm a successful immobilization of bacteriophages onto PEI-*f*-CNT using electric field-induced, charge directed immobilization method. About 140 phage particles were observed on a matrix size of 16 μm ×16 μm. Control experiment for phage immobilization without electric field (no voltage applied) resulted in only 9 phage particles on the PEI-*f*-CNT as shown in Figures 4.4c-d. No phage particles were observed in the negative control (in the absence phage) in Figure 4.4e. The fluorescence seen in Figure 4.4e is due to the autofluorescence of the CNTs which is well established in the literature and therefore should not be confused with that of the fluorescence from phage particles.[168] The higher intensity of the CNT in Figure 4.4e can be explained due to the higher intensity used while imaging (343 vs. 114 W/cm^2) and also from the fact that the substrate in Figure 4.4e was aligned in the focal plane as opposed to Figures 4.4a-d where the CNT were out of focus. From these results, it can be concluded that the electric field-induced immobilization methods result in 15 X higher loading of phage particles on the electrode surface, ensuring high bio-receptor loading on the electrode surface for host bacterial cell detection.

Since there is no feasible and reliable method for estimating the number of the receptors on the electrode surface, the activity of the immobilized phages was verified for their infectivity using disk diffusion method.[164] This infectivity study requires a flat electrode and therefore CNT-coated ITO glass was used as working electrode for this purpose. The ITO electrode was further incubated on a lawn of bacteria using soft agar overlay method. As shown in Figure 4.S1, a lysed rings up to 1 mm thick were found around the ITO electrode with immobilized phages, whereas ITO electrode without phage in Figure 4.S1b showed no such lysis rings around the electrode. The results indicate that the immobilized phages were able to lyse (kill) bacteria cells and were thus deemed active and infectious. The T2 phage modified PEI-*f*-CNT nanostructured electrode was

then evaluated as a biosensor for the detection of *E. coli* B using electrochemical impedance spectroscopy.

4.3.3 Electrochemical characterization and bacteria detection

Electrochemical impedance spectroscopy (EIS) was used to further characterize the assembly of the biosensor in a PBS (pH 7.4) containing 5 mM $Fe(CN)_6^{3-/4-}$ as the redox couple. EIS was reported as an effective and non-destructive method to monitor electrode surface characteristics. In the presence of $Fe(CN)_6^{3-/4-}$, the impedance measured is the Faradaic impedance of the redox couple.[67] Supplementary Figure 4.S2 illustrates the results of Nyquist plot ($-Z_{im}$ *vs* Z_r) of bare PEI-*f*-CNT and phage modified PEI- *f*-CNT in the presence of 5mM $Fe(CN)_6^{3-/4-}$ redox couple in PBS (pH 7.4). As shown in Figure 4.S2a, an obvious semicircle was observed at high to medium frequencies, corresponding to electron transfer-limited process, which was followed by a linear region representing the semi-infinite diffusion (mass transfer-limited process). After phage immobilization, the diameter of the semicircle was significantly increased in comparison with bare PEI-functionalized CNT. This is due to the fact that phage particles immobilized on the surface act as a protein-insulating layer with negative charge, resulting in hindered electron transfer of the redox couple. Herein, we compared three phage immobilization methods: (1) electric field-induced immobilization followed by PBSE covalent linkage; (2) PBSE covalent immobilization only for two hours; (3) PBSE covalent immobilization overnight. In covalent immobilization, electrodes were activated with PBSE and then incubated with phage suspension for 2h and overnight, respectively. In control experiment, the same procedures were performed using buffer solution (in the absence of T2 phages). Figure 4.S2b shows comparison of $\mathbf{\Delta}R_{CT}$, the charge transfer resistance variation after immobilization using different immobilization methods. After electric field-induced immobilization of phage particles, R_{CT} increased due to phage attachment. An average of an

increase of ~13Ω of charge transfer resistance was obtained with buffer containing T2 phage particles. There is no significant increase in charge transfer resistance in the absence of T2 phage upon application of voltage. As shown in Figure 4.S2b, with increase of incubation time, an increase of charge transfer resistance was observed. However, the charge transfer resistance did not increase as much as that for electric field-induced immobilization of phage. In these cases, the mechanism of phage immobilization was rather electrostatic interaction than electric field-induced interaction due to the positive charge on PEI-CNT surface. The results show that electric field-induced (EFI) immobilization of phage achieved higher loading of phage particles (as measured by the largest variation in the R_{CT} of the electrode upon phage immobilization) on the electrode surface compared to non-EIF immobilization. This observation is consistent with the results of the fluorescence images. The high phage loading on CNT could help to enhance the biosensor performance as evaluated and discussed below. Figure 4.5a illustrates the representative open circuit Nyquist plots measured using the phage-modified nanostructured electrodes for the 5mM $Fe(CN)_6^{3-/4-}$ redox couple obtained both in the absence and presence of bacteria (at different concentration expressed in CFU/mL) in the electrolyte solution. The equivalent electrical circuit, also called Randles circuit, used to fit the Nyquist data is also shown as an inset in Figure 4.5a. This model consists four circuit elements, including the electrolyte resistance (R_Ω), charge transfer resistance (R_{CT}), double layer capacitance (C_{dl}), and Warburg impedance (Z_w). Among them, R_Ω and Z_w represent the ohmic resistance of the electrolyte solution and the mass transfer impedance for the diffusion in and out of the redox couple from electrolyte bulk to the surface, respectively. C_{dl} represents a nonideal capacitance at the electrochemical interface. The arc of the Nyquist plot reflects the charge transfer resistance R_{CT}, which is determined by the type of surface modification and the kinetics of the redox reaction. The capture of bacterial cells on phage-modified electrode

surface could alter the surface properties of electrode which in turn vary the impedance measured on the biosensor electrode.

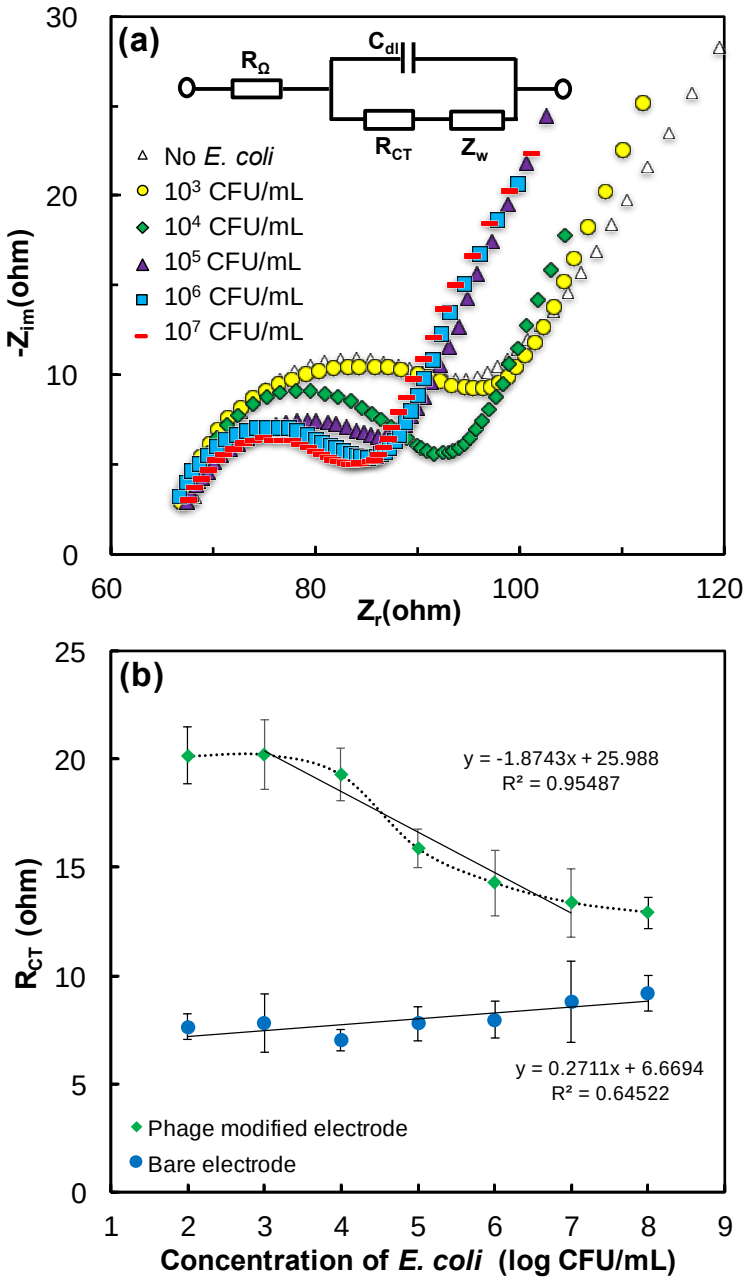

Figure 4.5: (a) Nyquist plot for T2-modified electrode in the absence and presence of *E. coli* B at different concentrations. (Inset: Randles equivalent circuit); (b) Variations of charge transfer resistance at different *E. coli* B concentrations with phage modified electrodes and bare electrode.

To evaluate the sensitivity of the biosensor, the phage-modified nanostructured CNT electrode was used for the detection of *E. coli* B from its suspensions of different concentrations (10^2-10^8 CFU/mL). The bacterial cell suspensions were incubated on the phage-modified electrode surface then rinsed before the AC impedance measurements. Impedance measurements were made at different *E. coli* B concentrations and the results were compared with that of the control where no *E. coli* was present. As shown in Figure 4.5a, the diameter of the Nyquist arc decreased with increasing bacterial cell concentrations suggesting a direct influence of bacterial cell attachment on the impedance of the above redox reaction. As expected, a significant variation was observed in R_{CT} upon the *E. coli* attachment onto phage modified nanostructured electrodes, and the difference is amplified at high *E. coli* concentrations (see magnitude of the arc in Figure 4.5a). Table 4.S1 shows the fitted data of parameters such as R_Ω and C_{dl}. A considerable decrease of charge transfer resistance was observed after 30 min contact between surface immobilized phage and *E. coli*. In many impedimetric biosensors, charge transfer resistance usually increases with increasing *E. coli* concentration.[169-172] Such increase in R_{CT} due to *E. coli* attachment could be attributed to the lowering of redox kinetics at the interface, as *E. coli* could act as a barrier on the electrode blocking the accessible CNT sites for $Fe(CN)_6^{3-/4-}$ redox reaction.

In order to completely understand the relation between charge transfer resistance and surface attached bacterial cells, a live/dead cell viability assay was performed to study the interaction between bacteria cells and surface immobilized phage particles. According to the fluorescence images shown in Figure 4.6, the immobilized T2 was seen to disturb the integrity of the cell membrane with increasing incubation time. The images in Figure 4.6 show a progressive decrease of green fluorescence (viable *E. coli* cells) and increase of red fluorescence (dead *E. coli* cells) due to phage infection. A distinct variation in the number of viable *E. coli* cells was noticed

after 20 minutes and the cells were completely compromised after 25 min, suggesting the infection time of *E. coli* and the lytic cycle of immobilized phages was around half an hour. It is reasonable to assume all *E. coli* cells that remained on the electrode surface were attached to phage particles. However, not all bacterial cells were compromised at the same time. The released phages from lysed cells may further infect surrounding bacterial cells resulting in increasing number of red fluorescence over longer periods of time. Above all, immobilization of phages onto electrode surface shortened the latent period of phage. The fluorescence study also indicated that the electrochemical measurements were conducted during the lysis of bacterial cells. In the present electrochemical impedance measurements, the subsequent decrease of charge transfer resistance happens presumably as the consequence of phage infection and bacterial cell lysis. Following the lysis of bacterial cells, progeny phages could be released and induce more disruption of cell walls and release of intracellular components. As observed by Shabani and Mejri, the released intracellular components may increase the surrounding medium conductivity at the electrode surface which contributes to the decrease of charge transfer resistance.[151,173] As shown in Table 4.S1, R_{CT} decreases with increasing number of bacteria cell concentration. Correspondingly, the values of C_{dl} at different bacterial concentrations shows a 40% increase in the double layer capacitance of the electrode at high bacterial concentrations. The slight increase of double layer capacitance (from 10^4 to 10^6 CFU/mL) may result from the increase of dielectric permittivity caused by higher number of bacterial cell lysis. Given that phage latent period would be shortened after surface immobilization, with high concentration of bacterial cells binding onto electrode surface, cell lysis may happen simultaneously on the electrode surface. More phages will be released and induce further infection of surrounding bacterial cells. This chain of events will contribute to greater amount and faster release of intracellular ions in the form of cell lysate, which

could influence the electrical double layer thickness and in turn influence the charge transfer resistance.[151]

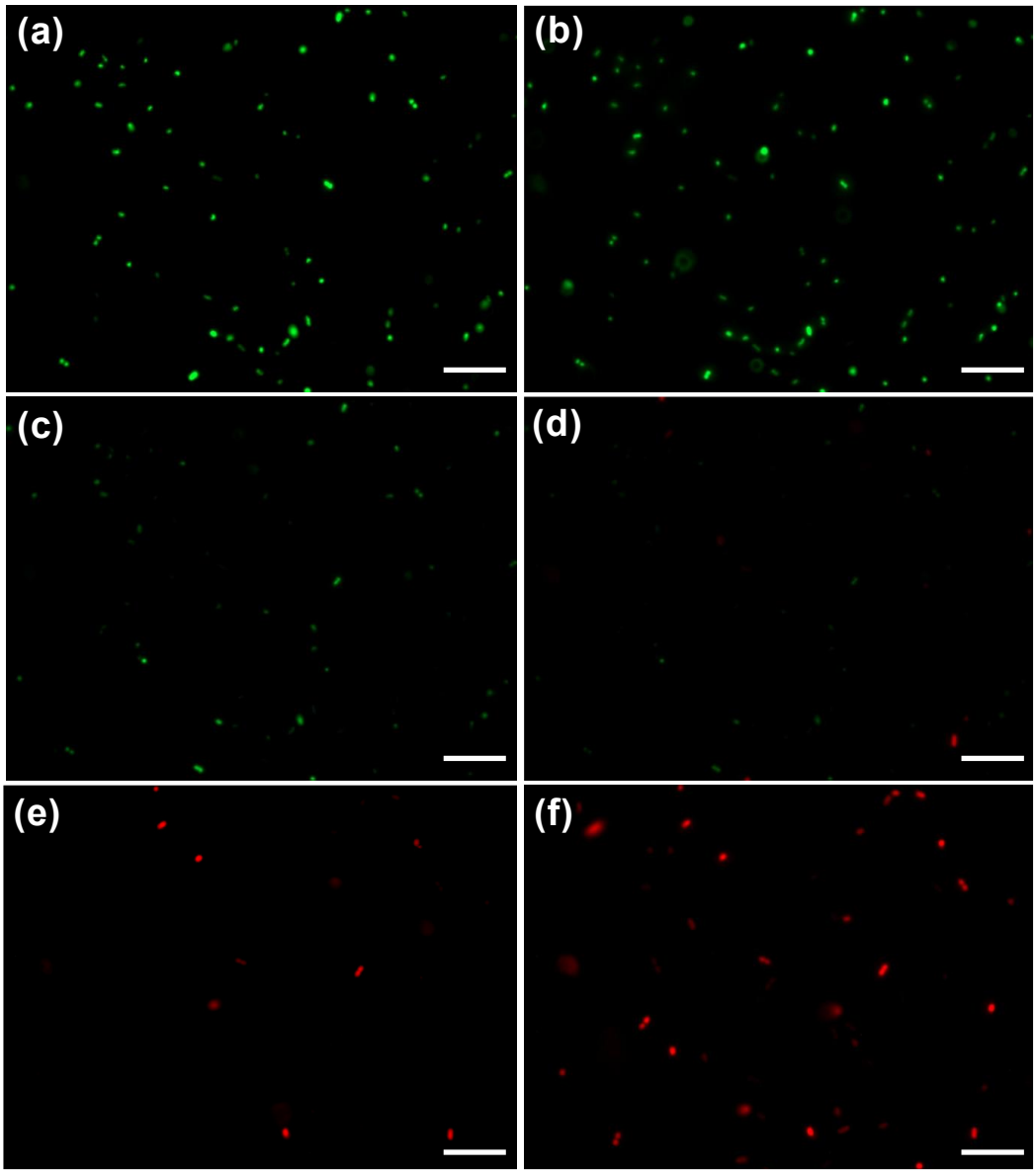

Figure 4.6: Representative images of bacterial cell lysis monitored by fluorescence microscope using the Backlight bacteria viability kit. (a) 10 min; (b) 15 min; (c) 20 min; (d) 25 min; (e) 30 min; (f) 35 min. Green dots represent live bacteria, and red dots represent lysed bacteria. The scale bar is 10 μm.

On the contrary, when only few bacterial cells bind to the electrode surface, the cell lysis may not have huge impact on surrounding bacterial cells and the charge transfer resistance. This effect was observed in Table 4.S1 for low bacterial cell concentrations (10^2-10^3 CFU/mL). Figure 4.S3 represents our hypothesis for the above argument. When high concentration of bacterial cells binds onto the electrode surface, the cell lysing process may happen simultaneously on the electrode surface. More phages will be released as a result which induce further infections of surrounding bacterial cells. This chain of events will contribute to greater amount and faster release of intracellular ions in the form of cell lysate, which could influence the electrical double layer thickness and in turn influence the charge transfer resistance. On the contrary, when only few bacterial cells bind to electrode surface, the lysis of few cell may not cause the same impact and does not cause a major change in charge transfer resistance. This effect was observed in Table 4.S1 for low bacterial cell concentrations (10^2-10^3 CFU/mL). As shown in Figure 4.S4, when bacterial cell concentration is high, lysis process releases high quantities of intracellular ions fairly quicker than that of low bacterial cell concentrations. So when the impedance was measured at 30-35 minutes (black dotted line), we observe low RCT for high concentration of cells. However further studies are needed to better understand the role of the intracellular ions during cell lysis on the interfacial impedance of the electrode.

A linear correlation between R_{CT} and the bacterial concentration was observed between 10^3 and 10^7 CFU/mL as shown in Figure 4.5b. No significant variation in R_{CT} was observed for concentrations below 10^2 CFU/mL in a 50 μL *E. coli* suspension. At and above bacterial cell concentrations of 10^7 CFU/mL, the change in charge transfer resistance is insensitive to changes in cell concentration, which may be due to surface saturation of adhered cells. The lowest concentration that can be determined to be statistically different from a blank (noise) is considered

as the limit of detection (LOD) of the sensor. The LOD is recommended to be a measurement level of 3σ units above the value of blank, where σ is the standard deviation of the blank.[4] The LOD was calculated from the slope of calibration curve according to the following equation: LOD = kσ/m, where k = 3, σ = standard deviation of blank, and m = slope of calibration curve. The calculated LOD is 10^2 CFU/mL which resides below the linear range, where calibration curve is no longer valid. Therefore, in order to define the smallest concentration of bacteria that can be detected, we used k = 5 for LOD calculation in order to provide a more conservative estimation of LOD. The detection limit of the biosensor hence determined was 1.5×10^3 CFU/mL in a 50 μL *E. coli* volume. For control experiment, the same set of detection experiments were performed using bare PEI-*f*-CNT electrodes (without phage) to identify non-specific adsorption of *E. coli* cells as shown in Figure 4.5b. A comparatively minor R_{CT} variation was observed over the same concentration range. The sensitivity of bacterial detection by phage-based biosensor could be influenced by the type of immobilization method used for attaching phage to the electrode surface as reported in the literature.[14,80,83,151-153] In the present study, the phage-based biosensor achieved a detection limit of 10^3 CFU/mL for *E. coli* B, which is better than most impedimetric sensors reported before.[169-172] Bacteriophages were treated as charged particles which could be immobilized onto working electrode. By electric field-induced alignment, a high loading of phage particles could be immobilized through charge directed orientation and covalent attachment. More importantly, the surface cationic polymer modified CNT interacts with negatively charged phage capsid followed by PBSE-based covalent linkage, leading to oriented immobilization and higher bacteria capture efficiency. As a result, the electric field-induced immobilization of phage particles could in turn affect the overall biosensor sensitivity.

4.3.4 Selectivity of the phage-based impedimetric biosensor

To evaluate the specificity of the T2 phage towards the B strain of *E. coli*, the biosensor was tested using non-host control bacteria *E. coli K* strain (at 10^3~10^6 CFU/mL,). As shown in Figure 4.S4, no plaques were observed after incubating T2 phage with K strain *E. coli*. When evaluated electrochemically using impedance, similar conclusion could be reached. Figure 4.7a shows the Nyquist plots of T2 phage-modified electrodes in the absence and presence of B (native host) and K strains (non-host) of *E. coli*. Figure 4.7b shows the variation in R_{CT} upon increasing bacterial concentrations. The figure shows little to no variation in charge transfer resistance for the K strain compared to the B strain, clearly demonstrating the biosensor is non-responsive to the non-host *E. coli* K strain. The results demonstrate that the phage-biosensor is highly specific only to the target host strains of the bacterial species.

4.3.5 Detection of *E. coli B* using screen printed electrode

In order to achieve real time detection, screen printed electrode was adopted using same phage immobilization strategy for detection of *E. coli B via* impedance spectroscopy as shown in Figure 4.8. Scanning electron microscopy (SEM) was used to verify the binding of bacteria to phage particles immobilized on SPE. As shown in Figure 4.9, the phage-modified CNT exhibited a homogenous morphology before the binding of the *E. coli* cells. The phage particles being too small are not visible in Figure 4.9a. After exposing the electrode surface to 50 μL (10_8 CFU/mL) of the host *E. coli* cells for 30 minutes, the SEM images clearly show the attachment of *E. coli* cells onto the phage-modified electrodes as shown in Figure 4.8b. Electrochemical impedance measurements were then performed using the T2 phage immobilized SPE. Figure 4.10 shows the impedance results (Nyquist plots) of the phage-modified electrode obtained with and without bacterial suspension. The bacterial suspensions at varying concentrations (10^3-10^9 CFU/mL) were

placed on the phage-modified surface for 30 minutes, and then rinsed before the AC impedance measurements.

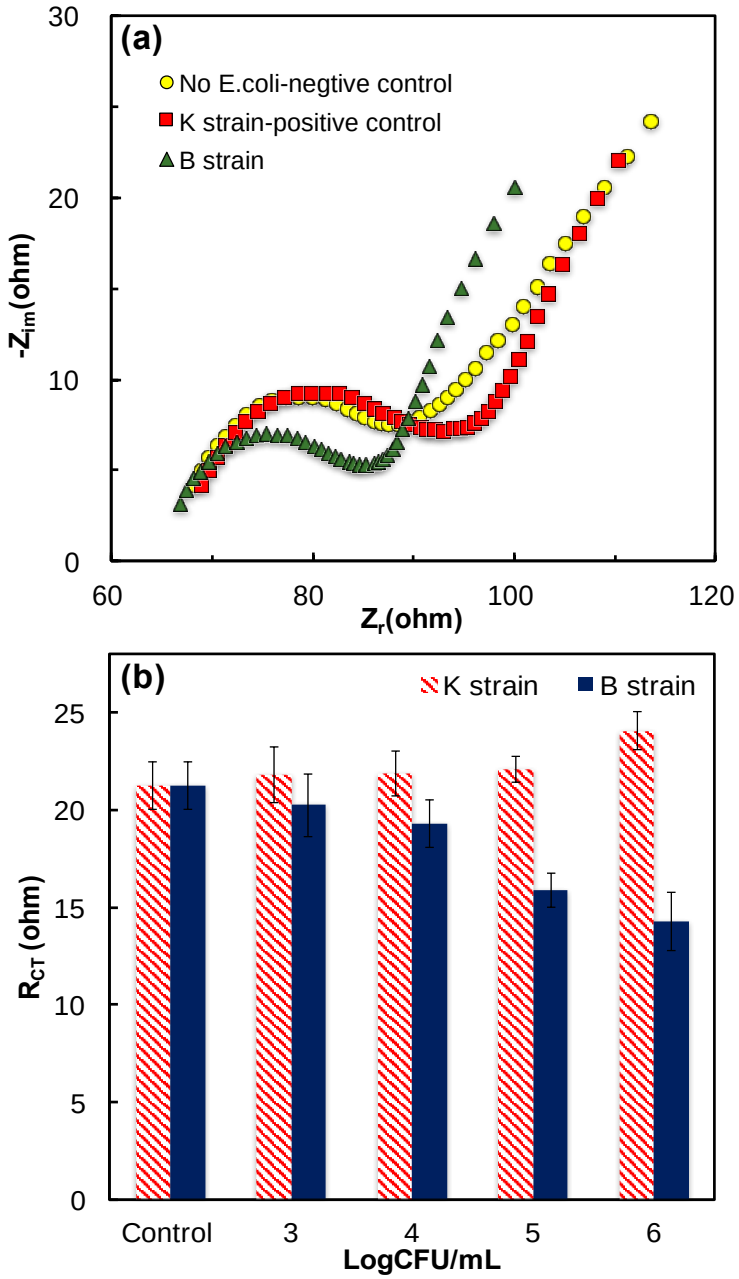

Figure 4.7. (a) Nyquist plot of T2-modified electrode in the absence and presence (10^6 CFU/mL) of native host (B strain) and non-host (K strain) *E. coli*. (b) Variation of R_{CT} with increasing bacterial concentrations for B and K strains of *E. coli*. (Values are the average of 3 replicates).

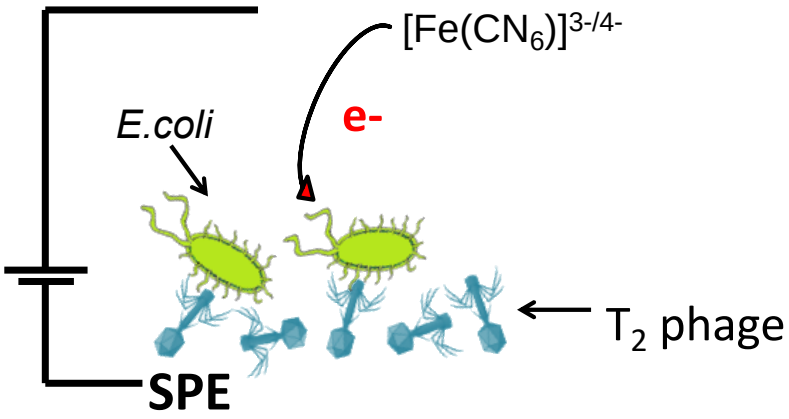

Figure 4.8: Schematic of electrochemical detection of *E. coli* using T2 bacteriophage modified screen printed electrode.

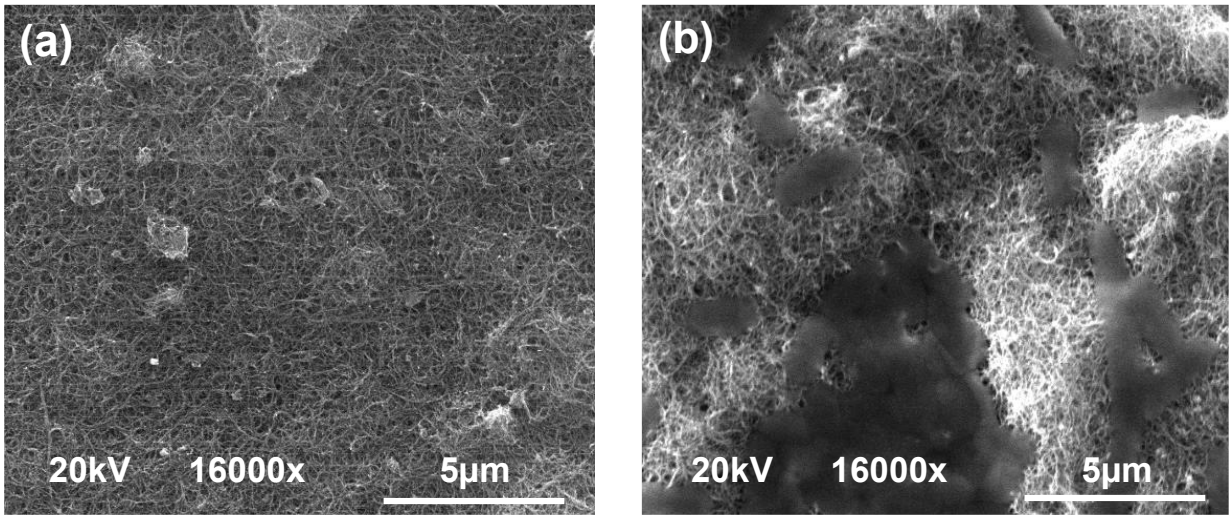

Figure 4.9: SEM images of phage-modified CNT electrodes: (a) before bacteria attachment; and (b) after bacteria attachment.

The equivalent circuit used for fitting the Nyquist plots is also shown in Figure 4.10. Figure 4.10 showed that charge transfer resistance, underwent a decrease with increasing bacterial concentration. No significant change in charge transfer resistance was observed for a concentration

below 10^2 CFU/mL in 50 µL bacteria suspension. A linear correlation between RCT and the bacterial concentration was observed as shown in Figure 4.10b.

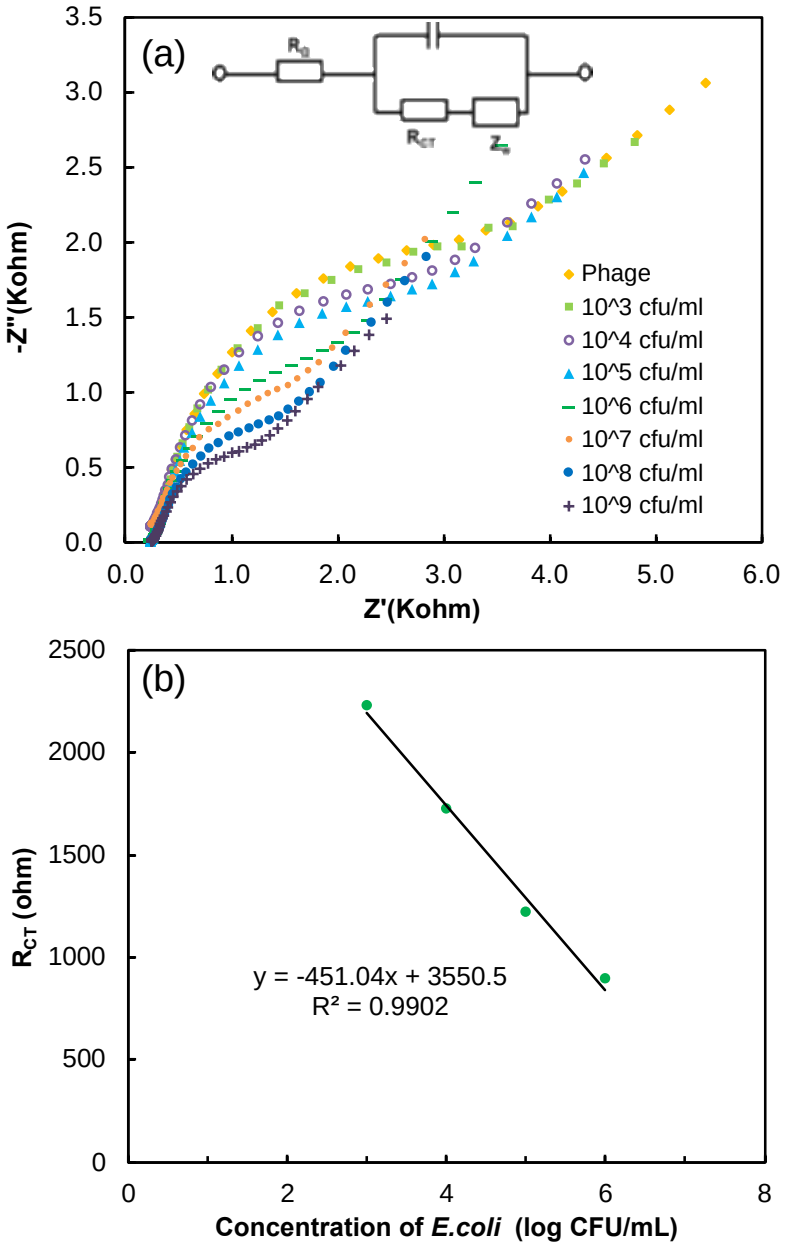

Figure 4.10: (a) Nyquist plot for T2-modified SPE in the absence and presence of *E. coli* B at different concentrations. The inset is the equivalent circuit used for fitting the Nyquist data; (b) Variation of charge transfer resistance at different *E. coli* concentrations.

The charge transfer resistance was found to be linear between bacterial concentration 10^3 and 10^7 CFU/mL with a lower detection limit of 50 CFU/mL. Finally, to evaluate the specificity of the T2 phage towards the B strain of *E. coli*, experiments were performed with phage-modified electrode in the present of *E. coli* K strain (at 10^8 CFU/mL, Figure 4.10) towards which T2 phage has no activity. As expected, there was no significant variation in the impedance spectra of the phage-modified electrode in the high-to-medium frequency region before and after exposure to *E. coli* K strain as shown in Figure 4.11. The results demonstrate that the phage-biosensor is highly specific only to the target host organisms, which in this case is the *E. coli* B strain.

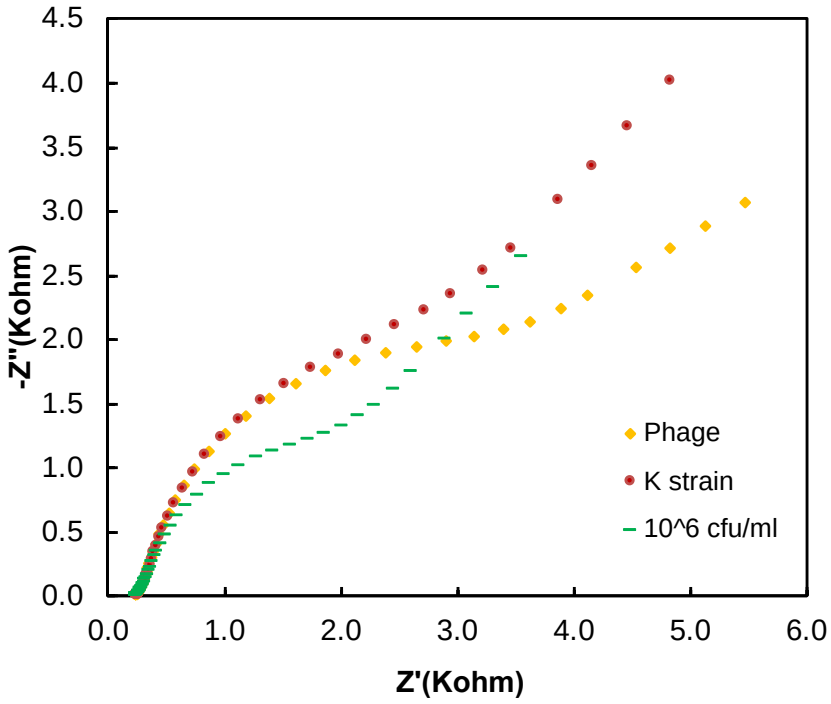

Figure 4.11: Nyquist plot for the detection of *E. coli* K strain.

4.4 Conclusion

We have demonstrated a new approach for whole cell bacteria detection using bacteriophage-assisted CNT-based electrochemical biosensor. A reliable method for oriented

immobilization of bacteriophages on CNT was developed by combining electric field-induced, charge-directed immobilization and covalent crosslinking. Bacteriophage particles was deposited with tail up and capsid down orientation, followed by covalent binding onto PEI-functionalized CNT sidewall through molecular crosslinkers. This new approach offers a high loading of bio-recognition molecule on the transducer surface, which in turn results in increased sensitivity of the biosensor. The immobilized phage particles retained their high infectivity towards host bacteria cells as confirmed by fluorescence microscopy. The biosensor was highly selective towards *E. coli* B strain with a reliable detection limit of 10^3 CFU/mL. Future studies would also focus on improving the performance of the biosensor by extending phage deposition time and increasing substrate surface area to obtain higher surface coverage of phages. Also a homogeneous electrode surface, for example, electrode with CNT directly grown on the surface, will definitely be helpful for uniform surface deposition, leading to oriented phage immobilization with minimal particle aggregation. The charge-directed immobilization method for bacteriophage attachment on CNT that has been developed in this work, could be widely applied for the developing of other type of biosensors and biological electrodes.

4.5 Supplementary Data

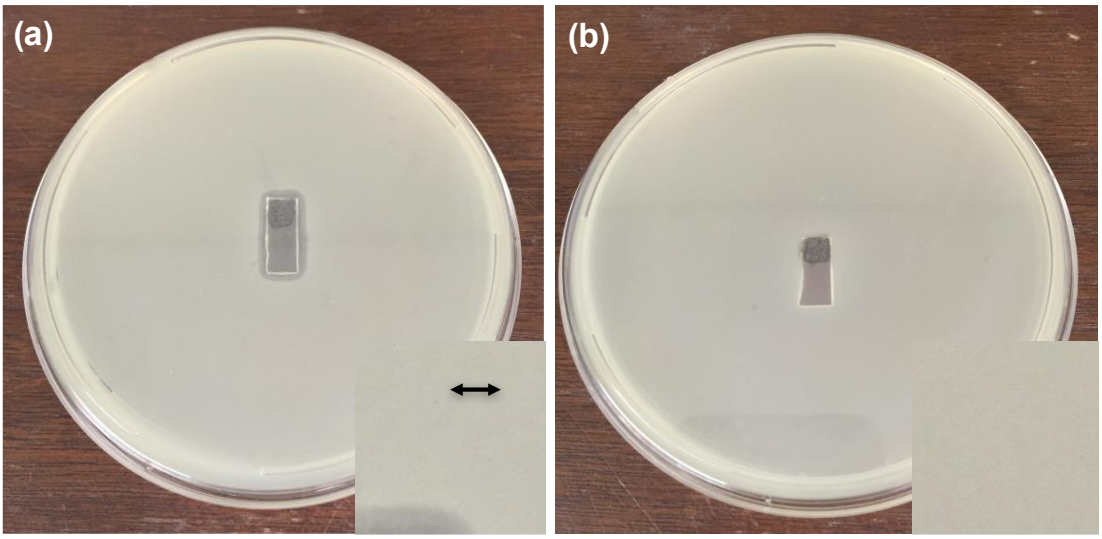

Figure 4.S1. Immobilized phage infectivity study. (a) Lysis rings were formed around the ITO electrode with immobilized phages. Inset shows the plaques formed around the ITO electrode up to 1 mm thick; (b) No plaque was formed around the ITO electrode without surface immobilized phages.

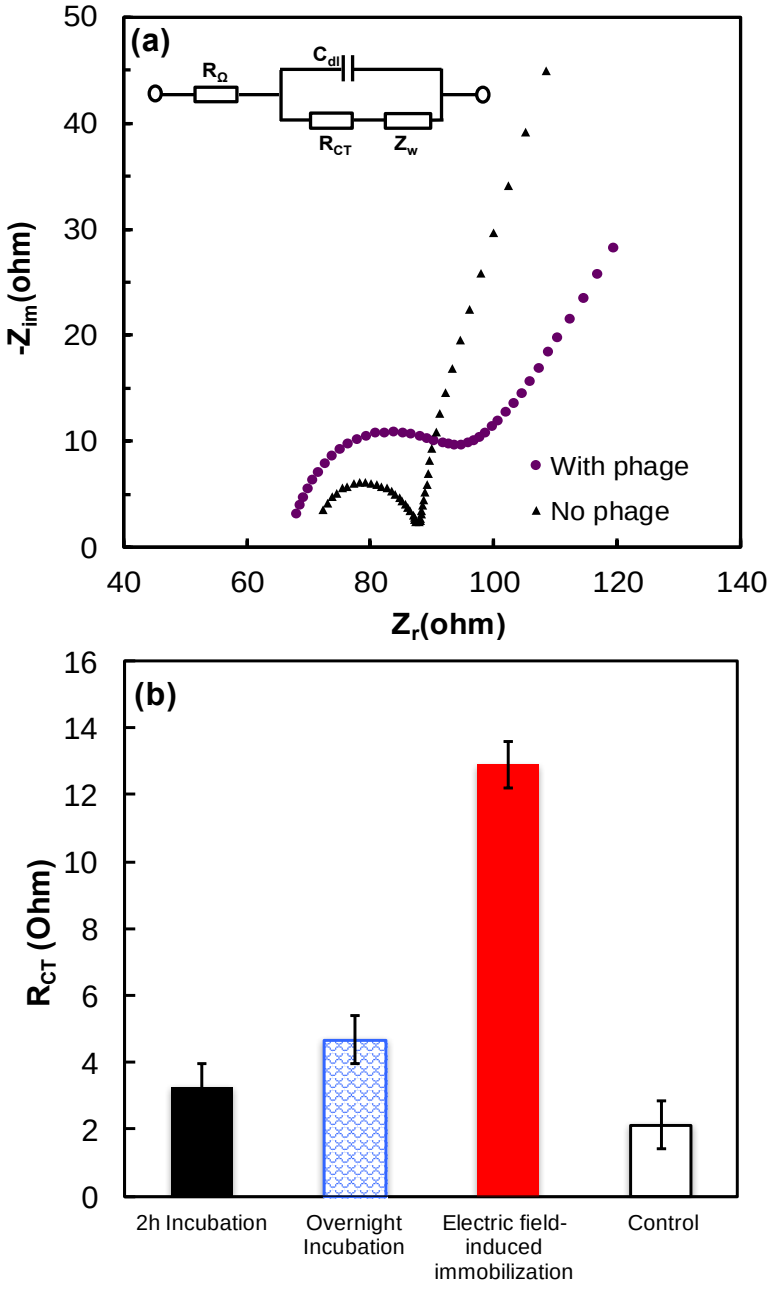

Figure 4.S2. (a) Nyquist plot for PEI-*f*-CNT electrode in the absence and presence T2 phages (Inset: Randles equivalent circuit). Phage was immobilized using charge- directed electric field-induced immobilization method; (b) Comparison of ΔR_{CT} of different immobilization methods. The highest ΔR_{CT} was obtained for electric field-induced immobilization, suggesting highest phage loading.

Table 4.S1. Values of equivalent circuit for bacteria detection. The geometric electrode surface area is 0.071cm^2

CFU/mL	R_S (Ω)	R_{CT} (Ω)	C_{dl} (F)
0	69.22	21.24	7.21E-07
10^2	70.11	20.57	7.74E-07
10^3	68.23	20.70	7.92E-07
10^4	68.27	19.33	5.32E-07
10^5	66.80	14.06	6.81E-07
10^6	67.62	13.32	8.91E-07
10^7	67.58	12.59	6.64E-07

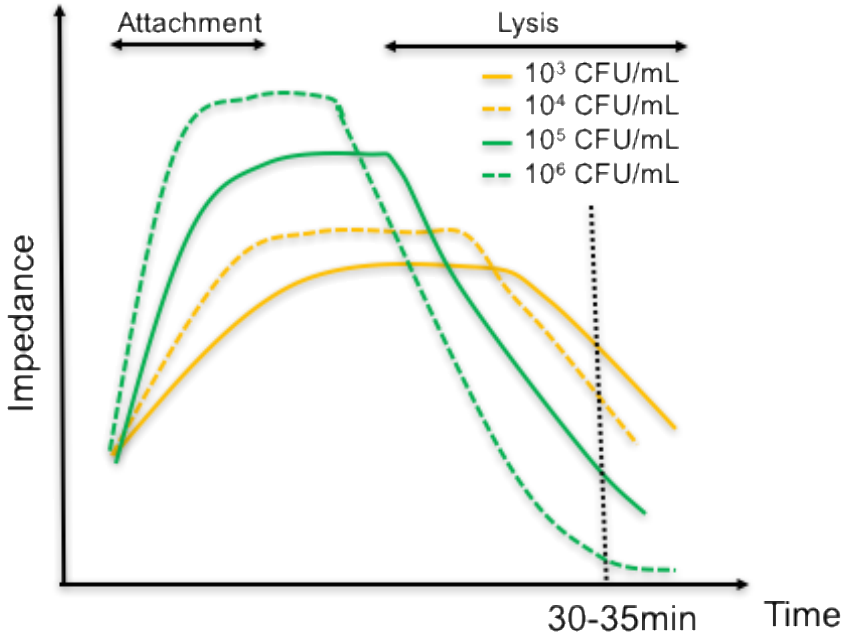

Figure 4.S3. Hypothesis of the relation between bacterial cell concentration and impedance variation from cell attachment to cell lysis process. The black dotted line represents the electrochemical measurement at 30-35 min.

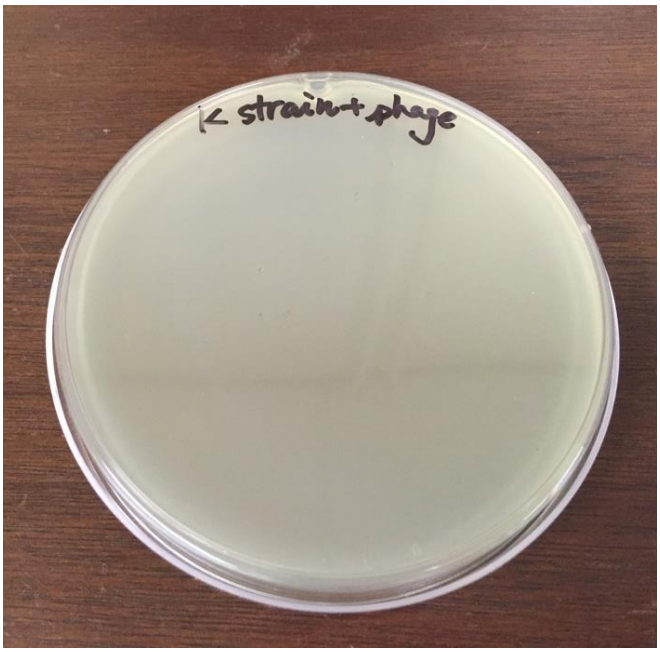

Figure 4.S4. Plaque assay of *E. coli* K strain with T2 phage. No plaques were observed after overnight incubation**.**

CHAPTER 5

ISOLATION AND SEPARATION OF LISTERIA MONOCYTOGENES USING BACTERIOPHAGE P100-MODIFIED MAGNETIC PARTICLES

Yan Zhou and Ramaraja P. Ramasamy. Submitted to Colloids and surfaces B: Biointerfaces.

Abstract

A bacteriophage-assisted magnetic separation method was developed for isolation of *L. monocytogenes* from complex food matrices. The aim of this study was to understand the importance of phage immobilization methods and the magnetic particle sizes on the effectiveness of phage coupling to the magnetic particles, the retention of phage's infectivity on the magnetic particle and the bacterial cell capture efficiency of the resulting phage-modified magnetic particle. More specifically, bacteriophage P100-modified magnetic particles (PMMP) were developed for separation of *L. monocytogenes* from complex food matrices. Three sizes of MP (150 nm, 500 nm, and 1 µm) were used for phage immobilization *via* chemical and physical methods. The coupling ratio of phage was investigated and the performance of each PMMP complex was evaluated by their *Listeria* capture efficiency. When compared to chemical immobilization method, physical immobilized PMMP complex achieved higher capture efficiency initially with excellent selectivity towards target strain. The PMMP was further tested for selective isolation of *L. monocytogenes* using real food samples such as ground beef and whole milk.

Keywords: Bacteriophage P100; *L. monocytogenes; Listeria* enrichment; magnetic separation; phage immobilization method; capture efficiency.

5.1 Introduction

Listeria monocytogenes is a food-borne pathogen frequently found in frozen vegetables, meat, raw milk, packed salad and raw milk cheese that causes severe foodborne illnesses. It has one of the highest fatality rates among common food-borne pathogens.[59] *L. monocytogenes* could grow over a wide temperature range from -0.4 to 45 °C, under both aerobic and anaerobic conditions and over a wide pH range.[60] Due to its high tolerance for harsh environments, *L. monocytogenes* could contaminate food at multiple points in the food processing chain. The FDA allowable limits for *Listeria monocytogenes* contamination in ready-to-eat (RTE) food products is <1 CFU/25 g of food that supports the growth of *L. monocytogenes* and 100 CFU/g of food that do not support its growth.[61,62]Conventional methods for identification of *Listeria* in food matrices include plating on selective and differential agar and/or biological and serological confirmation. These methods of identification require separate pre-concentration or enrichment steps in order to collect sufficient quantity of bacterial cells to enable a reliable identification. Moreover, during the enrichment process, nonpathogenic specie may compete and outgrow *L. monocytogenes*, leading to false-negative results during identification.[59,66] While being reliable and accurate, traditional methods are also time-consuming and need well-trained operators to conduct the experiment. Therefore, it is critical to develop new analytical methods that help in rapid and reliable identification of *Listeria* in food samples.

In recent years, immunomagnetic separation (IMS) has been widely used in the pathology labs for separation and identification of target bacteria from different food.[174,175] In IMS, mono-clonal antibodies are used as recognition elements that are immobilized onto magnetic particle surfaces for bacterial cell separation in the presence of a magnetic field.[63] IMS could significantly shorten enrichment time, and improve the sensitivity of detection, but it is prone to false positive

identification through non-specific interactions between non-target cells and magnetic particles.[176] Moreover, the antibodies are typically expensive, susceptible to pH and temperature variations making them less suitable for non-laboratory testing. Commercially available 2.8 µm Dynabeads coupled with polyclonal antibodies were proved to be capable of separating target bacterial cells but with a low capture efficiency generally (7-23 %).[59,64,177] Therefore, it is a pressing need to develop improved methods for bacterial cell isolation/enrichment/separation of *Listeria* from complex food matrices in order to enable rapid screening of *Listeria* in food samples.

Similar to antibodies, bacteriophages offer high selectivity toward their host bacteria and could discriminate between viable cells and dead cells.[178] In addition, phages are inexpensive, ubiquitous in the nature and possess robust stability under sub-optimal conditions. A phage could recognize the target bacteria through the receptors located on bacterial cell surface. Upon host recognition, the phage selectively binds to the bacterial cell wall. The genetic material of phage is then injected into the bacterial cell, which initiates protein synthesis, phage assembly and replication. The high selectivity of bacteriophage towards its host could be utilized for bacterial cell isolation and enrichment from food samples as an alternative to antibody-based bacterial separation methods.[179-183] The United States Department of Agriculture (USDA) has approved two bacteriophages for *L. monocytogenes* control in foods: LISTEX^{TM} P100 and LMP-102.[184,185] Phage-based magnetic separation of *Salmonella* cells from food samples has been previously reported.[186,187] However, there is very little information in the literature about the importance of phage immobilization methods on the effectiveness of phage coupling with magnetic particles, retention of phage's infectivity after immobilization and the bacterial cell capture efficiency.[13,188,189]

In this work, we have addressed major knowledge gaps in this area. Here, we report our

experimental study on the use of bacteriophage P100 as a model bio-receptor to study phage immobilization on magnetic particles for separation and isolation of *L. monocytogenes* from food matrices. More specifically, we studied the effect of phage immobilization methods and the size of magnetic particles on the effectiveness of phage attachment (coupling) to the magnetic beads and its bacterial cell capture efficiency. Three different sizes of magnetic particles (150 nm, 500 nm and 1 μm) and two different phage immobilization methods (physical and chemical) were investigated. In many literatures, covalent chemical immobilization method is commonly adopted for phage immobilization. However, very few studies have reported the importance of phage immobilization methods on the effectiveness of phage coupling with magnetic particles.[13,186] Upon immobilization, the P100 phage-modified magnetic particles (PMMP) were used for *L. monocytogenes* separation from dilute contaminated buffer solutions and the resulting capture efficiency were investigated. The PMMP were also used for selective isolation of *L. monocytogenes* from whole milk and ground beef samples to demonstrate their suitability for field applications in food industry.

5.2 Material and methods

5.2.1 Materials and instruments

The following chemicals were purchased and used without further purification: sodium chloride and sodium phosphate dibasic (both from EMD chemicals, Port Wentworth, GA), potassium chloride (J.T. Baker, Center Valley, PA), potassium dihydrogen phosphate (BDH, West Chester, PA), magnesium sulfate heptahydrate (J.T. Baker, Center Valley, PA), agar powder (Alfa Aesar, Ward Hill, MA), bis(sulfosuccinimidyl)suberate) (BS3) (Cova Chem, Loves Park, IL), Tris-HCl(Fisher Scientific, Fair Lawn, NJ), Brain heart infusion medium (Sigma-Aldrich, St. Louis, MO) SM buffer was prepared by mixing 5.8 g of NaCl, 2 g of $MgSO_4 \cdot 7H_2O$, 50 mL of 1M Tris-

HCl pH 7.5, and 1 mL of 10% (w/v) gelatin in deionized water. Brain heart infusion (BHI) medium was prepared by adding 37 g of BHI powder in deionized water and adjusted to pH 7.4. BHI-agar medium was prepared by adding 6 g of agar to 400 mL of BHI media. 2 g of agar was added to 400 mL of BHI media to obtain soft agar medium. 10X phosphate buffered saline (PBS) was prepared by mixing 16 g NaCl, 0.40 g KCl, 2.8 g Na_2HPO_4, and 0.49 g KH_2PO_4 in 200 mL deionized water yielding a buffer solution of pH 7.4. The prepared PBS was further diluted to 1X before use. All media, buffer and glassware were sterilized before use. *Listeria monocytogenes* Scott A strain was kindly provided by Dr. Michael Doyle (University of Georgia, Griffin). P100 bacteriophage (commercial name LISTEX^{TM}) was purchased from Micreos Food Safety (Wageningen, The Netherlands). The amine functionalized magnetic beads of 150 nm, 500 nm, and 1 µm size were purchased from Ocean Nanotech (Springdale, AR). The magnetic separation of the particles during the washing steps were carried out using a magnetic separation rack (Bel-Art, Wayne, NJ). A tube rotator (VWR, Suwanee, GA) was used for mixing steps at a speed of 18 rpm.

5.2.2 Bacterial strains and culture conditions

Listeria monocytogenes Scott A was used throughout the separation experiments unless otherwise stated. *L. monocytogenes* was cultured in 4 mL BHI medium overnight at 37 °C. 500 µL aliquot of the overnight culture was inoculated into 50 mL of fresh BHI medium by shaking at 200 rpm for 5 h at 37 °C in an incubator shaker. 1 mL of the bacteria culture was transferred into 1.5 mL centrifuge tube and the cell suspension was centrifuged at 4000 g for 10 min. The supernatant was removed and bacterial cell pellet was resuspended with 1X PBS buffer and washed twice before each separation experiment. Enumeration of bacteria was performed by plate counting

method and cell count was expressed in CFU/mL. All other bacterial strains were grown in LB medium using similar growth conditions as described above.

5.2.3 Preparation of bacteriophage-functionalized magnetic particles

Three different sizes of amine functionalized magnetic particles (MP) were used for phage immobilization: 150 nm, 500 nm and 1 μm. 20 μL of MP (10 mg/mL) was aliquoted and added into a 1.5 mL micro-centrifuge tube. Followed by sterilizing the particles with 70 % ethanol, the tube was placed on a magnetic separator to remove the ethanol. The particles were washed three times using 1X PBS buffer (coupled with 0.01% Tween 20). PBS buffer was then added into the tube to form a suspension of MP. As depicted in Figure 5.1a, phages were immobilized onto MP surface via two methods. The chemical immobilization of phages was achieved using bis(sulfosuccinimidyl)suberate) (BS3) crosslinker, which reacts with the surface amine moieties of phage particles resulting in amide bond formation. In physical immobilization method, the immobilization of phage particles was mainly driven by Van der Waals and electrostatic interactions.[12,70] For the preparation of chemical immobilization of phages onto MP surface, 10 mM of BS3 in PBS was prepared, syringe-filtered and added into the MP suspension. The mixture of BS3 and MP were reacted for 30 minutes at room temperature with continuous mixing using the tube rotator to allow the activation of MP surfaces. After 30 minutes, the tube was placed into the magnetic separator for activated MP separation. The particles were then washed three times with 500 μL of PBS buffer to remove excess BS3 and then re-suspended in 400 μL PBS buffer. Finally, phage particles (10^8 or 10^9 PFU) were added into the MP suspension to react overnight at 4 °C under continuous mixing at 18 rpm using tube rotator. The prepared phage-modified MP (PMMP) was then magnetically separated and washed three times with PBS buffer. The supernatant was removed and placed in another tube to perform plaque assay, in order to determine

the free phage quantity in the supernatant. The PMMP were resuspended in 500 μL SM buffer and incubated for two hours at 4 °C under continuous mixing to terminate the excess surface activated residuals. The thus-prepared phage chemically functionalized MP of different sizes were designated as PMMP-150Ch, PMMP-500Ch and PMMP-1000Ch, respectively. For physical immobilization, no pre-activation of MP surfaces was needed. Phage particles were directly added into sterilized MP suspension to react overnight at 4 °C under continuous mixing at 18 rpm using tube rotator. The phage-modified MP were then washed three time with PBS buffer. The supernatant was also obtained for plaque assay study. Excess surface activated residue was terminated using SM buffer as mentioned previously. The thus-modified MP were noted as PMMP-150Ph, PMMP-500Ph and PMMP-1000Ph, respectively. The phage-modified MP (PMMP) were finally stored at 4 °C for later use in bacterial cell separation experiments. Plaque assay was used to determine the phage quantity and infectivity of PMMP in the collected supernatant. Briefly, the obtained collected supernatant sample was serially diluted with 1X PBS buffer and added to a test tube containing 3 mL molten soft agar (0.5 %) with 250 μL of *L. monocytogenes* culture. The solution was poured over BHI agar plate and incubated overnight at 30 °C. The visible plaques were counted the following day. The initial phage quantity was also determined using plaque assay before each experiment. The remaining phage quantity in the supernatant was then compared with the initial phage quantity in order to calculate the phage coupling ratio (CR) of PMMP, which is defined as follows: $CR=1-C_S/C_I$, where C_S is the number of free phages remaining in the supernatant after separation and C_I is the initial number of phages used for immobilization. Data were collected from three independent experiments were analyzed in duplicate unless otherwise stated.

5.2.4 Bacterial capture efficiency determination

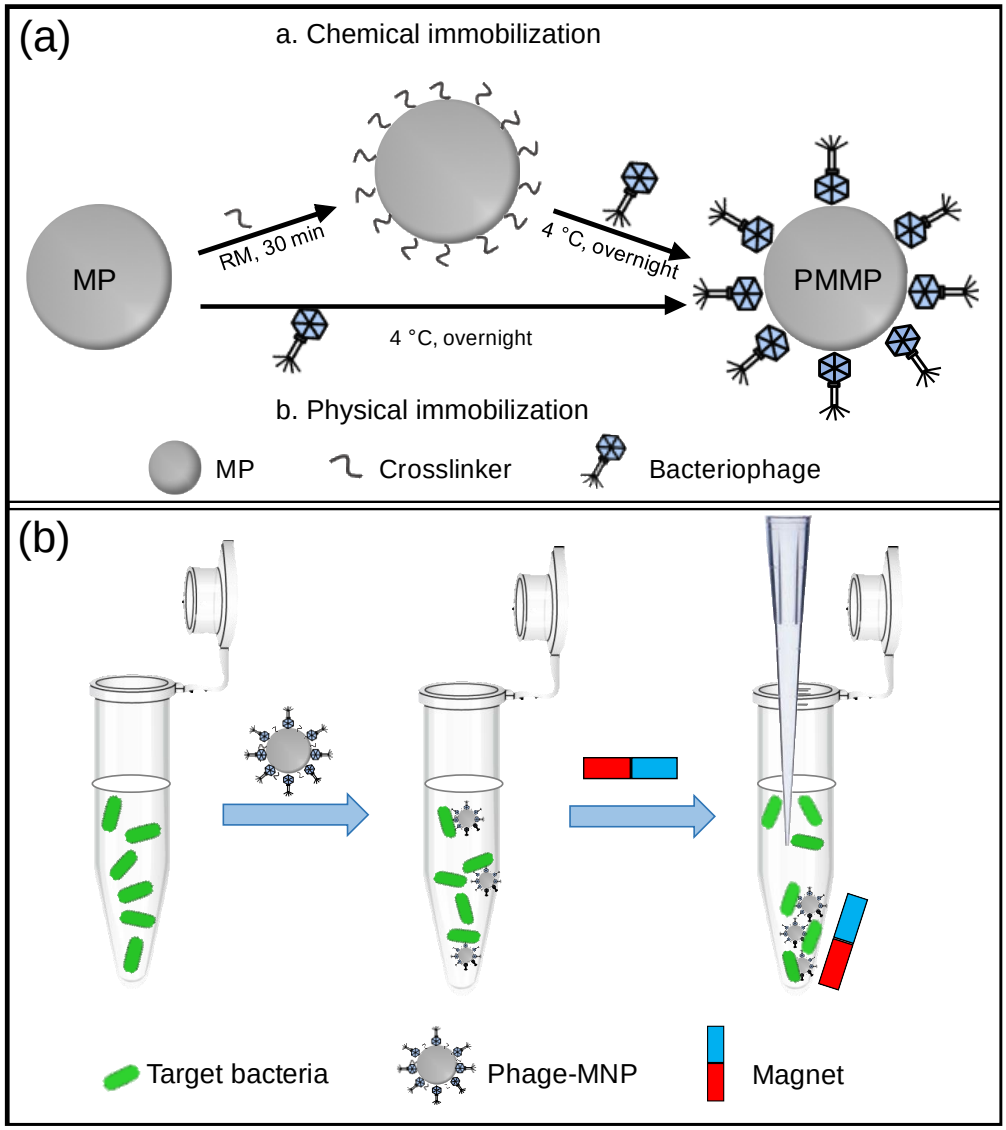

Figure 5.1: (a) MP modification with bacteriophage *via* chemical and physical immobilization methods; (b) Magnetic separation of *Listeria monocytogenes* captured on PMMP from bacterial suspension.

Bacterial cell separation was performed using 500 µL of bacterial cell suspension in micro-centrifuge tubes. The process of separation was illustrated in Figure 5.1b. *L. monocytogenes* cells were serial diluted to make 10^2 to 10^6 CFU/mL cell suspension in PBS buffer, as confirmed with

plate counting technique. Subsequently, different volumes of the 0.4 mg/mL functionalized magnetic particles (20 µL, 40 µL, 80 µL, 120 µL, and 140 µL) were added to the sample and incubated at room temperature for 10 min without agitation, and then for 5 min with rotation using tube rotator. The MP-bacteria complex was then separated using a magnetic separator over a period of 5 min. The supernatant was collected and plated on BHI agar plates which were then incubated at 37 °C for 24 to 48 hours for quantification. The initial *L. monocytogenes* cells were also plate-counted in order to calculate the number of captured cells. The capture efficiency (CE) was then calculated using the formula: $CE(\%)=(1-C_S/C_I)\times100$, where C_S is the number of *L. monocytogenes* cells remaining in the supernatant after separation and C_I is the initial total number of *L. monocytogenes* cells in the sample.

5.2.5 Microscopy characterization

The capture ability of PMMP was qualitatively observed using scanning electron microscopy. Each PMMP sample of 80 µL was added into 500 µL *L. monocytogenes* cell suspension of 10^6 CFU/ mL for bacterial capture. The mixture was incubated at room temperature for 10 min without agitation and then for 5 min with rotation using tube rotator. After that, the MP with attached bacteria were washed with PBST(X3), and then re-suspended in sterilized water. The resulting suspension was then filtered through a Nucleopore membrane (13 mm Ø, 0.1 µm/0.2 µm pore size). The filters were pre-fixed using 3% glutaraldehyde in pH 7.4 phosphate buffer for overnight at 4°C, and post-fixed with osmium tetroxide for 2h. After fixation, the samples were rinsed and dehydrated with ethanol gradient. Samples were then mounted on metallic stubs with adhesive carbon tapes and sputtered with gold for 30 s before scanning microscopy observation. The capture ability of PMMP were also characterized using fluorescence microscopy. PMMP (1 µm) suspension was added into 500 µL SYBR gold labeled *L. monocytogenes* sample for cell

separation, followed by the separation process as previously mentioned. After that, the PMMP with attached bacteria were washed with PBS(X3), and then resuspended in PBS buffer. A single drop of the resulting suspension on a glass slide was examined using fluorescence microscopy.

5.2.6 Selectivity and stability study

The selectivity of the PMMP towards *L. monocytogenes* was evaluated using other non-target bacterial strains such as *Escherichia coli B* (ATCC 11303), *Staphylococcus aureus* (ATCC 6538), *and Enterococcus faecalis*, provided by Dr. Hitesh Handa (University of Georgia, Athens). Each bacteria strain was cultured in LB medium at 37 °C and then serial diluted to 10^4 CFU/mL in PBS buffer. *L. monocytogenes* was also cultivated to a final concentration of 10^4 CFU/mL. Any binding of PMMP to non-target bacteria was tested by plate counting method as described above in order to determine the selectivity of the phage-MP towards *L. monocytogenes*. The long-term stability of the phage-modified MP was evaluated by monitoring the activity of PMMP using plaque assay. For this purpose, phage-MP complexes were prepared with 1 µm magnetic particles using both physical and chemical functionalization methods. The prepared PMMP-1000Ch and PMMP-1000Ph were stored at 4 °C in SM buffer, and intermittently warmed to room temperature before use in stability tests. Data were collected from three independent experiments were analyzed in duplicate and the mean values were obtained and compared with the initial activity of PMMP to determine the stability.

5.2.7 Capture of *L. monocytogenes* from contaminated food samples

In order to evaluate the capture of *L. monocytogenes* by PMMP from real food samples, whole milk and ground beef purchased from local grocery store were used as the food matrix for bacteria growth. For this test, 25 g of whole milk or beef was spiked with *Listeria monocytogenes* in 225 mL of PBS buffer to make the stock food sample (10^3 CFU/mL). Both PMMP-1000Ch and

PMMP-1000Ph were tested for *L. monocytogenes* separation and 80 µL of either was added to 500 µL of stock food sample. The mixture was incubated for 10 min without agitation and then for 5 min with rotation of 18 rpm. The supernatant was then serial-diluted and plated for bacterial cell counting. Data were collected for three individual experiments performed in duplicates.

5.3 Results and Discussion

5.3.1 Immobilization of bacteriophage on magnetic particles

As depicted in Figure 5.1a, P100 phages were immobilized onto magnetic particle surfaces through two immobilization methods: covalent chemical immobilization and physical immobilization. Plaque assay was performed using the collected supernatant and the phage coupling ratio (CR) was used as a parameter to determine the effectiveness of phage immobilization on MP. The CR of P100 phage binding on to MP could be influenced by several ratios, including type of immobilization method, phage quantity in sample and MP size. The influence of these on phage-magnetic particle CR is summarized in Table 5.1. Firstly, the influence of immobilization method on phage CR was studied by immobilizing 10^8 PFU phages onto MP surfaces using both chemical and physical immobilization methods. CR obtained from chemical immobilization of phages is higher than that obtained from physical immobilization of phages. For example, the CR of PMMP-150Ph is 0.46 and the CR of PMMP-150Ch is 0.43. This effect was also observed for 500 nm and 1 µm sized MP. Secondly, the influence of phage quantity on CR was studied by using 10^8 and 10^9 PFU (in 0.4 mL) of phages for immobilization on MP surface. When high quantity of phages (10^9 PFU) was employed for phage chemical immobilization on small MP, the CR of PMMP-150Ch increased from 0.46 to 0.6. However, for the medium sized MP, the CR of PMMP-500Ch decreased from 0.61 to 0.27 and for the large sized MP (1 µm), increasing phage quantity did not translate into increased CR as well. The results suggest that MP

size is an important parameter that determines the P100-MP coupling ratio and the resulting surface phage loading of P100 onto MP. The high CR of small MP (150 nm) over medium and larger MP could be attributed to the high surface/volume ratio and high mobility of small particles that could provide more opportunity to interact with phages.

Table 5.1: Phage-magnetic particle coupling ratios of three different sizes of magnetic particles using chemical/physical immobilization method.

Phage-magnetic particle coupling ratio						
Phage quantity	150Ch	150Ph	500Ch	500Ph	1000Ch	1000Ph
10^8 PFU	0.46	0.43	0.61	0.18	0.25	0.19
10^9 PFU	0.60	0.61	0.27	0.27	0.27	0.18

5.3.2 Retention of phage infectivity in PMMP

The infectivity of each PMMP was also studied to further establish the effectiveness of phage immobilization methods. Each PMMP was directly examined using plaque assay and the immobilized plaque quantity was obtained. The total plaque quantity could help to understand the overall lytic activity, which was defined as immobilized phage quantity/ MP number. As shown in Table 5.2, PMMP prepared with 10^9 PFU phages achieved 1-2 orders of magnitude higher lytic activity than that of PMMP prepared with 10^8 PFU phages. The increase of phage quantity improved the overall lytic activity of each PMMP. Besides high P100-MP coupling ratios, the smaller 150 nm MP exhibited very low lytic activity (0.001% and 0.01%), whereas medium (500 nm) and large (1 μm) PMMP showed 2-3 orders of magnitude higher lytic activity than small particle. These results are not in direct agreement with results of CR for 150 nm MP (40-60%) as mentioned previously. A high CR for 150 nm PMMP did not translate into a high PMMP lytic activity. This could due to high particle agglomeration for small MP that occurred during surface activation and phage immobilization. Moreover, the overall lytic activity of PMMP with

chemically immobilized phages was lower than that of PMMP with physically immobilized phages. Such variance in lytic activity was consistent with the obtained CR of two the immobilization methods. Given the fact that only phages with preferred orientation (e.g. head-down, tail-up fashion) could produce a plaque of the PMMP, the overall low lytic activity of MP with chemically immobilized phages could be the result of random immobilization of phages on MP surfaces, such as tail-down, head-up fashion.

Table 5.2: Lytic activity of each PMMP of three different sizes of magnetic particles using chemical/physical immobilization method.

	Lytic activity (%)					
Phage quantity	150Ch	150Ph	500Ch	500Ph	1000Ch	1000Ph
10^8 PFU	0.001	0.01	0.01	0.1	0.1	0.1
10^9 PFU	0.01	0.1	0.1	1	1	1

5.3.3 *L. monocytogenes separation with PMMP*

In order to further understand influence of phage immobilization method and the corresponding PMMP effectiveness toward bacteria cell separation, experiments were conducted using PMMP prepared with 10^9 PFU phages unless otherwise stated. Each PMMP (80 µL) was added into *L. monocytogenes* cell suspensions, and bacterial cells were isolated and separated using the method described in Figure 5.1b. As a model system, *L. monocytogenes* at a concentration of 10^3 CFU/mL was used for cell separation experiments, and the capture efficiency (CE) of each PMMP was evaluated and summarized in Figure 5.2. As shown in Figure 5.2, the capture efficiency of PMMP with chemically immobilized phages was lower than that of physically immobilized MP in all three sizes, which correlates with the observation about PMMP lytic activity. As mentioned previously, the low lytic activity of PMMP obtained using chemically immobilization may be due to the disorientation of phages on MP surface. These disoriented phages immobilized on PMMP may not be able to properly recognize and capture the host *L.*

monocytogenes cells, leading to low bacterial capture efficiency. PMMP with physically immobilized phages may contain higher numbers of "active" phage than that of PMMP with chemically immobilized phages. To evaluate the effect of the quantity of PMMP on *L. monocytogenes* capture efficiency, different volumes of 0.4 mg/mL PMMP (20 µL, 40 µL, 80 µL, 120 µL, 140 µL) of each size were added into 500 µL *L. monocytogenes* cell suspension of 10^3 CFU/mL. As shown in Table 5.3, the CE of PMMP-150Ph increased from 23.9±6.0%to 54.7±0.86% with increasing PMMP dosage from 20 µL to 140 µL, which may be due to the availability of more surface-active sites for bacteria attachment. Similar trend was also observed for PMMP-150Ch, PMMP-500Ch, PMMP-500Ph, PMMP-1000Ch and PMMP-1000Ph.

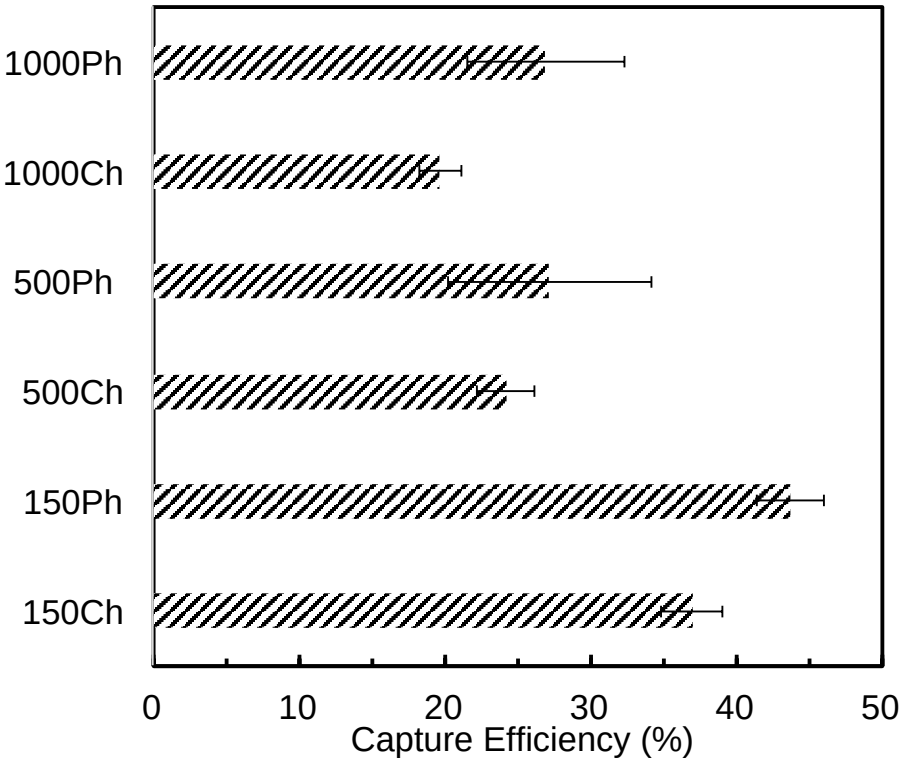

Figure 5.2: The capture efficiency of PMMP for the separation of *L. monocytogenes* from a suspension of 10^3 CFU/mL.

In order to assess the capture efficiency of PMMP with varying numbers of *Listeria monocytogenes* cells (10^2 -10^6 CFU/mL), 80 µL of each PMMP were added into respective cell

suspensions containing *L. monocytogenes* cells, and the CE was calculated as mentioned previously. Figure 5.3a shows the mean CE of PMMP from *L. monocytogenes* suspension, and the CE with standard deviations was included in supporting information as Table 5.S1. PMMP with physically immobilized phages showed higher CE than those with chemically immobilized phages. This effect was observed for all three sizes of PMMP. The CE of PMMP-150Ph at *L. monocytogenes* concentration of 10^2 CFU/mL is 47%, which is higher than the CE of PMMP-150Ch particles (9%). Physical immobilization of phages likely favors the preferred orientation of phages to interact with bacteria cells, as reflected in the capture efficiency values. As shown in Figure 5.3a, the CE at different *L. monocytogenes* concentrations showed that the highest capture efficiencies occur in the range of 10^3 to 10^5 CFU/mL for all particles studied. As expected, lowest capture efficiencies for all particles were observed for 10^2 CFU/mL. We also noticed that large MP showed higher CE at bacteria concentration above 10^4 CFU/mL, whereas PMMP-150Ph showed the peak CE at low cell concentration (10^2 CFU/mL). The poor performance of 150 nm PMMP for separation of high concentration of bacteria cell could be related to their particle aggregation, that reduces the number of particles that interact with bacteria cell.

Table 5.3: The effect of the MP quantity and immobilization method on the capture efficiency of bacteria cells using three sizes of MP (using 10^3 CFU/mL *L. monocytogenes* as model analyte).

		% of captured bacteria cells ± SD					
		150Ch	150Ph	500Ch	500Ph	1000Ch	1000Ph
Volume of MP	20	13.9±0.4	23.9±6.0	15.0±3.6	12.5±2.2	10.5±2.8	11.4±5.3
	40	18.3±5.3	34.6±10.4	15.2±2.2	21.2±5.4	11.5±3.1	18.4±8.9
	80	37.0±2.1	43.8±2.3	24.2±2.0	27.2±7.0	19.7±1.4	26.9±5.4
	120	36.9±5.0	58.0±7.2	32.6±7.1	41.1±6.6	24.5±5.0	40.9±3.9
	140	39.3±4.9	54.7±0.86	38.5±3.8	47.0±0.5	28.4±6.8	43.4±0.4

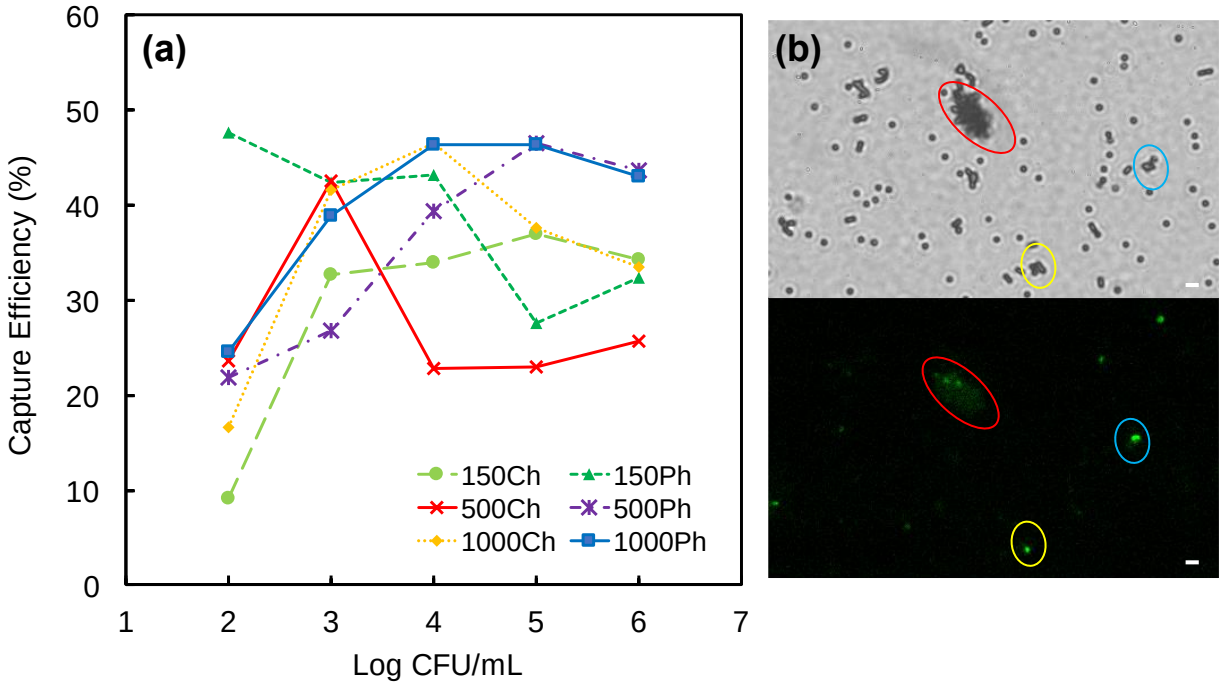

Figure 5.3: (a) The mean capture efficiency of phage-modified MP from cell suspension containing variable concentrations of *L. monocytogenes* (10^2-10^6 CFU/mL); (b) Transmitted (top) and fluorescence microscopy (bottom) images showing capture of bacteria using 1 µm MNP. Three spots were selected to show the captured bacteria on MP surfaces. The scale bar is 2 µm.

Figure 5.3b shows the capture of fluorescence-labeled *L. monocytogenes* by PMMP-1000Ph magnetic particle on glass slide. The circled areas indicate the binding of bacterial cells on to PMMP, which confirms the successful separation of cells by PMMP-1000Ph from the cell suspension. The captured bacteria attached on PMMP were also observed in the SEM images shown in Figure 5.4. Aggregation could be noticed in PMMP, and that the degree of aggregation is higher in small 150 nm MP, which explains the poor lytic activity obtained by soft agar overlay.

5.3.4 Selectivity test using other bacterial strains

The selectivity of the PMMP based magnetic separation towards *L. monocytogenes* was evaluated using three other randomly selected strains of non-target bacteria namely *E. coli*, *S. aureus*, and *E. faecalis*. As shown in Figure 5.5, the method achieved 40-50 % CE of the target bacteria (*L. monocytogenes* Scott A), whereas the CE for non-target bacteria was only about 15 %.

The 15 % capture of non-target cells could be due to the non-specific binding of bacteria cells on MP surface through FeO-P bonds between the bacterial cell membrane and the MP. [190,191]

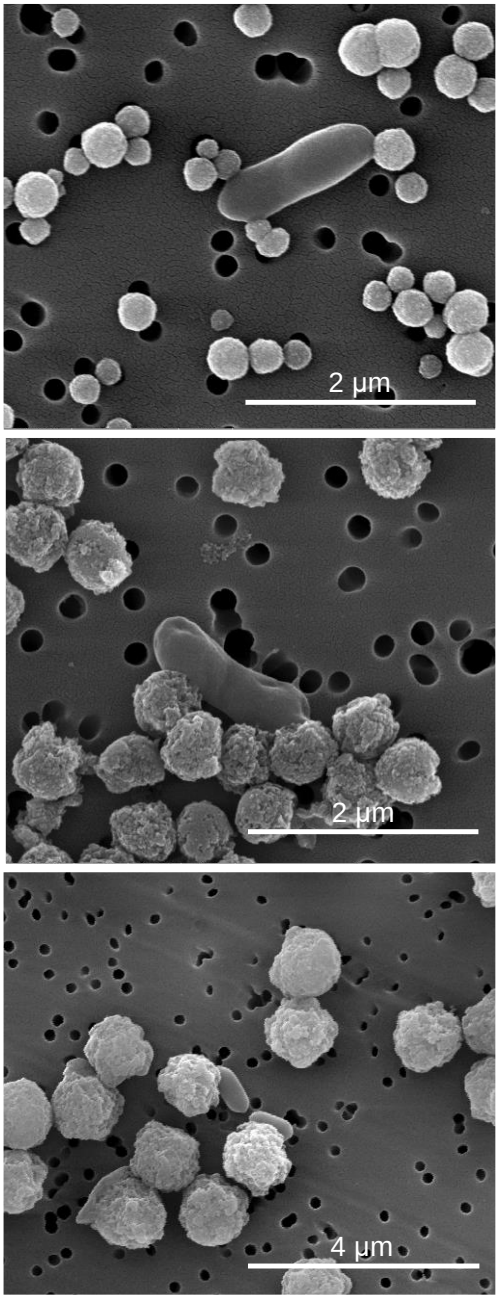

Figure 5.4: SEM images of PMMP used for the capture of *L. monocytogenes.* (top 150 nm, middle 500 nm and bottom 1 µm MP).

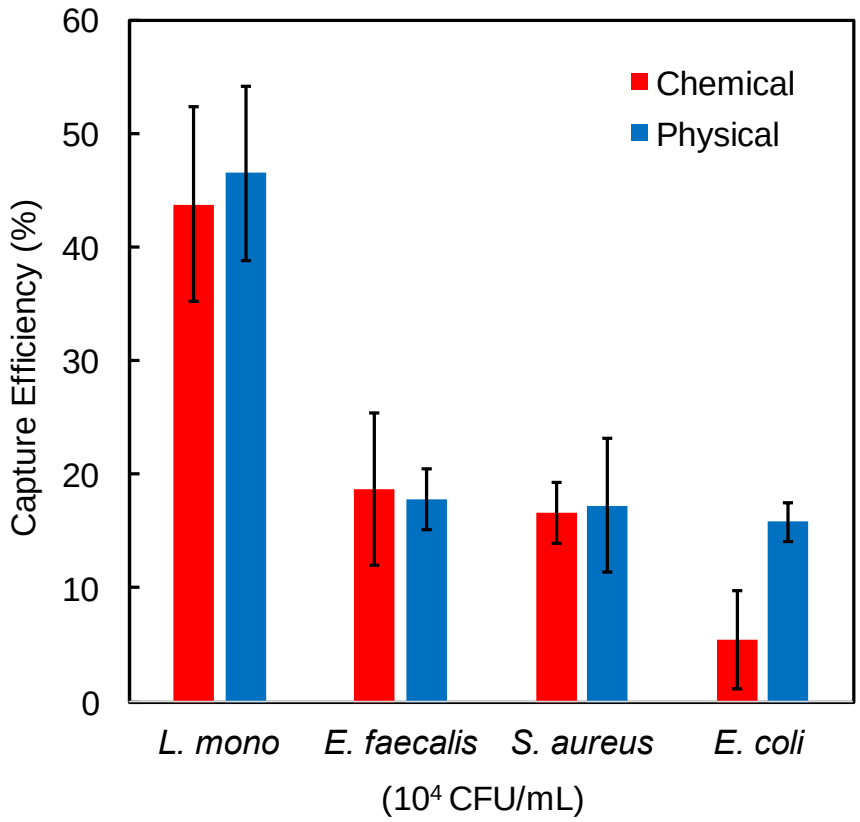

Figure 5.5: Selectivity study of phage-modified 1 µm MP with selected bacteria strains. Red bar represents P100 chemically-immobilized MP; blue bar represents P100 physically-immobilized MP.

5.3.5 Stability of PMMP

The stability of PMMP complexes was also studied by monitoring the immobilized phage activity using plaque assay. For this, PMMP were prepared using 1 µm magnetic particles *via* both physical and chemical immobilization methods. Plaque assay was performed using PMMP-1000Ch and PMMP-1000Ph for over 60 days. The PMMP lytic activity were obtained and compared to the first day lytic activity to evaluate their relative stability. Figure 5.6 shows the relative PMMP lytic activity obtained from plaque assay in terms of PFU/mL. PMMP-1000Ch showed a quick drop in lytic activity after 5 days and retained steady lytic activity of about 78 % after 66 days. On the other hand, the activity of PMMP-1000Ph fluctuated over a time range and remained 68 % after 66 days. The prolonged stability of PMMP using chemical immobilization

methods could be attributed to the strong covalent bonding between phages and MP, preventing phage desorption or disorientation, which may be the reason for the fluctuation of phage activity observed in physical immobilization method (as shown in Figure 5.6).

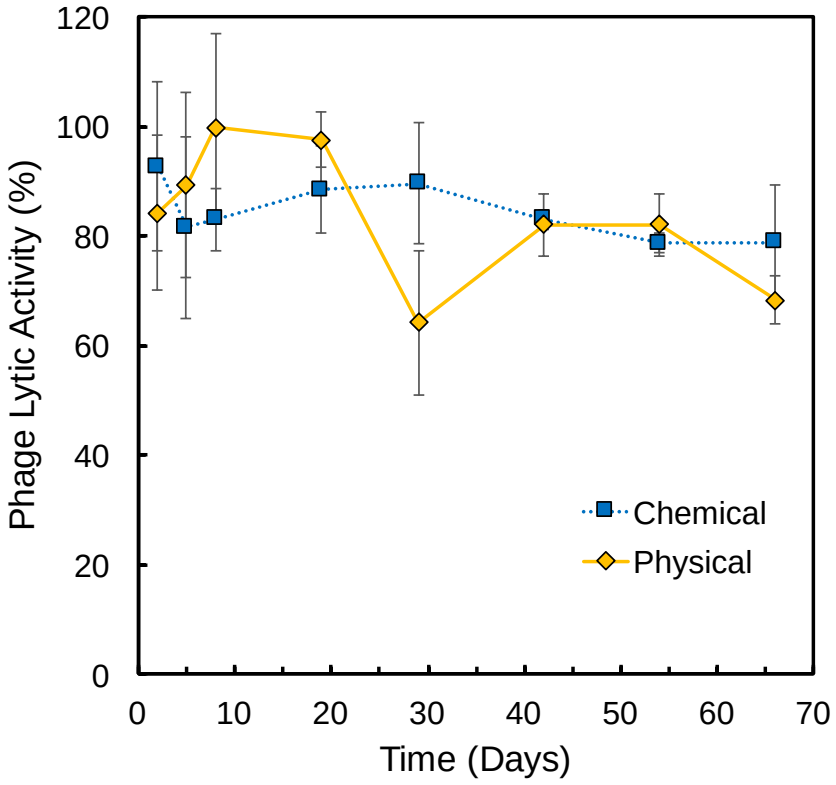

Figure 5.6: Stability of physical/chemical functionalized magnetic particles. The blue dotted line represents the phage lytic activity of PMMP-1000Ch, and the yellow solid line represents the phage lytic activity of PMMP-1000Ph.

It must be noted that the stability determination was based on relative activity of phages based on their activity on day 1 and therefore could not cross-compared between chemically and physically functionalized PMMP. Even though physical immobilization of phages likely favors the preferred orientation of phages, the resulting initial high lytic activity of physical immobilization may not necessarily result in long-term retention of lytic activity of immobilized phages in PMMP. This trade-off between initial lytic activity and long term lytic activity must be considered in determining the choice of immobilization methods for making PMMP for specific applications.

5.3.6 Real sample testing

The application of PMMP for *L. monocytogenes* isolation from whole milk and ground beef are presented in Figure 5.7. Pre-contaminated milk and ground beef samples with 10^3 CFU/mL of *L. monocytogenes* were used as real samples for magnetic separation. When PMMP-1000Ph and PMMP-1000Ch were used to capture 10^3 CFU/mL of *Listeria* in ground beef, the CE were 13 % and 18%, respectively. Both PMMP-1000Ph and PMMP-1000Ch were then used to capture *Listeria* from milk, the CE were 46% and 28%, respectively. The results indicated that the CE obtained for separation of bacteria from ground beef was much lower than that from milk, and the CE values obtained using milk as food matrix were also close to CE obtained using PBS buffer as matrix. CE of *Listeria* cells were dramatically influenced by different food matrix. A similar observation was reported for immuno-magnetic separation of *L. monocytogenes* cells from ground beef.[192] The low capture efficiency in ground beef may due to the fact that beef contains more solid content and fat than milk causing fouling and interference.

A comparison of the conventional methods (bacterial cell culture and IMS) with our PMMP-assisted method for *L. monocytogenes* separation is given in Table 5.4. Based on microbiology and biochemical analysis, conventional culture methods are highly accurate but overly time-consuming that take up to 48 hours for separation and identification of *Listeria* cells.[150,193,194] Moreover, an enrichment step is also required to grow the organisms, rendering it unsuitable for on-site separation and identification. IMS, on the other hand, has been widely used as an effective method for separation and isolation of *L. monocytogenes* from food, relying on the specificity of antibodies. Immunological based methods however suffer from harsh environmental conditions, high production cost of antibodies and the inconsistency in capture efficiency due to batch to batch variations.[59,64,65,192,195-197] Unlike antibodies, bacteriophages are inexpensive to

propagate and purify. PMMP obtained in this study could be used to separate *L. monocytogenes* cell within 20 minutes and cost about five dollars per sample. [193]

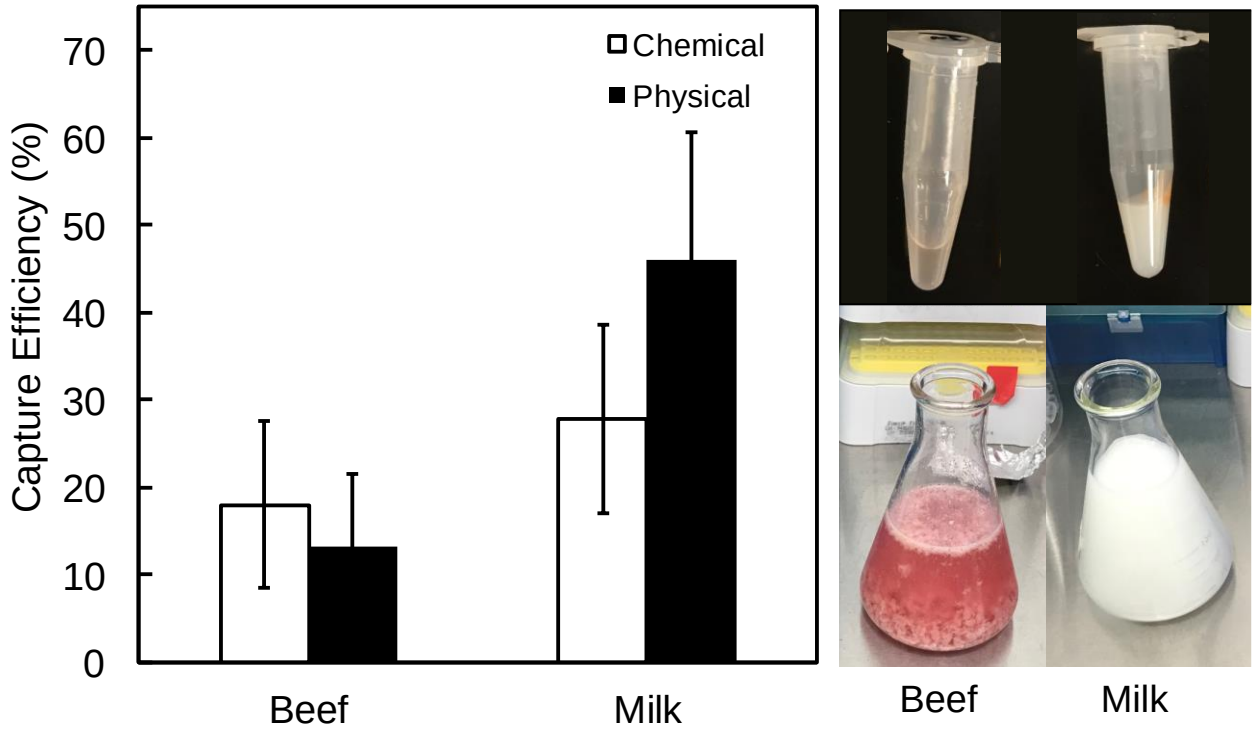

Figure 5.7: Separation of *L. monocytogenes* from pre-contaminated beef and milk samples (10^3 CFU/mL) using PMMP-1000Ch and PMMP-1000Ph.

Table 5.4: Comparison of methods for *L. monocytogenes* separation.

	Culture method [b]	**IMS**	**PMMP**
Time [a]	18 h-72 h	30 min~2 h	20 min
% CE	N/A	7 %-121 %	9-46 %
Estimated cost/sample	~$1	~$10-25	~$4
Labor	High	Medium	Medium

5.4 Conclusion

By chemical and physical immobilization method, P100 bacteriophages were immobilized onto three sizes of magnetic particles, which offered a useful label for rapid and specific separation of *Listeria monocytogenes*. The efficiency of bacterial capture by immobilized phage particles were influenced significantly by phage immobilization strategies and magnetic particle sizes. Physical immobilization method achieved preferred orientation of phages, which offers more active sites for bacteria attachment. The resulting PMMP could effectively capture *L. monocytogenes* in food matrix. The achieved bacteriophage-assisted separation technique could also be applied for the separation of other bacteria strains from food matrix, representing an improved isolation/ separation and concentration tool to the current standard method, IMS. Future work will be focused on analytical validation of the current methodology with more food samples and the integration of the current technique with bacteria detection method, such as biosensors or flow cytometry, thereby reducing the assay time from 2-4 days to less than 20 min.

CHAPTER 6

IMPEDIMETRIC DETECTION OF LISTERIA MONOCYTOGENES USING PHAGE-MODIFIED MAGNETIC PARTICLES

Yan Zhou, Ramaraja Ramasamy. To be submitted to Biosensors and Bioelectronics.

Abstract

In this study, an impedimetric electrochemical biosensor was developed and demonstrated for *Listeria monocytogenes* detection using magnetic particles bacteriophage functionalized magnetic particles on screen printed carbon electrodes. The purpose of this work is to investigate the feasibility of coupling a previously demonstrated bacterial cell enrichment method with an electrochemical biosensing platform. Our previous work has demonstrated that a successful isolation and separation (enrichment) of *L. monocytogenes* from contaminated food samples could be achieved using P100 phage-modified magnetic particles (PMMP). The thus separated *L. monocytogenes* bacteria cells on PMMP surfaces were further employed in this work for direct impedimetric biosensing of *L. monocytogenes* in the absence and presence of magnetic field. Electrochemical impedance spectroscopy (EIS) was used to monitor the changes in the interfacial impedance when *L. monocytogenes* cells attach onto the screen-printed electrode. An increase of charge transfer resistance was observed during the interaction, and the applied magnetic field was found to improve the limit of detection of *L. monocytogenes* from 10^4 to 10^3 CFU/mL.

Keywords: Bacteriophage P100; *Listeria monocytogenes*; bacteria detection; magnetic separation; impedance spectroscopy; screen-printed electrode.

6.1 Introduction

Among the large family of foodborne pathogens, *L. monocytogenes*, has been given considerable attention because of its high fatality rate. An estimation of 1600 people get listeriosis each year, and over 200 die from the disease.[61,62] Many approaches have been developed to monitor the contamination caused by *L. monocytogenes* and to prevent widespread outbreaks. Various techniques employed to detect *L. monocytogenes*, such as enzyme-linked immunosorbent assay (ELISA), polymerase chain reaction (PCR), flow cytometry, are either time consuming, low in sensitivity and limit of detection, expensive or require special laboratory set up and trained technician. Biosensors were introduced as an alternative analytical technique, which enable a rapid, real time detection of difference organisms. Several types of biosensors have been developed for detection of *L. monocytogenes* including immunosensors, fiber optic sensors, surface plasmon resonance (SPR) sensor, quartz crystal microbalance (QCM) and electrochemical biosensor etc.[196]

Impedance biosensor is a typical electrochemical biosensor, measuring the electrochemical impedance change on the electrode/interface of an electrode under an alternating potential with a direct current bias. The technique allows rapid detection, while the instrumentation is compact, low cost and easy to integrate into other analytical tools. Impedimetric biosensors have been used to detect bacteria cells based on the following mechanisms: a) measurement of changes in electric impedance in medium, resulting from bacterial metabolism; b) measurement of changes in impedance based on the highly ionic cytoplasm of cell; c) measurement of changes in impedance based on the insulating properties of bacteria cell membrane.[148] However, the first two mechanisms require long processing time, such as growing of bacteria in medium, or lysis of bacteria cells. Interference from other pseudo analytes present in the complex matrices, such as fats, food particles, enzymes, etc. Coupling the electrochemical transduction with magnetic enrichment

using microcarriers has contributed to improvements in the performance of the biosensor.[198] Magnetic particles based on iron oxide could be functionalized with diverse recognition elements for selective separation of pathogens from samples, and could be further coupled with electrochemical biosensors for detection. In our previous work discussed in Chapter 5, we have developed strategies for phage immobilization on magnetic particles for isolation and separation of *L. monocytogenes.* We studied the importance of phage immobilization methods and the magnetic particle sizes on the effectiveness of phage coupling and the bacterial cell capture efficiency of the resulting phage modified magnetic particles (PMMP). The successful capture of *L. monocytogenes* is confirmed with scanning electron microscopy and fluorescence microscopy. The resulting PMMP could also effectively capture *L. monocytogenes* from food matrix. The PMMP achieved 40~50 % selective capture efficiency of *L. monocytogenes.*

In this study, we investigated the feasibility of coupling the previously demonstrated magnetic separation with an impedance biosensor platform. The *L. monocytogenes* isolated using PMMP was introduced into the impedance biosensors in order to detect and quantify the bacteria on screen printed electrodes based on an impedance changes of the electrode surface. P100 bacteriophages modified 1 μm magnetic particles was used as a model to study the performance of magnetic particle assisted impedimetric biosensor. Screen-printed electrodes (SPEs) were used in this study over other types of electrodes, as they are disposable, low cost, and easy to fabricate.

6.2 Materials and methods

6.2.1 Material and instruments

The following chemicals were purchased and used without further purification: sodium chloride and sodium phosphate dibasic (both from EMD chemicals, Port Wentworth, GA), potassium chloride (J.T. Baker, Center Valley, PA), potassium dihydrogen phosphate (BDH, West

Chester, PA), magnesium sulfate heptahydrate (J.T. Baker, Center Valley, PA), agar powder (Alfa Aesar, Ward Hill, MA), bis(sulfosuccinimidyl)suberate) (BS3) (Cova Chem, Loves Park, IL), Tris-HCl(Fisher Scientific, Fair Lawn, NJ), Brain heart infusion medium (Sigma-Aldrich, St. Louis, MO). SM buffer was prepared by mixing 5.8 g of NaCl, 2 g of $MgSO_4 \cdot 7H_2O$, 50 mL of 1M Tris-HCl pH 7.5, and 1 mL of 10% (w/v) gelatin in deionized water. Brain heart infusion (BHI) medium was prepared by adding 37 g of BHI powder in deionized water and the pH was adjusted to pH 7.4. BHI-agar medium was prepared by adding 6 g of agar to 400 mL of BHI media. 2 g of agar was added to 400 mL of BHI media to obtain soft agar medium. 10X phosphate buffered saline (PBS) was prepared by mixing 16 g NaCl, 0.40 g KCl, 2.8 g Na_2HPO_4, and 0.49 g KH_2PO_4 in 200 mL deionized water yielding a buffer solution of pH 7.4. All media, buffer and glassware were sterilized before use. *Listeria monocytogenes* Scott A strain was kindly provided by Dr. Michael Doyle (University of Georgia, Griffin). P100 bacteriophage (commercial name LISTEX^{TM}) was purchased from Micreos Food Safety (Wageningen, The Netherlands). The amine functionalized magnetic beads 1 µm size were purchased from Ocean Nanotech (Springdale, AR). The magnetic separation of the particles during the washing steps were carried out using a magnetic separation rack (Bel-Art, Wayne, NJ). A tube rotator (VWR, Suwanee, GA) was used for mixing steps at a speed of 18 rpm.

6.2.2 Bacterial strains and culture conditions

Listeria monocytogenes Scott A strain was used throughout the separation experiments unless otherwise stated. *L. monocytogenes* was cultured in 4 mL BHI medium overnight at 37 °C. 500 µL aliquot of the overnight culture was inoculated into 50 mL of fresh BHI medium by shaking at 200 rpm for 5 h at 37 °C in an incubator shaker. Aliquots were prepared by transferring 0.5 mL of the culture into individual microcentrifuge tubes, and transferring the aliquots to a -80 °C freezer.

For each electrochemical experiment, a fresh aliquot of *L. monocytogenes* was used. In order to determine the concentration of the aliquots, the tube was thawed one tube on ice for at least 40 min, and then the tube was centrifuged at 4000g for 10 min to remove the medium. The supernatant was removed, and bacterial cell pellet was resuspended with 1XPBS buffer and washed twice before use. Multiple serial dilutions were performed using 1XPBS. Enumeration of bacteria was performed by plate counting method and cell count was expressed in CFU/mL.

6.2.3 Preparation of P100 bacteriophage-functionalized magnetic particles

Amine functionalized magnetic particles (MP) of 1 μm were used for phage immobilization. Each 20 μL of MP (10 mg/mL) was added into a 1.5 mL micro-centrifuge tube and sterilized with 70 % ethanol, the tube was placed on a magnetic separator to remove the ethanol. The particles were washed three times using 1X PBS buffer (coupled with 0.01% Tween 20). PBS buffer was then added into the tube to form a suspension of MP. The chemical immobilization of phages was achieved using bis(sulfosuccinimidyl)suberate) (BS3) crosslinker, which reacts with the surface amine moieties of phage particles resulting in amide bond formation. For the preparation of chemical immobilization of phages onto MP surface, 10 mM of BS3 in PBS was prepared, syringe-filtered and added into the MP suspension. The mixture of BS3 and MP were reacted for 30 minutes at room temperature with continuous mixing using the tube rotator to allow the activation of MP surfaces. After 30 minutes, the tube was placed into the magnetic separator for activated MP separation, followed by three times washing with 500 μL of PBS buffer to remove excess BS3. Finally, phage particles (10^9 PFU) were added into the MP suspension to react overnight at 4 °C under continuous mixing at 18 rpm using tube rotator. The supernatant was then removed and the PMMP were resuspended in 500 μL SM buffer to terminate the excess surface activated residuals. The thus-prepared phage chemically functionalized MP was designated as PMMP.

6.2.4 Electrode preparation for bacteria detection

Bacterial cell separation was performed using 500 µL of *L. monocytogenes* cell suspension in micro-centrifuge tubes. The separation of bacteria cells was illustrated in Figure 6.1 and *L. monocytogenes* cells were serial diluted to make 10^2 to 10^7CFU/mL cell suspension in PBS buffer for electrochemical detection. Eighty microliters of PMMP were mixed with 500 µL of *L. monocytogenes* in 1X PBS buffer (coupled with 0.01% Tween 20) in micro-centrifuge tubes. The mixture was then incubated at room temperature for 10 min without agitation, and then for 5 min with rotation using tube rotator. The MP-bacteria complex was separated using a magnetic separator over a period of 5 min. The supernatant was then removed, and the sample were washed for 2 times with PBS buffer. Finally, the magnetic particles were resuspended in 25 µL of 5 mM $Fe(CN)_6^{3-/4-}$ (1:1) mixture in 1X PBS buffer and kept on ice before detection. The thus-prepared PMMP separated *L. monocytogenes* was designated as magnetized *L. monocytogenes*.

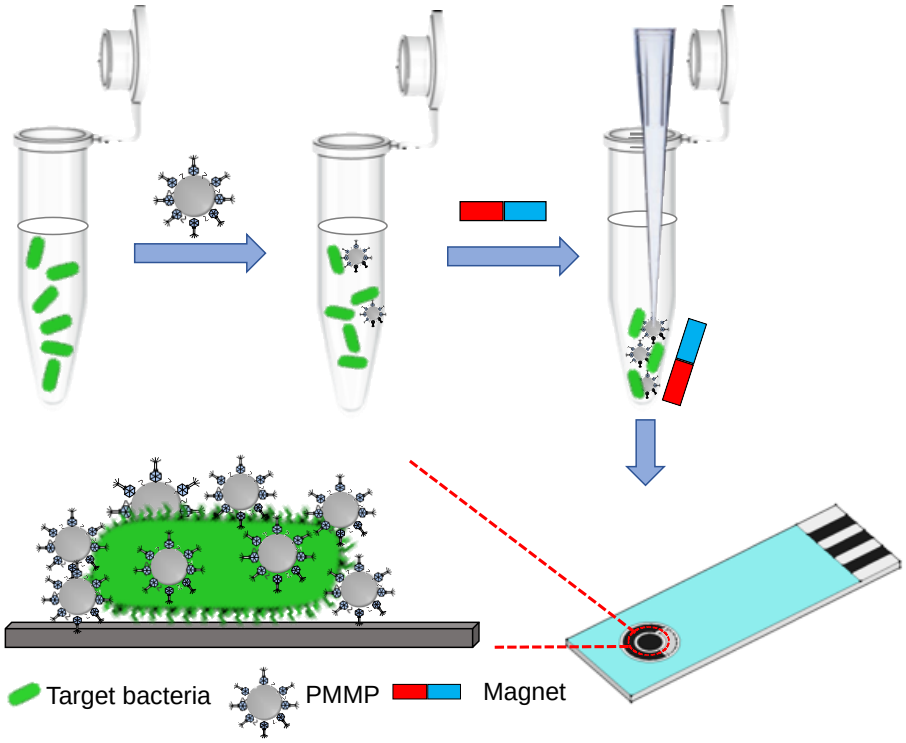

Figure 6.1: Magnetic separation and electrochemical detection of *L. monocytogenes*.

6.2.5 Electrochemical characterization

Electrochemical characterization was conducted using CHI-920c model potentiostat (CH Instruments Inc, Austin, TX). Screen-printed electrodes (SPE) from CHI instrument were used for all electrochemically measurements, which were carried out at 25 ºC ± 2 ºC in with 25 μL sample volume, unless otherwise stated. Impedance was measured at the open circuit potential, with a superimposed AC voltage of amplitude 5 mV between frequencies 100 kHz and 0.1Hz.

6.3 Results and Discussion

6.3.1 EIS of bacterial cell suspensions in DI water and PBS.

In order to choose the appropriate electrolyte system for the detection of magnetized *L. monocytogenes*, three different electrolyte systems were studied using impedance spectroscopy. Figure 6.S1 represents the Bode impedance plot of magnetized *L. monocytogenes* in a) DI water; b) PBS buffer; and c) 5 mM $Fe(CN)_6^{3-/4-}$ (1:1) in PBS buffer using screen-printed electrodes. In Figure 6.S1a, the impedance of PMMP in DI water showed a significant difference compared to DI water alone; however, the impedance of magnetized *L. monocytogenes* didn't show any difference compared to PMMP alone. When PBS was used as the electrolyte, no significant difference was found in impedance between PMMP and magnetized *L. monocytogenes* at any frequency, whereas impedance of magnetized *L. monocytogenes* in PBS supplemented with 5 mM $Fe(CN)_6^{3-/4-}$ showed significantly difference in impedance response from that of the case with control (PMMP without *Listeria*). This suggests that a redox couple is essential in monitoring the impedance change due to bacteria attachment on to the electrode. In the presence of $Fe(CN)_6^{3-/4-}$, the impedance measured is the Faradaic impedance of the redox couple.[67] Thus, electrolyte system of 5 mM $Fe(CN)_6^{3-/4-}$ (1:1) in PBS buffer was used for all electrochemical measurements unless otherwise stated.

6.3.2 Electrochemical characterization and *L. monocytogenes* detection

Figure 6.2 illustrate the representative open circuit Nyquist plot measured using screen-printed electrodes for the 5 mM $Fe(CN)_6^{3-/4-}$ redox couple obtained in the absence and presence of magnetized *L. monocytogenes* (at difference concentration expressed in CFU/mL) in the electrolyte solution. The equivalent electrical circuit used to fit the data is called Randles circuit. The model consists four elements, including charge transfer resistance (R_{CT}), the electrolyte resistance (R_Ω), double layer capacitance (C_{dl}), and Warburg impedance (Z_w). The width of the Nyquist plot reflects the charge transfer resistance R_{CT}, which is determined by the kinetics of the redox reaction and the type of surface modification. R_Ω represent the ohmic resistance of the electrolyte solution and Z_w represents the mass transfer impedance for the diffusion in and out of the redox couple from bulk electrolyte to the surface. C_{dl} represents a nonideal capacitance at the electrochemical interface. The magnetically separated bacteria cells on screen printed electrode surface could alter the surface properties of electrode which in turn varies the impedance measured on the electrode surface depending on the quantity of cells present in the bulk electrolyte solution. The electrode was thus used for the detection of magnetized *L. monocytogenes*. Impedance measurements were made at different magnetized *L. monocytogenes* concentrations and the results were compared with that of the controls where no *L. monocytogenes* was present in the sample (electrolyte). As shown in Figure 6.2, a significant variation was observed in R_{CT} upon the addition of magnetized *L. monocytogenes*. A considerable increase of charge transfer resistance was observed with increasing *L. monocytogenes* concentration. Such increase in R_{CT} due to magnetized bacteria attachment could be attributed to lowered $Fe(CN)_6^{3-/4-}$ redox the kinetics at the electrode interface, as the magnetized *L. monocytogenes* could act as a barrier on the electrode blocking the electron transfer pathway for $Fe(CN)_6^{3-/4-}$ redox reaction. However, no significant variation in R_{CT}

was observed for concentrations below 10^4 CFU/mL. At and above bacterial cell concentrations of 10^6 CFU/mL, the change in charge transfer resistance is insensitive to changes in cell concentration.

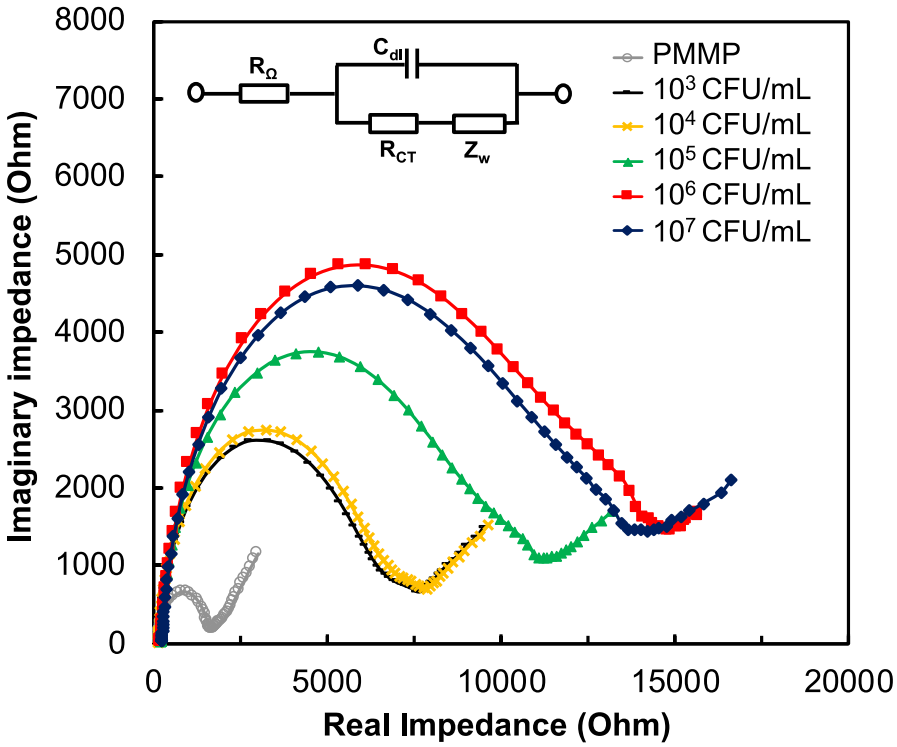

Figure 6.2: Nyquist plot measured using screen printed electrodes for the 5 mM $Fe(CN)_6^{3-/4-}$ in PBS obtained in the absence and presence of *L. monocytogenes* (at different concentration expressed in CFU/mL)

6.3.3 Integration of magnetic field for detection of *L. monocytogenes*

In order to further amplify the impedance change (signal) with varying bacterial concentrations, a magnetic field manipulation was enforced to assist the attachment of bacteria on electrode. After magnetized *L. monocytogenes* was deposited on the SPE electrode, a magnet was placed under the electrode for 30 second to attract the magnetic beads, along with the captured bacteria, to the sensor surface. First, a *L. monocytogenes* concentration of 10^5 CFU/mL was used to study the effect of magnetic field on the impedance signal due to bacteria cell attachment. It

could be hypothesized the presence of a magnetic field could mobilize more magnetized *L. monocytogenes* to the electrode surface resulting in a larger impedance signal. As shown in Figure 6.3, when magnetic field was applied, an amplification of the charge transfer resistance (magnitude of the arc) was observed from the Nyquist plot.

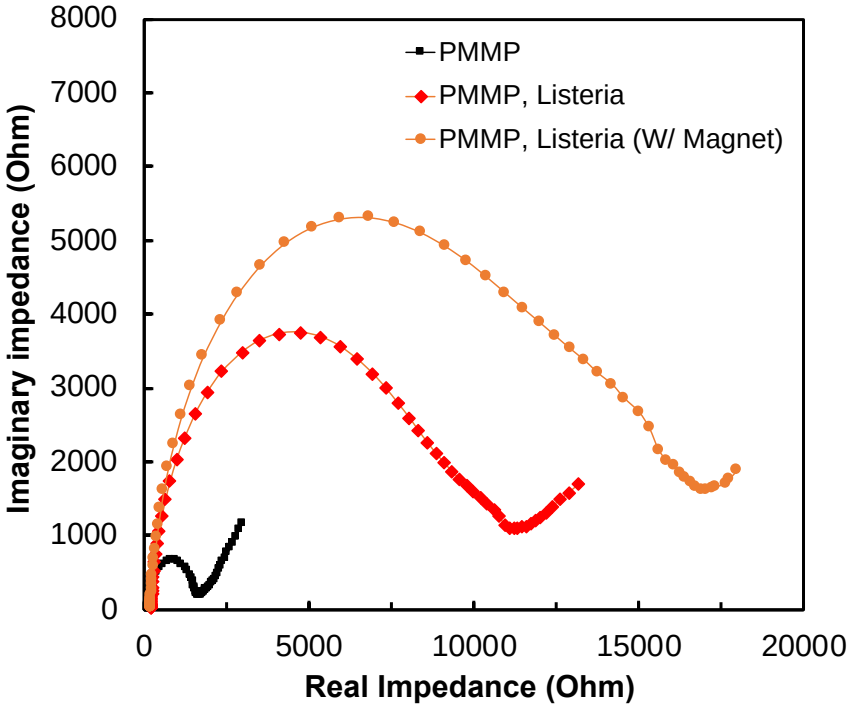

Figure 6.3: Nyquist plot of magnetized *L. monocytogenes* on SPE surface in the absence and presence of magnetic field.

Figure 6.4 presents the variation in charge transfer resistance as a function of bacteria concentration for detection of *L. monocytogenes* (from 10^3 to 10^8 CFU/mL) in the absence and presence of magnetic field. In the absence of magnetic field, a linear correlation between R_{CT} and the bacterial concentration was observed between 10^3 and 10^6 CFU/mL as shown in Figure 6.5. No significant variation in R_{CT} was observed for concentrations below 10^4 CFU/mL.

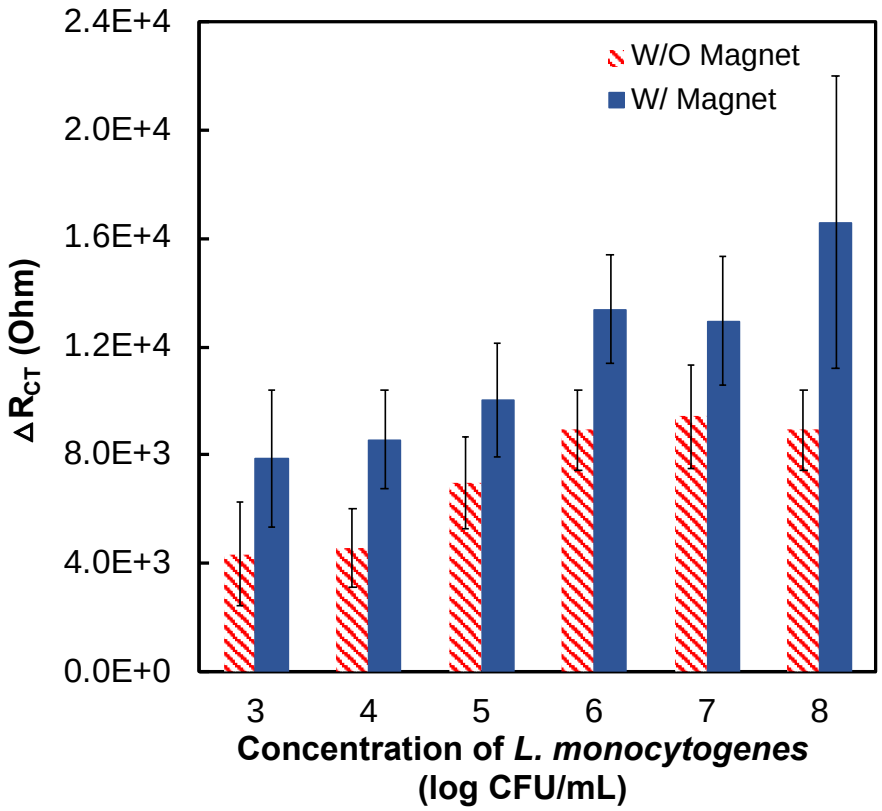

Figure 6.4: The variation in charge transfer resistance as a function of bacteria concentration for detection of *L. monocytogenes* (from 10^3 to 10^8 CFU/mL) in the absence and presence of magnetic field.

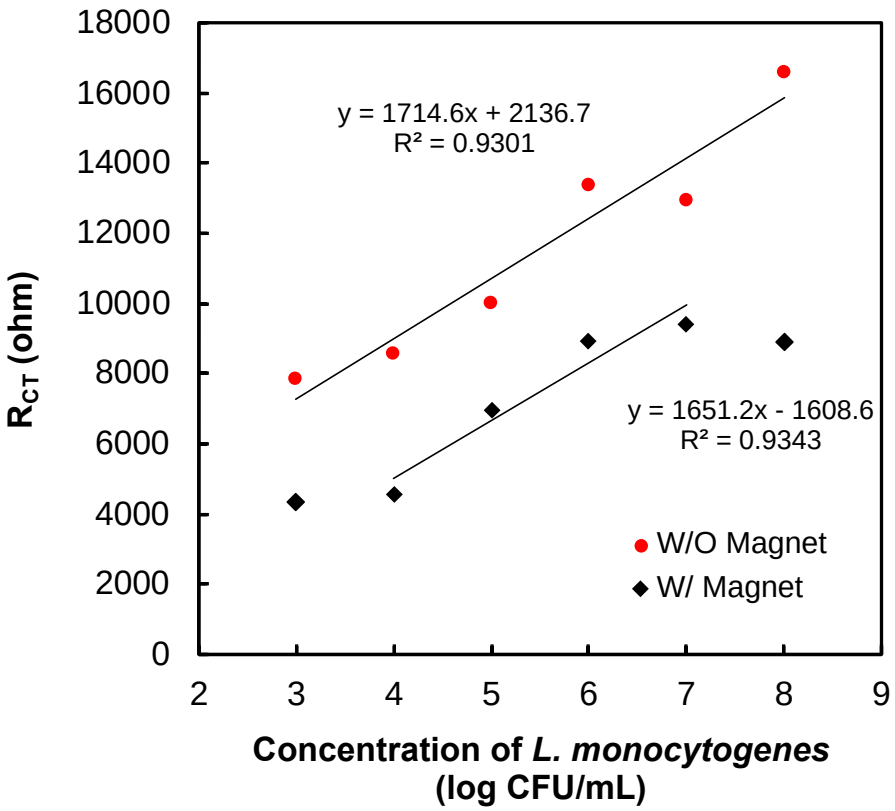

Figure 6.5: Variations of charge transfer resistance at different *L. monocytogenes* concentrations in the absence and in the presence of magnetic field.

At and above bacterial cell concentrations of 10^6 CFU/mL, the change in charge transfer resistance is insensitive to changes in cell concentration, which may be due to surface saturation of adhered cells. In the presence of magnetic field, a linear correlation between R_{CT} and the bacterial concentration was observed between 10^3 and 10^7 CFU/mL, with a detection limit of 10^3 CFU, which represents an order of magnitude improvement in *L. monocytogenes* detection limits in the presence of magnetic field.

6.4 Conclusion

We have demonstrated the feasibility of a screen-printed electrode-based impedimetric detection of *L. monocytogenes* using bacteriophage modified magnetic particles. The previously established bacteriophage-assisted separation was integrated with electrochemical impedance biosensor, which could potentially reduce the total test duration (sample collection to detection) for pathogen testing from 2-4 days to less than 20 min. It has been demonstrated that with the integration a simple magnet in the setup, an order of magnitude improvement in detection limits were achieved. Future studies would focus on further amplification of the sensitivity and improvement in detection limits by improving the nanoarchitecture of the electrode-electrolye interface. This work will also be expanded for detection of other bacterial cells using the respective bacteriophages as recognition molecules.

6.5 Supplementary Data

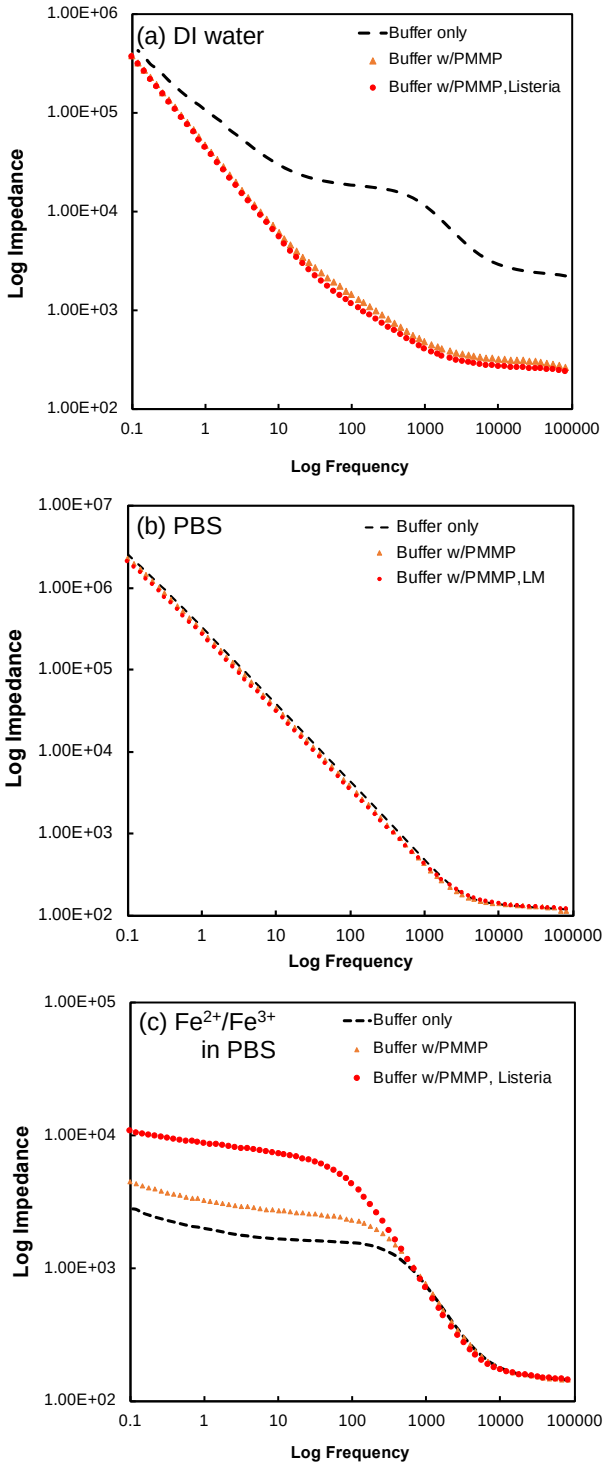

Figure 6.S1: Bode impedance plot of magnetized *L. monocytogenes* in a) DI water; b) PBS buffer; and c) 5 mM $Fe(CN)_6^{3-/4-}$ (1:1) in PBS buffer using screen-printed electrodes.

CHAPTER 7

CONSTRUCTION OF ENHANCED GREEN FLUORESCENCE PROTEIN LABELED BIOTINYLATED BACTERIOPHAGE P100 FOR DETECTION OF LISTERIA MONOCYTOGENES

Yan Zhou, Jian Wang, Yi Fang, Narendran Sekar and Ramaraja Ramasamy. To be submitted to Biotechnology and Bioengineering.

Abstract

Listeria bacteriophage P100 is a genus-specific, virulent Myovirus which infect 95 % of *Listeria monocytogenes.* The phage has broad host range and has potential application in *Listeria monocytogenes* identification and detection. The goal of this work is to develop a biotinylated bacteriophage P100 for achieving oriented immobilization of P100 on electrochemical transducer surfaces or magnetic particles via affinity interaction, which could then be utilized for detection of *Listeria monocytogenes* using electrochemical tools with improved sensitivity and selectivity. Plasmid PZE12-luc was first used for gene insertion carrying P100 DNA flanking *egfp* gene. A recombinant plasmid PDL276-Y5 was constructed, which carries the genes for biotin carboxyl carrier protein (*bccp*), and enhanced green fluorescence protein (*egfp*), that were inserted immediately downstream of the major capsid protein gene (*cps*). This site-specific construction of the plasmid can be further introduced into P100 genome via homologous recombination.

Keywords: Bacteriophage P100; *Listeria monocytogenes;* biotin carboxyl carrier protein; enhanced green fluorescence protein; major capsid protein gene.

7.1 Introduction

Listeria monocytogenes is widely recognized as an opportunistic food-borne pathogen. A number of outbreaks of listeriosis have been traced back to foods, such as frozen vegetables, meat, raw milk, and packed salad.[59] *L. monocytogenes* could grow over a wide temperature range, under both aerobic and anaerobic conditions.[60] Conventional methods for identification of *Listeria monocytogenes* in food matrices include selective enrichment and plating on selective and differential agar, followed by biological testing and species confirmation. While being reliable and accurate, these procedures are also laborious and time-consuming, which takes up 5 to 6 days for confirmation. In recent years, immunomagnetic separation (IMS) has been widely used in the pathology labs for separation and identification of *Listeria monocytogenes* from different food.[174,175] Commercially available 2.8 μm Dynabeads coupled with polyclonal antibodies were proved to be capable of separating target bacterial cells but with a low capture efficiency generally (7-23 %).[59,64,177] IMS could significantly shorten enrichment time; however, the antibodies are prone to harsh environmental conditions, such as pH and temperature variations, making them less suitable for non-laboratory testing.[63] Bacteriophages offer many advantages over antibodies for magnetic separation of *L. monocytogenes* as discussed in chapters 5 and 7.

The number and diversity of bacteriophages offer high selectivity toward their host bacteria, which provide a promising tool for specific detection of pathogenic bacteria.[178] Phage-based magnetic separation of *Salmonella* cells from food samples has been previously reported.[186,187] Bacteriophages have been chemically immobilized on magnetic particles for capture and separation of target bacteria cells. The surface protein structure of bacteriophages are chemically tethered onto magnetic particle surfaces. However, for Myrovirdea bacteriophages, only tail fibers are responsible for bacteria recognition. Simple chemical immobilization of phages

may result in mis-orientation of bacteriophages with a tail down-head up fashion, which does not benefit in achieving high bacteria capture efficiencies and limits of detection. In order to facilitate the bacterial separation using phage modified magnetic particles, methods have been developed to introduce either reporter genes followed by monitoring the gene expression products or introduce affinity tag on bacteriophage capsid protein for a specific diagnostic purpose. A511 bacteriophage, have been previously studied to express bacteria luciferase for the detection of *L. monocytogenes* using bio-luminescence. Among the various affinity tags, biotin acceptor protein containing specific amino acids can be biotinylated. Tolba et al. have successfully engineered coliphage T4 to express biotinylated protein for oriented immobilization of T4 for capture and detection of *E. coli*. The affinity between the biotinylated phage capsid protein and functionalized magnetic particle surfaces could achieve oriented immobilization of phages on magnetic particle surfaces for improved capture and detection of target bacteria cells.[179-183]

The aim of our study is to genetically modify a *Listeria* specific bacteriophage to introduce biotin tags on phage capsids that would be applied in *Listeria monocytogenes* separation and detection. LISTEX^{TM} P100 and LMP-102 bacteriophages have been approved for *L. monocytogenes* control in foods by the United States Department of Agriculture (USDA).[184,185] Currently, there are no reports in the literature for genetic engineering of P100 bacteriophage for *Listeria* separation and detection. In order to incorporate biotin tag onto P100 phage capsid, the biotin carboxyl carrier protein gene (*bccp*) was incorporated into phage genome for transcription. An enhanced green fluorescence protein gene (*egfp*) was also used as a fluorescence label for selection of the biotinylated bacteriophage P100. The purpose of this study was to design site-specific introduction of *bccp* genes and *egfp* genes into P100 bacteriophage genome in order to results in effective biotin tag expression on P100 phage capsid.

7.2 Material and methods

7.2.1 Materials and instruments

The following chemicals were purchased and used without further purification: sodium chloride and sodium phosphate dibasic (both from EMD chemicals, Port Wentworth, GA), magnesium sulfate heptahydrate (J.T. Baker, Center Valley, PA), potassium chloride (J.T. Baker, Center Valley, PA), potassium dihydrogen phosphate (BDH, West Chester, PA), agar powder (Alfa Aesar, Ward Hill, MA), Brain heart infusion medium (Sigma-Aldrich, St. Louis, MO). Brain heart infusion (BHI) medium was prepared by adding 37 g of BHI powder in deionized water and adjusted to pH 7.4. BHI-agar medium was prepared by adding 6 g of agar to 400 mL of BHI media. Soft agar medium was prepared by adding 2 g of agar into 400 mL of BHI media. All media, buffer and glassware were sterilized before use. P100 bacteriophage (commercial name LISTEX^{TM}) was purchased from Micreos Food Safety (Wageningen, The Netherlands). *Listeria monocytogenes* Scott A strain was kindly provided by Dr. Michael Doyle (University of Georgia, Griffin). Standard molecular biology and cloning protocols were used for the construction of plasmid as explained in detail in Appendix K.

7.2.2 Bacterial strains, phages, and plasmids

The organisms and vectors used for construction of P100:bccp are listed in Table 7.1. *L. monocytogenes* was cultured in 4 mL BHI medium overnight at 37 °C. 500 µL aliquot of the overnight culture was inoculated into 50 mL of fresh BHI medium by shaking at 200 rpm for 5 h at 37 °C in an incubator shaker. *E. coli* cells were grown in standard Luria-Bertani media at 37 °C. For selection of plasmid-bearing bacteria cells, ampicillin or kanamycin was used at concentration of 50 µg/mL, respectively.

Table 7.1. Phages, bacterial strains, and plasmids involved in construction of P100:bccp.

Phages, strains, or plasmid	Genotype or relevant properties	Source or references
Phage P100	Virulent, *Listeria* specific, wild type	LISTEX^{TM}
Strains		
L. monocytogenes Scott A	*Wild type*	
E. coli X blue	*Wild type*	
E. coli BL21	*Wild type*	
Plasmids		
PZE12-luc	Amp^{R} General cloning vector	This study
PZE12-luc-Y3	5.4kb constructed cloning vector	This study
PDL 276	Gram^{-}Gram^{+} shuttle vector, Kan^{R}	This study
PDL 276-Y5	10.0 kb constructed shuttle vector	This study

7.2.3 Construction of PZE12-luc-Y3

The protocol used to construct plasmid PZE12-luc-Y3 is outlined in Figure 7.1. P100 phage genome is isolated and purified for PCR reactions. A 175 bp *pcps* fragment and a 417 bp *orf3* fragment were selected and amplified by PCR from P100 phage genome using primers listed in Table 7.2. Overlapping PCR was applied to fuse *pcps* gene with *egfp* gene using pcps-F, pcps-fus-F, pcps-fus-R, egfp-R. Ligation of the modified *orf3* gene into PZE12-luc plasmid resulted in PZE12-luc-Y3. Colonies of *E. coli* X blue carrying plasmids with functional *bccp* and *egfp* genes were identified by their fluorescence.

7.2.4 Construction of PDL 276-Y5

A 1404 bp *cps* fragment were selected and amplified with PCR from phage P100 genome using the primers listed in Table 7.2. A 468 bp *bccp* fragment was obtained by PCR from *E. coli*. The *pcps-egfp-orf3* cassette was removed with *Bam*HI and *Xba*I from plasmid PZE12-luc-Y3, ligated with *cps* gene, *bccp* gene into *Eco*RI-*Xba*I-digested PDL276. Transformation of the ligated plasmid was performed into *E. coli* BL 21 yielded PDL276-Y5 plasmid. Again, positive colonies were identified by their green fluorescence. The protocol used to construct plasmid PDL276-Y5 is

outlined in Figure 7.1. The plasmid was then purified from *E. coli* BL 21 and checked for correct structure and insertion orientation.

7.2.5 Verification of *bccp-egfp* gene insertion

The correct orientation and integrity of the *cps* 3' end was checked by performing restriction endonuclease digestion and determining the nucleotides sequences of the respective regions in plasmid mini-preparations.

Table 7.2. List of primers

S. No	Primer name	Sequence
1	cps-F	GGGAAAGAATTCATGCCAAAAAATAACAAAGAAGAAG
2	cps-R	GGGAAAGTCGACGTTGCTATGAACGTTTTTTACAGGAATATA
3	bccp-F	GGGAAAGTCGACGATATTCGTAAGATTAAAAAACTGAT
4	bccp-R	GGGAAAGGATCCTTACTCGATGACGACCAGCGGCTCGTC
5	pcps-F	GGGAAAGGATCCTAAAGGTAACTGTATAGAGTATTTTTTG
6	pcps-fus-F	GGTGATAAATATAAATGAGTAAAGGAGAAGAACTTTTCAC
7	pcps-fus-R	TCTTCTCCTTTACTCATTTATATTTATCACCTTTCAGTTTC
8	egfp-R	GGGAAAGCATGCCTATTTGTATAGTTCATCCATGCCATG
9	orf3-F	GGGAAAGCATGCTAATTATAGGATAATTGAATAAAAAC
10	orf3-R	GGGAAATCTAGATTACCCTCTCTTTAGTTCTTCAATT

7.2.6 Overall concept of P100 phage genetic engineering by homologous recombination

P100 phage host *L. monocytogenes* Scott A can be transformed with PDL276-Y5 by electroporation of penicillin-treated cells. Homologous recombination process as shown in Figure 7.2 helps the insertion of *bccp* and *egfp* genes for downstream of the major capsid protein gene, *cps*. *L. monocytogenes* could be infected with P100 (wild type) by using standard soft-agar overlay plates supplemented with 50 μg of kanamycin per mL. After overnight incubation at 37 °C, phage

from plates showing confluent lysis with green fluorescence could be eluted with 5 ml of SM buffer. The propagation process could be conducted following the procedure given in Appendix F, and the titer of the phage could thus be determined.

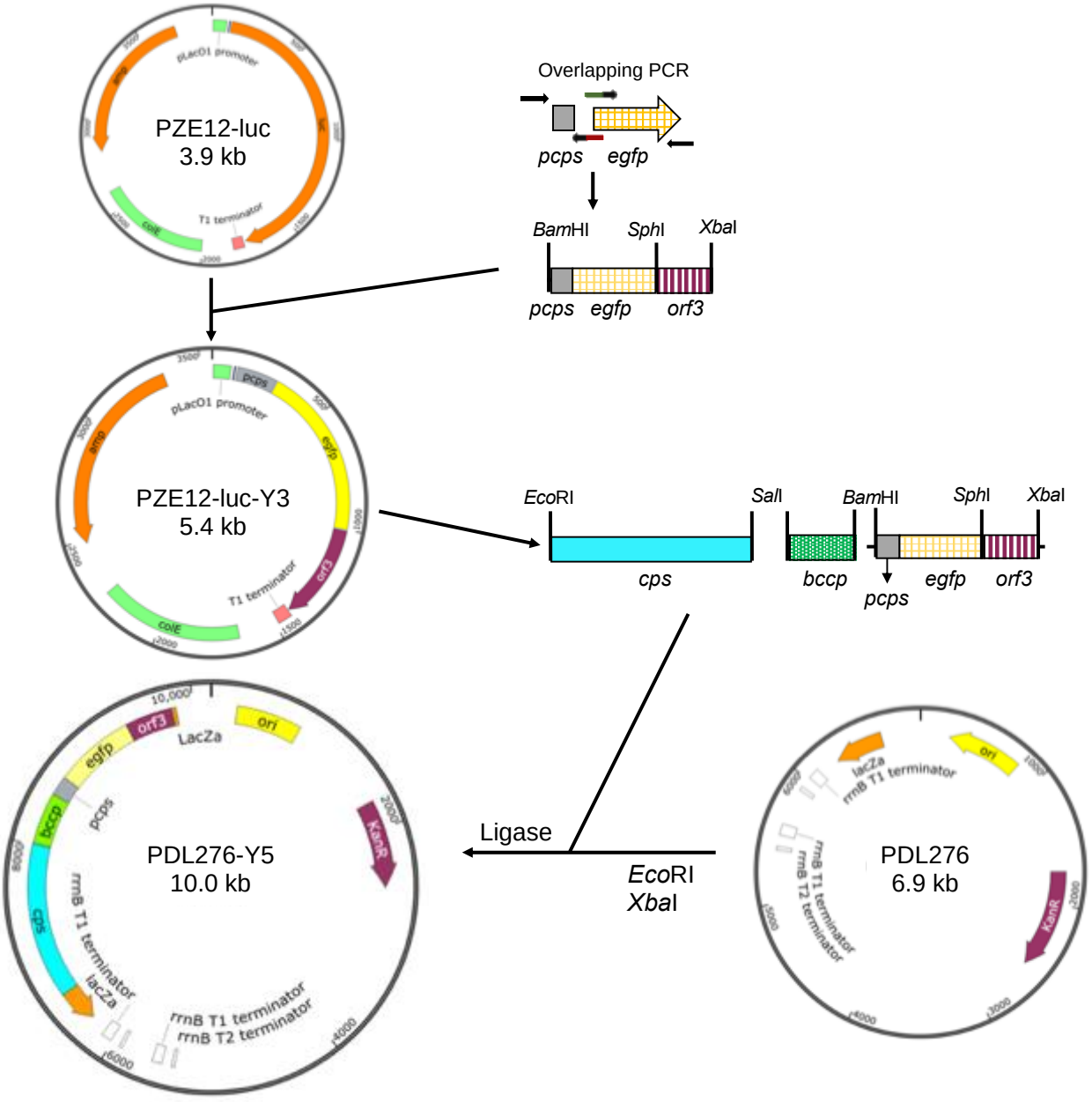

Figure 7.1: Construction of PDL276-Y5, which carries an P100 flanked *bccp* gene designed for *in vivo* homologous recombination with phage DNA.

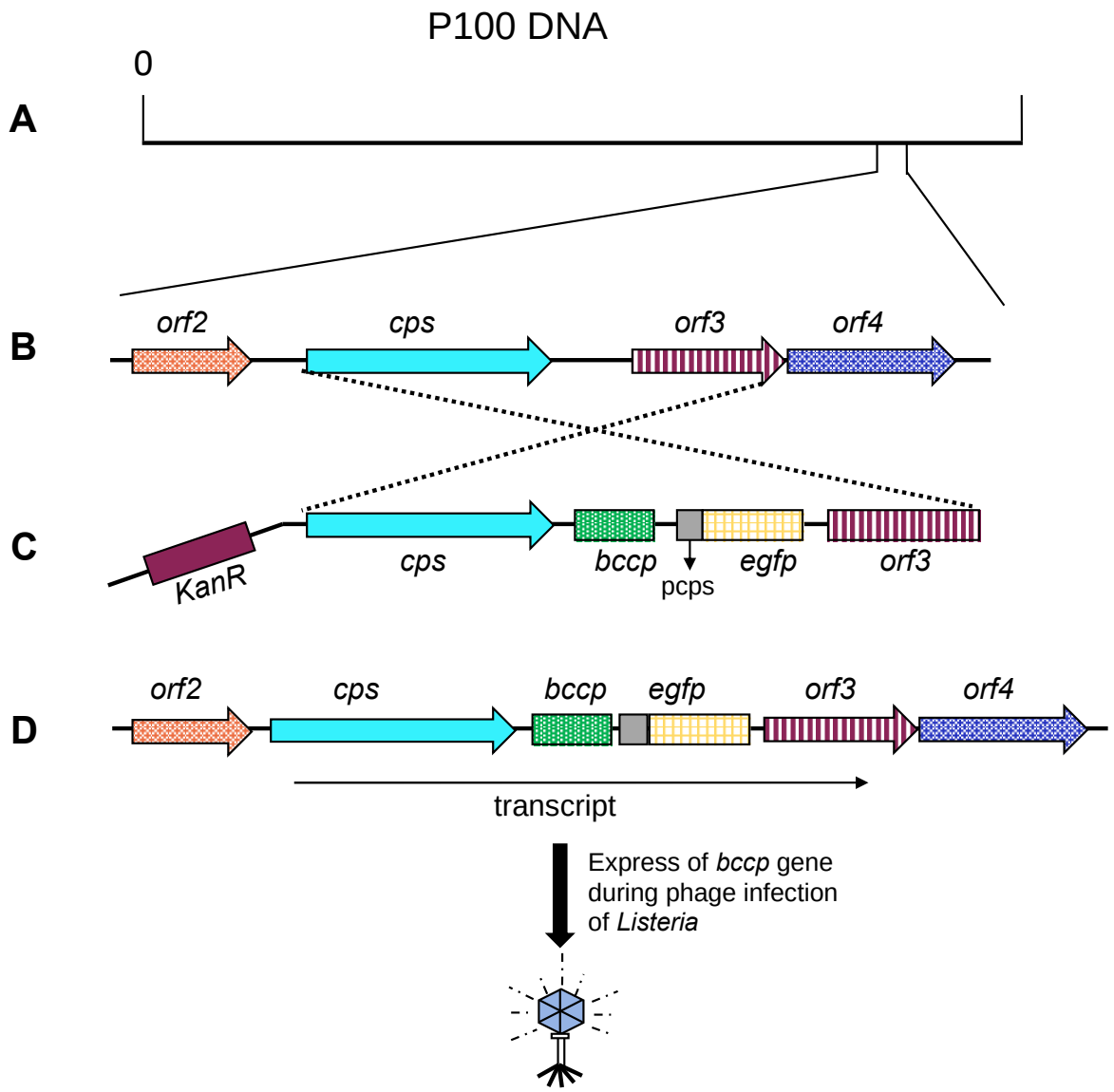

Figure 7.2: Outline of the homologous recombination process leading to insertion of *bccp, egfp* downstream of the major capsid protein gene, *cps*. (A) Simplified physical map of phage P100. (B) Approximately 3 kb segment of P100 genetic map. The multiplication signs indicate the recombination event between phage P100 DNA present in infected cells and PDL276-Y5 (C). (D) The resulting incorporation of *bccp* gene and *egfp* gene between the 3' end of *cps* and downstream transcription terminator.

7.3 Results and Discussion

7.3.1 Site specific introduction of *bccp* gene into PDL276 plasmid

The goal was to insert the *bccp* genes directly downstream of the P100 major capsid protein gene, *cps*, without disrupting any phage-encoded genes. Transcription initiation from the strong *cps* promotor should result in high level expression of *bccp* gene. Direct cloning into P100 phage DNA was not feasible because of its large size, the lack of appropriate, unique restriction sites for *Listeria* strains. Therefore, homologous recombination between phage DNA and a plasmid carrying *bccp* flanked by P100 DNA was the cloning strategy which we used. In order to select the genetically modified P100 phages, a fluorescence enhanced green fluorescence protein gene was also inserted. After the plasmid transformation, colonies were observed in antibiotic selective agar plates. The colonies were then cultivated and used for plasmid verification. Figure 7.3 showed the colonies with fluorescence in comparison with wild type *L. monocytogenes*. The cells were then centrifuged for plasmid extraction as shown in Figure 7.4, yellow pellets were obtained, which confirmed the successful transformation of PDL276-Y5. Thus the inserted *egfp* genes were successfully transcribed and expressed. To further verify the construction of the plasmid, the PDL276-Y5 plasmid, PCR was used with gene specific primer sets as mentioned in Table 7.2. Specific band corresponding to the *cps-bccp-pcps-egfp-orf3* gene was observed in Figure 7.5. Further, restriction endonuclease digestion was performed using PDL276 and PDL276-Y5 and the gel images are shown in Figure 7.6. Two types of endonuclease digestions were performed, which confirmed the successful construction of the PDL276-Y5 plasmid. A ~1800 bp band in lane 2 was observed after *Eco*RI/ *Bam*HI digestion, which confirmed the successful insertion of *cps-bccp* gene in PDL276-Y5 plasmid. In lane 5, a ~3000 bp band was observed after *Eco*RI/*Xba*I digestion, which confirmed the insertion of *cps-bccp-pcps-egfp-orf3* gene in PDL276-Y5 plasmid.

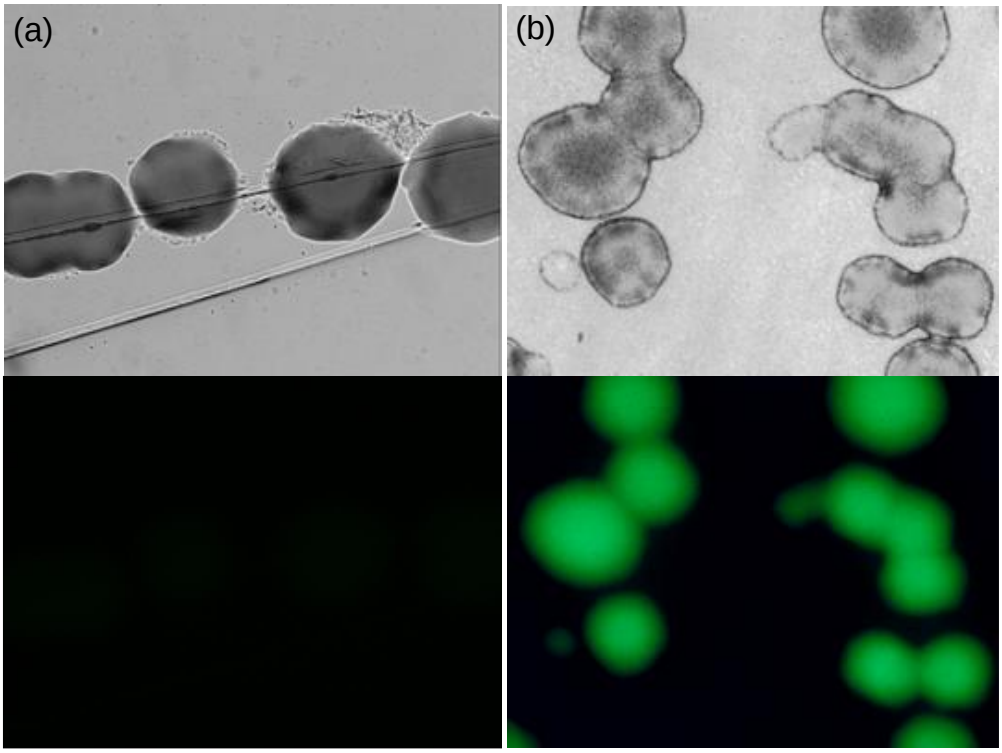

Figure 7.3: (a) Wild type *L. monocytogenes* under transmission microscopy (top), and fluorescence microscopy (bottom); (b) Transformed PDL276-Y5 in BL 21 cells under transmission microscopy (top), and fluorescence microscopy (bottom).

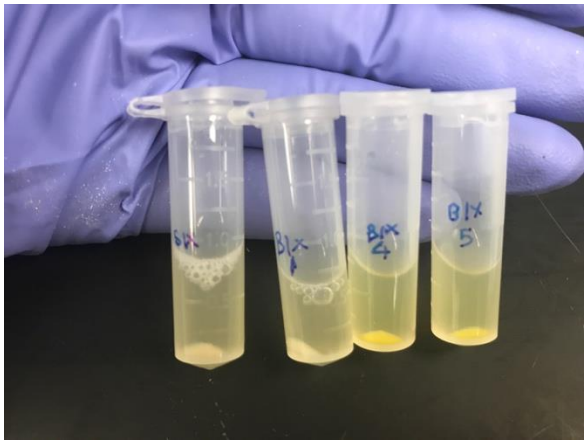

Figure 7.4: PDL276-Y5 transformed *E. coli XL* blue cells.

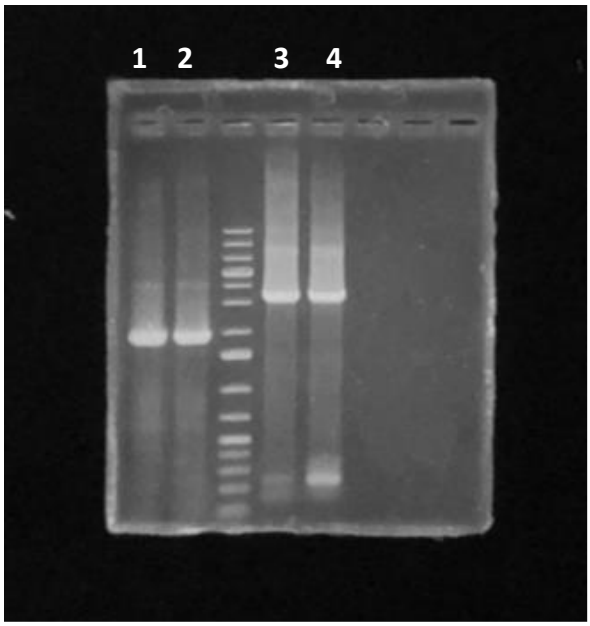

Figure 7.5: Verification of PDL276-Y5 plasmid by PCR using (1) cps-F and bccp-R primers; (2) cps-F and bccp-R primers (duplicate); (3) cps-F and orf3-R primers; (4) cps-F and orf3-R primers (duplicate). 1 kb DNA ladder is also shown in the image.

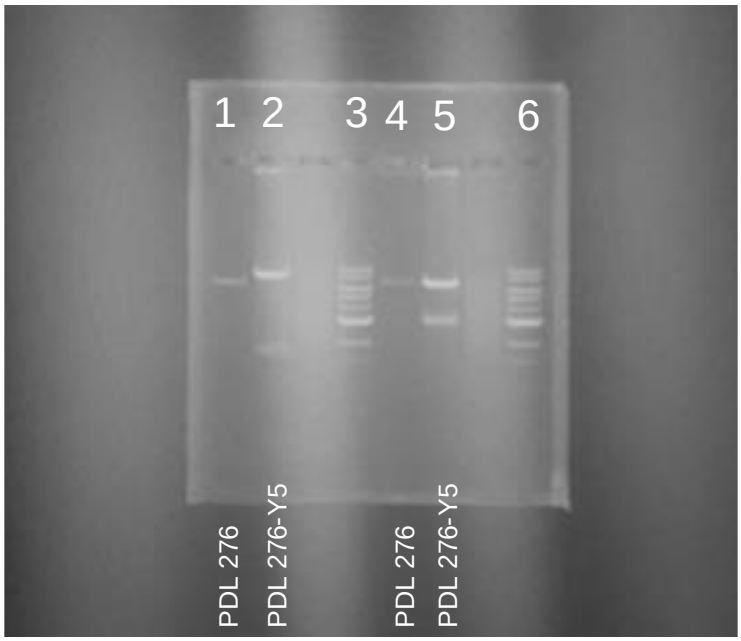

Figure 7.6: Verification of PDL276-Y5 plasmid by restriction endonuclease digestion. Lane 1-2 shows the digestion results using *Eco*RI/*Bam*HI; Lane 4-5 shows the digestion using *Eco*RI/*Xba*I.

7.4 Conclusion

In this work, a plasmid PDL276-Y5 plasmid was constructed for genetic engineering of phage P100 for bio-functionalization purpose. A biotin carboxyl carrier protein gene, *bccp* was inserted directly downstream of the P100 major capsid protein gene, *cps*, without disrupting any phage-encoded genes. In order to select the constructed phages, an enhanced green fluorescence protein gene, *egfp* was also introduced downstream of *bccp* genes. A promotor of *cps* gene is adopted upstream of *egfp* for successful transcription of green fluorescence protein. Transcription initiation from the strong *cps* promotor should result in high level of *bccp* and *egfp*. The constructed plasmid PDL276-Y5 could be used for in vivo homologous recombination in *Listeria monocytogenes.* Subsequent analysis of the recombinant phage P100 DNA can be performed, which could further be used for oriented immobilization of this genetically modified phage onto magnetic particles for *Listeria* separation as described in earlier chapters.

CHAPTER 8

CONCLUSIONS AND FUTURE DIRECTION

Modification of nanostructured electrodes using biological molecules could impart new functionalities on the electrodes and enable them to be used for a specific end application. This dissertation research demonstrates that a variety of different bio-functionalization approaches could be used for modification of electrode surface for two biosensor applications: laccase-nanoconjugates for oxygen sensing and bacteriophage-based biosensors for foodborne pathogen detection. Multi-disciplinary approaches to develop bio-functionalization methods for specific application, especially in achieving site-specific, or oriented immobilization of biomolecules have huge advantages and scopes to further improve the performance of the biosensors. A comprehensive approach towards bio-functionalization for biosensing application has been undertaken in this dissertation under three thematic focus areas:

(1) Enhancing the Electrocatalytic Activity of Laccase Nanoconjugates

The research work on this topic in the dissertation has demonstrated an enhanced electrocatalytic activity of laccase enzyme from both fungi and bacterial sources upon forming bio-nanoconjugates of laccase and their supporting materials. Laccase from *Trametes versicolor* (TVL) was initially used to functionalize metal oxide nanoparticles on electrode surfaces and was evaluated as electrocatalyst for oxygen sensing. Two different crosslinkers were studied to tether laccase enzyme onto metal oxide. The length of the crosslinker used for enzyme immobilization

was found to have a significant influence over the electron transfer between the nanoparticles and the enzyme. The TVL- *s*TiO_2 nanoconjugates as bio-electrocatalysts for O_2 reduction revealed competitive activity via direct electron transport and excellent activity via mediated electron transfer. However, TVL-based catalysts are currently limited by their poor stability on electrodes caused by the susceptibility of enzymes to denaturation and eventual activity loss. The above limitation could be overcome by developing bio-nanoconjugate catalysts using a recombinant laccase obtained from a thermophilic bacterium namely *Bacillus sp. FNT* (FNTL). *Bacillus sp.* FNTL exhibited superior stability over 2 weeks compared to TVL. An electro-kinetic study of FNTL-MWCNT bio-nanoconjugates also revealed high electrocatalytic activity of the conjugate catalysts towards bio-electrochemical reduction of oxygen to water. The kinetic parameters such as Tafel slopes, number of electrons transferred, electrochemical rate constant and electron transfer rate were calculated from rotating disk electrode experiments. The slope value obtained from Tafel plot was close to that of the ideal four-electron transfer oxygen reduction, which indicates the electroactivity of the immobilized FNT laccase.

(2) Exploring Bacteriophage-based Detection of Pathogens

In addition to the study of enzyme functionalized electrodes for electrochemical sensing applications, bacteriophages, were also used as biorecognition molecules for the electrochemical detection of pathogens using novel electric-field induced bio-functionalization methods. Charge-directed, orientated immobilization of bacteriophage particles on carbon nanotubes was achieved through covalent linkage of phage capsid onto the carbon nanotubes. Proof of concept study was conducted using T2 bacteriophage-based biosensors for electrochemical detection of non-pathogenic *Escherichia coli* B. The detection was highly selective towards the B strain of *E. coli*

as no signal was observed for the non-host K strain of *E. coli.* The present achievable detection limit of the biosensor is 10^3 CFU/mL.

Further investigations were conducted to evaluate the feasibility of using bacteriophage as recognition element for detection of pathogenic bacteria *L. monocytogenes.* Bacteriophage P100-modified magnetic particles (PMMP) was tested for selective isolation of *L. monocytogenes* using real food samples such as ground beef and whole milk. This study demonstrated the importance of phage immobilization methods and the magnetic particle sizes on the effectiveness of phage coupling to the magnetic particles, the retention of phage's infectivity on the magnetic particle and the bacterial cell capture efficiency of the resulting phage-modified magnetic particle. In order to develop a simultaneous isolation and detection platform for foodborne pathogens, the magnetically separated *L. monocytogenes* cells were used for direct impedimetric sensing in the absence and presence of magnetic field. The detection of PMMP isolated *L. monocytogenes* (magnetized *Listeria*) was studied in the presence of magnetic field, and it was found that the magnetic field-assisted detection resulted in significant improvement in sensitivity and detection limits.

Lastly, an attempt to improve the oriented immobilization of phage on magnetic particles to enable highly selective capture of bacterial cells with minimal non-specific binding was carried out. P100 was proposed to be genetically engineered to express biotin at the capsid of the phage structure, which could be oriented in head-down, tail-up fashion on the magnetic particle or on the electrode surface using complementary affinity receptors on the surface. A recombinant plasmid PDL276-Y5, was constructed with gene for biotin carboxyl carrier protein (*bccp*), and enhanced green fluorescence protein (*egfp),* which can be further introduced into P100 genome via homologous recombination. The resulting recombinant P100 can be used as an improved recognition molecule for both bacterial isolation and detection purposes.

Future Directions

Based on the scope of the research discussed in this dissertation, the following paths could be taken for future research on these topics:

1) The relative low onset potential from bacterial laccase FNT could be overcome by genetic engineering FNT to exhibit high redox potential for T1 Cu site, in order to make them attractive catalysts for fuel cell cathode application.
2) Genetic engineering offers a great opportunity to functionalize the bacteriophages genome with affinity tag, or expression of specific proteins or enzymes. New genetic engineering approaches to modify phage or the bacteria cells to enable better detection on the electrode could offer opportunities in the area of bacterial cell detection.
3) Fabrication of a lab on a chip device for simultaneous separation and detection of pathogens using the fundamental methods described in this dissertation, could also be a natural next step in the develop of bacterial cell biosensors.

REFERENCE

(1) Pangule, R. C.; Brooks, S. J.; Dinu, C. Z.; Bale, S. S.; Salmon, S. L.; Zhu, G.; Metzger, D. W.; Kane, R. S.; Dordick, J. S. *ACS Nano* **2010**, *7*, 3993-4000.
(2) Senthil Kumar, A.; Gayathri, P.; Barathi, P.; Vijayaraghavan, R. *The Journal of Physical Chemistry C* **2012**, *116*, 23692-23703.
(3) Turner, A. P. *Chem. Soc. Rev.* **2013**, *42*, 3184-3196.
(4) Long, G. L.; Winefordner, J. D. *Anal. Chem.* **1983**, *55*, 712-724.
(5) Poltronieri, P.; Mezzolla, V.; Primiceri, E.; Maruccio, G. *Foods* **2014**, *3*, 511-526.
(6) Sin, M. L.; Mach, K. E.; Wong, P. K.; Liao, J. C. *Expert Rev Mol Diagn* **2014**, *14*, 225-244.
(7) Upadhyay, L. S. B.; Verma, N. *Role of Biosensors in Environmental Monitoring* ; Springer, Cham, 2015; Vol. 45.
(8) Shi, J.; Claussen, J. C.; McLamore, E. S.; ul Haque, A.; Jaroch, D.; Diggs, A. R.; Calvo-Marzal, P.; Rickus, J. L.; Porterfield, D. M. *Nanotechnology* **2011**, *22*, 355502.
(9) Wooten, M.; Karra, S.; Zhang, M.; Gorski, W. *analytical Chemistry (Washington, DC, United States)* **2014**, *86*, 752-757.
(10) Zhu, L.; Yang, R.; Zhai, J.; Tian, C. *Biosens. Bioelectron.* **2007**, *23*, 528-535.
(11) Kalogianni, D. P.; Koraki, T.; Christopoulos, T. K.; Ioannou, P. C. *Biosens. Bioelectron.* **2006**, *21*, 1069-1076.
(12) Singh, A.; Arutyunov, D.; Szymanski, C. M.; Evoy, S. *Analyst* **2012**, *137*, 3405-3421.
(13) Chen, J.; Duncan, B.; Wang, Z.; Wang, L. S.; Rotello, V. M.; Nugen, S. R. *Nanoscale* **2015**, *7*, 16230-16236.
(14) Arya, S. K.; Singh, A.; Naidoo, R.; Wu, P.; McDermott, M. T.; Evoy, S. *Analyst* **2011**, *136*, 486-492.
(15) Chen, J.; Alcaine, S. D.; Jiang, Z.; Rotello, V. M.; Nugen, S. R. *Anal. Chem.* **2015**, *87*, 8977-8984.
(16) BarreirosdosSantos, M.; J.P.Agusil; B.Prieto-Simo´n; C.Sporer; V.Teixeira; Samitier, J. *Biosensors Bioelectron.* **2013**, *45*, 174-180.
(17) Aravind, S. S. J.; Ramaprabhu, S. *Sensors Actuators B: Chem.* **2011**, *155*, 679-686.
(18) Grieshaber, D.; MacKenzie, R.; Vörös, J.; Reimhult, E. *sensors* **2008**, *8*, 1400-1458.
(19) Blanford, C. F.; Foster, C. E.; Heath, R. S.; Armstrong., F. A. *Faraday Discuss.* **2009**, *140*, 319-335.
(20) Tilmaciu, C. M.; Morris, M. C. *Front Chem* **2015**, *3*, 59.
(21) Bellino, M. G.; Soler-Illia, G. J. A. A. *small* **2014**, *10*, 2834-2839.
(22) Besteman, K.; Lee, J.-O.; Wiertz, F. G. M.; Heering, H. A.; Dekker, C. *Nano Lett.* **2003**, *3*, 727-730.
(23) Jain, S. *Journal of Biosensors & Bioelectronics* **2012**, *01*.
(24) Bonanni, A.; Esplandiu, M. J.; del Valle, M. *Biosens. Bioelectron.* **2009**, *24*, 2885-2891.
(25) Bourourou, M.; Elouarzaki, K.; Lalaoui, N. m.; Agns, C.; Goff, A. L.; Holzinger, M.; Maaref, A.; Cosnier, S. *Chem. Eur. J.* **2013**, *2013*, 9371-9375.
(26) Hartmann, M.; Kostrov, X. *Chem. Soc. Rev* **2013**, *42*, 6277-6289.
(27) Jia, F.; Shan, C.; Li, F.; Niu, L. *Biosens. Bioelectron.* **2008**, *24*, 951-956.

(28) Holzinger, M.; Le Goff, A.; Cosnier, S. *Front Chem* **2014**, *2*, 63.
(29) Zhou, Y.; Umasankar, Y.; Ramasamy, R. P. *J. Electrochem. Soc.* **2015**, *162*, H911-H917.
(30) Guo, X. *J Biophotonics* **2012**, *5*, 483-501.
(31) Iijima, S. *Nature* **1991**, *354*, 56-58.
(32) Balasubramanian, K.; Burghard, M. *Small* **2005**, *1*, 180-192.
(33) Zhao, Q.; Gan, Z.; Zhuang, Q. *Electroanalysis* **2002**, *14*, 1609-1613.
(34) Lawal, A. T. *Mater. Res. Bull.* **2016**, *73*, 308-350.
(35) Mundra, R. V.; Wu, X.; Sauer, J.; Dordick, J. S.; Kane, R. S. *Curr. Opin. Biotechnol.* **2014**, *28*, 25-32.
(36) Li, S.; Zhu, X.; Zhang, W.; Xie, G.; Feng, W. *Appl. Surf. Sci.* **2012**, *258*, 2802-2807.
(37) Qiu, H.; Xu, C.; Huang, X.; Ding, Y.; Qu, Y.; Gao, P. *J. Phys. Chem. C* **2008**, *112*, 14781-14785.
(38) Solanki, P. R.; Kaushik, A.; Agrawal, V. V.; Malhotra, B. D. *NPG Asia Materials* **2011**, *3*, 17-24.
(39) Mohamad, N. R.; Marzuki, N. H.; Buang, N. A.; Huyop, F.; Wahab, R. A. *Biotechnol. Biotechnol. Equip.* **2015**, *29*, 205-220.
(40) Palmore, G. T. R.; Kim, H.-H. *J. Electroanal. Chem.* **1999**, *464*, 110-117.
(41) Gupta, G.; Rajendran, V.; Atanassov, P. *Electroanalysis* **2004**, *16*, 1182-1185.
(42) Fernández-Fernández, M.; Sanromán, M. Á.; Moldes, D. *Biotechnol. Adv.* **2013**, *31*, 1808-1825.
(43) Mate, D. M.; Alcalde, M. *Microb Biotechnol* **2017**, *10*, 1457-1467.
(44) Ivnitski, D.; Atanassov, P. *Electroanalysis* **2007**, *19*, 2307-2313.
(45) Willner, I.; Yan, Y. M.; Willner, B.; Tel-Vered, R. *Fuel Cells* **2009**, *9*, 7-24.
(46) El Ichi-Ribault, S.; Zebda, A.; Tingry, S.; Petit, M.; Suherman, A. L.; Boualam, A.; Cinquin, P.; Martin, D. K. *J. Electroanal. Chem.* **2017**, *799*, 26-33.
(47) Chen, R. J.; Zhang, Y.; Wang, D.; Dai, H. *J. Am. Chem. Soc* **2001**, *123*, 3838-3839.
(48) Ramasamy, R. P.; Luckarift, H. R.; Ivnitski, D. M.; Atanassov, P. B.; Johnson, G. R. *Chem Commun (Camb)* **2010**, *46*, 6045-6047.
(49) Parimi, N. S.; Umasankar, Y.; Atanassov, P.; Ramasamy, R. P. *ACS Catalysis* **2012**, *2*, 38-44.
(50) Rahman, M. M.; Ahammad, A. J.; Jin, J. H.; Ahn, S. J.; Lee, J. J. *Sensors (Basel)* **2010**, *10*, 4855-4886.
(51) Zhou, Y.; Umasankar, Y.; Ramasamy, R. P. *ECS Transactions* **2014**, *61*, 9-15.
(52) Sandra, H.; Tobenna, A., Making Sens of Recent Cost-of-Foodborne-Illness Estimates; USDA Economic Information Bulletin 118; U.S. Department of Agriculture2013.
(53) Scallan, E.; Hoekstra, R. M.; Angulo, F. J.; Tauxe, R. V.; Widdowson, M. A.; Roy, S. L.; Jones, J. L.; Griffin, P. M. *Emerg Infect Dis* **2011**, *17*, 7-15.
(54) Levinson, R. K. *N J Med* **1998**, *95*, 37-39.
(55) Nugen, S. R.; Baeumner, A. J. *Anal Bioanal Chem* **2008**, *391*, 451-454.
(56) Baeumner, A. *Anal Bioanal Chem* **2008**, *391*, 449-450.
(57) Batt, C. A. *Science* **2007**, *316*, 1579-1580.
(58) Breidt, F., Jr.; Caldwell, J. M. *J. Food Sci.* **2011**, *76*, M198-203.
(59) Conrad, M. M. N. L.; Conceição, F. R.; Moreira, Â. N.; Silva, W. P. d.; Aleixo, J. A.; Bhunia, a. A. K. *BMC Microbiol.* **2012**, *12*.
(60) Välimaa, A.-L.; Tilsala-Timisjärvi, A.; Virtanen, E. *Food Control* **2015**, *55*, 103-114.

(61) Administration, U. S. F. a. D. *Available at https://www.fda.gov/ICECI/ComplianceManuals/CompliancePolicyGuidanceManual/ucm136694.htm* **2008**.
(62) Buchanan, R. L.; Gorris, L. G. M.; Hayman, M. M.; Jackson, T. C.; Whiting, R. C. *Food Control* **2017**, *75*, 1-13.
(63) Xiong, Q.; Cui, X.; Saini, J. K.; Liu, D.; Shan, S.; Jin, Y.; Lai, W. *Food Control* **2014**, *37*, 41-45.
(64) Yang, H.; Qu, L.; Wimbrow, A. N.; Jiang, X.; Sun, Y. *Int. J. Food Microbiol.* **2007**, *118*, 132-138.
(65) Wang, H.; Li, Y.; Wang, A.; Slavik, M. *J. Food Prot.* **2011**, *74*, 2039-2047.
(66) Oravcova, K.; Trncikova, T.; Kuchta, T.; Kaclikova, E. *J. Appl. Microbiol.* **2008**, *104*, 429-437.
(67) Ahmed, A.; Rushworth, J. V.; Hirst, N. A.; Millner, P. A. *Clin. Microbiol. Rev.* **2014**, *27*, 631-646.
(68) Mothershed, E. A.; Whitney, A. M. *Clin. Chim. Acta* **2006**, *363*, 206-220.
(69) Stephen Inbaraj, B.; Chen, B. H. *J. Food Drug Anal.* **2016**, *24*, 15-28.
(70) Anany, R. C. H.; Gross, I.; Bhayani, R.; Griffiths, M.; Brook, M. A. *Biomaterials* **2010**, *31*, 1904-1910.
(71) Carlton, R. M.; Noordman, W. H.; Biswas, B.; de Meester, E. D.; Loessner, M. J. *Regul. Toxicol. Pharmacol.* **2005**, *43*, 301-312.
(72) Singh, A.; Poshtiban, S.; Evoy, S. *Sensors* **2013**, *13*, 1763-1786.
(73) Wu, L.; Luan, T.; Yang, X.; Wang, S.; Zheng, Y.; Huang, T.; Zhu, S.; Yan, X. *Anal. Chem.* **2014**, *86*, 907-912.
(74) Liébana, S.; Brandão, D.; Alegret, S.; Pividori, M. I. *Anal. Methods* **2014**, *6*, 8858-8873.
(75) Lu, T. K.; Bowers, J.; Koeris, M. S. *Trends Biotechnol.* **2013**, *31*, 325-327.
(76) Edgar, R.; McKinstry, M.; Hwang, J.; Oppenheim, A. B.; Fekete, R. A.; Giulian, G.; Merril, C.; Nagashima, K.; Adhya, S. *Proc. Natl. Acad. Sci. USA* **2006**, *103*, 4841-4845.
(77) Gervais, L.; Gel, M.; Allain, B.; Tolba, M.; Brovko, L.; Zourob, M.; Mandeville, R.; Griffiths, M.; Evoy, S. *Sensors and Actuators B* **2007**, *125*, 615-621.
(78) Handa, H.; Gurczynski, S.; Jackson, M. P.; Auner, G.; Mao, G. *Surf. Sci.* **2008**, *602*, 1392-1400.
(79) Nanduri, V.; Sorokulova, I. B.; Samoylov, A. M.; Simonian, A. L.; Petrenko, V. A.; Vodyanoy, V. *Biosensors Bioelectron.* **2007**, *22*, 986-992.
(80) Singh, A.; Glass, N.; Tolba, M.; Brovko, L.; Griffiths, M.; Evoy, S. *Biosensors Bioelectron.* **2009**, *24*, 3645-3651.
(81) Park, J. A.; Kim, S. B.; Lee, C. G.; Lee, S. H.; Choi, J. W. *J Environ Sci Health A Tox Hazard Subst Environ Eng* **2014**, *49*, 1116-1124.
(82) Hosseinidoust, Z.; Olsson, A. L.; Tufenkji, N. *Colloids Surf. B. Biointerfaces* **2014**, *124*, 2-16.
(83) Ahn, S.; Jeon, S.; Kwak, E.-A.; Kim, J.-M.; Jaworski, J. *Colloids Surf. B. Biointerfaces* **2014**, *122*, 851-856.
(84) Barton, S. C.; Kim, H.-H.; Binyamin, G.; Zhang, Y.; Heller, A. *J. Am. Chem. Soc* **2001**, *123*, 5802-5803.
(85) Barton, S. C.; Gallaway, J.; Atanassov, P. *Chem. Rev.* **2004**, *104*, 4867-4886.
(86) Durán, N.; Rosa, M. A.; D'Annibal, A.; Gianfreda, L. *Enzyme Microb. Technol.* **2002**, *31*, 907-931.

(87) Umasankar, Y.; Ramasamy, R. P. *Catalysis Science & Technology* **2013**, *3*, 2546-2549.
(88) Shleev, S.; Tkac, J.; Christenson, A.; Ruzgas, T.; Yaropolov, A. I.; James W. Whittaker, L. G. *Biosensors Bioelectron.* **2005**, *20*, 2517-2554.
(89) Kim, J.; Jia, H.; Wang, P. *Biotechnol. Adv.* **2006**, *24*, 296-308.
(90) Cracknell, J. A.; Vincent, K. A.; Armstrong, F. A. *Chem. Rev.* **2008**, *108*, 2439-2461.
(91) Solomon, E. I.; Sundaram, U. M.; Machonkin, T. E. *Chem. Rev.* **1996**, *96*, 2563-2605.
(92) Parimi, N. S.; Umasankar, Y.; Atanassov, P.; Ramasamy, R. P. *ACS Catalysis* **2012**, *2*, 38-44.
(93) Agbo, P.; Heath, J. R.; Gray, H. B. *J. Am. Chem. Soc.* **2014**, *136*, 13882-13887.
(94) Ramasamy, R. P.; Luckarift, H. R.; Ivnitski, D. M.; Atanassov, P. B.; Johnson, G. R. *Chemical Communications (Cambridge, United Kingdom)* **2010**, *46*, 5977-6188.
(95) Barton, S. C. *Handbook of Fuel Cells—Fundamentals, Technology and Applications*; John Wiley & Sons, London, 2009, p 112–130.
(96) Armstrong, F. A.; Hill, H. A. O.; Walton, N. J. *Q. Rev. Biophys.* **1985**, *18*, 261-322.
(97) Kenausis, G.; Taylor, C.; Katakis, L.; Heller, A. *J. Chem. Soc., Faraday Trans.* **1996**, *92*, 4131-4136.
(98) Sassolas, A.; Blum, L. J.; Leca-Bouvier, B. D. *Biotechnol. Adv.* **2012**, *30*, 489-511.
(99) Blanford, C. F.; Heath, R. S.; Armstrong., F. A. *Chem. Commun.* **2007**, *17*, 1710-1712.
(100) Vaze, A.; Hussain, N.; Tang, C.; Leech, D.; Rusling, J. *Electrochem. Commun.* **2009**, *11*, 2004-2007.
(101) Shrier, A.; Giroud, F.; Rasmussen, M.; Minteer, S. D. *J. Electrochem. Soc.* **2014**, *161*, H244-H248.
(102) Poulpiquet, A. d.; Ciaccafava, A.; Lojou, E. *Electrochemica Acta* **2014**, *126*, 104-114.
(103) Ivnitski, D.; Artyushkova, K.; n, R. A. R.; Atanassov, P.; Luckarift, H. R.; Johnson, G. R. *small* **2008**, *4*, 357-364.
(104) Miyake, T.; Yoshino, S.; Yamada, T.; Hata, K.; Nishizawa, M. *J.Am.Chem. Soc.* **2011**, *133*.
(105) Meredith, M. T.; Minson, M.; Hickey, D.; Artyushkova, K.; Glatzhofer, D. T.; Minteer, S. D. *ACS Catal.* **2011**, *1*, 1683-1690.
(106) Gutiérrez-Sánchez, C.; Pita, M.; Vaz-Domínguez, C.; Shleev, S.; Lacey, A. L. D. *J. Am. Chem. Soc.* **2012**, *134*, 17212-17220.
(107) Wong, L. S.; Khan, F.; Micklefied, J. *Chem. Rev* **2009**, *109*, 4025-4053.
(108) Wang, Q.; Peng, L.; Li, G.; Zhang, P.; Li, D.; Huang, F.; Wei, Q. *International Journal of Molecular Sciences* **2013**, *14*, 12520-12532.
(109) Sanlier, S. H.; Gider, S.; Koprulu, A. *Artificial Cells Nanomedicine and Biotechnology* **2013**, *41*, 259-263.
(110) Hou, J.; Dong, G.; Ye, Y.; Chen, V. *J. Membr. Sci.* **2014**, *452*, 229-240.
(111) Dagys, M.; Haberska, K.; Shleev, S.; Arnebrant, T.; Kulys, J.; Ruzgas, T. *Electrochem. Commun.* **2010**, *12*, 933-935.
(112) Guo, C. X.; Li, C. M. *Phys. Chem. Chem. Phys.* **2010**, *12*, 12153-12159.
(113) Oliveira, E. M.; Beyer, S.; Heinze, J. *Bioelectrochemistry* **2007**, *71*, 186-191.
(114) Strack, G.; Luckarift, H. R.; Nichols, R.; Cozart, K.; Katzd, E.; Johnson, G. R. *Chem. Commun.* **2011**, *47*, 7662-7664.
(115) Minussi, R. C.; Miranda, M. A.; Silva, J. A.; Ferreira, C. V.; Aoyama, H.; Marangoni, S.; Rotilio, D.; Pastore, G. M.; Durán, N. *African Journal of biotechnology* **2007**, *6*, 1248-1254.
(116) RIDE, J. P. *Physiological Plant Pathology* **1980**, *16*, 187-196.
(117) Nuzzo, R. G.; Allara, D. L. *J.Am.Chem.Soc* **1983**, *105*, 4481-4483.

(118) Lavrich, D.; Wetterer, S.; Bernasek, S.; Scoles, G. *J. Phys. Chem. B* **1998**, *102*, 3456-3465.
(119) Mallakpour, S.; Madani, M. *Bull. Mater. Sci.* **2012**, *35*, 333-339.
(120) McCarthy, S. A.; Davies, G.-L.; Gun'ko, Y. K. *Nature Protocols* **2012**, *7*, 1677-1693.
(121) Halámková, L.; Halámek, J.; Bocharova, V.; Szczupak, A.; Alfonta, L.; Katz, E. *J.Am.Chem. Soc.* **2012**, *134*, 5040-5043.
(122) Chakraborty, D.; Barton, S. C. *J. Electrochem. Soc.* **2011**, *158*, B440-B447.
(123) Elegir, G.; Daina, S.; Zoia, L.; Bestetti, G.; Orlandi, M. *Enzyme Microb. Technol.* **2005**, *37*, 340-346.
(124) Morozova, O. V.; Shumakovich, G. P.; Shleev, S. V.; Iaropolov, A. I. *Appl. Biochem. Microbiol.* **2007**, *43*, 523-535.
(125) Salaj-Kosla, U.; Pöller, S.; Schuhmann, W.; Shleev, S.; Magner, E. *Bioelectrochemistry* **2013**, *91*, 15-20.
(126) Shervedani, R. K.; Amini, A. *Bioelectrochemistry* **2011**, *84*, 25-31.
(127) Damjanovic, A.; Brusic, V. *Electrochim. Acta* **1967**, *12*, 615-628.
(128) Damjanovic, A.; Sepa, D. B.; Vojnovic, M. V. *Electrochim. Acta* **1979**, *24*, 887-889.
(129) Jones, S. M.; Solomon, E. I. *Cell. Mol. Life Sci.* **2015**, *72*, 869-883.
(130) Blanford, C. F.; Heath, R. S.; Armstrong, F. A. *Chem. Commun.* **2007**, 1710-1712.
(131) Sammond, D. W.; Kastelowitz, N.; Himmel, M. E.; Yin, H.; Crowley, M. F.; Bomble, Y. J. *PLOS ONE* **2016**, *11*, e0145848.
(132) I, L.; J., B. *Microbiologia* **1993**, *9*, 77-89.
(133) Beneyton , T.; Beyl , Y.; Guschin, D. A.; Griffiths, A. D.; Taly, V.; Schuhmann , W. *Electroanalysis* **2011**, *23*, 1781-1789.
(134) Atalah, J.; Zhou, Y.; Espina, G.; Blamey, J. M.; Ramasamy, R. P. *Catalysis Science & Technology* **2018**, *8*, 1272-1276.
(135) Millington, R. J. *Science* **1955**, *122*, 1090-1091.
(136) Gnanamuthu, D. S.; Petrocelli, J. V. *Journal of Electrochemical Society* **1967**, *114*, 1036-1041.
(137) Anastasuević, N. A.; Dimitruević, Z. M.; Adźić, R. R. *Electrochim. Acta* **1986**, *31*, 1125-1130.
(138) Bordley, J. A.; El-Sayed, M. A. *The Journal of Physical Chemistry C* **2016**, *120*, 14643-14651.
(139) Gojković, S. L.; Gupta, S.; Savinell, R. F. *Electrochim. Acta* **1999**, *45*, 889-897.
(140) Hsueh, K. L.; Chin, D. T. *J. Electroanal. Chem.* **1983**, *153*, 79-95.
(141) Barton, S. C.; Kim, H.-H.; Binyamin, G.; Zhang, Y.; Heller, A. *J. Am. Chem. Soc.* **2001**, *123*, 5802-5803.
(142) *Estimates of Foodborne Illness in the United States, Centers for Disease Control and Prevention* **2011**.
(143) *Centers for Disease Control and Prevention* **2015**.
(144) *Health topics on Tuberculosis, World Health Organization* **2014**.
(145) Ivnitski, D.; Abdel-Hamid, I.; Atanasov, P.; Wilkins, E. *Biosensors Bioelectron.* **1999**, *14*, 599-624.
(146) Ivnitski, D.; Abdel-Hamid, I.; Atanasov, P.; Wilkins, E.; Stricker, S. *Electroanalysis* **1999**, *12*, 317-325.
(147) Setterington, E. B.; Alocilja, E. C. *Biosensors* **2012**, *2*, 15-21.

(148) Maalouf, R.; Fournier-Wirth, C.; Coste, J.; Chebib, H.; Saı1kali, Y.; Vittori, O.; Errachid, A.; Cloarec, J.-P.; Martelet, C.; Jaffrezic-Renault, N. *Analytical Chemistry (Washington, DC, United States)* **2007**, *79*, 4879-4886.
(149) Viswanathan, S.; Rani, C.; Ho, J.-a. A. *Talanta* **2012**, *94*, 315-319.
(150) Stevens, K. A.; Jaykus, L. A. *Crit. Rev. Microbiol.* **2004**, *30*, 7-24.
(151) Shabani, A.; Zourob, M.; Allain, B.; Marquette, C. A.; Lawrence, M. F.; Mandeville, R. *Anal. Chem.* **2008**, *80*, 9475-9482.
(152) Pearson, H. A.; Sahukhal, G. S.; Elasri, M. O.; Urban, M. W. *Biomacromolecules* **2013**, *14*, 1257-1261.
(153) Tolba, M.; Minikh, O.; Brovko, L. Y.; Evoy, S.; Griffiths, M. W. *Appl. Environ. Microbiol.* **2010**, *76*, 528-535.
(154) Hosseinidoust, Z.; Ven, T. G. M. V. d.; Tufenkji, N. *Langmuir* **2011**, *27*.
(155) Anany, H.; Chen, W.; Pelton, R.; Griffiths, M. W. *Appl. Environ. Microbiol.* **2011**, *77*, 6379-6387.
(156) Han, J.-H.; Wang, M. S.; Das, J.; Sudheendra, L.; Vonasek, E.; Nitin, N.; Kennedy, I. M. *ACS Applied materials and Interfaces* **2014**, *6*, 4758-4765.
(157) Richter, Ł.; Matuła, K.; Leśniewski, A.; Kwaśnicka, K.; Łoś, J.; Łoś, M.; Paczesny, J.; Hołyst, R. *Sensors Actuators B: Chem.* **2016**, *224*, 233-240.
(158) Li, R.; Wang, X.; Ji, Z.; Sun, B.; Zhang, H.; Chang, C. H.; Sijie Lin; Meng, H.; Liao, Y.-P.; Wang, M.; Li, Z.; Hwang, A. A.; Song, T.-B.; Xu, R.; Yang, Y.; Zink, J. I.; Ne, A. E.; Xia, T. *ACS Nano* **2013**, *3*, 2352-2368.
(159) Lau, C.; Adkins, E. R.; Ramasamy, R. P.; Luckarift, H. R.; Johnson, G. R.; Atanassov, P. *Advanced Energy Materials* **2012**, *2*, 162-168.
(160) Calkins, J. O.; Umasankar, Y.; O'Neill, H.; Ramasamy, R. P. *Energy Environ. Sci.* **2013**, *6*, 1891-1900.
(161) Sekar, N.; Umasankar, Y.; Ramasamy, R. P. *Phys. Chem. Chem. Phys.* **2014**, *16*, 7862-7871.
(162) Van Valen, D.; Wu, D.; Chen, Y. J.; Tuson, H.; Wiggins, P.; Phillips, R. *Curr. Biol.* **2012**, *22*, 1339-1343.
(163) Ovesny, M.; Krizek, P.; Borkovec, J.; Svindrych, Z.; Hagen, G. M. *Bioinformatics* **2014**, *30*, 2389-2390.
(164) Andrews, J. M.; Testing, B. W. P. o. S. *J. Antimicrob. Chemother.* **2009**, *64*, 454-489.
(165) Zhang, G.; Dang, L.; Li, L.; Wang, R.; Fu, H.; Shi, K. *CrystEngComm* **2013**, *15*, 4730.
(166) Sadeghi, G.; Schijven, J. F.; Behrends, T.; Hassanizadeh, S. M.; Gerritse, J.; Kleingeld, P. J. *Ground Water* **2011**, *49*, 12-19.
(167) Zweckstetter, M.; Hummer, G.; Bax, A. *Biophys. J.* **2004**, *86*, 3444-3460.
(168) Zhou, B.; Lin, Y.; Harruff, B. A.; Sun, Y.-P. *Photoluminescence Properties of Carbon Nanotubes*; Springer-Verlag Berlin Heidelberg, 2008; Vol. 4.
(169) Tlili, C.; Sokullu, E.; Safavieh, M.; Tolba, M.; Ahmed, M. U.; Zourob, M. *Anal. Chem.* **2013**, *85*, 4893-4901.
(170) Shabani, A.; Marquette, C. A.; Mandeville, R.; Lawrence, M. F. *Analyst* **2013**, *138*, 1434-1440.
(171) Bekir, K.; Barhoumi, H.; Braiek, M.; Chrouda, A.; Zine, N.; Abid, N.; Maaref, A.; Bakhrouf, A.; Ouada, H. B.; Jaffrezic-Renault, N.; Mansour, H. B. *Environ Sci Pollut Res* **2015**, *22*, 15796-15803.
(172) Li, Y.; Afrasiabi, R.; Fathi, F.; Wang, N.; Xiang, C.; RyanLove; She, Z.; Kraatz, H.-B. *Biosensors Bioelectron.* **2014**, *58*, 193-199.

(173) Mejri, M. B.; Baccar, H.; Baldrich, E.; Del Campo, F. J.; Helali, S.; Ktari, T.; Simonian, A.; Aouni, M.; Abdelghani, A. *Biosens. Bioelectron.* **2010**, *26*, 1261-1267.
(174) Martelet, A.; L'Hostis, G.; Nevers, M.-C.; Volland, H.; Junot, C.; Becher, F.; Muller, B. H. *Anal. Chem.* **2015**, *87*, 5553-5560.
(175) Suo, Z.; Yang, X.; Avci, R.; Deliorman, M.; Rugheimer, P.; Pascual, D. W.; Idzerda, Y. *Anal. Chem.* **2009**, *81*, 7571-7578.
(176) Steingroewer, J.; Bley, T.; Bergemann, C.; Boschke, E. *J. Magn. Magn. Mater.* **2007**, *311*, 295-299.
(177) Koo, O. K.; Aroonnual, A.; Bhunia, A. K. *J. Appl. Microbiol.* **2011**, *111*, 93-104.
(178) Zhou, Y.; Marar, A.; Kner, P.; Ramasamy, R. P. *Anal. Chem.* **2017**, *89*, 5734-5741.
(179) Wang, Z.; Wang, D.; Chen, J.; Sela, D. A.; Nugen, S. R. *Analyst* **2016**, *141*, 1009-1016.
(180) Tolba, M.; Minikh, O.; Brovko, L. Y.; Evoy, S.; Griffiths, M. W. *Appl. Environ. Microbiol.* **2010**, *76*, 528-535.
(181) Hagens, S.; Loessner, M. J. *Front Microbiol* **2014**, *5*, 159.
(182) Smartt, A. E.; Xu, T.; Jegier, P.; Carswell, J. J.; Blount, S. A.; Sayler, G. S.; Ripp, S. *Anal. Bioanal. Chem.* **2012**, *402*, 3127-3146.
(183) Kanayeva, D. A.; Wang, R.; Rhoads, D.; Erf, G. F.; Slavik, M. F.; Tung, S.; Li, Y. *J. Food Prot.* **2012**, *75*, 1951-1959.
(184) U.S.D.A. *pp. 47729–47732, 2006 Available at: http://edocket.access.gpo.gov/2006/E6-13621.htm.* **2006**.
(185) U.S.D.A. *Available at https://www.accessdata.fda.gov/scripts/fdcc/index.cfm?set=grasnotices&id=198* **2006**.
(186) Laube, T.; Cortés, P.; Llagostera, M.; Alegret, S.; Pividori, M. I. *Appl. Microbiol. Biotechnol.* **2014**, *98*, 1795-1805.
(187) Liebana, S.; Spricigo, D. A.; Cortes, M. P.; Barbe, J.; Llagostera, M.; Alegret, S.; Pividori, M. I. *Anal. Chem.* **2013**, *85*, 3079-3086.
(188) Zhan, S.; Yang, Y.; Shen, Z.; Shan, J.; Li, Y.; Yang, S.; Zhu, D. *J. Hazard. Mater.* **2014**, *274*, 115-123.
(189) Jin, Y.; Liu, F.; Shan, C.; Tong, M.; Hou, Y. *Water Res.* **2014**, *50*, 124-134.
(190) Parikh, S. J.; Chorover, J. *Langmuir* **2006**, *22*, 8492-8500.
(191) Cagnasso, M.; Boero, V.; Franchini, M. A.; Chorover, J. *Colloids Surf. B. Biointerfaces* **2010**, *76*, 456-467.
(192) Shan, S.; Zhong, Z.; Lai, W.; Xiong, Y.; Cui, X.; Liu, D. *Food Control* **2014**, *45*, 138-142.
(193) Gasanov, U.; Hughes, D.; Hansbro, P. M. *FEMS Microbiol. Rev.* **2005**, *29*, 851-875.
(194) Law, J. W.; Ab Mutalib, N. S.; Chan, K. G.; Lee, L. H. *Front Microbiol* **2015**, *6*, 1227.
(195) Wadud, S.; Leon-Velarde, C. G.; Larson, N.; Odumeru, J. A. *J. Microbiol. Methods* **2010**, *81*, 153-159.
(196) Bilir Ormanci, F. S.; Erol, I.; Ayaz, N. D.; Iseri, O.; Sariguzel, D. *Br Poult Sci* **2008**, *49*, 560-565.
(197) Šafařík, I.; Šafaříková, M. *Journal of Chromatography B: Biomedical Sciences and Applications* **1999**, *722*, 33-53.
(198) Yáñez-Sedeño, P.; Campuzano, S.; Pingarrón, J. M. *Sensors* **2016**, *16*, 1585
.

APPENDICES

APPENDIX A

Laccase Enzyme Activity Assay

Reagents:

A: 100 mM Potassium phosphate buffer, pH 6.5 at 30°C (Adjust the pH at 30 °C with 1M KOH)

B: 0.216 mM Syringaldazine Solution in absolute methanol.

C: Laccase enzyme solution. (Prepare immediately before use, 25-50 U/mL of laccase in cold DI water)

Sample preparation:

1. Prepare "Blank" cuvette following the table below.

	Blank
DI water	0.5 mL
Reagent A (Buffer)	2.2 mL
Equilibrate to 30°C, monitor A530nm until constant, then add Reagent B	
Reagent B	0.3 mL

2. Use the "Blank" cuvette to zero the instrument
3. Prepare "Sample" cuvette following the table below.

	Sample
Reagent A (Buffer)	2.2 mL
Reagent C (Enzyme solution)	0.5 mL
Equilibrate to 30°C, monitor A530nm until constant, then add Reagent B	
Reagent B	0.3 mL

4. Immediately mix by pipetting and record the increase in A_{530nm} for 10 min using the MULTISKAN GO thermostatted spectrophotometer.
5. Obtain the ΔA_{530nm}/min using the maximum linear rate.

Calculations:

$$\text{Units/mL enzyme} = \frac{(\Delta A530nm/\min(\text{Sample})-\Delta A530nm/\min(\text{Blank}))(Df)}{(0.001)(0.5)}$$

Df: Dilution factor;

0.001: The change in ΔA_{530nm}/min per unit of Laccase at pH 6.5, 30°C in a 3mL reaction mix.

0.5: Volume of the enzyme sample.

$$\text{Units/mg solid} = \frac{\text{Units/mL enzyme}}{\text{mg solid/mL enzyme}}$$

Reference: Ride, J.P. (1980) Physiological Plant Pathology, 16, 187-196.

APPENDIX B

Bradford Assay

1. The Bradford assay can be performed using 96-well plates.
2. Remove the 1X dye reagent from 4 °C storage and let it warm to ambient temperature. Invert the dye reagent a few times before use.
3. Use BSA stock 0.5 mg/mL to protein standard analysis. Pipette the stock solution and sample mix with Bradford 1X dye agent following the table below.

Standard protein BSA (µL)	DI water (µL)	Braford 1X dye reagent (µL)
0	10	190
2	8	190
4	6	190
6	4	190
8	2	190
10	0	190
Protein Sample (µL)		
10	0	190

4. Mix the samples in the microplate mixer using MULTISKAN GO thermostatted spectrophotometer.
5. Incubate at room temperature for at least 5 min. (do not incubate for more than 1 hr at room temperature).
6. Set the spectrophotometer to 595 nm. Measure the absorbance of the standards and unknown samples.

7. All standards and samples could be assayed in duplicates and triplicates.
8. Create a standard curve by plotting the 595 nm values (y axis), versus their concentration in µg/mL (x axis). Determine the unknown sample concentrations using the standard curve.
9. If the sample is diluted, adjust the final concentration of the unknown samples by multiplying the dilution factor.

APPENDIX C

Laccase Enzyme Dialysis

Materials and reagents:

Slide-A-Lyzer™ Dialysis Cassettes (10K MWCO)

10mL of 10mM $CuSO_4$ in DI water

Laccase enzyme solution: 3 mL of 50 mg/mL of Laccase in cold DI water

2.88 L of 20mM of pH 5.8 phosphate buffer

Procedures:

1. Weigh 150 mg of Laccase and dissolve in 1.5 mL of ice cold water.
2. Centrifuge the laccase solution at 14000 rpm for 15 min, collect the supernatant.
3. Add another 1.5 mL of water into the residue, and centrifuge at 14000 rpm for 15 min.
4. Collect the supernatant ~3 mL.
5. Keep the enzyme solution on ice before dialysis.
6. Prepare the dialysis buffer by adding 5.76 mL of 10mM $CuSO_4$ into the phosphate buffer and stir at 4 °C.
7. Slip the Cassette into the groove of an appropriate size buoy, immerse the cassettes in dialysis buffer to hydrate the cassette for at least 2 min, as shown below,

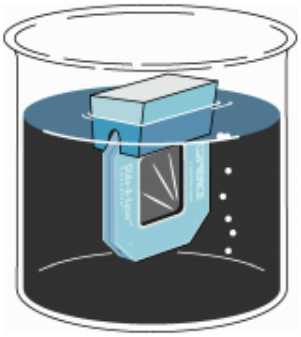

8. Remove cassette from buffer and remove excess liquid by tapping the edge of the cassette gently on paper. (Do not blot the membrane.)
9. Fill a 10 mL syringe with a volume of air equal to the sample size. For low-volume samples, fill the syringe with a volume of air approximately equal to two times of the sample volume.
10. With the bevel sideways, insert the tip of the needle through another syringe port located at a corner of the cassette. Inject air slowly into the cassette to separate the membranes.
11. Turn the unit so that needle is on the bottom and allow the sample to collect near the port. Withdraw the sample into the syringe.
12. Dialyze the laccase enzyme solution for overnight at 4 °C.
13. Add air into the cassette containing the sample before removing the laccase solution from the cassette.
14. Conduct laccase enzymatic activity assay the next day following Appendix A.

APPENDIX D

Bacteria Cultivation

Escherichia coli B

LB (Luria-Bertani) medium

	1 L medium
Tryptone 1%	10 g
Yeast Extract 0.5%	5 g
NaCl 1%	10 g
Agar plates 1.5%	15 g
Soft agar 0.5%	5 g

Adjust to pH 7.0. Autoclave the medium at 121 °C, 30 min, 18 psi.

1. Use a sterile inoculation loop/ pipette tip to scrape a small quantity of frozen material and streak for isolated colonies on LB plates.
2. Incubate the agar plate overnight at 37 °C.
3. Use a sterile inoculation loop to pick a single, freshly isolated colony of *E. coli*, and introduce the colony into a sterile LB medium in a culture tube by gently swirling the loop within the broth.
4. Inoculate the culture at 37 °C with orbital shaking at 200-250 rpm.
5. To prepare bacteria in exponential phase of growth for plaque assay or phage propagation, take the overnight culture and add to a fresh LB medium based on 1:100 ratio, and incubate for 3-4 hours.

a. A bacteria growth curve can be generated by take the OD_{600nm} of the culture every 30 min to 1h.

Listeria monocytogenes

Brain Heart Infusion (BHI) medium

37 grams into 1 L DI water.

Adjust to pH 7.4. Autoclave the medium at 121 °C, 30 min, 18 psi.

1. Use a sterile inoculation loop/ pipette tip to scrape a small quantity of frozen material and streak for isolated colonies on BHI plates.
2. Incubate the agar plate overnight at 37 °C/ 30 °C.
3. Use a sterile inoculation loop to pick a single, freshly isolated colony of *Listeria monocytogenes*, and introduce the colony into a sterile LB medium in a culture tube by gently swirling the loop within the broth.
4. Inoculate the culture at 37 °C/30 °C with/without orbital shaking at 200-250 rpm.
5. To prepare bacteria in exponential phase of growth for plaque assay or phage propagation, take the overnight culture and add to a fresh LB medium based on 1:100 ratio, and incubate for 3-4 hours.
    b. A bacteria growth curve can be generated by take the OD_{600nm} of the culture every 30 min to 1h.

APPENDIX E

Buffer Preparation

pH 7.4 Phosphate buffer saline (10X)

	200 mL
NaCl	16.0 g
KCl	0.40 g
Na_2HPO_4	2.8 g
KH_2PO_4	0.49 g

Adjust the pH to 7.4, and store at room temperature. Dilute to 1X PBS and sterilize using autoclave every time before use.

Sodium magnesium (SM) buffer

	400 mL
NaCl	2.338 g
$MgSO_4$ $7H_2O$	0.789 g
Tris base	2.423 g
10% Gelatin	200 µL

Filter-sterilize. Store at room temperature or 4 °C.

Reference: Protocol adopted from Cold Spring Harbor Protocols.

APPENDIX F

Phage Propagation and Plaque Assay

The following protocol was used to propagate bacteriophage T2.

1. Serial dilution of phage stocks (~10^{10} PFU/mL).
2. To each 100 μL of phage stock, 250 μL of bacteria culture were added and mixed.
    a. *E. coli* bacteria culture needs to be grown to log phase, O.D.~ 1.0, so all cells are in active growing condition. For efficient propagation, use the mid-log phase cultures.
3. Take 100 μL phage solution and mix with 250 μL bacteria culture. The mixture was then added into 3 mL molten soft agar (LB containing 0.5 % agar)
    a. Pre-warm plates of the LB plates in the incubator.
4. Poure the mixed soft agar onto LB plates.
    a. Incubated the plates under 37 °C for one hour before the experiment to prevent solidify of soft agar on LB plates.
5. Incubate the plates upside down at 37 °C at room temperature.
6. Collect the plates on the following day. (usually after 24 hours)
    a. Plaques are formed on the soft agar plates, and the concentration of the phage stock can be counted and expressed in PFU/mL. (Stop in here for plaque assay, and quantify the phages by counting the plaques)

7. Add 2-5 mL of SM buffer onto the plates and the plate was placed on the bench rocker for two hours at room temperature, (or longer time at 4 °C)
    a. I generally use 2 mL of SM buffer in order not to dilute the phage concentration.
8. Scraped off the surface and collect the soft agar in centrifuge tubes.
9. Centrifuge at 4000 g for 10 min to sediment the cellular debris and agar. Conserve the supernatant.
10. Use syringe filter to remove the bacteria debris from the supernatant.
    a. The supernatant was collected and passed through a 0.22 μm Millipore filter.
11. Centrifuge the filtered supernatant at high speed 17200 g at 4°C for three hours or more.
    a. Confirm the formation of phage pellets in the centrifuge tubes. (a transparent pellet)
12. The supernatant was removed, and the phage pellet was resuspended in 1 mL SM buffer.
13. For long term storage, freeze the tube in liquid nitrogen and store it at -80°C.

APPENDIX G

Preparation of Phage Modified Magnetic Particles

Buffer: 100 mM PBS pH 7.4, 0.01% Tween 20.

Magnetic particle: 150 nm/ 500 nm/ 1 μm amine functionalized (10 mg/ml)

Surface activation

1. Aliquot 20 μL (1×10^{10} beads) of magnetic beads into low-binding micro-centrifuge tube.
2. Add 70% ethanol to sterilize the MNP, and remove the ethanol using magnetic separator.
    a. Make sure to separate the beads for at least 9 min.
3. Add 500 μL sterilized PBS to wash the particle for twice.

a. When withdrawing the clear suspension from the tube, slowly take up the supernatant without disturbing the beads. (Don't have to take all supernatant is you are not sure about that)

4. Add 300 μL PBS the magnetic beads and vortex the solution for 15 seconds.
5. Add 200 μL BS3 (10 mM in PBS) to the magnetic beads solution.
    a. Equilibrate the BS3 tube to room temperature before open the bottle cap. Syringe filter the BS3 solution before use.
6. React at room temperature for 30 minutes with continuous mixing.
7. Place tube into the magnetic separator and allow the activated magnetic beads to separate. Remove the supernatant and add 500 μL coupling buffer. Re-suspend the magnetic beads.

8. Place the tube into the magnetic separator and allow the activated magnetic beads to separate. Wash the activated beads two more time with 0.5 mL coupling buffer. Note: This purification step should be done as soon as possible.
9. Remove the supernatant and add 0.4 mL coupling buffer. Re-suspend the magnetic beads with vortex.
10. Add 360 μL bacteriophages suspension. React at 4°C for overnight using the tube rotator.
11. Collect the tube, place it into the magnetic separator, and allow the phage modified magnetic beads to separate.
12. Remove the supernatant, place it in another tube for further analysis.
    a. The collect supernatant could be used to perform plaque assay to calculate phage coupling ratio.
13. Resuspend the beads in 0.5 mL PBS and wash the beads with PBS for three times.
14. Add 0.5 mL SM buffer and keep it rotate 4 °C for 2 hours at to terminate the activated residual groups.
15. Keep the phage modified magnetic beads at 4 °C for long term storage.

APPENDIX H

Electrochemical Experiments

Three-electrode system

The three-electrode system or half-cell electrochemical system consists of three electrodes:

1. Working electrode. The electrode where the concerned electrochemical reaction under study happens.

The glassy carbon electrode (cylindrical in shape with a dimension of 3 mm) and screen-printed electrode are used as the working electrode in the research unless otherwise specifically mentioned. The glassy carbon electrodes have been modified with different biocatalyst such as TVL/sMOx/GC or Phage/PEI-MWCNT/GC**.**

2. Reference electrode. The potential at the working electrode is measured or a fixed constant potential is applied to the working electrode with respect to this reference electrode. In the entire thesis work, silver/silver chloride reference electrode (Ag/AgCl, sat. KCl) is used as the reference electrode. The equilibrium potential of the Ag/AgCl, sat. KCl is + 0.197 V with respect to Standard Hydrogen Electrode (SHE, whose equilibrium potential is 0 V). All the potential values are reported with respect to the Ag/AgCl, sat. KCl unless otherwise specifically mentioned.

3. Counter electrode. It is also called auxiliary electrode that closes the circuit for an electrochemical measurement. A thin platinum wire is usually used as the counter electrode. The three-electrode system is an electrochemical system used to study the oxidation/reduction reaction

that is happening at the working electrode with respect to the reference electrode (Ag/AgCl, sat. KCl). All the three electrodes are dipped into the electrolyte and the leads from the three electrodes are connected to the potentiostat. A specific function (explained below) in the potentiostat is chosen based on the type of electrochemical parameter measured.

Open Circuit Potential

Open Circuit Potential (OCP) is the potential difference between the two electrodes (the anode and the cathode) measured without closing the circuit with an external load, i.e., no current is flowing through the circuit. Throughout the research work, the OCP is measured by choosing the "Open Circuit Potential" function in the potentiostat.

Polarization Curve

Polarization curve is a plot of current density (A/m_2) on the x-axis versus potential (V) in the y-axis. By using a potentiostat, the Amperometric I-t curve can be achieved by applying a different constant potential at a time to measure the steady state current

The polarization curve clearly explains the type of losses (such as ohmic losses, charge transfer losses and concentration losses) that predominates the electrochemical system and is very useful to improve the system performance.

APPENDIX I

Microscopy Sample Preparation

Fluorescence microscopy imaging of bacteria and phages

A. Fluorescence imaging of immobilized phage on ITO electrodes.

1. Incubate bacteriophage with SYBR GOLD 100X for 30 min.
2. Free dye on phage particles were removed by diluting 100 µL of the phage suspension and then centrifuging the sample across a 100 kDa (EDM Millipore, UFC 910008) filter four times.
    a. Each centrifugation step led to a 40-fold of dilution of dye, reducing the final concentration of dye.
3. After 4-step of centrifugation, the phage was resuspended in saline to the original volume of 100 µL.
4. The fluorescence imaging of the bacteriophage was performed on a STORM microscope system that has been previously described with modification.
5. The sample was excited with a 488nm laser (Cyan 488, Newport). The laser is reflected off of a long-pass dichroic (DMLP567T, Thorlabs) so that excitation in both blue and red channels can be combined. The emission and excitation paths are separated by a multiband dichroic (XF2054 485-555-650 TBDR, Omega Optical) and a multiband emission filter is placed before the CCD camera (BrightLine triple-band bandpass filter; FF01-515/588/700-

25, Semrock). The objective is a 60X oil immersion objective (1.42 N.A., 60X oil immersion, Plan Apo N, Olympus) and the image is magnified by an additional factor of 3 before the CCD camera so that the effective pixel size at the sample plane is 89nm. The CCD camera is a 14-bit EMCCD that was used in emgain mode for these experiments (Ixon DV887DCS-BV, ANDOR). Fluorescently labeled phage particles were counted by first using a wavelet filter and then detecting the molecules using a local maximum algorithm which detects if the pixel intensity of each pixel in the filtered image is above an intensity threshold which was set to be 1.3 times the standard deviation of the first wavelet level of the input image.[33]

B. Fluorescence imaging of bacteria cells using LIVE/DEAD BacLight kit

1. The images were obtained using EVOS fluorescence microscopy (Invitrogen) with a 100X objective.
    a. Deionized water was used to prepare all solutions.
2. Host bacteria were stained with SYTO9 and PI, a red fluorescent nucleic acid dye with EX/EM of 490 nm/635 nm.
    a. The SYTO 9 stain labels all bacteria in a population, whereas PI penetrates only bacteria with damaged membranes. Thus, a mixture of the SYTO 9 and PI will label bacteria with intact cell membranes fluorescent green and bacteria with damaged membranes fluorescent red.
3. Following contact with the bacterial suspension, the slide was monitored for 40 min with fluorescence microscope to observe cell membrane disruption.
    a. It should be noted that the phage remained hydrated throughout the preparation and testing of the phage-functionalized substrates.

Scanning electron microscopy imaging of PMMP (with bacteria attached onto it).

Buffers: PBS/PBST/water/ethanol/glutaraldehyde/OsO_4

Materials: Nucleopore membrane: 0.2 μm, 0.13 μm track-etch membrane.

Membrane holder.

All related materials and buffers are sterilized before use.

Bacteria concentration: 10^6 CFU/mL in PBS pH 7.4.

1. 80μL of PMMP is added into 500μL of bacteria suspension in PBST and react for 15 min at room temperature (10 min stationary, 5 min rotation).
2. After magnetic actuation, wash the PMMP with PBST(X3), and then resuspend in sterilized water.
3. Filter the PMMP through a Nucleopore membrane.
    a. Assemble a membrane holder set up for syringe filtration.
4. Fix the membrane by immersing it in 3mL of a 3% glutaraldehyde in pH 7.4 phosphate buffer for overnight at 4°C.
5. Wash the membrane for 4 times using PBS buffer.
6. Fix the membrane in 1% w/v OsO_4 in 0.1M PBS for 2h at 4°C. Wash again for 4 times with PBS buffer.
7. Dehydrate the membrane with ethanol: 15 min in 30% ethanol, 30 min in 50% ethanol, 12 hours in 2% acetate uranyl in 70% ethanol, 30 min in 90% ethanol, and twice 30 min in 100% ethanol.
8. Remove all remaining ethanol by critical point drying with CO_2.
9. The filter is then submitted to metallization with gold to improve electric conductivity.
10. The gold sputtered sample is then ready for SEM imaging.

APPENDIX J

Preparation of PEI-functionalized CNT

1. Carboxyl functionalized multi-walled CNT (COOH-CNT) was synthesized by adding 40 mg CNT to concentrated 20 mL HNO_3 and H_2SO_4 (1:3, v/v) solution at 120 °C in an oil bath to react while stirring for 30 min.
2. The product was then washed with DI water to a neutral pH and vacuum dried at 70 °C.
3. For preparation of PEI-CNT, 30 mg COOH-CNT was dissolved in 15 mL dry DMF following which the suspension was sonicated for 5 min and 6 mL $SOCl_2$ was added gradually in an ice-bath to acylate the COOH group.
4. Reflux for 24 h at 120 °C with continuous stirring, the reaction mixture was centrifuged at 10000 rpm.
5. The pellet was washed with anhydrous THF, dried under vacuum at room temperature for 2 h. Resuspend the pellet in 5 mL of DMF.
6. After stirring for 1 h under N_2 atmosphere at 90 °C, 100 mg PEI was added into reaction flask and reacted with acylated COOH-CNT for 3 days.
7. The reaction mixture was centrifuged, washed with methanol and dried at 70 °C.

APPENDIX K

Cloning in *E. coli*

1. Design of cloning strategy and primer design using the software. Selection of restriction enzymes and buffers.
2. *E. coli* XL-1 Blue/BL21 chemical competent cells (stock maintained in -80°C freezer in vials, each vial of 80 µL competent cells).
3. Obtaining DNA fragment by PCR (using genomic DNA of the desired microorganism or phage P100: usually the gene sequence is codon optimized for expression in the desired microorganism and synthesized in Genscript).
4. PCR product purification
5. Restriction digestion of the plasmid and the PCR product
6. Ligation, transformation and plating in antibiotic selective agar plates
7. Design of screening strategy: Grow the colonies, isolate the plasmid and do PCR verification

I. Plasmid Isolation: Plasmid Miniprep - Zippy Protocol

II. PCR: Phusion Polymerase (25 µL system)

H_2O	12.7 µL
5×Phusion HF Buffer	5 µL
2.5 mM dNTP	2.5 µL

Primer mix	2.5 μL
Template	1 μL
Phusion Polymerase	0.3 μL

Annealing Temperature (T_A) should be the lowest T_m - 5 °C

Extension Time: 30s/kb at 72 °C

Reaction:

Step 1: 98 °C – 45 sec

Step 2: 98 °C – 15 sec

Step 3: T_A°C – 30 sec

Step 4: 72 °C – 30s/kb

Repeat Steps 2-3, 30 cycles

Step 5: 72 °C – 5 min

Step 6: 10 °C --- infinite hold

III. PCR product purification: ZYMO Protocol

IV. Restriction Digestion

1. Purified PCR product, plasmid to be digested separately- choose the correct restriction enzymes and the compatible buffer (refer NEB buffer charts)

2. Restriction digestion Set up (20 μL system for DNA fragment, 10 μL system for Vector)

Water (Vector/DNA)	4 μL/0 μL
10x Buffer (1/2/3/4)	2 μL
Restriction Enzyme 1	1 μL
Restriction Enzyme 2	1 μL
Vector/ DNA	4 μL/16 μL

3. Incubate at 37°C for 2-4 hours in water bath.

V. Gel Extraction

1. Use fresh 1x TAE buffer. Run 20 µL digested samples + 10 µL loading buffer in 1% Agarose gel.

2. Observe under UV Transilluminator. (wear UV protective glasses)

3. Cut the fragments and place it in their respective centrifuge tubes. Vector fragment and DNA-right size in separate tubes.

4. Add 300 µl - 600 µl of ADB buffer

5. Incubate at 55 °C for 10 min in water bath or as long as it takes to fully melt.

6. After the gel melts, add the solution on a spin column with collection tube.

7. Centrifuge at 10000 rpm for 1 min

8. Add 400 µL of DNA wash buffer.

9. Centrifuge at 12,000 rpm for 2 min.

10. Transfer spin column to centrifuge tube and add X µL milli- Q water. (The quantity of water added depends on the brightness of each fragments)

11. Wait for 2 min and spin at 12,000 rpm for 2 min.

VI. Ligation

1. Use DNA Insert: Plasmid as 3:1 or 5:1

2. Set up

a. Three fragments system

2x Buffer	16.5 µL
Vector	2 µL
Fragment 1	4.5 µL

Fragment 2	4.5 µL
Fragment 3	4.5 µL
Ligase	1 µL

b. Two fragments system

2x Buffer	12 µL
Vector	2 µL
Fragment 1	4.5 µL
Fragment 2	4.5 µL
Ligase	1 µL

c. One fragment system

2x Buffer	8µL
Vector	2 µL
Fragment 1	5µL
Ligase	1 µL

3. Wait for 20 min (room temperature), and then proceed for transformation.

VII. Heat shock Transformation

1. 10 µL sample + 60 µL chemical competent cell. (XLBlue1/ BL21)

2. Keep on ice for 20-30 min

3. Heat shock at 42°C for 1.5 min

4. Keep on ice for 2 min

5. Add 700 µL LB

6. Keep in 37 °C shaker for 30-45 min, 250 rpm

7. Centrifuge at 5000 rpm for 1 min

8. Discard 600 µL supernatant

9. Resuspend the 100 µL culture.

10. Spread the 100 µL culture on LB plate with the appropriate antibiotic.

11. Place it in 37 °C oven incubator overnight.

VIII. Screening

1. Pick 3-9 colonies and make overnight culture for all, separately.

2. Extract the plasmid from all cultures.

3. Verification of clones/mutants by enzyme digestion or PCR.

APPENDIX L

P100 Phage Genetic Information

gp 16 (orf2)

ATGAATAACAGTGAAGAAAAGTTCGAAGATGTTTTAAACGAATTTGGTAATACAGTAG
AAAAAGATAAAGAAGAAATTTCTAAGTCTACCGAAGAAAAAGAGGAGGTTACAGAT
ATTAATAAAGATAAAAAATCAGAAGAAGAAACTGCTGAGGAAGAAGTAACTGAGGC
TCCCGAAGTAGACGTTGCAGAAGACAAAGAAGTGTCCACTGAGACTCCCGAAGAAG
AGTCTACTAGTAAGTCAGCTAAGGAAGAAAAGAAAGAAAAAGATAGTGAAGAAGAC
AAGGACGAAGACGAGAACAAAAAAGGTAAGAAAGACAAAAAAGACAAAAAAGAA
GAAGACAGCAAAGAAGAAAAAACGGAGAAGTCTGATGAAGAAGATTCCGAAGAGG
CTGTAAAAAATACTAACTCTGATGCAGATATTGCAGGAGCATTGAATGCTGTTGCTAA
GTCTTATGAGAATGTTAAAGAAAGCCAAAGAGAGCAAAATACAACTGTAGAACGCTT
AGAGAAGAATATCGGTAGCTTAGTCAGTAAATTAGACAGCTTGGTAGATTTAATGAGT
GAACGTGTATCTAAGAGTGTAGTAGAAGATATTGAAACTCTTGAAGGAGCTAGTGAA
AAAGCTGTTGGCTATGTAGCAAAAAACGTAGATAGCAGTGTAGTAGAAGTTATTGAA
GGAGAAGAAACTTCTAAGAGTGTAGATGCAGAAGTGAGTCCTAGAGATGAGTTTCTA
GCTAATAAGAGTGCTTTCCTAGAGTCTTTTGAATATGCAAGTCGTAACGGTGCTGAGC
GTAGAGATTTAACTGATGTTCGTCACGCTCATGGGAACATTACAAATGATATTGCTAGT
AAAGCAGATTATAACCGAGTTAACGACTTTATGAAAAAATGGAGTAAGTAA

TAAAGGTAACTGTATAGAGTATTTTTTGTAAACAGTATGCTATATTATAGGAACATG
GGAAACATGTTACGTTATGAGAGAGCTTGCCCGTTTTAGGACTCCTCCCCTAGGGCA
GGTTATCTCACTAACAAAAAAATAAAACTATGAAACTGAAAGGTGATAAATATAA

gp 17 (capsid protein s)

ATGCCAAAAAATAACAAAGAAGAAGAAGTTAAAGAAGTAAACCTTAATTCAGTACA
AGAGGACGCGTTAAAGTCCTTTACAACTGGTTATGGTATCACACCTGATACACAAAC
AGATGCAGGAGCATTAAGACGTGAGTTCCTAGACGACCAAATCTCAATGCTTACTTG
GACAGAGAATGATTTAACATTCTATAAAGACATCGCTAAAAAACCAGCTACATCTA
CAGTAGCAAAATACGATGTATACATGCAACATGGTAAGGTAGGTCATACTAGATTT
ACTCGTGAGATTGGGGTAGCACCAGTAAGTGACCCTAACATCCGTCAAAAAACAGT
AAATATGAAATTTGCTTCCGATACTAAAAACATCAGTATCGCAGCAGGTCTAGTAAA
CAACATTCAAGACCCAATGCAAATTTTGACTGACGATGCTATCGTAAATATTGCTAA
AACAATTGAGTGGGCTTCATTCTTTGGAGATTCTGACTTATCAGATAGCCCAGAACC
ACAAGCAGGACTAGAATTTGACGGCTTGGCTAAACTTATTAACCAAGATAACGTTCA
TGATGCTCGTGGAGCTAGCTTGACTGAAAGCTTGTTAAACCAAGCAGCAGTAATGAT
TAGTAAAGGTTATGGTACACCTACAGATGCTTACATGCCAGTAGGGGTTCAAGCAG
ACTTTGTTAACCAACAACTTTCTAAACAAACACAGCTTGTTCGTGATAACGGAAACA
ACGTAAGCGTTGGTTTCAACATCCAAGGTTTCCATTCAGCTCGTGGATTTATCAAAC
TTCACGGTTCTACAGTAATGGAAAACGAACAAATCTTAGATGAACGTATTCTTGCTT
TACCAACAGCTCCACAACCAGCTAAGGTAACTGCAACACAAGAAGCAGGTAAAAAA
GGACAATTTAGAGCAGAAGACTTAGCAGCACACGAATACAAAGTTGTTGTAAGTTC
TGACGATGCAGAGTCTATTGCAAGTGAAGTGGCTACAGCTACAGTTACTGCAAAAG
ATGACGGCGTTAAACTAGAAATCGAGTTAGCTCCAATGTACAGCTCCCGTCCACAAT
TCGTTTCAATCTATAGAAAAGGTGCAGAAACAGGTTTATTCTACCTAATCGCTCGTG
TACCTGCTAGCAAAGCAGAGAACAACGTAATCACTTTCTATGACTTAAACGACTCTA
TTCCTGAAACAGTAGACGTATTCGTTGGTGAAATGTCTGCTAACGTAGTACACTTGT
TTGAATTACTACCAATGATGAGATTACCTCTAGCTCAAATTAACGCATCTGTTACATT
TGCAGTTTTATGGTATGGAGCATTAGCTCTAAGAGCACCTAAGAAATGGGTACGTAT
TAGAAACGTTAAATATATTCCTGTAAAAAACGTTCATAG CAACTAA

TAATTATAGGATAATTGAATAAAAACAGTATAGAGAGCAGATAAATACTGCTCTCT
ATTTTACTAATAAGGAGGATTTAAA

gp 18 (orf3)

TTGCTAAAAAATACAAACTTAGCTAATTATAAAAAAGTGAATACACGATTTGGAAA
TCTTAGTTTTGATGATAAAGGTATTTCTAATGACCTAACGGAAGAGCAGCAAAAAGA
ATTAGGTAAGCTTAGAGGATTCGAATATATTAAGACAGAACAGAAAACGAAAGAAG
AACCTAAGAAAGAAGAACCTAAGAAAGAAAGTACAGAAAATGAATTAGACAGCTT
CTTAGCTAAAGAACCTTCAATCAAAGAATTAAAAGAATTTGCGAGTAAAAAAGGCA
TTAAAATTGAAAAAACTAAGAAAAATGATATAATTGAAGAACTAAAGAGAGGGTAA

APPENDIX M

List of Abbreviations

ABTS: 2,2'-azino-bis(3-ethylbenzothiazoline-6-sulfonic acid)

APTES: (3-aminopropyl)-triethoxysilane

BHI: Brain heart infusion

BS3: bis(sulfosuccinimidyl)suberate)

CE: Capture efficiency

CNT: Carbon nanotube

CR: Phage coupling ratio

CV: Cyclic voltammetry

DET: Direct electron transfer

DFDNB: 1,5-difluoro-2,4-dinitrobenzene

DSP: dithiobis-(succinimidyl propionate)

ELISA: Enzyme linked immunosorbent assays

EIS: Electrochemical impedance spectroscopy

$Ep_{1/2}$: Half peak potentials

FNTL: Laccase from bacterium *Bacillus sp.* FNT

GCE: Glassy carbon electrode

GMO: Genetically modified organisms

IMS: Immunomagnetic separation

LOD: Limit of detection

LOQ: Limit of quantification

LSV: Linear sweep voltammetry

MET: Mediated electron transfer

MO: Metal oxide

MWCNT: Multi-wall carbon nanotube

OCP: Open circuit potential

ORR: Oxygen reduction reaction

PBSE: 1-pyrenebutanoic acid succinimidyl ester

PCR: Polymerase chain reaction

PBS: Phosphate buffered saline

PEI: Polyethylenimine

PMMP: P100-functionalized magnetic particles

PMZ: Promazine

RRDE: Rotating ring disk electrode

SEM: Scanning electron microscopy

SPE: Screen-printed carbon electrode

SWCNT: Single-wall carbon nanotube

sTiO_2: Silylated TiO_2 nanoparticles

SYR: Syringaldazine

TEM: Transmission electron microscopy

TVL: Laccase from *Trametes versicolor*